Study on Secondary Metabolites of Marine-derived Actinomycetes

Toyama Prefectural University

Zhiwei Zhang

Feb. 10, 2022

List of Abbreviations

1-BuOH	1-butanol
CH_3Cl	Chloroform
DMSO	Dimethyl sulfoxide
MeCN	Acetonitrile
MeOH	Methanol
HCO_2H	Formic acid
HPLC	High performance liquid chromatography
HPLC-UV	High performance liquid chromatography-ultraviolet
HR-ESI-TOFMS	High resolution-electrospray ionization-time of flight-mass spectrometry
GC-MS	Gas chromatography–mass spectrometry
NMR	Nuclear magnetic resonance
COSY	Correlation spectroscopy
TOCSY	Total correlation spectroscopy
HSQC	Heteronuclear single-quantum correlation spectroscopy
HMBC	Heteronuclear multiple-bond correlation spectroscopy
NOESY	Nuclear overhauser effect spectroscopy
ROESY	Rotating-frame nuclear overhauser effect spectroscopy
ECD	Electronic circular dichroism
DDBJ	DNA data bank of Japan
MIC	Minimum inhibitory concentration
MTT	3-(4,5-Dimethylthiazol-2-yl)-2,5-diphenyl tetrazolium bromide
ODS	Octadecyl-silica
XTT	Sodium 3′-[1-[(phenylamino)-carbony]-3,4-tetrazolium]-bis(4-methoxy-6-nitro)benzene-sulfonic acid hydrate

Contents

CHAPTER 1

Introduction

1-1 Background

Although human medicine has made great progress, infectious diseases caused by bacteria, fungi, and viruses still pose a significant threat to public health. The lack of effective drugs and the persistent threat of resistant microorganisms have further intensified this situation [1]. In particularly, cancer is still one of the most life-threatening diseases in the world. In 2018, approximately 18 million new cancer cases were reported worldwide, causing approximately 10 million deaths [2]. In addition, according to the World Health Organization, more than 10 million people die each year from lifestyle diseases caused by smoking, drinking alcohol or simply lack of physical exercise [2-3].

1-2 Natural products as a major source of available drugs

Natural products are small organic molecules derived from natural sources, including plants, animals, and microorganisms. Historically, natural products are the majority source of medicine to treat a wide area of human diseases [4-5]. Before the 20th century, the only available medicines that could be used to treat human and livestock diseases were crude and semi-pure extracts of plants, animals, microorganisms, and minerals. The 20th century completely changed the idea of drug use, as the receptor theory of drug action. The role of drugs in the human body is determined by the idea of specific interactions between drug molecules and biological macromolecules that allow scientists to draw conclusions about individual compounds in the extract [6]. This led to the beginning of a new era in pharmacology, as pure, isolated chemicals, rather than extracts which became the standard treatment for diseases. Therefore, biological activity is the main factor required for drugs. In fact, many biologically active compounds are responsible for crudely extracting drugs and elucidating their chemical structures [7-8].

The most legendary example is the discovery of penicillin in 1928, the first antibiotic, isolated from a fungus *Penicillium.* Penicillin contains a characteristic quaternary β-lactam ring, which kills bacteria by combining the β-lactam ring with DD-transpeptidase, inhibits its cross-linking activity and prevents the formation of new cell walls [9]. The modern era of antibiotic chemotherapy was started with the introduction of penicillin in the 1940s in clinical trials for the treatment of bacterial infections.

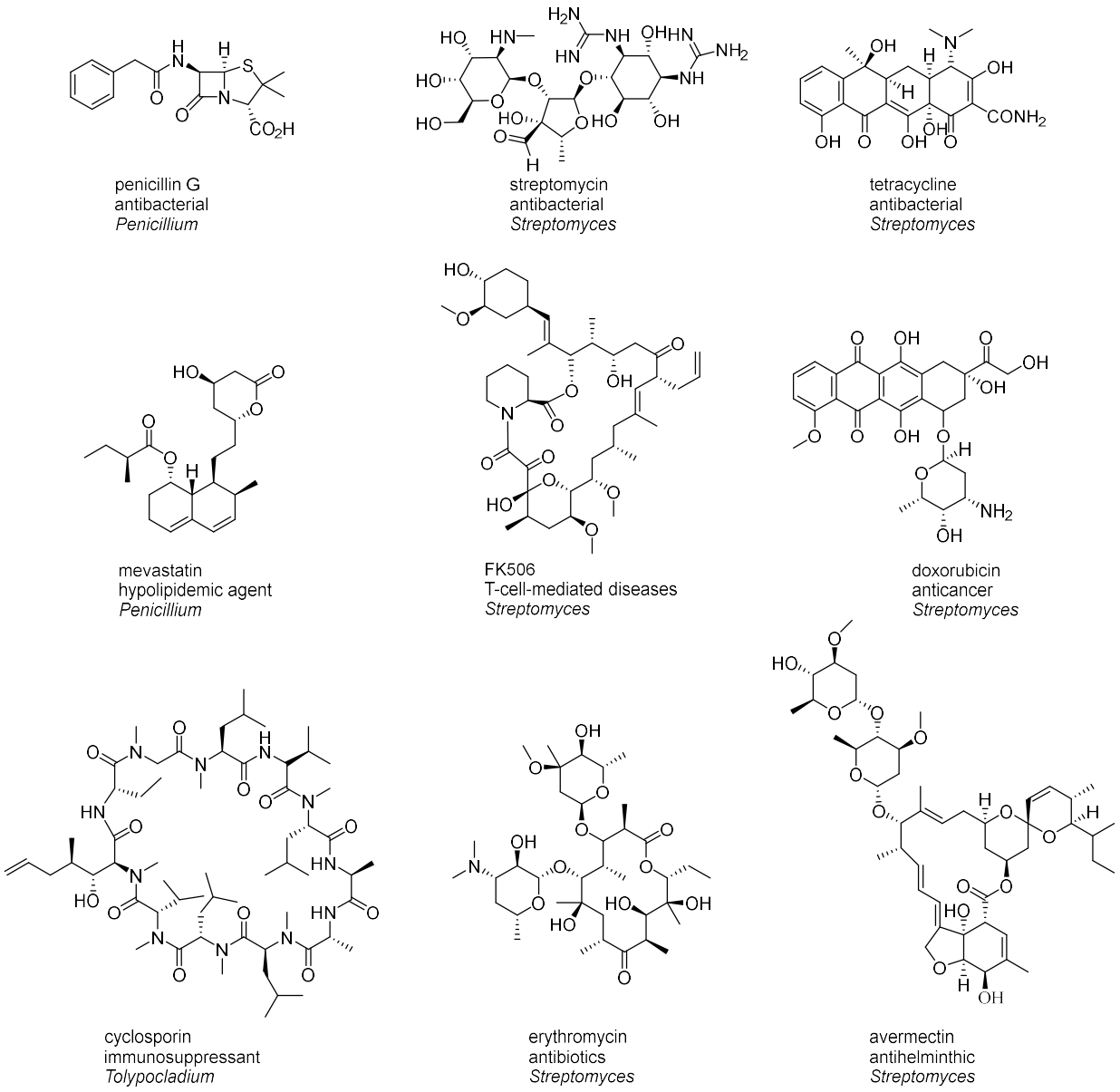

Figure 1-1. Microbial metabolites used as clinical medicines or drug leads.

Accompanying the successful case of penicillin, soil-derived bacteria and fungi have been shown be a rich source of structurally unique bioactive compounds. Streptomycin is the first antibiotic to treat tuberculosis, discovered from *Streptomyces* by Waksman [10]. Soon after discovery of tetracycline from *Streptomyces aureofaciens*, doxorubicin and other classes of antibiotic microbial natural products were discovered one after another. A hypolipidemic agent mevastatin, an immunosuppressant FK506, and anthelminthic avermectin all provided new remedies [11-12] (Figure 1-1).

In the 1980s, the application of NMR, high performance liquid chromatography (HPLC) and mass spectrometry in the research of natural product chemistry accelerated the discovery of new natural products [13]. There has been a remarkable increase of

interest in natural product research after the 2000s, with more and more renewed attention for providing novel and interesting scaffolds with improved pharmacokinetics and pharmacodynamics properties. In addition, newer outstanding resources have been stepped up in the area of isolation, analysis, biological assay, and many more hyphenated techniques, for example, GC–MS, LC-MS, LC-NMR and many more [14].

Recently, intensive and concentrated screening activities on traditional terrestrial sources resulted in the repeated isolation of known compounds and the number of novel natural products is declining year by year [15]. In response to the increasing demand for new antibacterial compounds for drugs, the focus on natural product discovery has turned to underexplored habitats. Especially the marine environment represents one of the most abundant and underexploited habitats with rich microbial diversity showing potential for discovery of new and chemically diverse antimicrobial compounds [16]. Considering the difference in biosynthetic pathways, unexplored organisms are the best way to discover new metabolites. Further, organisms of unexplored geographic origin generally receive more attention.

1-3 Marine environment as an important source for drugs and drug candidates

The higher terrestrial plants and soil microorganisms were considered to be the major biological sources of natural products for a long time. In the past few decades, more than 20,000 natural products have been found from marine environmental research, which indicated not only the increase in the number of known natural products but also excellent structures and activities [17]. In addition, the first researchers were surprised by the fact that marine organisms very rarely contained already known compounds. Therefore, the biochemistry of their secondary metabolism is very different from that of terrestrial organisms.

Oceans cover nearly 70% of the earth surface and host a huge ecological, chemical and biological diversity. The unique characteristics of the marine environment have equipped marine organisms with the appropriate mechanisms to survive in a hostile milieu in terms of extreme temperatures, changes in pressure and salinity, and attacks by bacteria and viral pathogens [18]. The harsh chemical and physical conditions of the marine have also favored the production of a wide variety of novel molecules in marine

organisms that are unique in terms of diversity. Therefore, marine organisms are considered as a potential source of essential and novel biologically active compounds for the development of therapeutics. Nevertheless, the marine habitat is still poorly explored.

After decades of exploration of natural products derived from the marine environment, eleven drugs have successfully reached the market, out of five are for the treatment of cancer, including cytarabine, trabectedin, eribulin mesylate, and the antibody-drug conjugates brentuximab vedotin and polatuzumab vedotin, three are for the treatment of hypertriglyceridemia, two are for antivirus treatment, including vidarabine and iota-carrageenan and one is for the amelioration of severe chronic pain, namely ziconotide [19] (Figure 1-2).

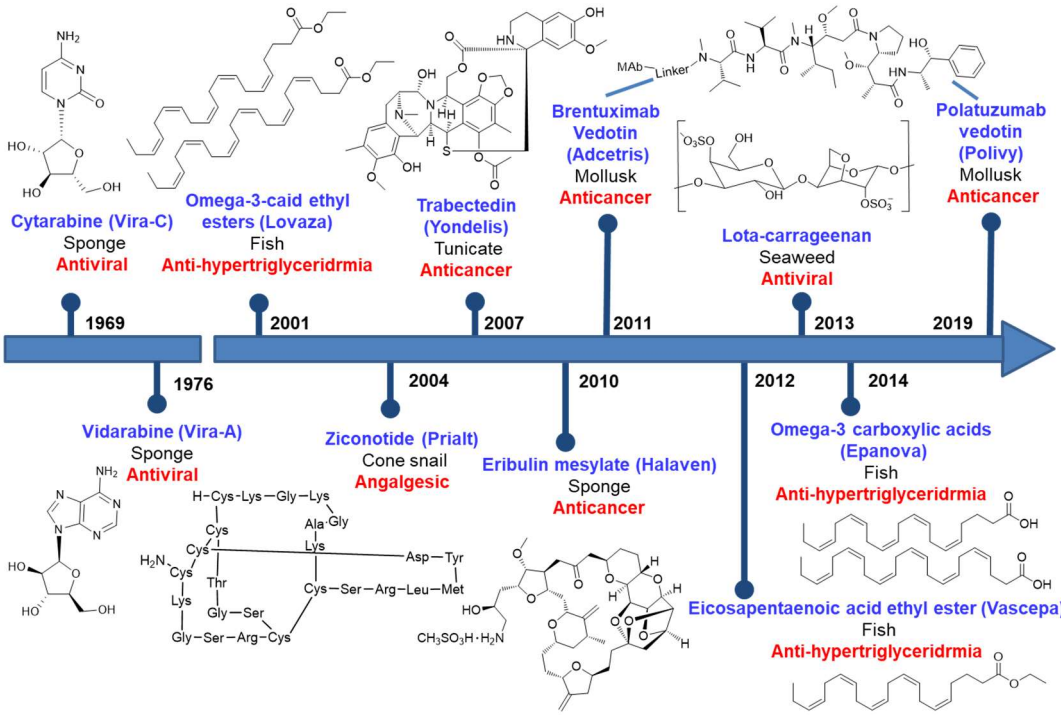

Figure 1-2. Timeline for drugs from marine.

So far, more than twenty marine natural products have been investigated as drug candidates in different phases of clinical trials, and a large number of drugs are undergoing extensive preclinical development for various applications. Marine natural products increasingly stimulate the development of new drug therapies for various applications [20].

The cyclic depsipeptide plitidepsin (Aplidin, Figure 1-3) was isolated from the

marine tunicate *Aplidium albicans* and known to interact with eukaryotic elongation factor 1A2 (eEF1A2) in tumor cells. It has reached Phase III clinical trial for the treatment of relapsed/refractory multiple myeloma in combination with dexamethasone [21].

Plinabulin (NPI-2358, Figure 1-3) is a potent and selective vascular disrupting agent (VDA), isolated from the marine fungus *Aspergillus* sp. CNC139. Plinabulin is now under investigation in Phase III trials to assess its application in combination with docetaxel in patients with advanced non-small cell lung cancer due to its function as a vascular-disrupting agent and its apoptotic effect on tumor cells [22].

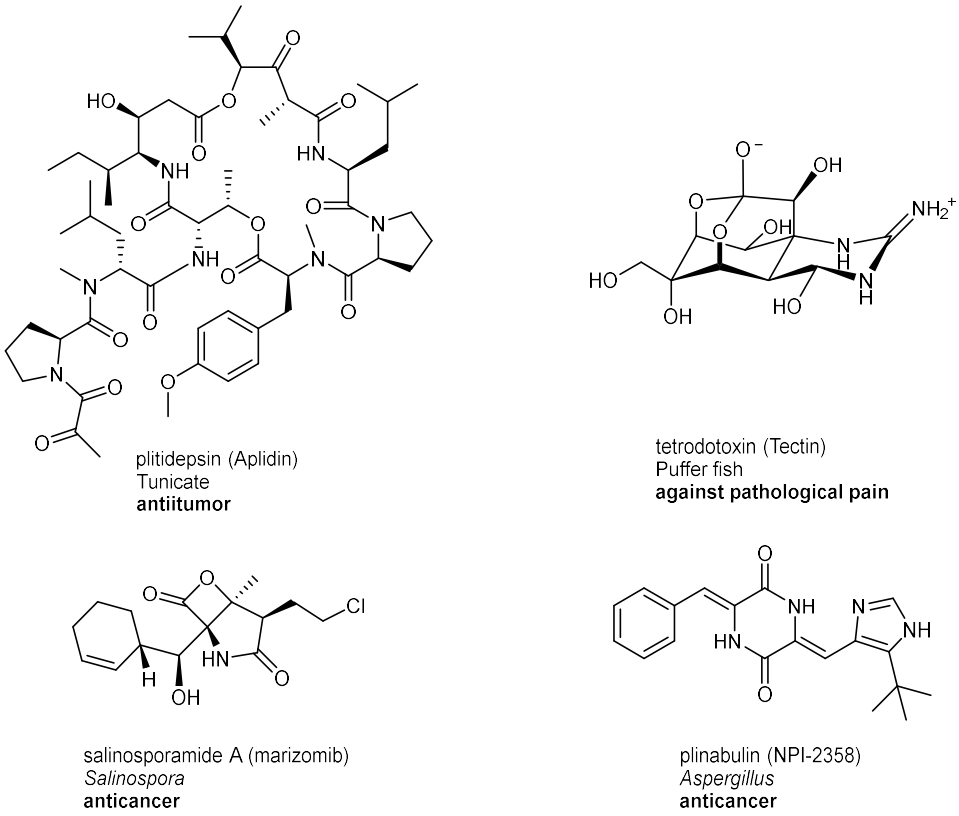

Figure 1-3. Drug candidates found from the marine organisms reaching clinical trials.

Tetrodotoxin (Tectin, Figure 1-3) is a guanidine derivative with a highly oxygenated carbon skeleton, found from puffer fish the *Tetraodontidae* family. Tetrodotoxin is probably the most well-known marine toxin, binding to VGSCs in nerve cell membranes to prevent depolarization and propagation of action potentials and lead to the loss of sensation. More recently, it has been extensively used as a chemical tool to functionally characterize VGSCs and has been applied as an analgesic agent against pathologic pain. Two Phase III safety and efficacy studies for management of moderate

to severe inadequately controlled cancer-related pain were completed [23].

Salinosporamide A (Marizomib, Figure 1-3), a novel long-lasting proteasome inhibitor isolated from marine actinomycetes *Salinispora tropica* and *Salinispora arenicola*, which entered phase I clinical trials for the treatment of multiple myeloma only three years after its discovery. To examine the safety, pharmacokinetics and pharmacodynamics of salinosporamide A, a phase II clinical trial in patients with relapsed/refractory multiple myeloma has been completed [24].

1-4 Marine microorganisms as an unexploited source for bioactive compounds

Marine microorganisms, including fungi, actinobacteria, proteobacteria, firmicutes, and cyanobacteria, have shown to be great reservoirs of bioactive molecules. Most marine microorganisms survive in a stressful habitat, under high salinity, without oxygen, extreme temperature (low and high), high pressure and limited light availability conditions [25]. These factors have resulted in the development of novel metabolisms, resulting in the production of unique metabolites that differ from terrestrial organisms. Thus, marine microbes provide an excellent resource for the discovery of new compounds with interesting biological activities, including antimicrobial, antifungal, antiprotozoal, antituberculosis, and antiviral properties.

Among marine microorganisms, there are many unknown species, and genera of bacteria, such as *Listonella*, *Marinomonas*, *Oceanospirillum*, and *Prochloron* [26]. Many obligate marine microorganisms are associated with marine fish, invertebrates, or algae. The adaptation of obligate marine bacteria to marine conditions often leads to the selection of such metabolic pathways that produce previously unknown metabolites. This explains the significant biochemical diversity in these microorganisms and helps to study them as a new source of antibiotics [27].

The main species of bacteria found in seawater belong to the genera *Vibrio*, *Pseudomonas*, *Flavobacterium*. *Achromobacter*, and *Micrococcus*. However, the genus *Streptomyces* has been the major provider of new molecules so far. Marine bacteria are supposed to have different physiological, biochemical and molecular properties from their terrestrial equivalents, so they may produce different compounds [27-28].

Although many actinomycete isolates from marine environments display high similarity of 16S rRNA gene sequence to the terrestrial isolates, their secondary metabolites often have unprecedented skeletons or unreported combination of known structural units, suggesting the specific adaption of secondary metabolism in marine microorganisms [29].

1-5 Secondary metabolites isolated from marine actinomycetes

Actinomycetes are the rich source of bioactive natural products, accounting for approximately 60% of all known antibiotics, and more than 70% of them are found from the genus *Streptomyces* [30]. Marine environment is largely an untapped source for deriving actinobacteria, having potential to produce novel, bioactive natural products. Marine actinomycetes are widely distributed in biological sources such as fishes, molluscs, sponges, seaweeds, mangroves, besides seawater and sediments [31]. The secondary metabolites of marine actinomycetes enhance distinct biological properties, including antibacterial, antifungal, anticancer, insecticidal antiviral, and enzyme inhibitory activities. They have attracted global in the last few years for their ability to produce pharmaceutically active compounds [32-33].

1-5-1 Antibacterial activity

Antibacterial substances are agents that inhibit the growth or kill bacteria. Infectious diseases are still one of the main causes of death caused by antibiotic resistant microorganisms. The frequency of drug resistance of microbial pathogens continues to increase at an alarming rate throughout the world [34]. Pathogens have reduced efficacy and resistance to antibiotics, so new alternatives need to be developed. In order to overcome this problem, there is an urgent need to develop effective new drugs without any side effects. The antibacterial activity of marine actinomycetes has been extensively studied, and many natural products with novel structure and excellent antibacterial activity have been reported [35].

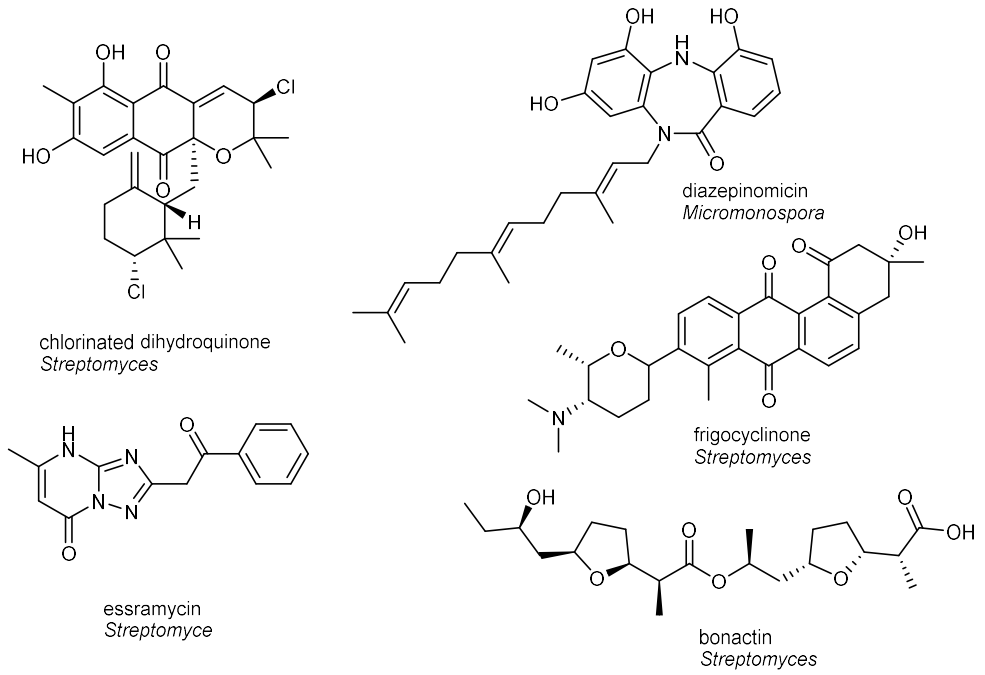

Figure 1-4. Chemical structure of chlorinated dihydroquinones, diazepinomicin, frigocyclinone, essramycin and bonactin.

Bonactin (Figure 1-4) has been isolated from *Streptomyces* isolated from a shallow-seawater sediment sample. This compound showed antimicrobial activity against both Gram-positive and Gram-negative bacteria, and antifungal activity [36]. Chlorinated dihydroquinone (Figure 1-4) is a new antibiotic produced by a marine *Streptomyces* sp. This compound formally possess novel carbon skeleton, but is related to several previously reported metabolites of the napyradiomycin class. Structures of the this compound have significant antibacterial and cytotoxicities [37].

Diazepinomicin (Figure 1-4) is a novel farnesylated dibenzodiazepinone produced by a *Micromonospora*. It displayed antibacterial, antitumor and anti-inflammatory activity [38]. Frigocyclinone (Figure 1-4) is a angucyclinone antibiotic isolated from *Streptomyces griseus*, consisting of a tetrangomycin moiety attached through a *C*-glycosidic linkage with the aminodeoxysugar ossamine. This compound showed antibacterial activities against Gram-positive bacteria. Essramycin (Figure 1-4) is a new triazolopyrimidine antibiotic isolated from the genus *Streptomyces*. This compound has antibacterial activity and has an MIC of 2–8 μg/mL against Gram-positive and Gram-negative bacteria [39].

1-5-2 Antifungal activity

Marine actinomycetes are useful biological tools for the production of antifungal compounds. In general, *Streptomyces* are saprophytic, usually related to soil, and they make a great contribution to the turnover of complex biopolymers and antibiotics. However, marine *Streptomyces*, particularly related to marine invertebrates associated with invertebrate, produced the enzyme chitinase and shows antifungal activity in order to protect the host [40].

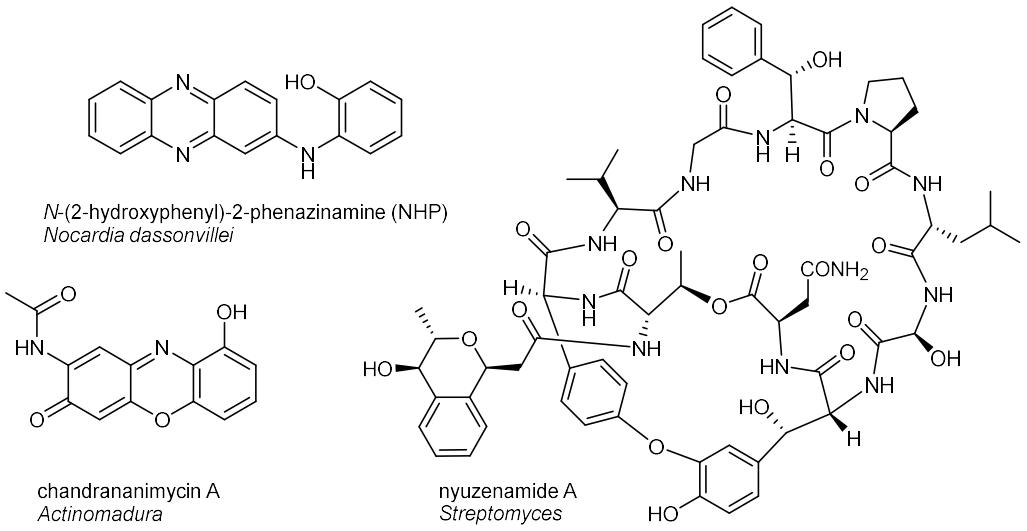

Figure 1-5. Chemical structure of *N*-(2-hydroxyphenyl)-2-phenazinamine (NHP), chandrananimycin A, and nyuzenamide A.

Chandrananimycin A (Figure 1-5) was an unique antibiotic discovered from *Actinomadura*. This compound possesses potent antifungal activity against *Mucor miehei*. It also exhibits antialgal activity against the microalgae *Chlorella vulgaris* and *Chlorella sorokiniana* and antibacterial activity, along with anticancer activity [41]. *N*-(2-hydroxyphenyl)-2-phenazinamine (NHP) (Figure 1-5) is a new antibiotic isolated from *Nocardia dassonvillei*. This compound showed significant antifungal activity against *C. albicans* and high cancer cell cytotoxicity [42].

Nyuzenamide A (Figure 1-5), a bicyclic peptide, was discovered from *Streptomyces* isolated from suspended matter in deep sea water collected in the Sea of Japan. Nyuzenamide A was inactive against Gram positive and -negative bacteria and a yeast but selectively inhibited the growth of filamentous fungi. Nyuzenamide A was active against plant and human pathogens, *Glomerella cingulata* NBRC5907 and

Trichophyton rubrum NBRC5467, with a minimum inhibitory concentration (MIC) of 3.1 and 6.3 μg/mL, respectively. In addition, this compound exhibited cytotoxicity against P388 murine leukemia cells with IC_{50} of 4.9 μM [43].

1-5-3 Anticancer activity

Cancer still remains one of the most serious human health problems. Therapies for cancer treatment include surgery, radiotherapy, immunotherapy, and chemotherapy. Many of antitumor natural products from marine drugs are derived from marine actinomycetes and these metabolites play an important role in the identification of pharmaceutical compounds. Currently, it appears that only a few studies have focused on finding biologically active compounds derived from marine actinomycetes for use of anticancer agents. In particular, salinosporamide A (Figure 1-3) is a novel rare bicyclic β-lactone γ-lactam isolated from an obligate marine actinomycetes, Phase II clinical trial in patients with relapsed/refractory multiple myeloma has been completed [44].

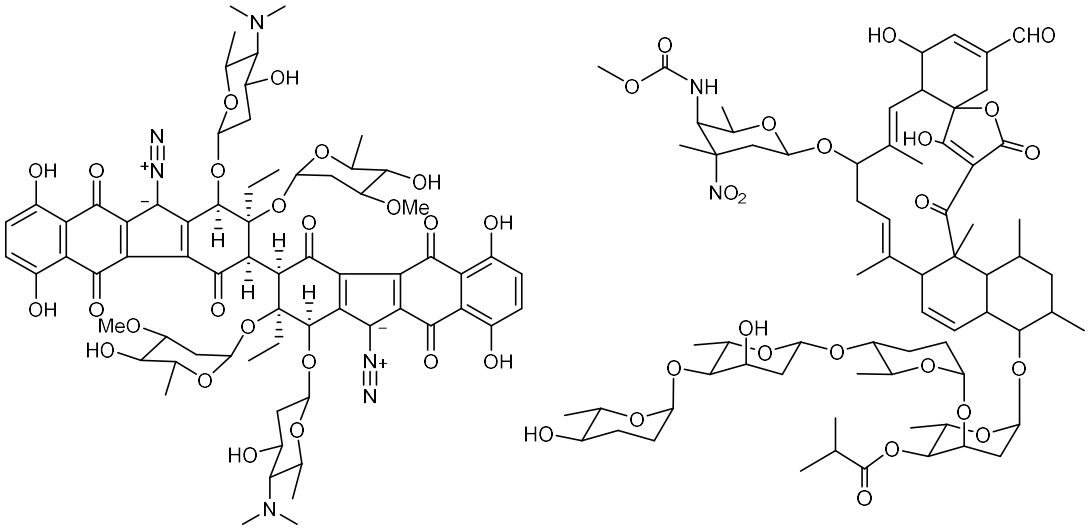

Figure 1-6. Chemical structure of lomaiviticin A and arisostatin A.

Lomaiviticin A (Figure1-6), dimeric angucycline with dimeric diazobenzofluorene glycoside structure, produced by fermentation of *Micromonospora lomaitiensis* in a seawater medium. Lomaiviticin A is an extremely potent cytotoxic compound reactive with DNA through a radicalic mechanism, is under preclinical studies for an anticancer agent [45]. Arisostatin A (Figure 1-6), a new member of tetrocarcin class of antibiotic

was isolated from the culture broth of an actinomycete *Micromonospora* collected from a seawater sample in Japan. Arisostatin A showed *in vitro* antitumor activity against cancer cell lines derived from organs such as breast, brain, colon and lung with IC_{50} values of 0.059-0.26 μM, and showed antibiotic activity against Gram-positive bacteria [46].

Arenicolide A (Figure 1-7), 26-membered polyunsaturated macrolactone, was produced by the obligate marine actinobacteria *Salinispora arenicola*. Arenicolide A was displayed to exhibit moderate cytotoxicity toward the human colon adenocarcinoma cell line HCT-116 with an IC_{50} of 30 μg/mL [47]. Resistoflavine (Figure 1-7) is a cytotoxic compound, isolated from *Streptomyces chibaensis*. It showed cytotoxic activity against human gastric adenocarcinoma HMO2 and hepatic carcinoma HePG2 cell lines [48].

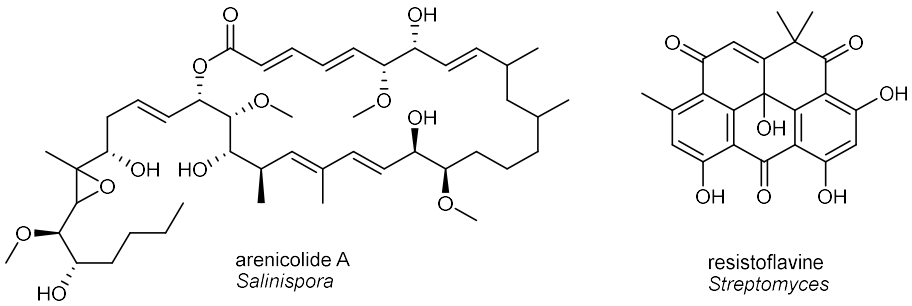

Figure 1-7. Chemical structure of arenicolide A and resistoflavine.

1-5-4 The objective of this thesis

As discussed already, marine environment is still largely underexploited in comparison with terrestrial one as new drug resources. The number of new natural products from marine actinomycetes is constantly increasing year by year.

To validate the potential of marine actinomycetes to produce new bioactive metabolites, four marine actinomycetes, two *Streptomyces* strains isolated from marine invertebrates and two *Actinomadura* strains isolated from deep seawater, were investigated. The results will be detailed in the following chapters.

References

1) Foreman, K. J.; Marquez, N.; Dolgert, A.; Fukutaki, K.; Fullman, N.; et al. *Lancet.* **2018**, *392*, 2052–2090.
2) WHO. **2017**. Noncommunicable diseases. Fact Sheet.
3) Tabish, S. A. *J. Cardiol. Curr. Res.* **2017**, *9*, 00326.
4) Siddiqui, A. A.; Iram, F.; Siddiqui, S.; Sahu, K. *Int. J. Drug. Dev. Res*. **2014**, *6*, 172–204.
5) Pham, J. V.; Yilma, M. A.; Feliz, A.; Majid, M. T.; et al. *Front. Microbiol.* **2019**, *10*, 01404.
6) Lahlou, M. *Pharmacol. Pharm.* **2013**, *4*, 17–31.
7) Thomford, N. E.; Senthebane, D. A.; Rowe, A.; Munro, D.; Seele, P.; et al. *Int. J. Mol. Sci.* **2018**, *19*, 1578.
8) Sorkin, B. C.; Kuszak, A. J.; Bloss, G.; Fukagawa, N. K.; Hoffman, F. A. et al. *FASEB. J.* **2020**. *34*, 41-65.
9) Fleming, A. *Br. J. Exp. Pathol.* **1929**, *10*, 226–236.
10) Wainwright, M.; *Hist. Philos. Life Sci.* **1991**, *13*, 97–124.
11) Jukes, T. H. *Rev. Infect. Dis.* **1985**, *7*, 702–707.
12) Dumont, F. J. *Curr. Med. Chem.* **2000**, *7*, 731–748.
13) Pye, C. R.; Bertin, M. J.; Lokey, R. S.; Gerwick, W. H.; Linington, R. G.; *PNAS.* **2017**, *114*, 5601–5606.
14) Bobzin, S. C.; Yang, S.; Kasten, T. P. *J. Chromatogr. B. Biomed. Sci. Appl.***2000**, *748*, 259–267.
15) Manivasagan, P.; Venkatesan, J.; Sivakumar, K.; Kim, S. K.; *Microbiol. Res.* **2014**, *169*, 262–278.
16) Sayed, A. M.; Hassan, M. H. A.; Alhadrami, H. A.; Hassan, H. M.; Goodfellow, M.; Rateb, M. *E. J. Appl. Microbiol.* **2019**, *51*, 72.
17) Carroll, A. R.; Copp, B. R.; Davis, R. A.; Keyzers, R. A.; Prinsep, M. R. *Nat. Prod. Rep.* **2021**, *38*, 362–413.
18) Newman, D. J.; Cragg, G. M.; *Planta. Med.* **2016**, *82*, 775–789.
19) Liang, X.; Luo, D.; Luesch, H. *Pharmacol. Res.* **2019**, *147*, 104373–104391.
20) McCauley, E. P.; Piña, I. C.; Thompson, A. D.; Bashir, K.; Weinberg, M.; et al. *J. Antibiot.* **2020**, *73*, 504–525.
21) Alonso-Álvarez, S.; Pardal, E.; Sánchez-Nieto, D.; Navarro, M.; Caballero, M. D.; Mateos, M. V.; Martín, A. *Drug. Des. Devel. Ther.* **2017**, *11*, 253–264.
22) Yan, J.; Chen, J.; Zhang, S.;, Hu, J.; Huang, L.; Li, X. *J. Med. Chem.* **2016**, *59*, 5264–5283.
23) Lago, J.; Rodríguez, L. P.; Blanco, L.; Vieites, J. M.; Cabado, A. G. *Mar. Drugs.* **2015**, *13*, 6384–6406.
24) Feling, R. H.; Buchanan, G. O.; Mincer, T. J.; Kauffman, C. A.; Jensen, P. R.; Fenical, W. *Chem. Intl. Ed.* **2003**, *42*, 355–357.
25) Carroll, A. R.; Copp, B. R.; Davis, R. A.; Keyzers, R. A.; Prinsep, M. R. *Nat. Prod. Rep.* **2020**, *37*, 175–223.
26) Schinke, C.; Martins, T.; Queiroz, S. C. N.; Melo, I. S.; Reyes, F. G. R. *J. Nat. Prod.* **2017**, *80*, 1215–1228.
27) Stonik, V. A.; Makarieva, T. N.; Shubina, L. K. *Biochemistry (Mosc)* **2020**, *85*, 1362–1373.
28) Jin, M.; Gai, Y.; Guo, X.; Hou, Y.; Zeng, R. *Mar. Drugs.* **2019**, *17*, 656.
29) Blunt, J. W.; Copp, B. R.; Munro, M. H. G.; Northcote, P. T.; Prinsep, M. R. *Nat. Prod. Rep.* **2005**, *22*, 15−61.
30) Berdy, J. *J. Antibiot*. **2005**, *58*, 1-26.
31) Manivasagan, P.; Venkatesan, J.; Sivakumar, K.; Kim, S. K.; *Microbiol. Res.* **2014**, *169*, 262–278.
32) Stincone, P.; Brandelli, A. *Crit. Rev. Biotechnol.* **2020**, *40*, 306–319.
33) Bull, A. T.; Stach, J. E.; Ward, A. C.; Goodfellow, M.; *Antonie. Van. Leeuwenhoek*. **2005**, *87*,

65–79.
34) Ravikumar, S.; Gnanadesigan, M.; Saravanan, A.; Monisha, N.; Brindha, V.; Muthumari, S. *Asian. Pacific. J. Tropical. Med.* **2012**, *5*, 887–890.
35) Valliappan, K.; Sun, W.; Li, Z. *Appl. Microbiol. Biotechnol.* **2014**, *98*, 7365–7377.
36) Schumacher, R. W.; Talmage, S. C.; Miller, S. A.; Sarris, K. E.; Davidson, B. S.; Goldberg, A. *J. Nat. Prod.* **2003**, *66*, 1291–1293.
37) Soria-Mercado, I. E.; Prieto-Davo, A.; Jensen, P. R.; Fenical, W. *J. Nat. Prod.* **2005**, *68*, 904–910.
38) Charan, R. D.; Schlingmann, G. Janso, J.; Bernan, V.; Feng, X.; Carter, G. T. *J. Nat. Prod.* **2004**, *67*, 1431–1433.
39) El-Gendy, M. M.; Shaaban, M.; Shaaban, K. A.; El-Bondkly, A. M.; Laatsch, H. *J. Antibiot.* **2008**, *61*, 149–157.
40) Wanner, L. A. *Am. J. Potato. Res.* **2009**, *86*, 247–264.
41) Maskey, R. P.; Li, F.; Qin, S.; Fiebig, H. H.; Laatsch, H. *J. Antibiot.* **2003**, *6*, 622–634.
42) Gao, X.; Lu, Y.; Xing, Y.; Ma, Y.; Lu, J.; Bao, W.; et al. *Microbiol. Res.* **2012**, *167*, 616–622.
43) Karim, M. R. U.; In, Y.; Zhou, T.; Harunari, E.; Oku, N.; Igarashi, Y. *Org. Lett*. **2021**, *23*, 2109–2113.
44) Prudhomme, J.; McDaniel, E.; Ponts, N.; Bertani, S.; Fenical, W. et al. *PLoS. ONE.* **2008**, *3*, e2335.
45) Colis, L. C.; Hegan, D. C.; Kaneko, M.; Glazer, P. M.; Herzon, S. B.; *J. Am. Chem. Soc*. **2015**, *137*, 5741–5747.
46) Furumai, T.; Takagi, K.; Igarashi, Y.; Saito, N.; Oki, T. *J. Antibiot.* **2000**, *53*, 227-232.
47) Williams, P. G.; Miller, E. D.; Asolkar, R. N.; Jensen, P. R.; Fenical, W. *J. Org. Chem.* **2007**, *72*, 5025–5034.
48) Gorajana, A.; Vinjamuri, S.; Kurada, B. V.; Peela, S. Jangam, P.; Poluri, E. et al. *Microbiol. Res.* **2007**, *162*, 322–327.

CHAPTER 2

Iseolides A–C, Antifungal Macrolides from a Coral-Derived Actinomycete of the Genus *Streptomyces*

2-1 Background

Actinomycetes are the prolific source of bioactive compounds, accounting for approximately 60% of all known antibiotics, and more than 70% of them are produced by the genus *Streptomyces* [1]. Marine actinomycetes are considered to be a potential source of new natural products with high structural diversity, unique biological activity, and molecular mode of action beneficial to drug development [2]. Actinomycetes in the marine environment can be recovered from a variety of sources, including sediments, water, and invertebrates such as corals, sponges and molluscs [3-4]. Among the isolated sources of marine actinomycetes, a number of researches have been devoted to sponges, and it has been clarified that various species of actinomycetes can produce interesting natural products [5-6]. Corals are another large group of marine invertebrates, and they also have a variety of symbiotic or associated microorganisms [7-9]. However, only few natural products such as, streptochloritides [10], nahuoic acids B–E [11], and pteridic acids C–G [12], were reported from actinomycetes isolated from soft corals.

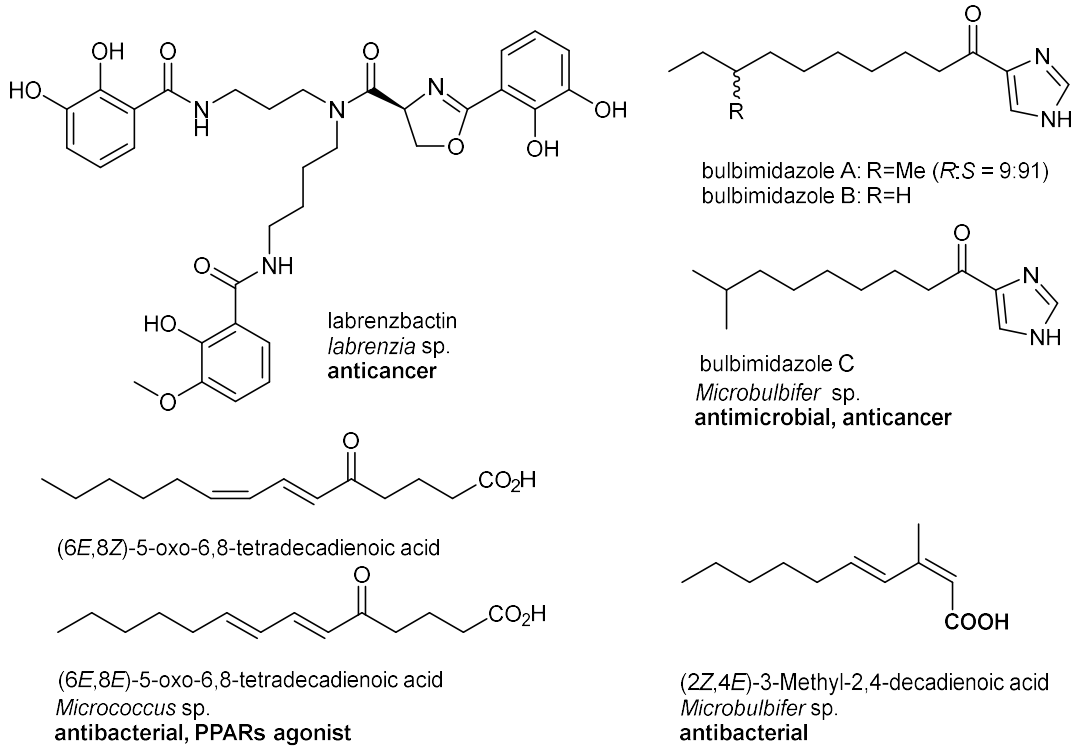

Figure 2-1. Chemical structure of labrenzbactin, bulbimidazoles A–C, (6*E*,8*Z*)/ (6*E*,8*E*)-5-oxo-6,8-tetradecadienoic acids and (2*Z*,4*E*)-3-methyl-2,4-decadienoic acid.

In addition, a few natural products were reported from stony corals. The reason may be that researchers suspect that stony corals rarely produce biologically active metabolites as a chemical defense, because its exoskeleton is made of calcium

carbonate, which is used to study the secondary metabolites of microorganisms isolated from stony corals. However, in our laboratory we continue to investigate stony coral-derived microorganisms as an unexplored source, and some new biologically active compounds have been discovered one after another, including labrenzbactin [13], an unsaturated fatty acid [14], two new keto fatty acids [15], and bulbimidazoles A–C [16] from stony coral-associated microorganisms, *Labrenzia, Microbulbifer,* and *Micrococcus* (Figure 2-1).

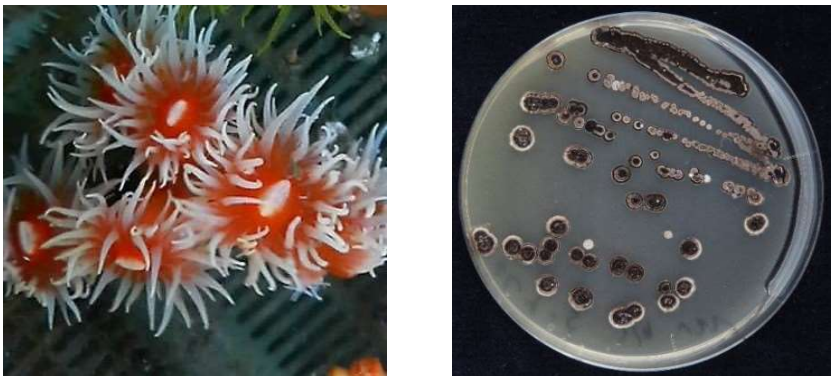

Figure 2-2. Stony coral *Dendrophyllia* (left) and *Streptomyces* sp. DC4-5 on Bn-2 agar (right).

Following the successful experiences of new compounds discovered in microorganisms derived from stony corals, *Streptomyces* strain DC4-5 isolated from a stony coral *Dendrophyllia* was found to produce three new polyhydroxy macrolides, iseolides A (**1**), B (**2**), and C (**3**), which are efficacious against the fungus *G. cingulate* NBRC5907. Herein, I describe the isolation, structure determination, and biological activity of compounds **1**–**3** (Figure 2-3).

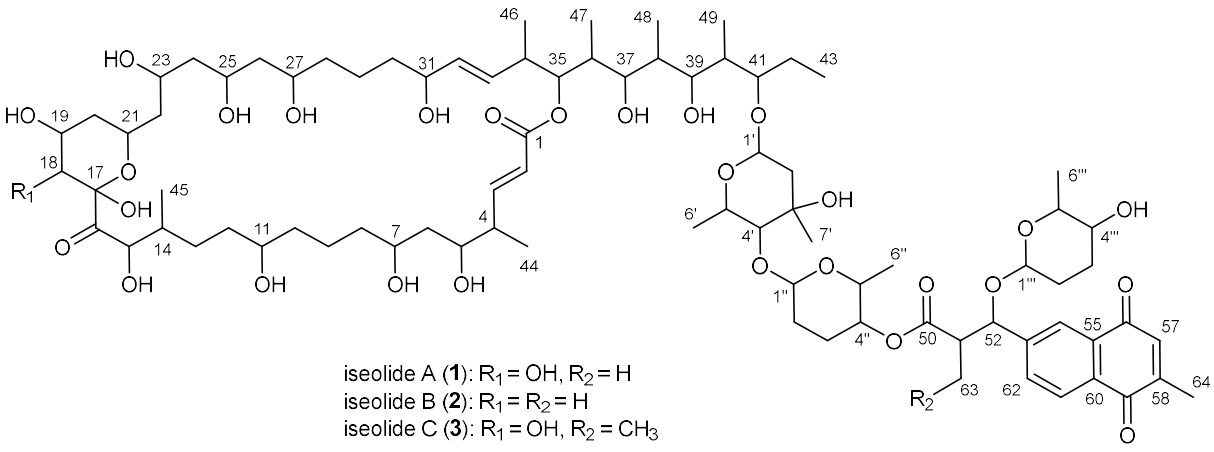

Figure 2-3. Structures of iseolides A–C (**1**–**3**).

2-2 Results and discussion

2-2-1 Fermentation and isolation

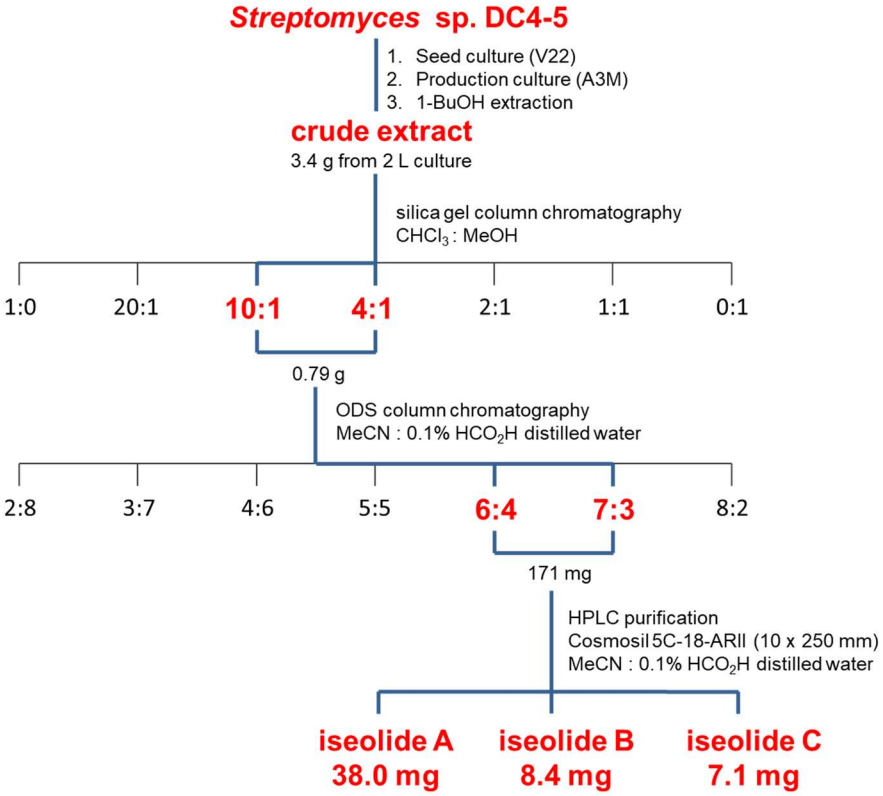

Scheme 2-1. Isolation of iseolides (**1**–**3**).

The producing strain *Streptomyces* sp. DC4-5 was isolated from a scleractinia coral of the genus *Dendrophyllia* collected near the coast of Mie prefecture, Japan. Strain DC4-5 was cultured in A3M medium, and the whole culture broth was extracted with 1-butanol. The extract was consecutively subjected to silica gel and ODS column chromatography, and the final purification was achieved by reversed-phase HPLC to yield iseolides A (**1**, 38.0 mg), B (**2**, 8.4 mg), and C (**3**, 7.1 mg).

2-2-2 Structure determination

Iseolide A (**1**) was obtained as pale yellow amorphous solid. The molecular formulae was determined to be $C_{83}H_{132}O_{29}$ on the basis of HR-ESITOFMS that gave sodium adduct ions $[M + Na]^+$ at *m*/*z* 1615.8744 (calcd for $C_{83}H_{132}O_{29}Na$, 1615.8746). The IR spectra of indicated the presence of hydroxy (3386 cm^{-1}) and carbonyl (1729 cm^{-1}) functional groups.

The structure of **1** was determined by extensive analysis of one- and two-dimensional NMR (COSY, TOCSY, ROESY, HSQC, HMBC) spectroscopic data. While the ^{1}H NMR spectrum displayed heavily overlapped signals around 1.2 to 1.6 ppm, ^{13}C NMR spectrum together with HSQC spectrum allowed to assign 83 signals including 13 methyl, 20 methylene, 39 methine, and 11 non-protonated carbons (Table 2-1). COSY correlation data identified 14 fragments, **A** to **N**, as shown in Figure 2-4. Linkage between fragments **A** and **B** was deduced from the HMBC correlations from H6 to C8, H7 to C9, and H8 to C7. HMBC correlations from H11 and H12 to C13 established the connectivity between fragments **B** and **C**. Further connectivity from C15 to fragment **D** was suggested by the HMBC correlations from H15 and H18 to a carbonyl carbon C16 (δ_C 208.8) and from H18 to a deshielded sp^3 carbon C17 (δ_C 99.8). Similarly, connectivities among the fragment pairs, **D**/**E**, **E**/**F**, and **F**/**G**, were established by HMBC correlations illustrated in Figure 2-4.

Finally, an HMBC correlation from H35 to C1 (δ_C 168.9) established the ester linkage between C1 and C35, thereby completing the macrolactone structure of **1**. Structural similarity of this 36-membered macrolide skeleton to a known macrolide PM100117 [17], as well as the deshielded chemical shift δ_C 99.8 of C17, implied the six-membered hemiacetal ring cyclized by the ether bond between C17 and C21, however HMBC or ROESY/NOESY correlations that could support this linkage were not detected. In order to distinguish ether-bonding oxymethines from free hydroxy oxymethines, ^{13}C NMR spectrum was taken in CD_3OH and compared with the chemical shifts obtained in CD_3OD. The overlaid ^{13}C NMR spectra are shown in Figure 2-5, displaying the chemical shift change for eleven oxymethine carbons (C5, C7, C11, C15, C18, C19, C23, C25, C27, and C31) caused by exchange of alcoholic proton with deuteron while no change for two oxymethines C21 and C35. The ether-bonding of C21 oxygen to C17 and the hemiacetal structure were thus established.

The presence of three deoxysugars **S1**, **S2**, and **S3** were evident from the ^{1}H and ^{13}C NMR resonances for H1′ (δ_H 5.03) and C1′ (δ_C 96.6), H1″ (δ_H 4.96) and C1″ (δ_C 101.1), H1‴ (δ_H 4.98) and C1‴ (δ_C 101.3), corresponding to the anomeric protons and carbons. COSY-defined fragments **H**/**I**, **J**, and **K** were assigned to constitute deoxysugars, **S1**, **S2**, and **S3**, respectively, on the basis of HMBC analysis (Figure 2-4). Deoxysugar **S1** was connected at C41 of the macrolide part by an HMBC correlation from H1′ to C41. Deoxysugar **S2** was next connected to C4′ of **S1** by the correlation

from H1″ to C4′. As for deoxysugar **S3**, an HMBC correlation from a methine H52 to C1‴ indicated its connectivity to fragment **L** which was expanded to include a carbonyl carbon C50 (δ_C 175.8) by HMBC correlations from H51, H52, and H63 to this carbon. C50 was also correlated with H4″, whereby the ester linkage of deoxysugar **S2** to fragment **L** was established. A set of HMBC correlations from an olefinic methine H54 to the sp^2 carbons C56, C60, and C62 and an sp^3 methine C52, together with the correlations from H57, H61, and H64 to the sp^2 carbons present in two-bond or three-bond distance, established the naphthoquinone moiety containing fragments **M** and **N**. The geometries of the two double bonds of the macrolide moiety were assigned both to *E* by the large coupling constants of $J_{H2,H3}$ = 15.8 Hz. whereas that for C32–C33 double bond could not be determined due to the signal overlapping of H32 and H33. However, the (*E*)-configuration was suggested for the C32–C33 double bond because the carbon chemical shifts for C31, C32, C33, and C34 of **1** were closely similar to those of PM100117 [17] and astolides, another member of this class of macrolides [18], both of which were shown to possess *E*-double bond at the same position.

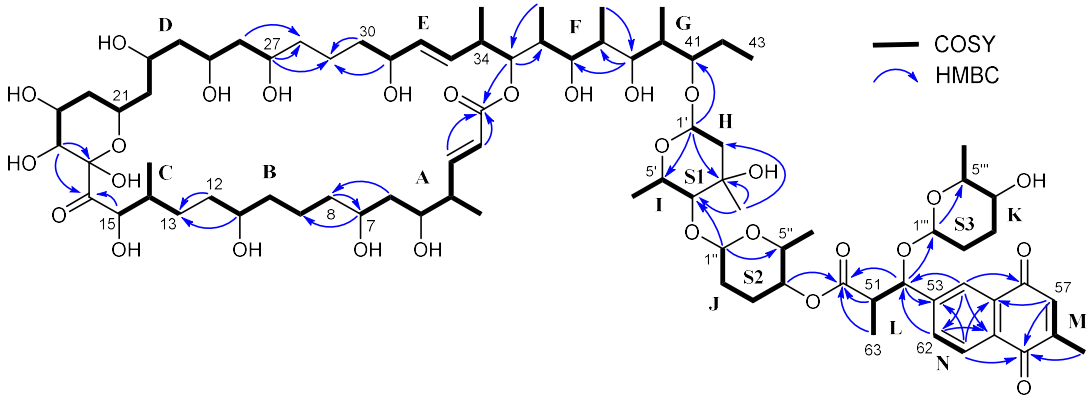

Figure 2-4. COSY and key HMBC correlations for **1**.

Table 2-1. ^{1}H and ^{13}C NMR data for iseolide A (**1**) in CD_3OD.

No.	δ_H,mult (*J* in Hz)[a]	δ_C[b]	HMBC[a,c]	no.	δ_H,mult (*J* in Hz)[a]	δ_C[b]	HMBC[a,c]
1		168.9		43	0.99, t (7.2)	11.6	41, 42
2	5.86, d (15.8)	122.3	1, 4	44	1.09, d (6.9)	14.2	3, 4, 5
3	7.05, dd (7.1, 15.8)	153.7	1, 2, 4, 5, 44	45	0.82, d (6.9)	14.0	13, 14, 15
4	2.46, m	43.7	2, 3, 5, 6, 44	46	1.03, d (5.9)	17.5	33, 34, 35
5	3.78, m	74.3	3, 4, 44	47	0.90[d]	9.9	35, 36, 37
6	1.54, m; 1.61, m	41.9	8	48	0.90[d]	5.0	37, 38, 39
7	3.37, m	71.3	9	49	0.79, d (7.2)	10.8	39, 40, 41
8	1.35-1.56, m	38.8		1′	5.03, brd (3.6)	96.6	3′, 5′, 41
9	1.40, m	22.9		2′	1.61, m; 1.97, m	38.3	1′, 4′, 7′
10	1.35-1.56, m	38.8		3′		71.5	
11	3.53, m	72.8	10, 13	4′	3.28, brs	83.8	1”, 2′, 5′, 7′
12	1.43, m; 1.56, m	36.4	13	5′	4.49, d (6.5)	65.3	1’, 4′, 6′
13	1.27, m; 1.64, m	31.6		6′	1.20, d (6.6)	17.8	4′, 5′
14	2.2, m	36.8	13, 45	7′	1.29, s	27.5	2′, 3′, 4′
15	4.61, d (3.4)	75.7	13, 14, 16	1″	4.96, d (2.3)	101.1	2″, 5″, 4′
16		208.8		2″	1.75, m; 1.93, m	25.3	
17		99.8		3″	1.76, m; 2.14, m	24.0	
18	3.51, m	75.5	16, 17, 19, 20	4″	4.92, m	71.3	3″, 50
19	3.88, m	69.8	18, 20	5″	4.24, m	67.6	1″, 4″, 6″
20	1.43, m; 1.98, m	41.1	18, 19	6″	1.12, d (6.6)	17.6	4″, 5″
21	4.23, m	67.5	19	1‴	4.98, d (2.2)	101.3	2‴, 3‴, 5‴, 52
22	1.50-1.66, m	45.9	20, 21, 23	2‴	1.49, m; 1.92, m	24.6	
23	4.01, m	65.8	22	3‴	1.62, m; 1.93, m	26.8	1‴
24	1.50-1.66, m	46.3	26	4‴	3.33, m	67.6	
25	4.03, m	68.5	23, 24	5‴	3.18, q (6.7)	68.4	1‴, 3‴, 4‴, 6‴
26	1.50-1.66, m	45.1	28	6‴	0.47, d (6.6)	16.9	4‴, 5‴
27	3.79, m	71.8	29	50		175.8	
28	1.35-1.66, m	38.5		51	2.99, dt (9.8, 7.3)	49.6	50
29	1.50, m	22.8		52	4.80, d (9.8)	84.1	50, 51, 53, 54, 62, 63, 1‴
30	1.35-1.56, m	38.5	29	53		148.7	
31	3.95, m	72.7	29, 32, 33	54	8.04, s	126.1	52, 56, 60, 62
32	5.51, m	135.4	31, 33, 34	55		133.6	
33	5.50, m	133.3	32, 34, 46	56		186.3	
34	2.54, m	40.6	32	57	6.90, s	136.7	55, 59, 64
35	5.14, dbr (9.4)	77.6	1, 33, 34, 36, 47	58		150.1	
36	1.96, m	39.0		59		186.4	
37	3.39, dbr (9.4)	78.8	35, 38, 39, 47, 48	60		133.1	
38	1.82, m	36.2		61	8.10, d (7.9)	127.8	53, 55, 59

39	3.52, m	79.6	37, 38, 41, 48, 49	62	7.85, d (7.9)	134.1	52, 54, 60
40	2.00, m	38.8		63	0.92[d]	14.7	50, 51, 52
41	3.88, m	80.8	39, 40	64	2.18, s	16.5	57, 58, 59
42	1.41, m; 1.62, m	23.0					

[a] Recorded at 500 MHz
[b] Recorded at 125 MHz
[c] Proton showing HMBC correlation to indicated carbon
[d] Coupling constant could not be determined due to signal overlapping

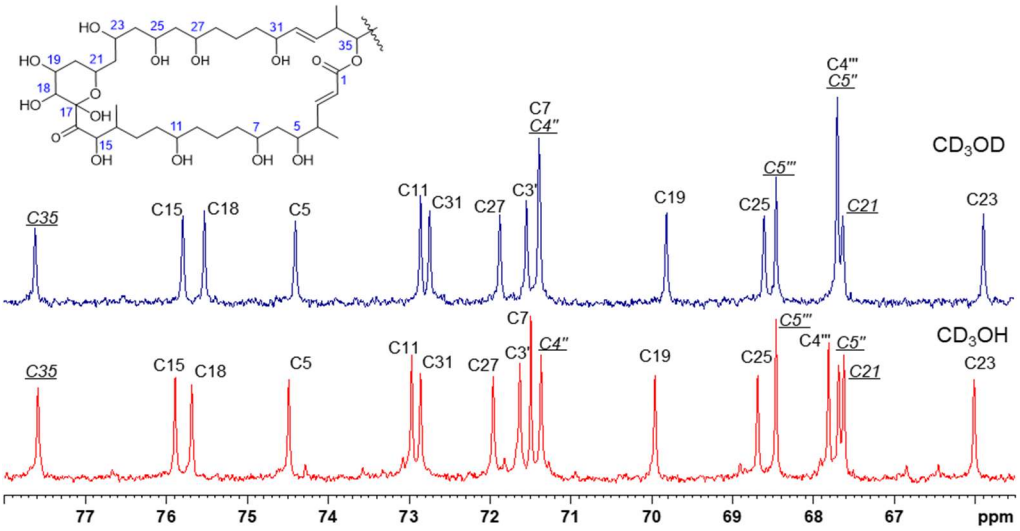

Figure 2-5. Partial ^{13}C NMR spectra of **1** for the oxymethine region measured in CD_3OD (blue) and CD_3OH (red). Carbons of which chemical shifts are unchanged in two solvents are indicated with underline.

The small coupling constant between H1′ and H2′ (J = 3.6 Hz) of deoxysugar **S1** suggested the equatorial orientation of the anomeric proton and thereby the α-glycosidic bonding to the aglycon. ROESY correlations for H5′/H41, H4′/H7′, H6′/H1″, and H7′/H5″ suggested the equatorial positioning of the two methyl groups in **S1**, and thus α-axenose was established for **S1**. Deoxysugar **S2** was assigned to α-rhodinose by the following observations.

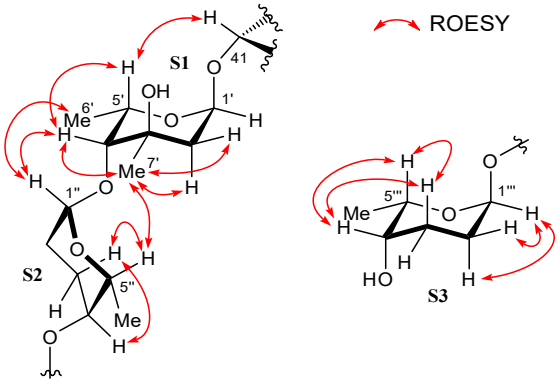

Figure 2-6. Relative configuration of deoxysugars in **1**.

The anomeric proton H1″ showed a small coupling constant $J_{1'',2''}$ = 2.3 Hz, a typical value for α-glycosides. ROESY correlations were detected between H3″ax and H5″ and between H3″ax and H4″, which suggested the axial orientation of H5‴ and the equatorial orientation of H4″. Similarly, deoxysugar **S3** was determined to be α-rhodinose. First, the small coupling constant $J_{1''',2'''}$ = 2.2 Hz and ROESY correlations between H1‴ and both axial and equatorial H2‴ protons indicated the α-glycosidic linkage. Second, ROESY correlation for H3‴/H5‴ supported axial orientation of these protons, and also ROESY correlations for H4‴/H3‴ax and H4‴/ H5‴ established the equatorial orientation of H4‴ (Figure 2-6). Additionally, the relative configuration of C51 and C52 was speculated to be *anti* on the basis of the coupling constant $J_{H51,H52}$ = 9.8 Hz which was close to the *J* value for the same proton pairs in PM100117 (10 Hz) [17] and that in caniferolide A (8.3 Hz) [19].

Iseolides B–C (**2**–**3**) were obtained as pale yellow amorphous solid. The molecular formulae of **2** and **3** were determined to be $C_{83}H_{132}O_{28}$, and $C_{84}H_{134}O_{29}$ on the basis of HR-ESITOFMS that gave sodium adduct ions $[M + Na]^+$ at *m*/*z* 1599.8798 (calcd for $C_{83}H_{132}O_{28}Na$, 1599.8797) and *m*/*z* 1629.8904 (calcd for $C_{84}H_{134}O_{29}Na$, 1629.8903), respectively. The IR spectra of iseolides indicated the presence of hydroxy (3390–3350 cm^{-1}) and carbonyl (1730–1725 cm^{-1}) functional groups. Comparison of ^1H and ^{13}C NMR spectra of **1** with the other two congeners, **2** and **3**, showed extensive similarities and the presence of a common macrocyclic aglycon and the equivalent decoration units in **2** and **3** (Table S1). The only notable difference between **1** and **2** was found in the macrolide moiety. C18 oxymethine in **1** was replaced by a methylene (δ_H 1.34, 2.09; δ_C 41.3) in **2**. H18 methylene protons were correlated with H17 methine and were long-range coupled with C16, C17, C19, and C20. Additional evidence for this structure was shown by MS/MS fragmentation analysis, which gave a 16 amu smaller fragment corresponding to the aglycon part of **2** (Figure 2-7). Two-dimensional NMR analysis of **3** revealed that the methyl group at C51 of **1** was replaced by an ethyl group in **3**. A triplet methyl H65 (δ_H 0.83) was COSY-correlated with H63 methylene and long-range correlated with C63 and C51. This structural difference proven by NMR analysis was consistent with 14 amu larger molecular mass of **3** and the MS/MS analytical data which indicated a 14 amu increment in the naphthoquinone moiety esterified with **S2** (Figure 2-7).

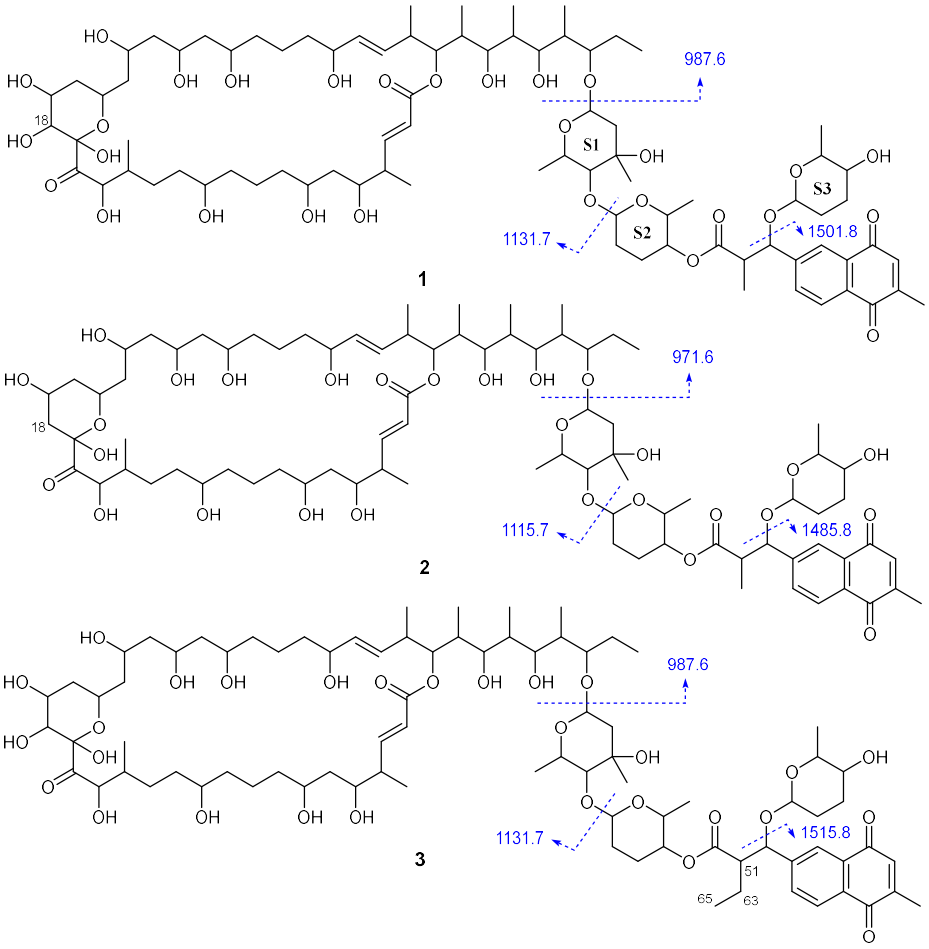

Figure 2-7. MS/MS fragmentation of **1**–**3**. The numbers indicate *m*/*z* values of sodium adduct ions observed in the positive mode.

2-2-3 Bioactivity

Iseolides A (**1**), B (**2**), and C (**3**) showed potent antifungal activity against *Glomerella cingulata* NBRC5907, a causative agent of anthracnose disease, with MIC of 0.19–0.78 μg/ml. They were also active against human pathogens *Candida albicans* NBRC0197 and *Trichophyton rubrum* NBRC5467 with MIC values in the range of 0.39 to 6.25 μg/ml (Table 2-2). Among the three congeners, **1** was most potently antifungal. Compounds **1**, **2**, and **3** were not active against *Micrococcus luteus* ATCC9341, *Staphylococcus aureus* FDA209P JC-1, and *Rhizobium radiobacter* NBRC14554, but weakly active against *Ralstonia solanacearum* SUPP1541, a causative bacterium of wilt disease of plants, with MIC of 25, 100, and 50 μg/ml, respectively. Additionally, compounds **1**, **2**, and **3** exhibited moderate cytotoxicity against P388 murine leukemia cells with IC_{50} of 0.55, 1.1, and 0.85 μM, respectively.

Table 2-2. Antimicrobial activity of compounds **1**–**3**.

	MIC (μg/mL)		
Microorganisms	**1**	**2**	**3**
Kocuria rhizophila ATCC9341	＞100	＞100	＞100
Staphylococcus aureus FDA209P JC-1	＞100	＞100	＞100
Rhizobium radiobacter NBRC14554	＞100	＞100	＞100
Ralstonia solanacearum SUPP1541	25	100	50
Candida albicans NBRC0197	0.39	6.25	3.16
Glomerella cingulata NBRC5907	0.19	0.78	0.78
Trichophyton rubrum NBRC5467	0.78	1.56	3.16

2-3 Conclusion

In summary, screening of anti-anthracnose substances from marine actinomycetes resulted in the discovery of three new macrolides, iseolides A–C (**1**–**3**). Iseolides are the new members of PM10017-class polyketides comprising the 36-membered macrocyclic aglycon, an alkylnaphthoquinone, and deoxysugars. To date, PM100117 and PM100118 [17], astolides [18], GT35 [20], deplelides [21], and caniferolides [19] are known within this class (Figure 2-8). Their cytotoxic and antifungal activities are described but effectiveness against *Glomerella cingulate* had not been known. Actinomycetes associated with scleractinian (stony) corals are a neglected source of new bioactive compounds. This study provides an additional support to the idea that microorganisms residing in underexplored sources still can offer new bioactive compounds.

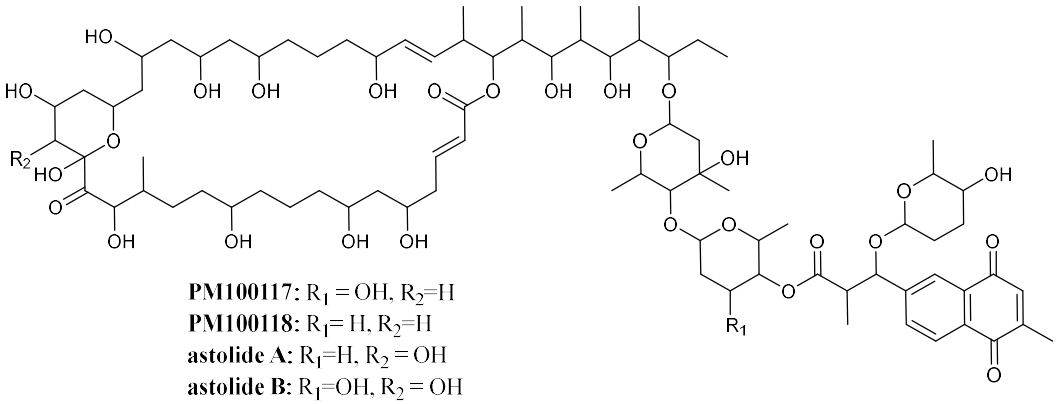

PM100117: R_1 = OH, R_2=H
PM100118: R_1= H, R_2=H
astolide A: R_1=H, R_2 = OH
astolide B: R_1=OH, R_2 = OH

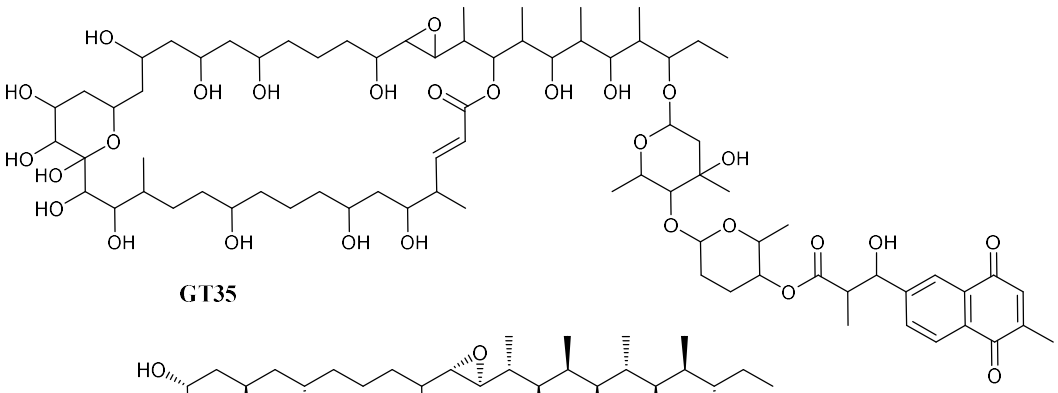

GT35

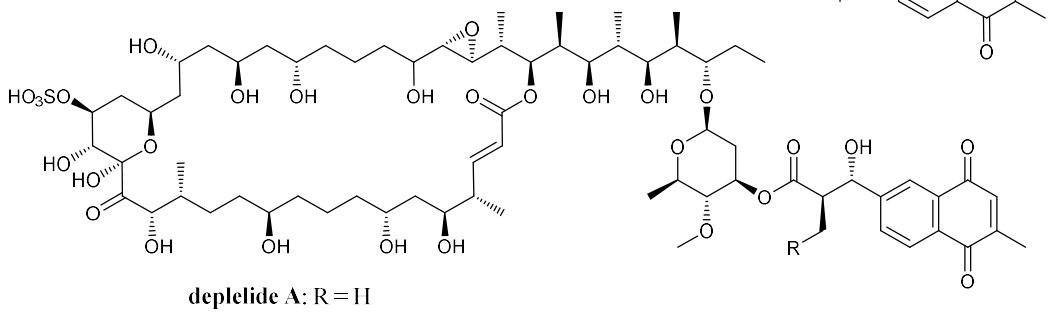

deplelide A: R = H
deplelide B: R = OH

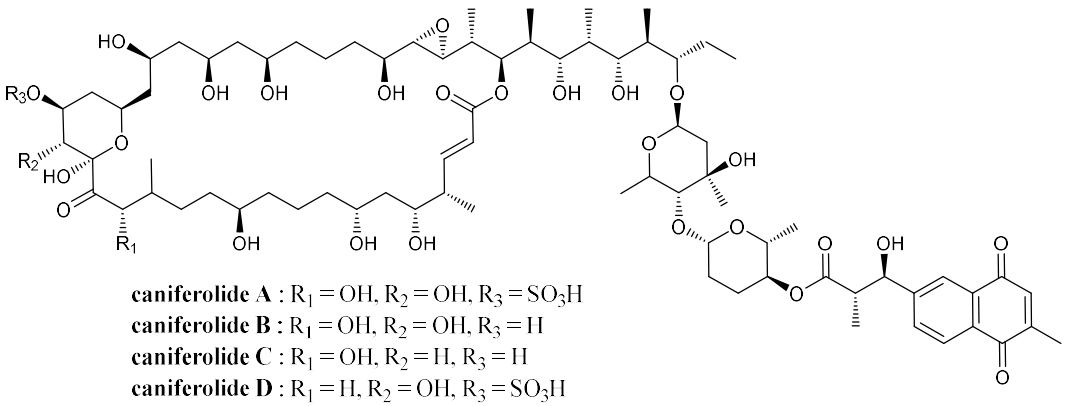

caniferolide A : R_1 = OH, R_2 = OH, R_3 = SO_3H
caniferolide B : R_1 = OH, R_2 = OH, R_3 = H
caniferolide C : R_1 = OH, R_2 = H, R_3 = H
caniferolide D : R_1 = H, R_2 = OH, R_3 = SO_3H

Figure 2-8. Structures of macrolides related to iseolides.

2-4 Experimental section

2-4-1 General experimental procedures

Optical rotations were measured using a JASCO P-1030 polarimeter. The UV spectra and IR spectra were recorded on a Shimadzu UV-1800 spectrophotometer and a PerkinElmer Spectrum 100, respectively. NMR spectra were obtained on a Bruker AVANCE 500 spectrometer in CD_3OD. The residual solvent signals (δ 3.31 for ^{1}H and 49.2 for ^{13}C) were used as internal references. MS/MS and HR-ESITOFMS were recorded on a Bruker microTOF focus mass spectrometer.

2-4-2 Microorganism

A scleractinian coral, *Dendrophyllia* sp., was collected at -20~25 m in depth near the coast of Minami-Ise, Mie prefecture, Japan, as fishery waste and was obtained through a local aquarium vendor in Mie prefecture, Japan. The coral specimen was washed with 70% ethanol and then washed with sterile natural seawater. A piece of the coral (*ca* 1 g) was homogenized by mortar and pestle with equal amount of sterile natural seawater (1 mL), and the suspension was spread on an ISP 4 agar medium (Difco). After cultivation at 23 °C for 14 days, a single colony was transferred onto ISP 2 agar medium to obtain the pure isolate of strain DC4-5. The isolated strain DC4-5 was identified as a member of genus *Streptomyces* on the basis of 99.2% similarity in the 16S rRNA gene sequence (1428 nucleotides; DDBJ accession number LC476780) to *Streptomyces kronopolitis* NEAU-ML8^{T} (accession number KP050495).

2-4-3 Fermentation

The producing strain DC4-5 was maintained on Bn-2 agar medium consisting of soluble starch 0.5%, glucose 0.5%, meat extract (Kyokuto Pharmaceutical Industrial Co., Ltd.) 0.1%, yeast extract (Difco Laboratories) 0.1%, NZ-case (Wako Chemicals USA, Inc.) 0.2%, NaCl 0.2%, $CaCO_3$ 0.1%, and agar 1.5%. Strain DC4-5 was inoculated into a 500 mL K-1 flask containing 100 mL of V-22 seed medium consisting of soluble starch 1%, glucose 0.5%, NZ-case 0.3%, yeast extract 0.2%, Tryptone (Difco Laboratories) 0.5%, K_2HPO_4 0.1%, $MgSO_4 \cdot 7H_2O$ 0.05%, and $CaCO_3$ 0.3% (pH 7.0) in distilled water. The flask was cultivated on a rotary shaker (200 rpm) at 30 °C for 4 days. The seed culture (3 mL) was transferred into twenty 500 mL K-1 flasks each containing 100 mL of A3M production medium consisting of glucose 0.5%, glycerol

2%, soluble starch 2%, Pharmamedia (Traders Protein, Memphis, TN, USA) 1.5%, yeast extract 0.3%, and Diaion HP-20 (Mitsubishi Chemical, Kanagawa, Japan) 1% in distilled water. The pH of the medium was adjusted to 7.0 before sterilization. The inoculated flasks were placed on a rotary shaker (200 rpm) at 30 ˚C for 7 days.

2-4-4 Extraction and isolation

At the end of the fermentation period, 100 mL of 1-butanol was added to each flask, and they were agitated on a rotary shaker for 1 h. The mixture was centrifuged at 6,000 rpm for 10 min, and the organic layer was separated from the aqueous layer with the mycelium. Evaporation of the solvent gave 3.44 g of crude extract from 2 L of culture. The crude extract was subjected to silica gel column chromatography with a step gradient of $CHCl_3$/MeOH (1:0, 20:1, 10:1, 4:1, 2:1, 1:1, and 0:1 v/v). Fraction 4 (4:1) was concentrated to provide 0.79 g of brown oil, which was further fractionated by reversed-phase ODS column chromatography with a gradient of MeCN/0.1% HCO_2H (2:8, 3:7, 4:6, 5:5, 6:4, 7:3, and 8:2 v/v). Fractions 5 and 6 (6:4 and 7:3) were concentrated to provide 171 mg of dried material containing the target compounds. The final purification was achieved by preparative HPLC (Cosmosil 5C-18-ARII, 10 x 250 mm, 4 mL/min, UV detection at 254 nm) with a mixture of MeCN and 0.1% HCO_2H solution (49:51) to yield iseolides A (**1**, 38 mg, t_R 22.6 min), B (**2**, 8.4 mg, t_R 24.1 min), and C (**3**, 7.1 mg, t_R 27.5 min).

Iseolide A (**1**): brown amorphous solid; $[\alpha]^{23}_D$ -11 (*c* 0.10, MeOH); UV (MeOH) λ_{max} (log ε) 198 (4.61), 204 (4.51), 247 (5.20) and 332 (3.30) nm; IR (ATR) ν_{max} 3386, 2935, 1665, 1115, 1081, 997 cm^{-1}; For ^1H and ^{13}C NMR data, see Table 2-1; HR-ESITOFMS $[M + Na]^+$ 1615.8744 (calcd for $C_{83}H_{133}O_{29}Na$, 1615.8746).

Iseolide B (**2**): brown amorphous solid; $[\alpha]^{23}_D$ -6.1 (*c* 0.10, MeOH), UV (MeOH) λ_{max} (log ε) 196 (4.27), 204 (4.44), 221 (4.21), 267 (3.53) and 331 (2.63) nm; IR (ATR) ν_{max} 3347, 2933, 1665, 1115, 1061, 976 cm^{-1}; For ^1H and ^{13}C NMR data, see Table S1; HR-ESITOFMS $[M + Na]^+$ 1599.8798 (calcd for $C_{83}H_{133}O_{28}Na$, 1599.8797).

Iseolide C (**3**): brown amorphous solid; $[\alpha]^{23}_D$ -11 (*c* 0.10, MeOH), UV (MeOH) λ_{max} (log ε) 196 (4.26), 203 (4.37), 248 (4.06), 323 (3.23) nm; IR (ATR) ν_{max} 3383, 2934, 1666, 1115, 1000, 977 cm^{-1}; For ^1H and ^{13}C NMR data, see Table S1; HR-ESITOFMS $[M + Na]^+$ 1629.8904 (calcd for $C_{84}H_{134}O_{29}Na$, 1629.8903).

2-4-5 Antimicrobial assay

Antimicrobial activity was evaluated by the liquid microculture method using round-bottom 96-well microtiter plates against six bacteria, *Bacillus subtilis* ATCC6633, *Micrococcus luteus* ATCC9341, *Staphylococcus aureus* FDA209P JC-1, *Ralstonia solanacearum* SUPP1541, *Rhizobium radiobacter* NBRC14554, and *Escherichia coli* NIHJ JC-2, and three fungus such as, *Candida albicans* NBRC0197, *Glomerella cingulata* NBRC5907, and *Trichophyton rubrum* NBRC5467 as indication strains. Tryptic Soy Broth (DIFCO Laboratories) and Potato Dextrose Broth (DIFCO Laboratories) were used for bacteria and fungus, respectively. Iseolides A, B and C and reference drugs, kanamycin sulfate for bacteria and amphotericin B for fungi were made in 2-fold dilution series along the longer side of the plates by sequential transfer of 100-μL aliquots between the adjacent wells, to which the same amount of medium was pre-dispensed. To each well was added a 100 μL suspension of the indication strains prepared at ~10^6 cfu/mL from a culture at the logarithmic growth phase. The solvent vehicle added to the top rows was set at the 0.5% of the final culture volume to avoid the effect on the growth of microbes. The plates were incubated for 48 h at 37 °C for bacteria and at 32 °C for fungi. The tests were done in triplicate and the MIC values were read from the lowest drug concentrations at which no growth was observed.

2-4-6 Cytotoxicity assay

P388 murine leukemia cells were maintained in RPMI-1640 medium containing phenol red, L-glutamine, and HEPES (product no. 189-02145) supplemented with 10% fetal bovine serum and 0.1 mg/mL gentamicin sulfate. Iseolides A, B and C and doxorubicin as a reference were serially diluted by a factor of 3.16 (half-logarithmic dilution) in a 96-well round bottom microtiter plate. To each well were seeded the cells at a final density of 1 x 10^4 cells/mL, and 200-μL cultures thus made were incubated for 48 h at 37 °C in an atmosphere of 5% CO_2 in air with 100% humidity. Viability of the cells was visualized by MTT, added to each well as a 50 μL solution in phosphate-buffered saline without Ca^{2+} prepared at 1 mg/mL. After incubating for 4 h at 37 °C, medium was carefully removed by a suction aspirator, and formazan dye formed by respiratory reduction by living cells was solubilized by 100 μL of DMSO. The absorption at 540 nm was read by a microplate reader to calculate the rate of cell growth inhibition at each concentration, and the results of triplicate experiments were plotted

on single-logarithmic charts to deduce IC_{50} values.

References

1) Berdy, J. *J. Antibiot*. **2005**, *58*, 1-26.
2) Yi, M. Q.; Lin, S. X.; Zhang, B.; Jin, H. X.; Ding, L. *J. Eur. J. Med. Chem*. **2020**, *207*, 112790.
3) Schinke, C.; Martins, T.; Queiroz, S. C. N. Melo, I. S.; Reyes, F. G. R. *J. Nat. Prod.* **2017**, *80*, 1215−1228.
4) Ameen, F.; Alnadhari, S.; Al-Homaidan, A. A. *Saudi J. Biol. Sci.* **2021**, *28*, 224–231.
5) Valliappan, K.; Sun, W.; Li, Z. Y.; *Appl. Microbiol. Biotechnol.* **2014**, *98*, 7365–7377.
6) Manivasagan, P.; Venkatesan, J.; Sivakumar, K.; Kim, S. K. *Microbiol. Res*. **2014**, *169*, 262-278.
7) Abdelmohsen, U. R.; Bayer, K.; Hentschel, U. *Nat. Prod. Rep*. **2014,** *31,* 381-399.
8) Frias-Lopez, J.; Zerkle, A. L.; Bonheyo, G. T.; Fouke, B. W. *Appl. Environ. Microbiol.* **2002**, *68*, 2214–2228.
9) Leal, M. C.; Calado, R.; Sheridan, C.; Alimonti, A.; Osinga, R. *Trends. Biotechnol.* **2013,** *31*, 555-561.
10) Fu, P.; Kong, F.; Wang, Y. F.; Wang, Y. *Chin. J. Chem.* **2013**, *31*, 100-104.
11) Nong, X. H.; Zhang, X. Y.; Xu, X. Y.; Wang, J.; Qi, S. H. *J. Nat. Prod.* **2016**, *79*, 141-148.
12) Nong, X. H.; Wei, X. Y.; Qi, S. H. *J. Antibiot.* **2017**, *70*, 1047–1052.
13) Sharma A. R.; Zhou T.; Harunari E.; Oku N.; Trianto A.; Igarashi Y. *J. Antibiot.* **2019**, *72*, 634-639.
14) Sharma, A. R.; Harunari, E.; Zhou, T.; Trianto, A.; Igarashi, Y. *Beilstein J. Org. Chem.* **2019**, *15*, 2327–2332.
15) Sharma, A. R.; Harunari, E.; Oku, N.; Matsuura, N.; Trianto, A.; Igarashi, Y. *Beilstein J. Org. Chem.* **2020**, *16*, 297–304.
16) Karim, M. R. U.; Harunari, E.; Oku, N.; Akasaka, K.; Igarashi, Y. *J. Nat. Prod.* **2020,** *83*, 1295−1299.
17) Pérez, M.; Schleissner, C.; Fernández, R.; Rodríguez, P.; Reyes, F.; Zuñiga, P.; et al. *J. Antibiot.* **2016**, *69*, 388-394.
18) Alferova. V. A.; Novikov, R. A.; Bychkova, O. P.; Rogozhin, E. A.; Shuvalov, M. V.; Prokhorenko, I. A. et al. *Tetrahedron* **2018**, *74*, 7442-7449.
19) érez-Victoria, I.; Oves-Costales, D.; Lacret, R.; Martín, J.; Sanchez-Hidalgo, M.; Díaz-Navarro, C. et al. *Org. Biomol. Chem.* **2019**, *17*, 2954–2971.
20) Takahashi, I.; Nishiie, Y.; Uosaki, Y.; Ochiai, K. New substance GT35 and its production. Jpn. Kokai Tokkyo Koho. 1995: JPH09100290A.
21) Takeuchi, T.; Hatano, M.; Umekita, M.; Hayashi, C.; Wada, S.; Nagayoshi, M.; et al. *Org. Lett.* **2017**, 19, 4207−4210.

2-5 Spectral data

Table of contents

Figure S1. UV spectrum of iseolide A (**1**).

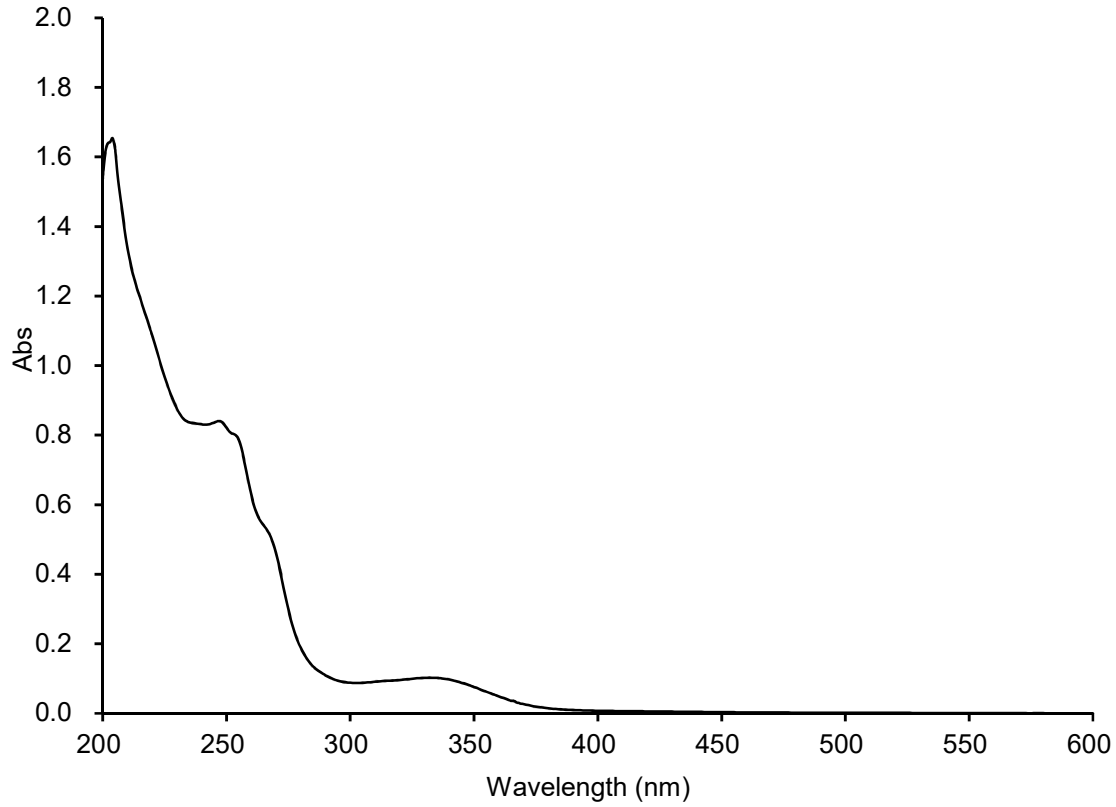

Figure S2. IR spectrum of **1.**

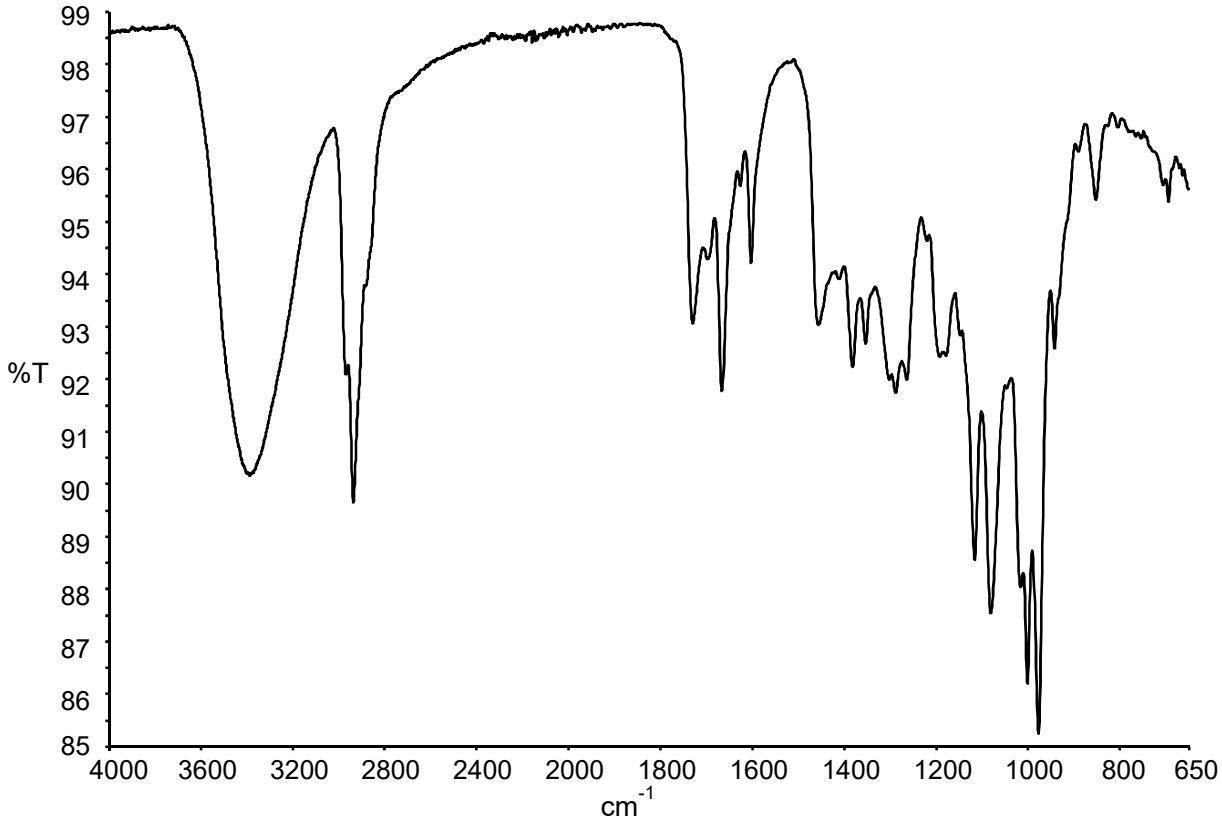

Figure S3. ^{1}H NMR spectrum of **1** (500 MHz, CD_3OD).

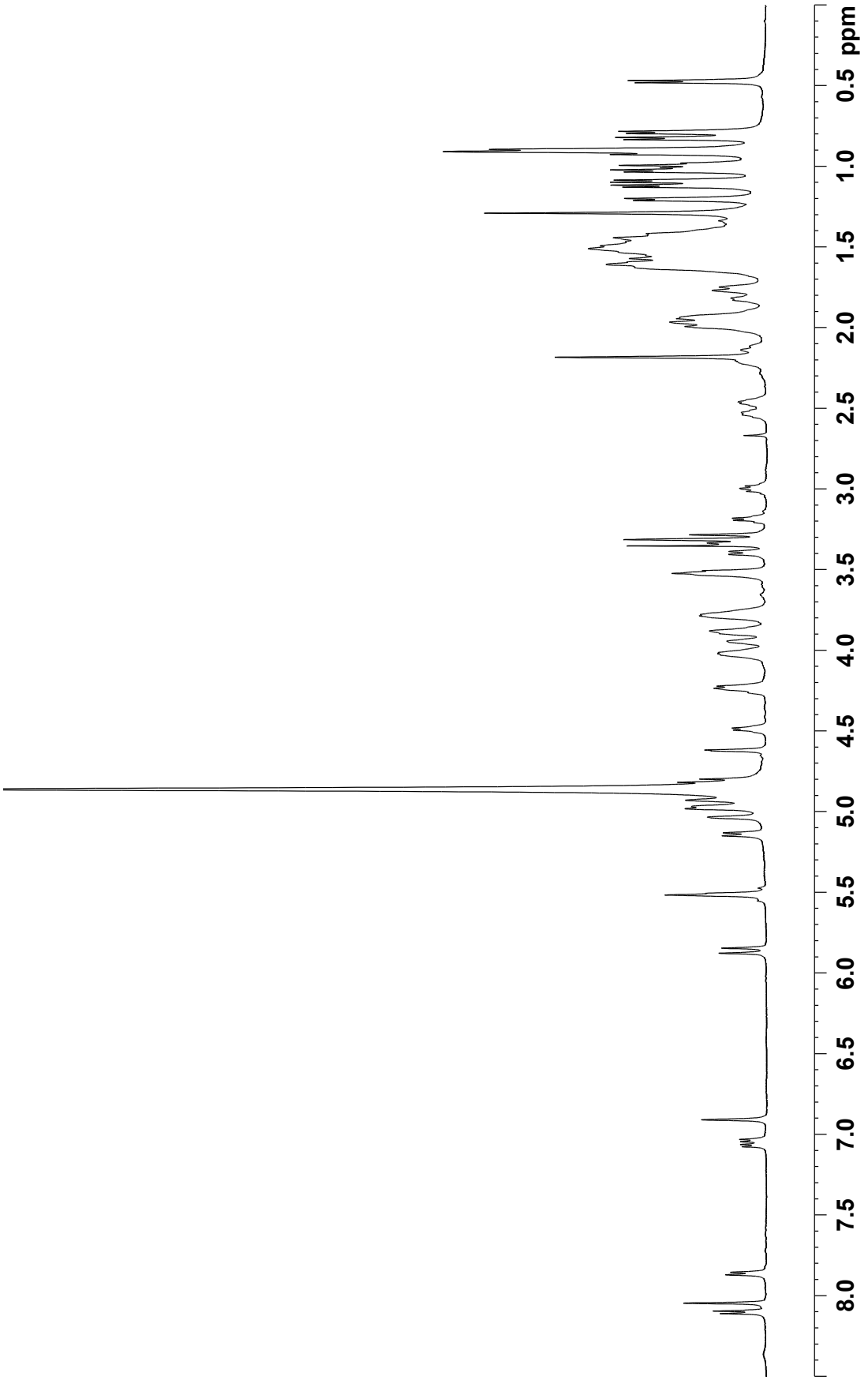

Figure S4. ^{13}C NMR spectrum of **1** (125 MHz, CD_3OD).

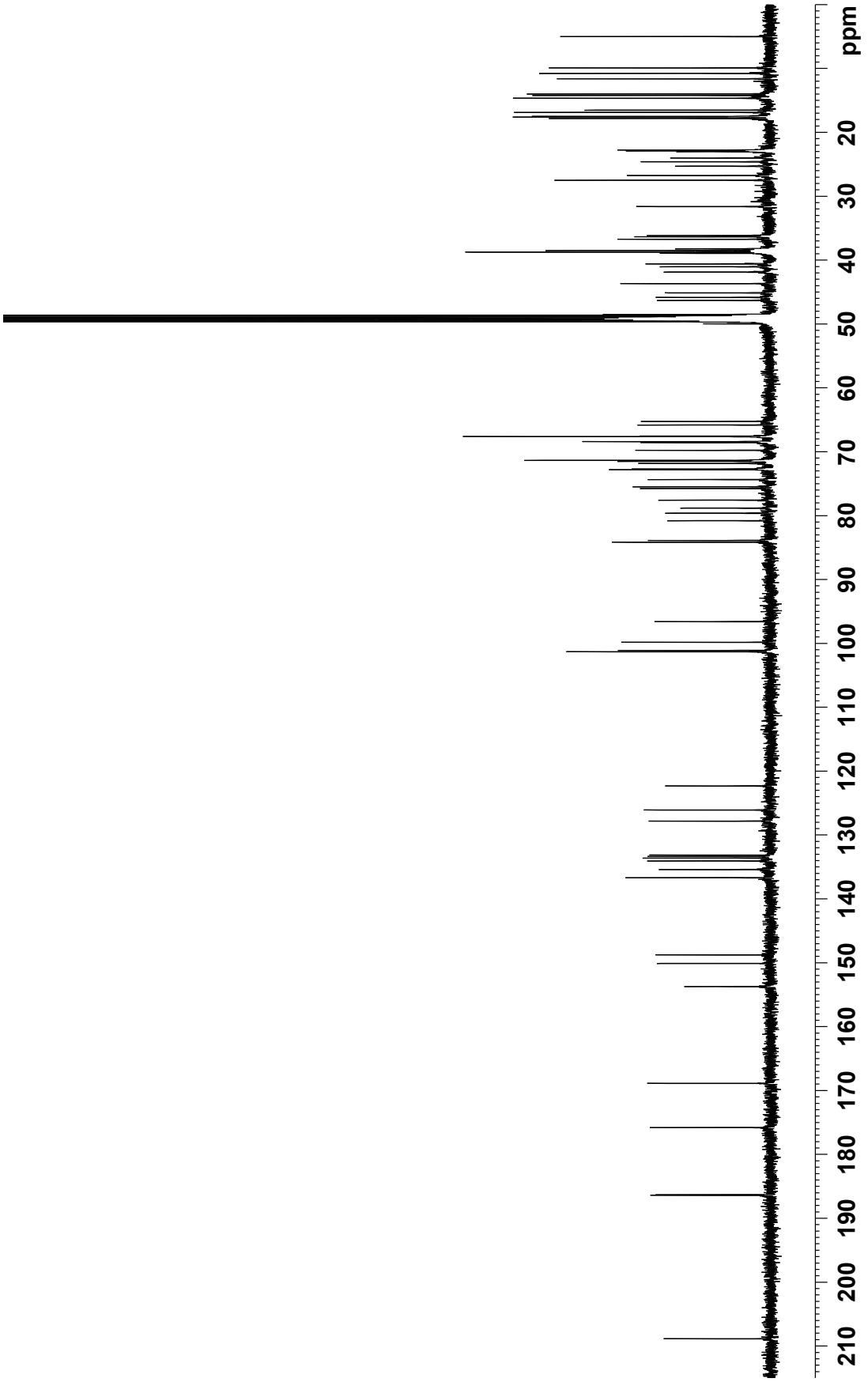

Figure S5. COSY spectrum of **1** (500 MHz, CD_3OD).

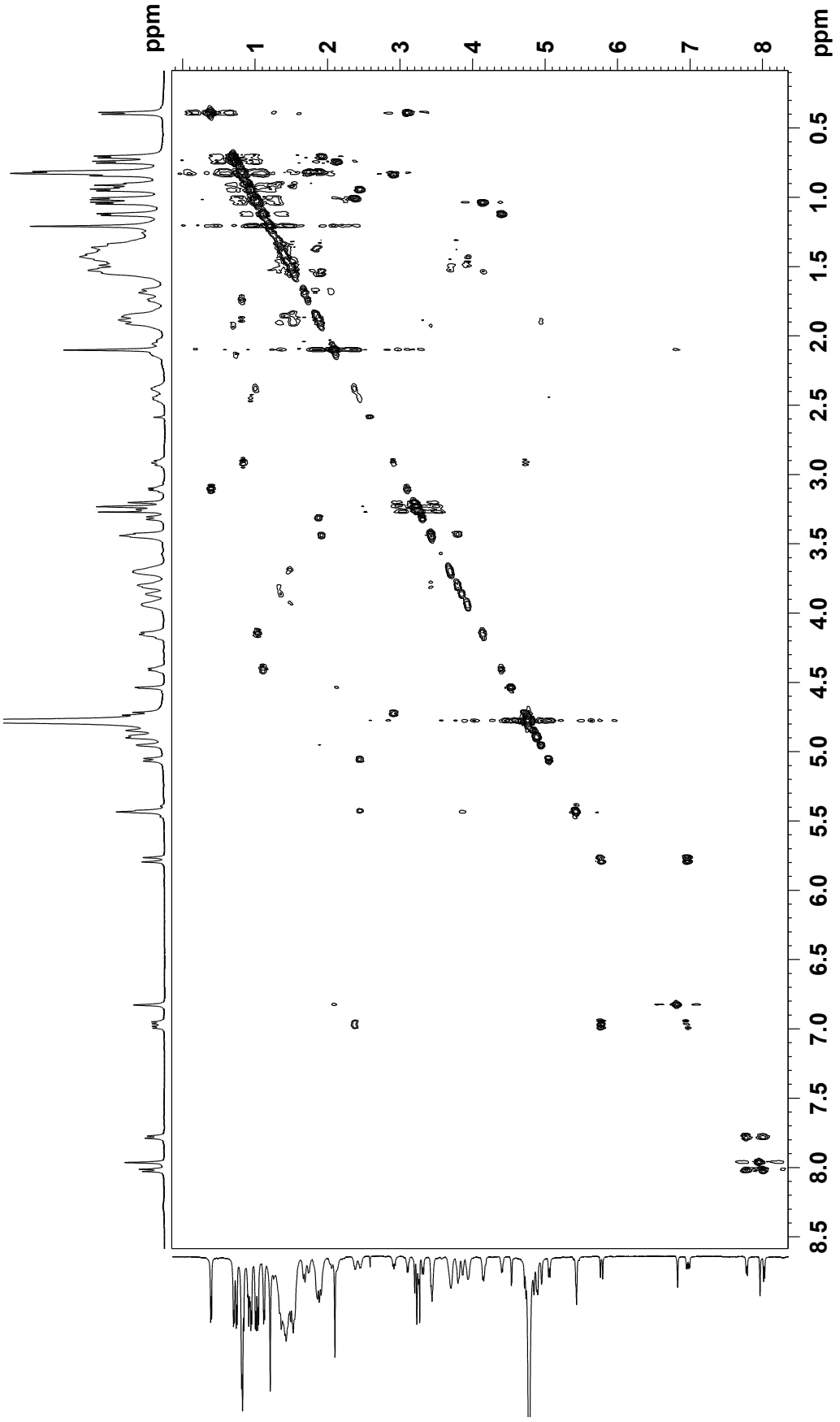

Figure S6. TOCSY spectrum of **1** (500 MHz, CD_3OD).

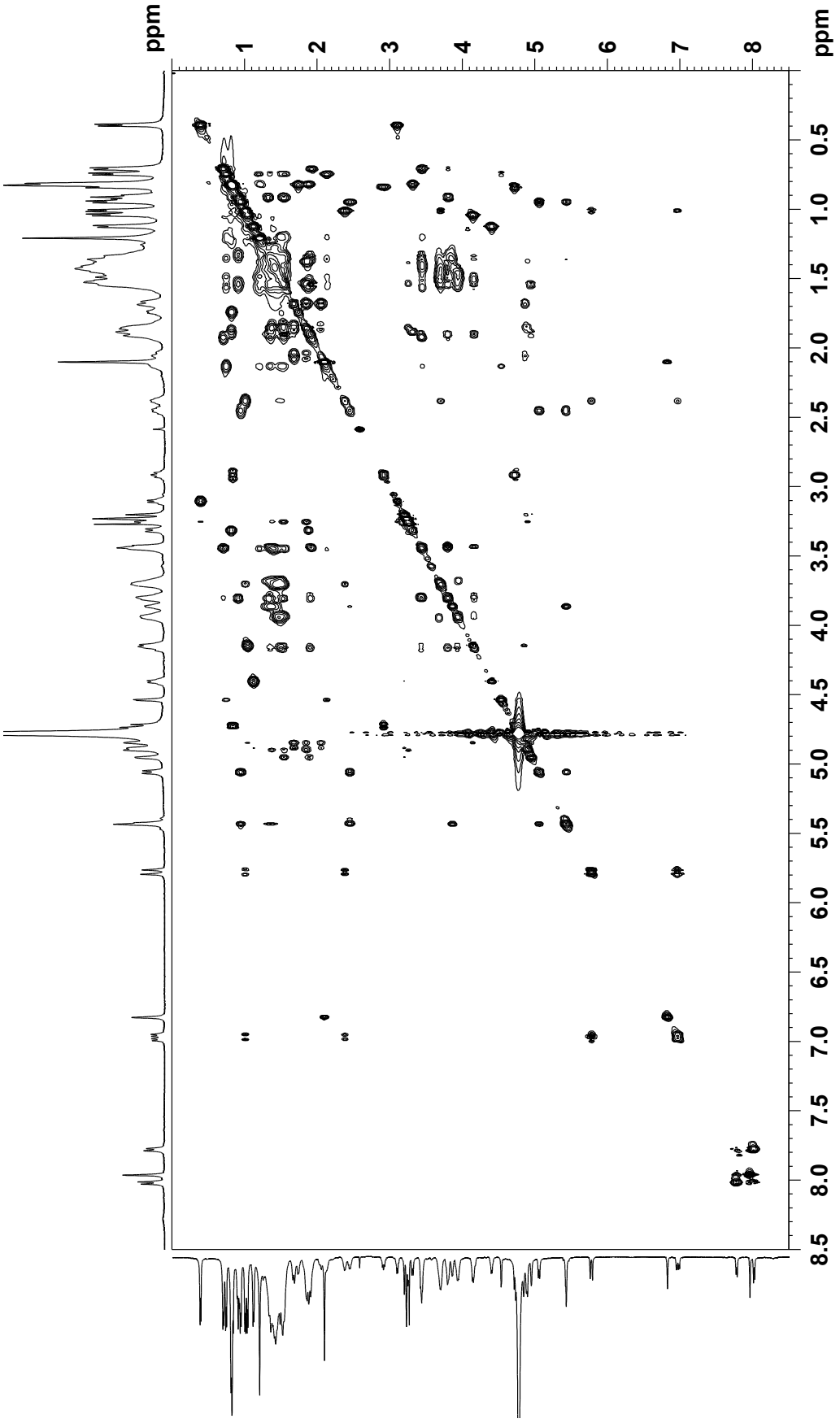

Figure S7. HSQC spectrum of **1** (500 MHz, CD_3OD).

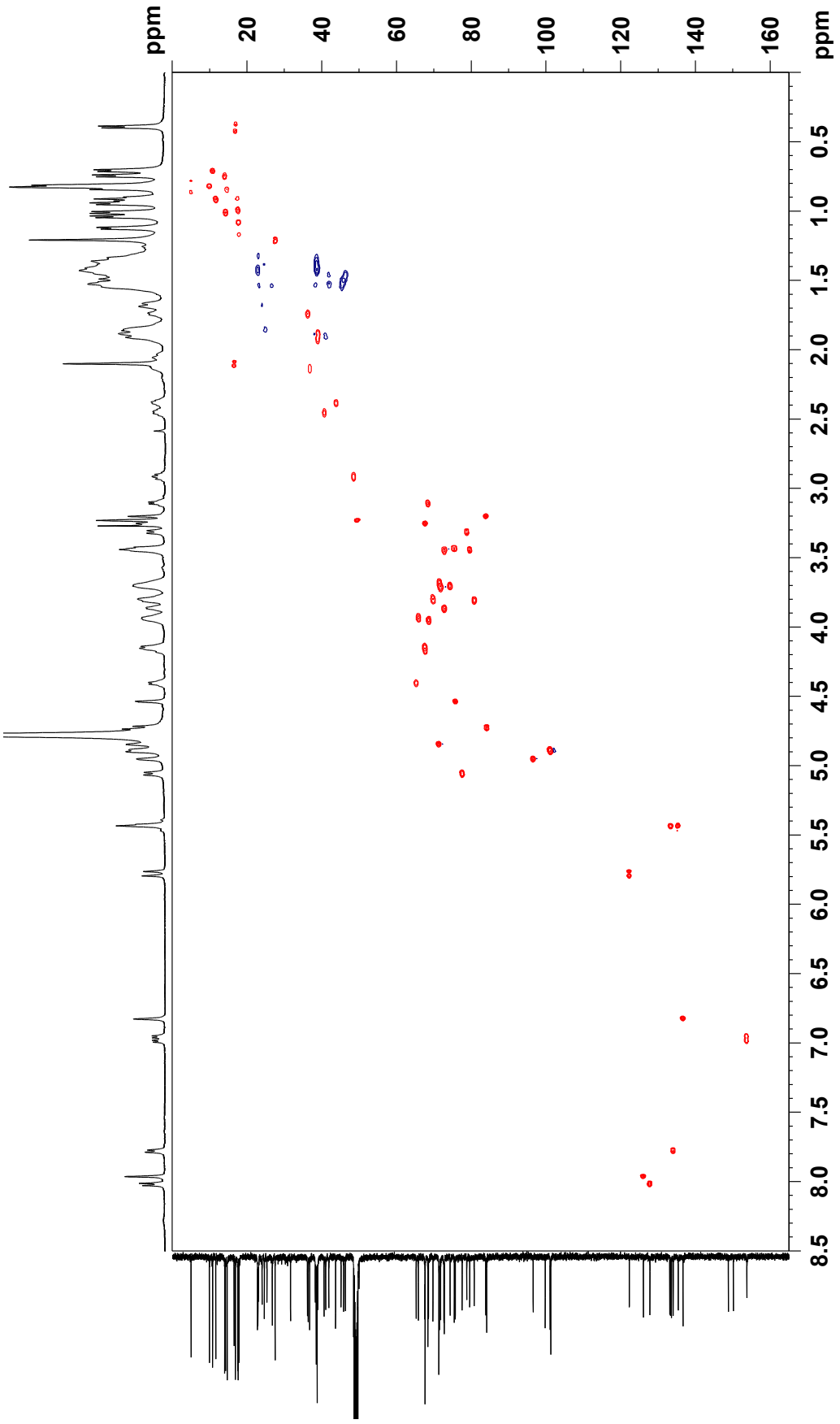

Figure S8. HMBC spectrum of **1** (500 MHz, CD_3OD).

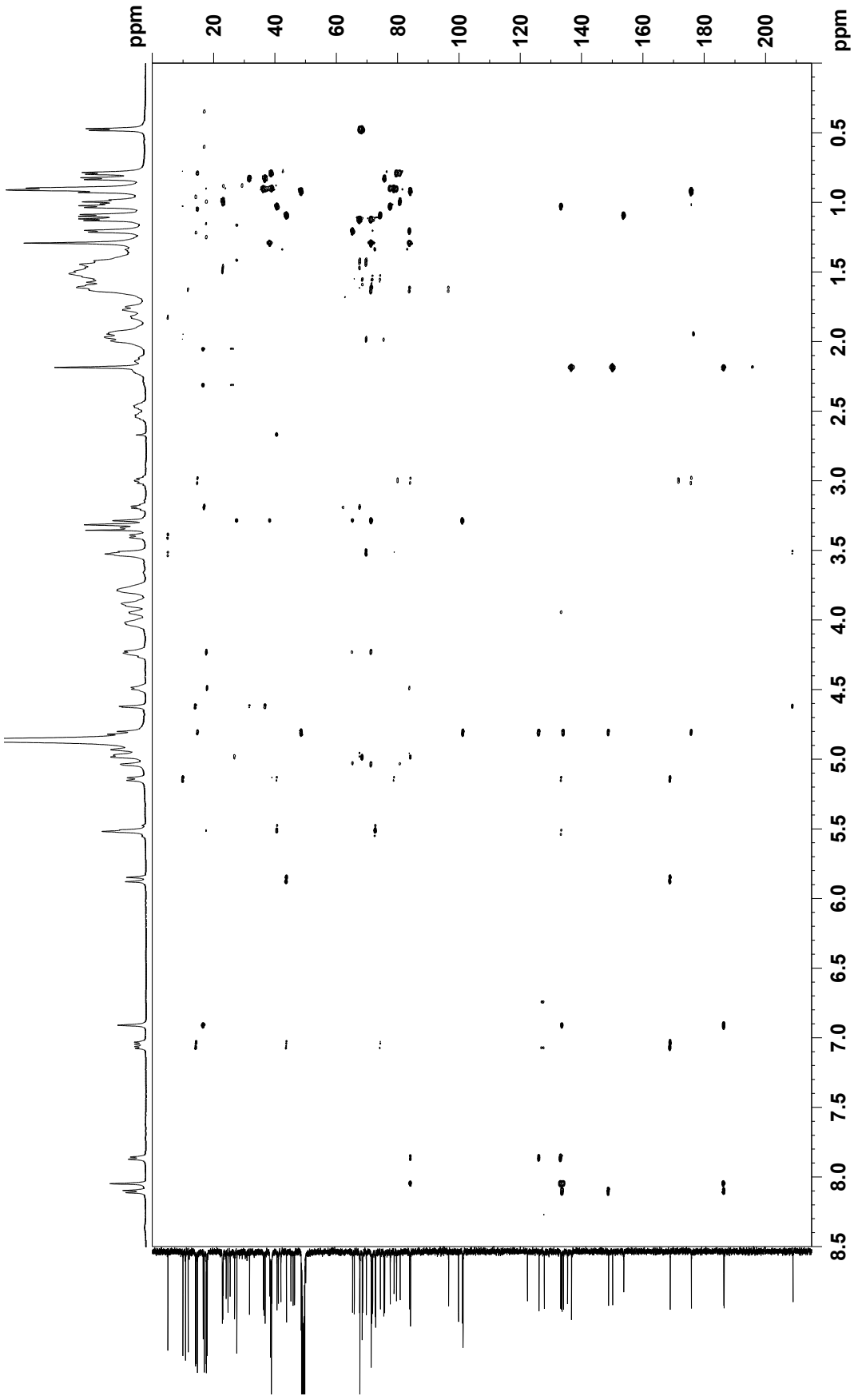

Figure S9. ROESY spectrum of **1** (500 MHz, CD_3OD).

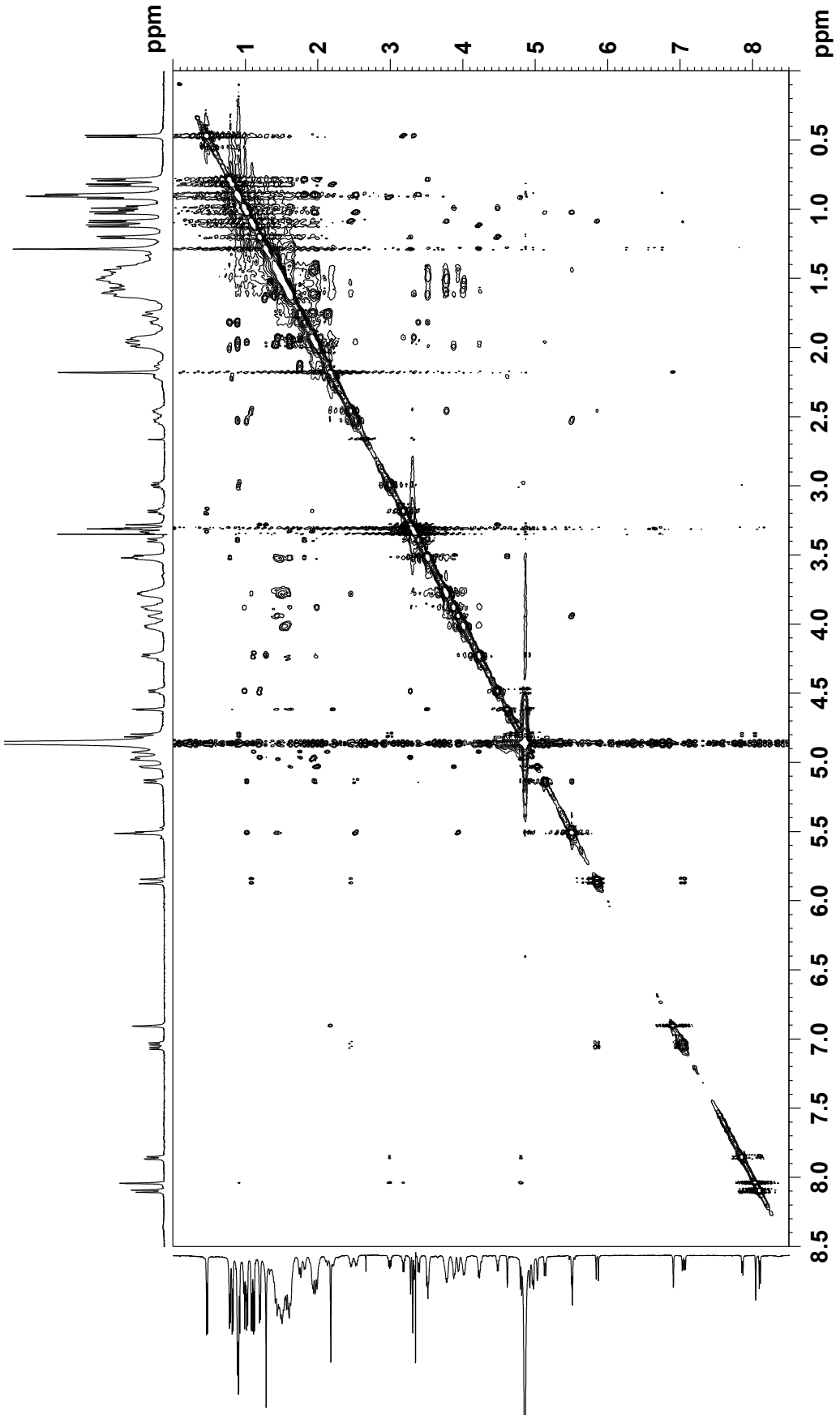

Figure S10. UV spectrum of iseolide B (**2**).

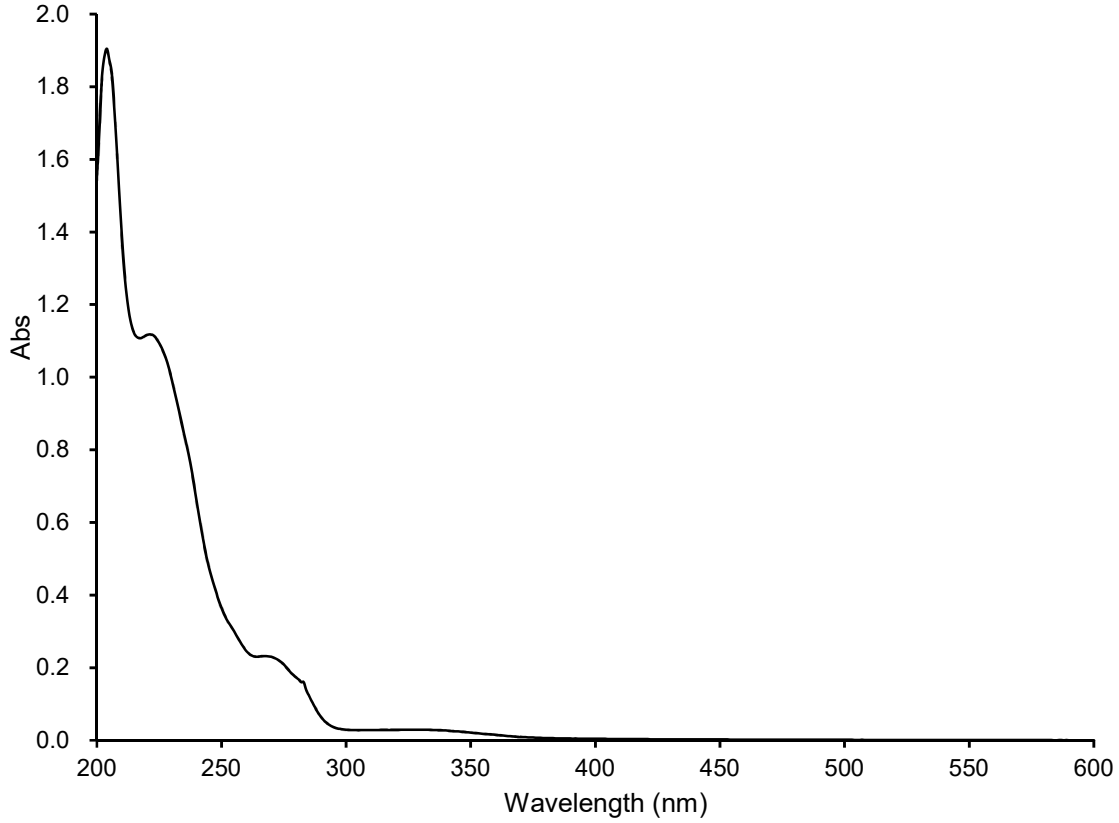

Figure S11. IR spectrum of **2**.

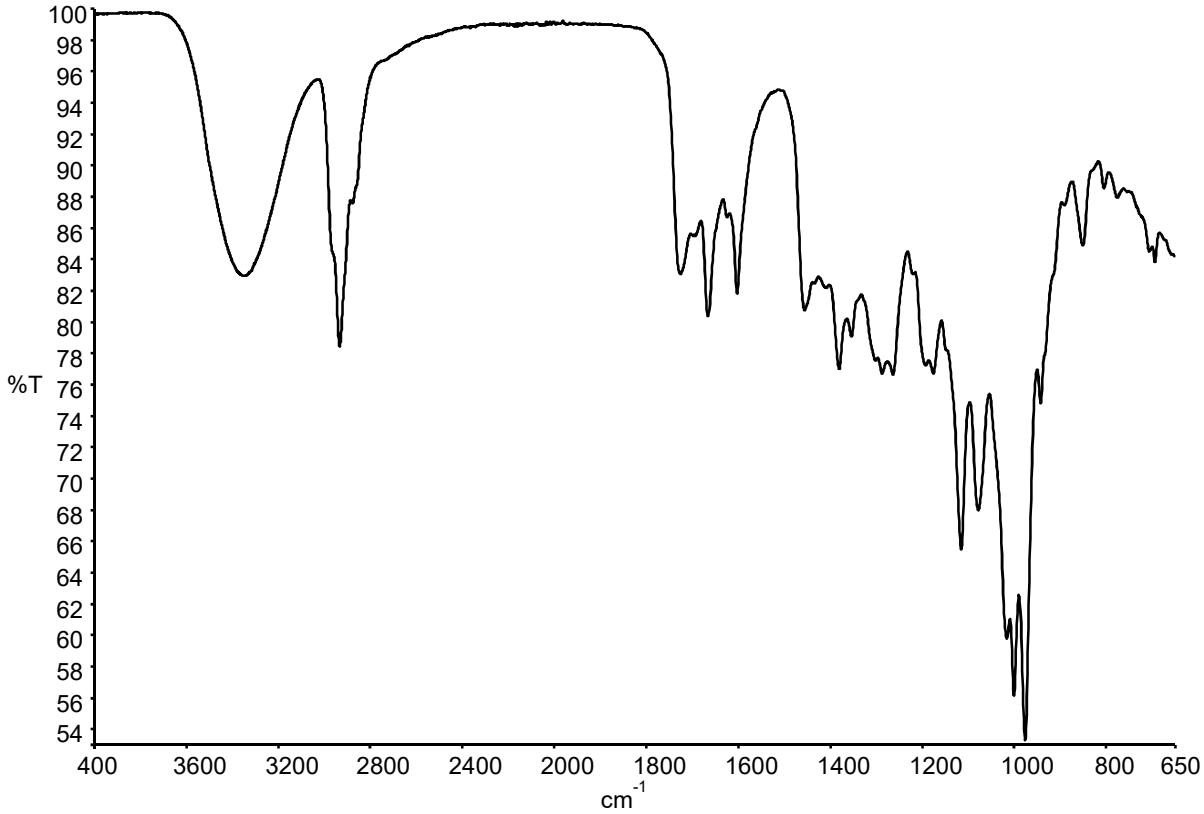

Figure S12. ^{1}H NMR spectrum of **2** (500 MHz, CD_3OD).

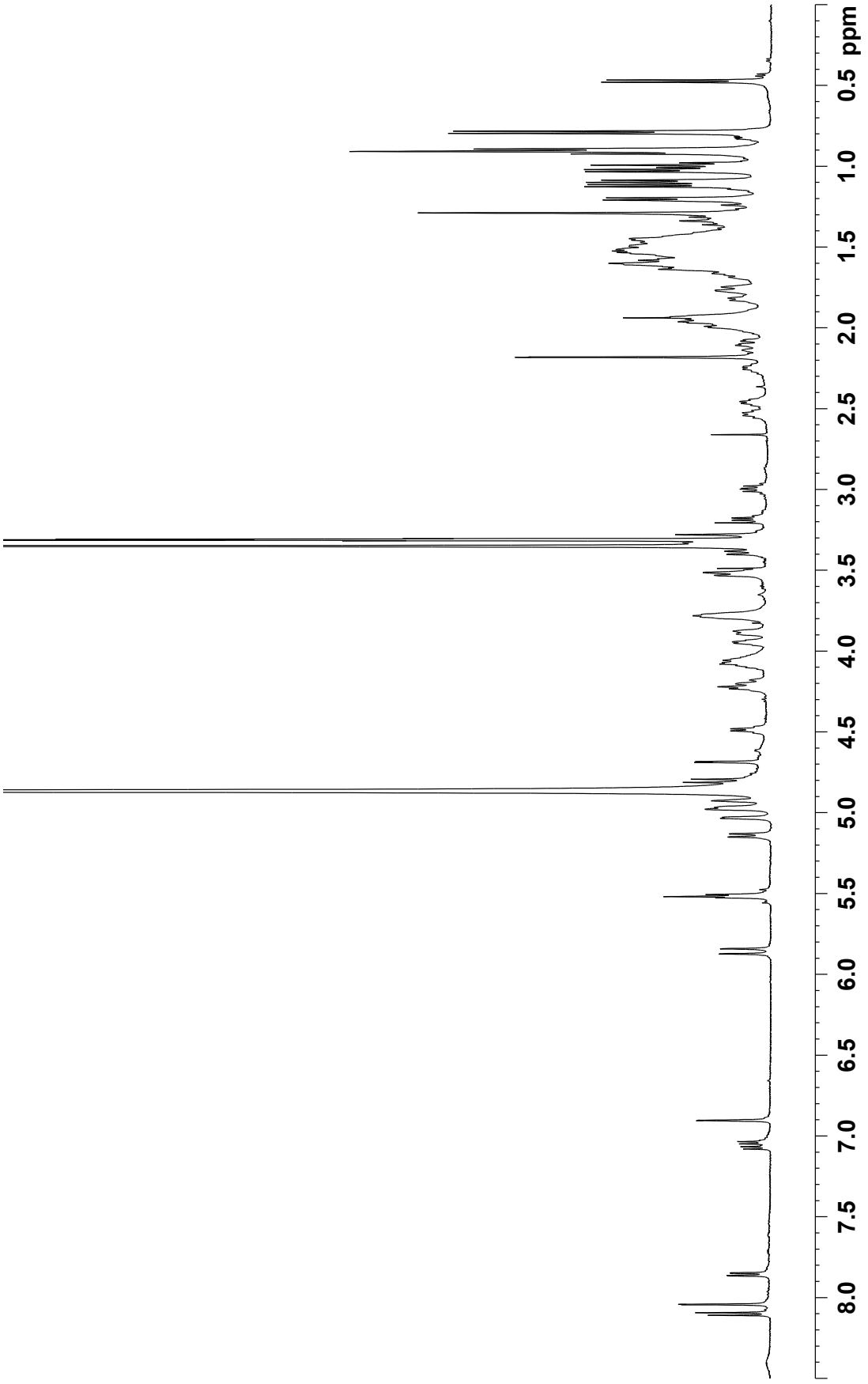

Figure S13. ^{13}C NMR spectrum of **2** (125 MHz, CD_3OD).

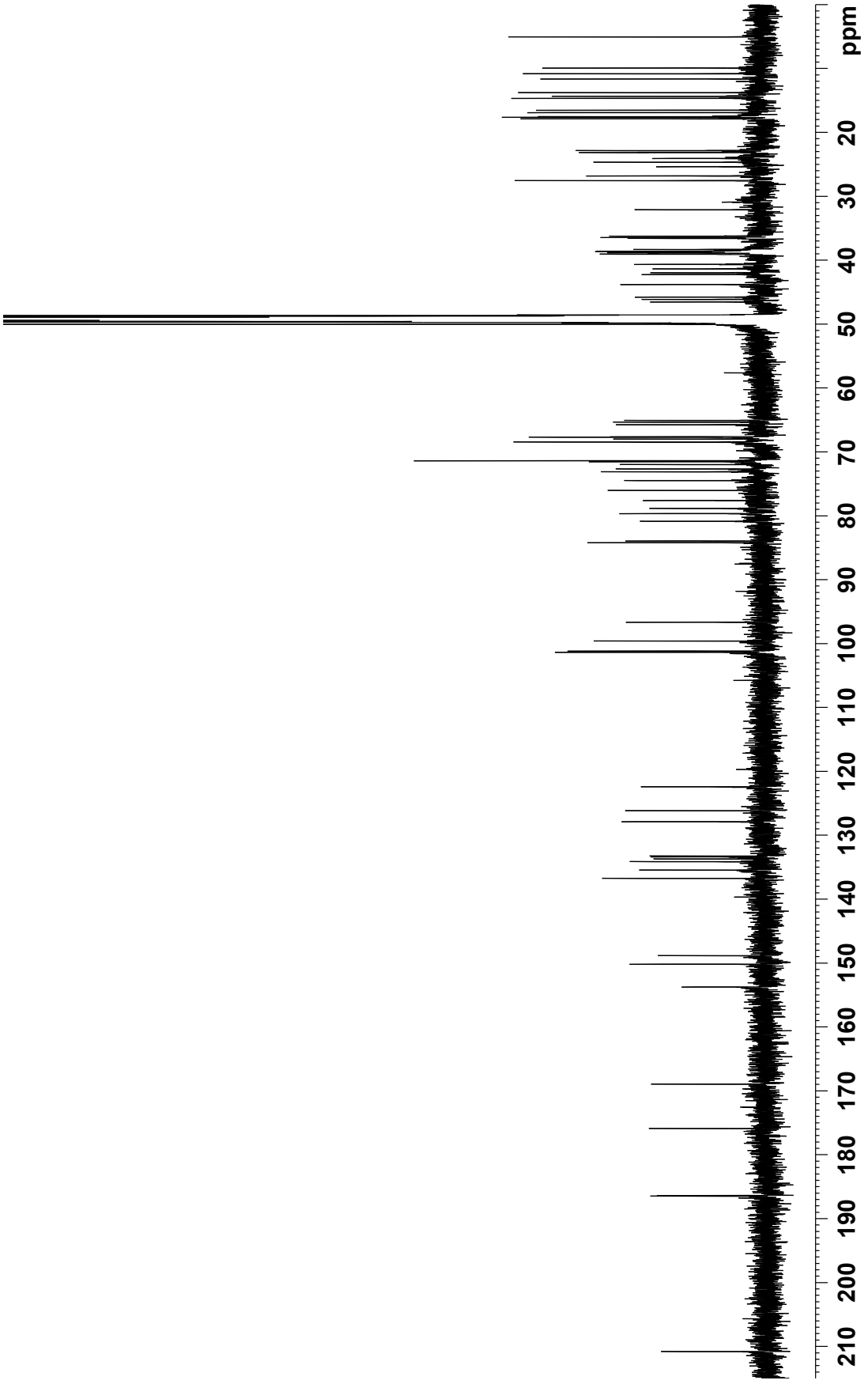

Figure S14. COSY spectrum of **2** (500 MHz, CD_3OD).

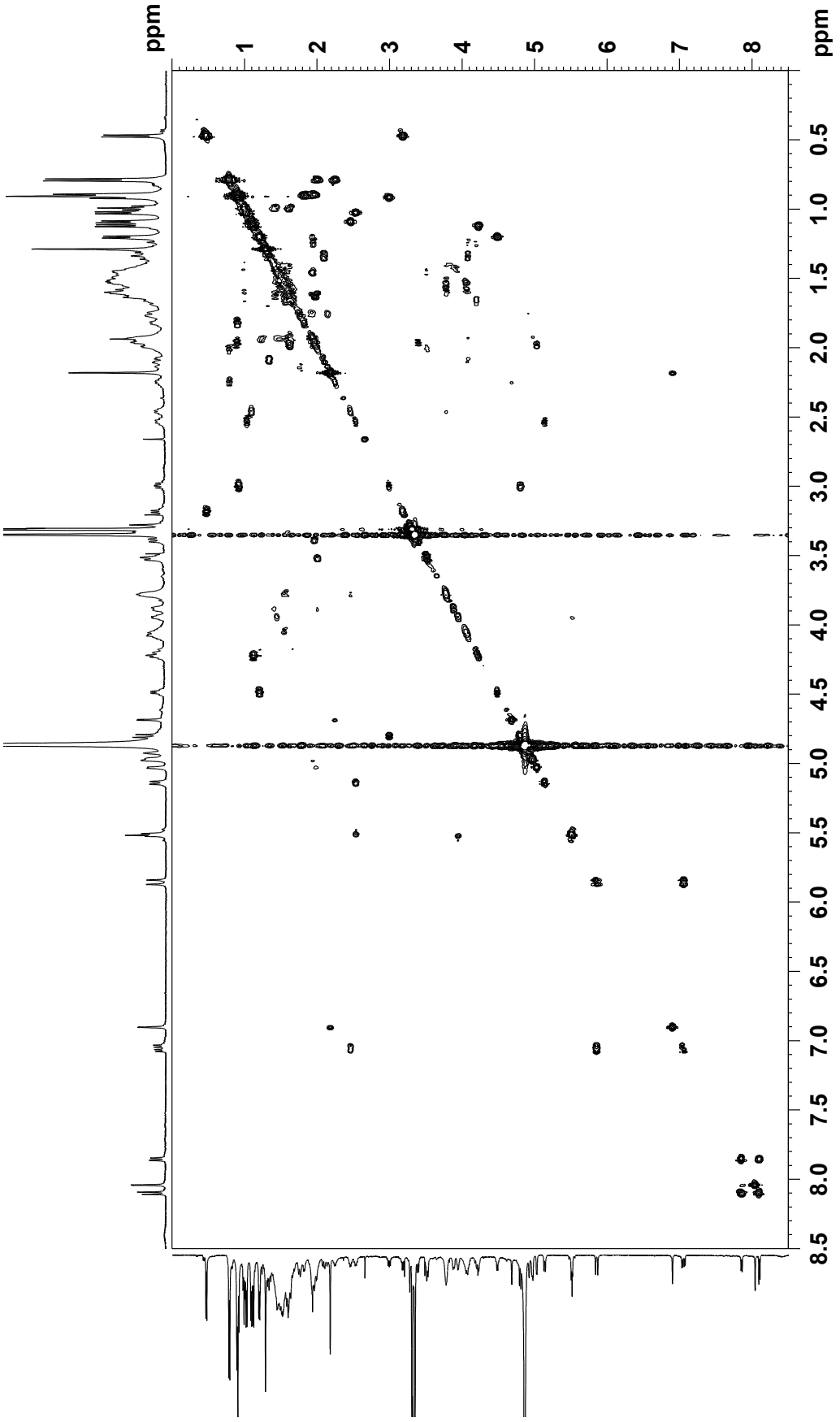

Figure S15. TOCSY spectrum of **2** (500 MHz, CD_3OD).

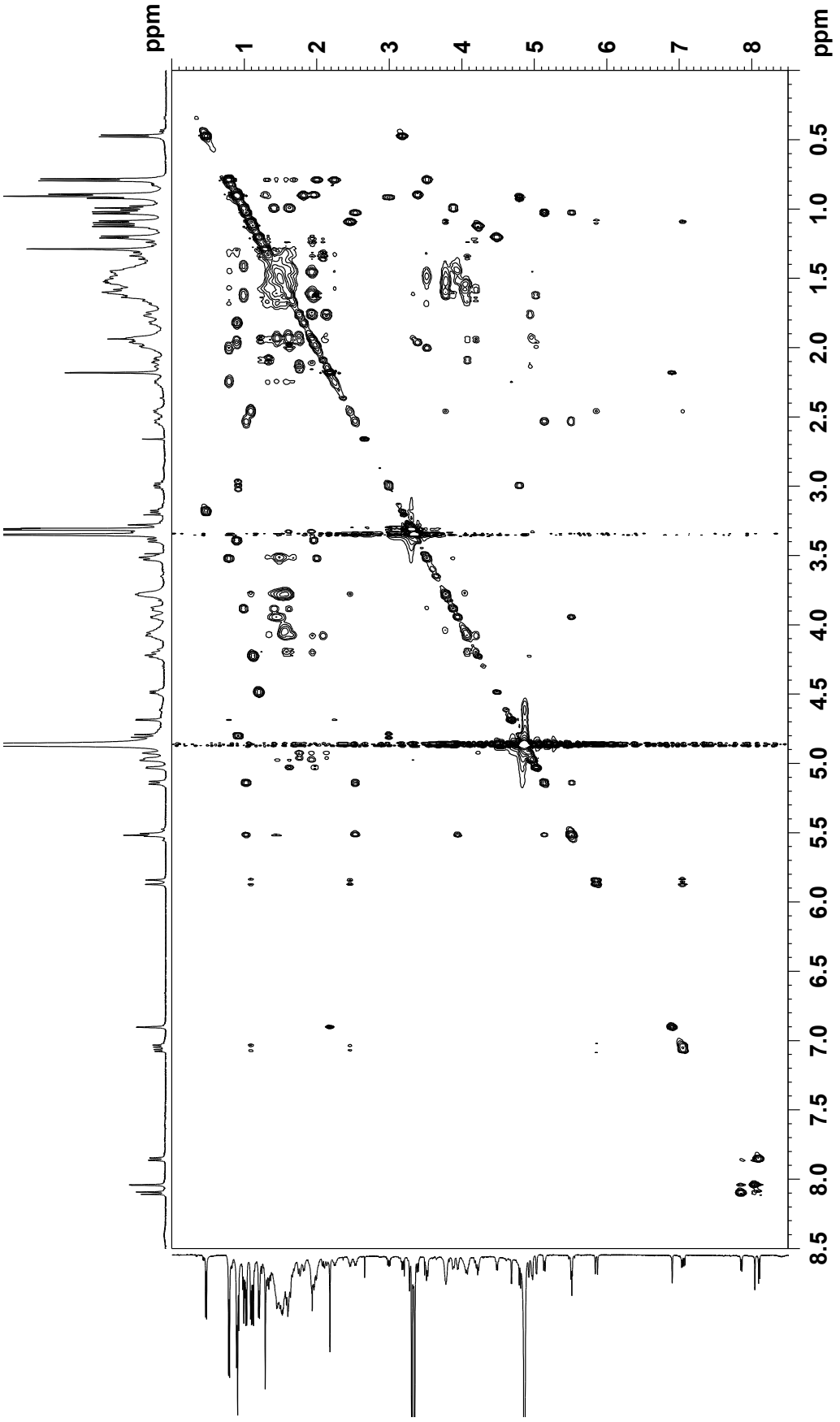

Figure S16. HSQC spectrum of **2** (500 MHz, CD_3OD).

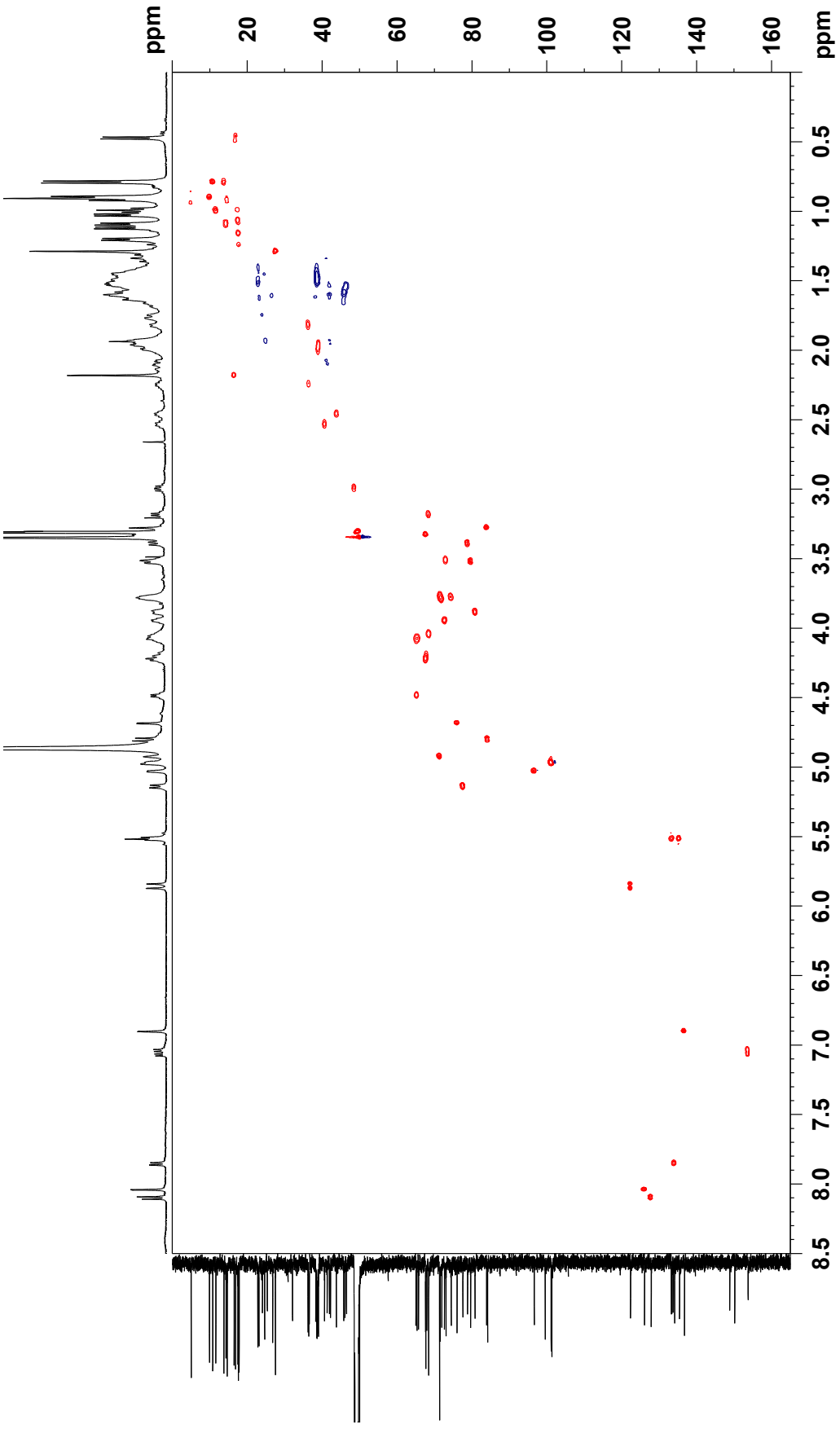

Figure S17. HMBC spectrum of **2** (500 MHz, CD_3OD).

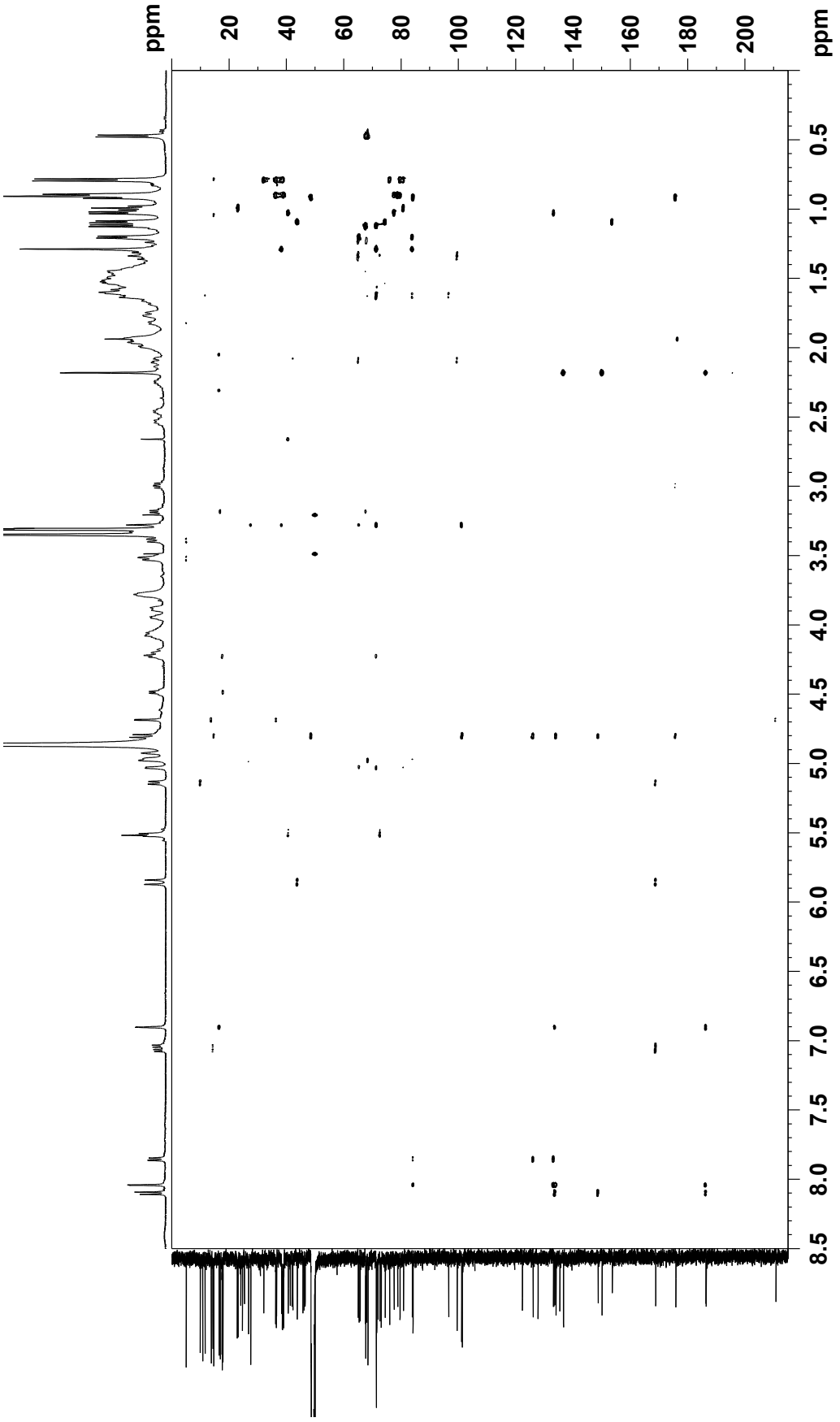

Figure S18. ROESY spectrum of **2** (500 MHz, CD_3OD).

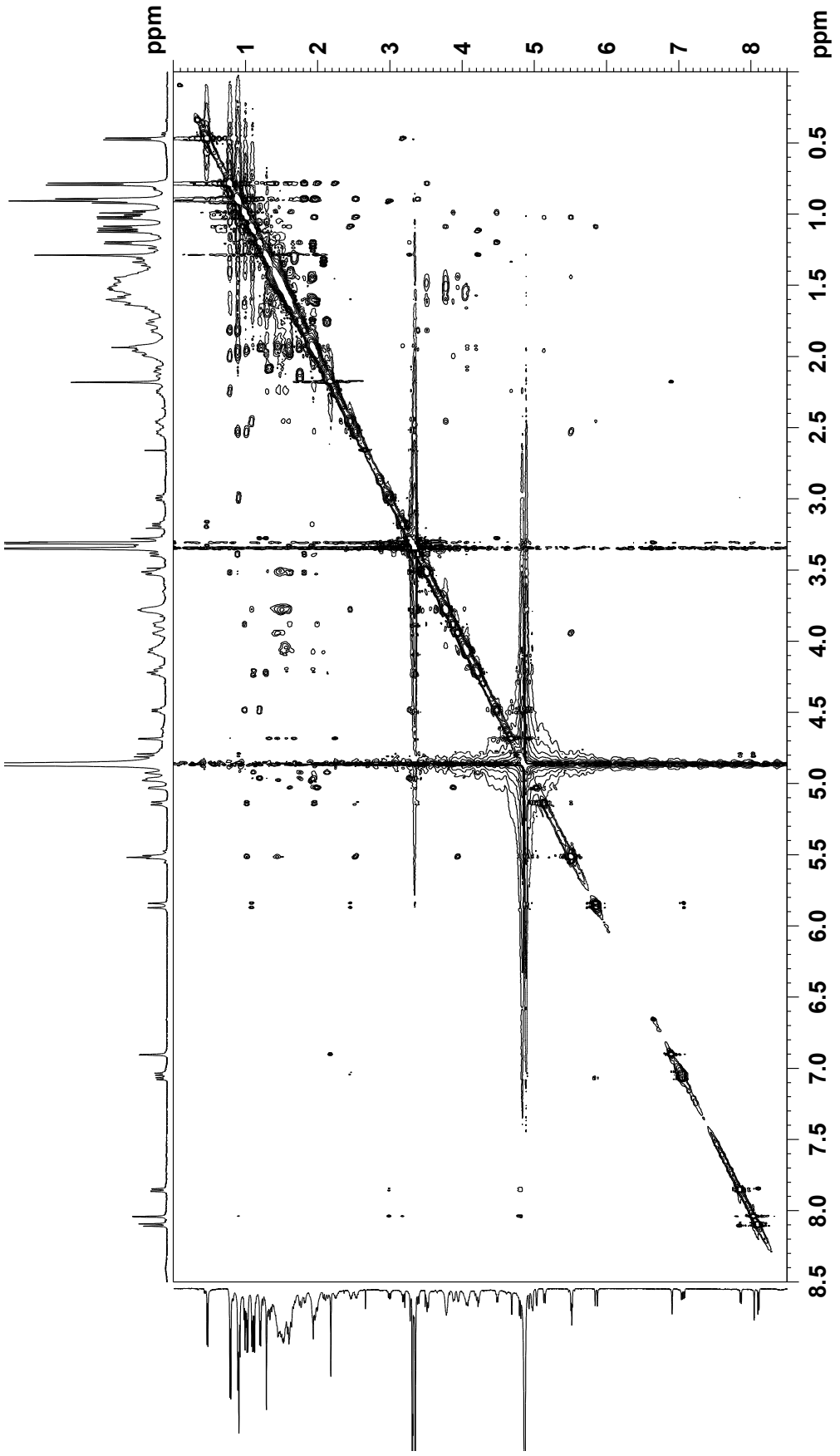

Figure S19. UV spectrum of iseolide C (**3**).

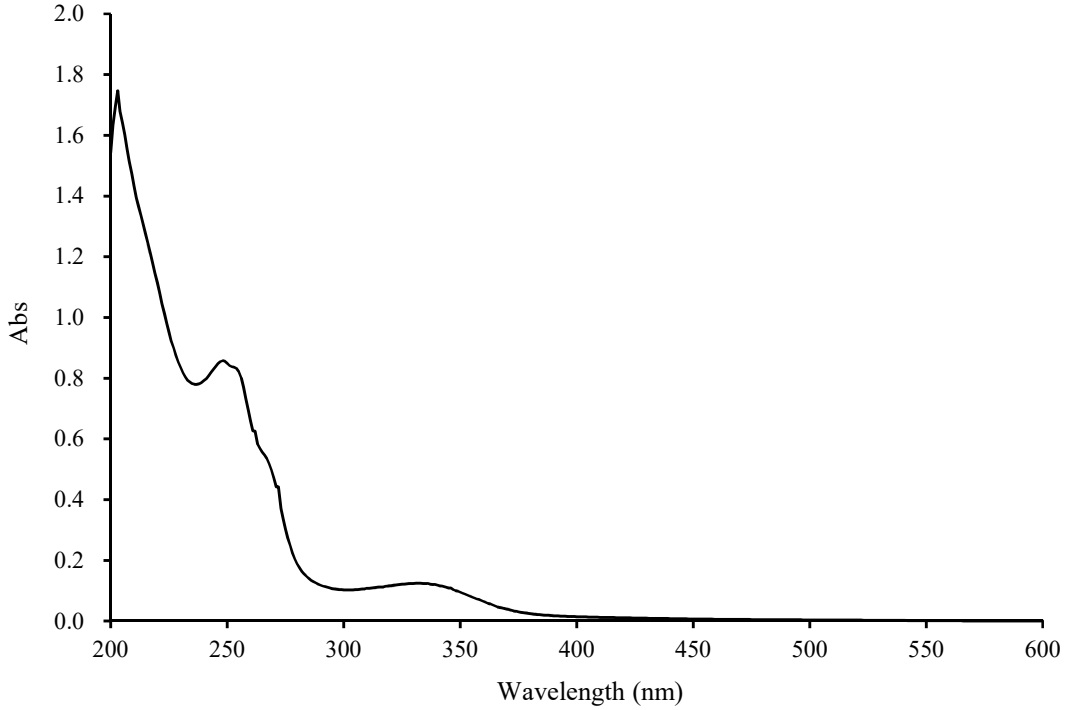

Figure S20. IR spectrum of **3**.

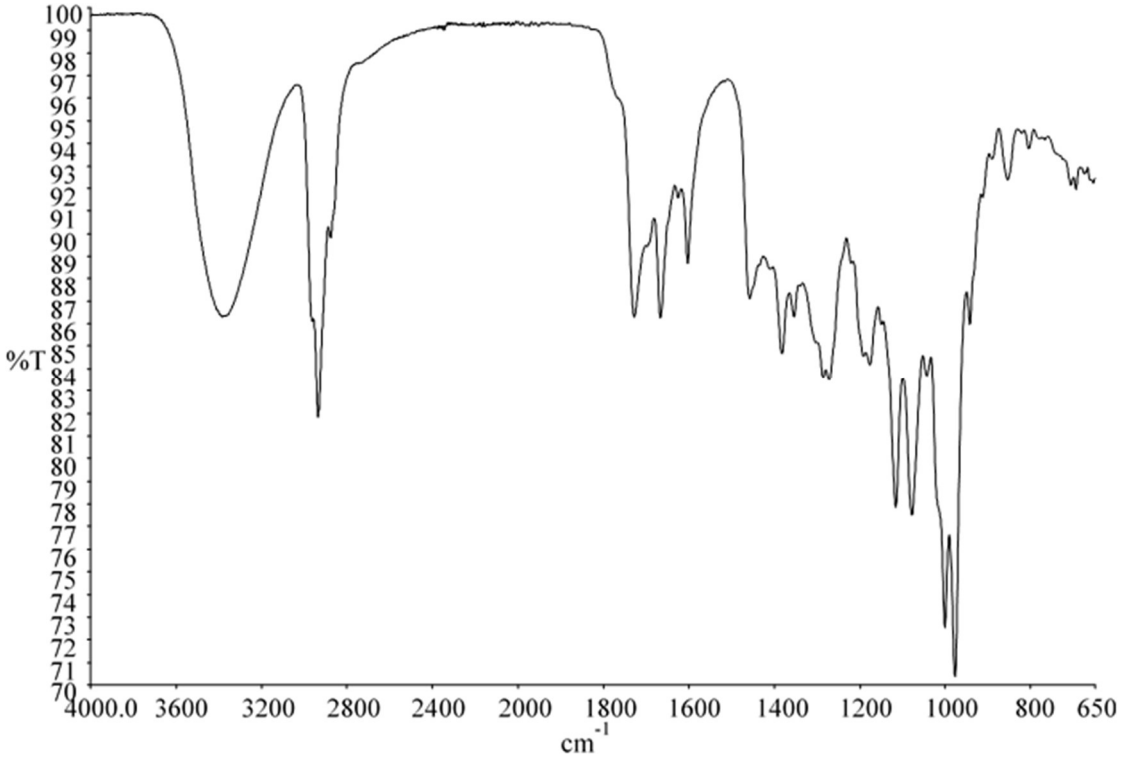

Figure S21. ^{1}H NMR spectrum of **3** (500 MHz, CD_3OD).

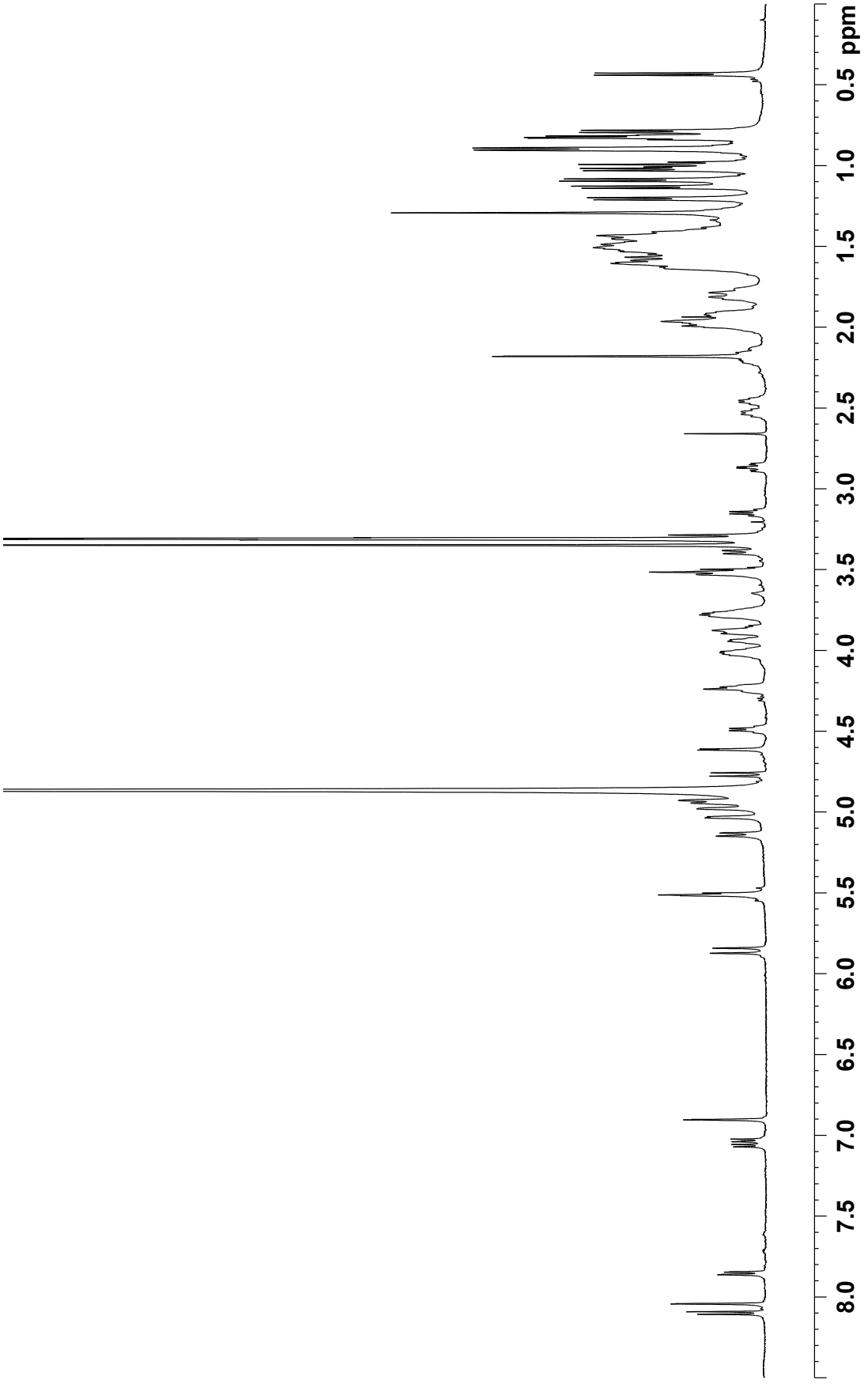

Figure S22. ^{13}C NMR spectrum of **3** (125 MHz, CD_3OD).

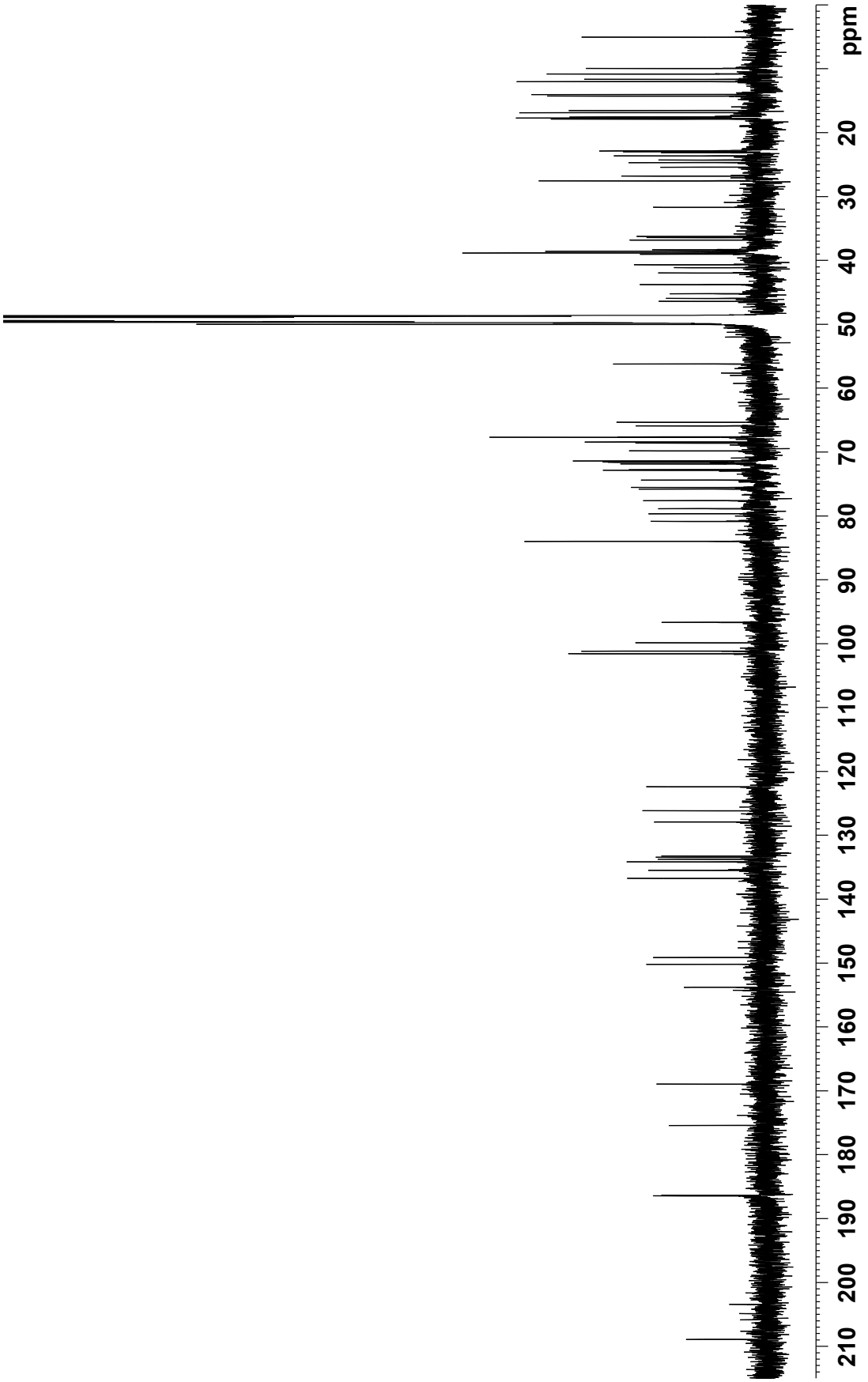

Figure S23. COSY spectrum of **3** (500 MHz, CD_3OD).

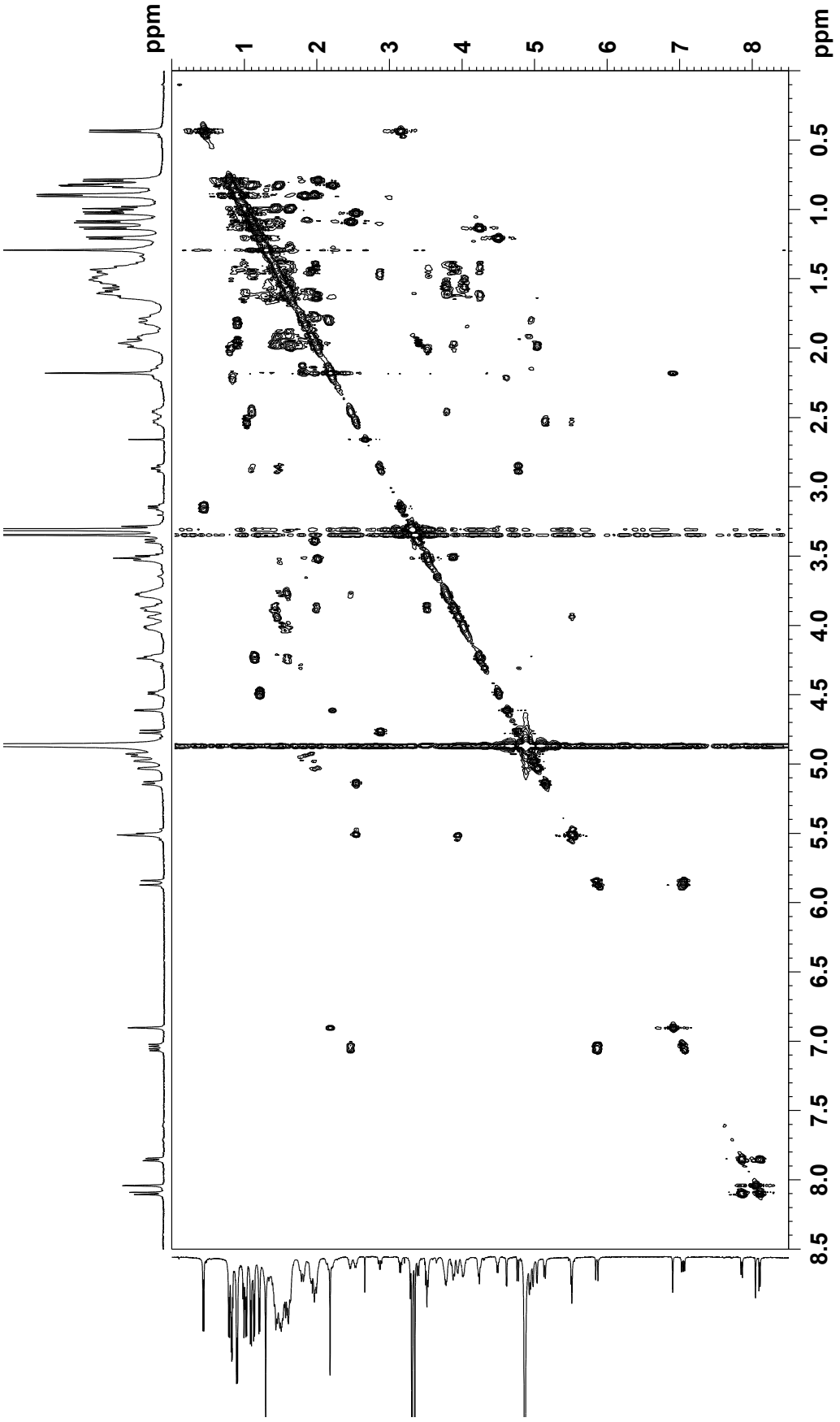

Figure S24. TOCSY spectrum of **3** (500 MHz, CD_3OD).

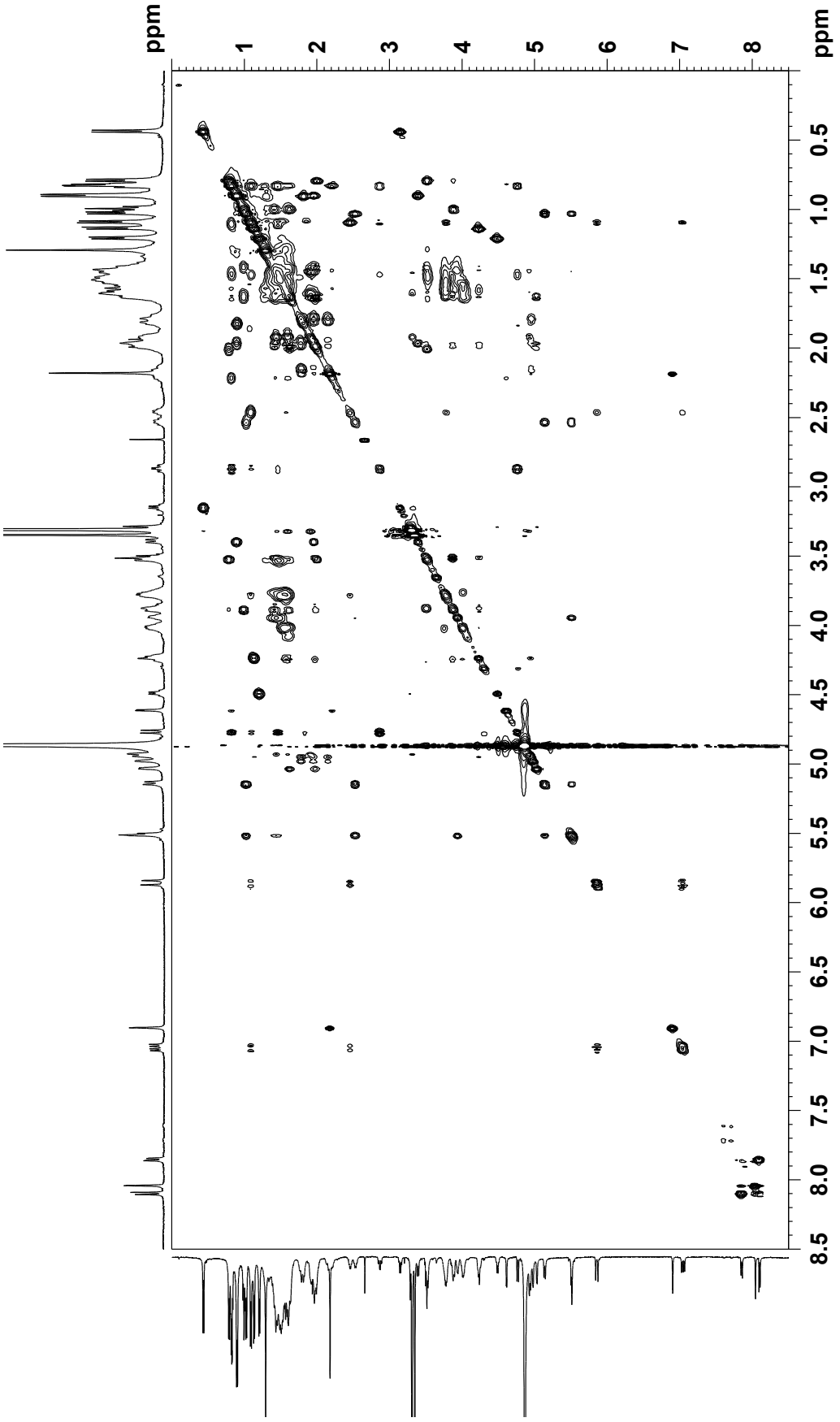

Figure S25. HSQC spectrum of **3** (500 MHz, CD_3OD).

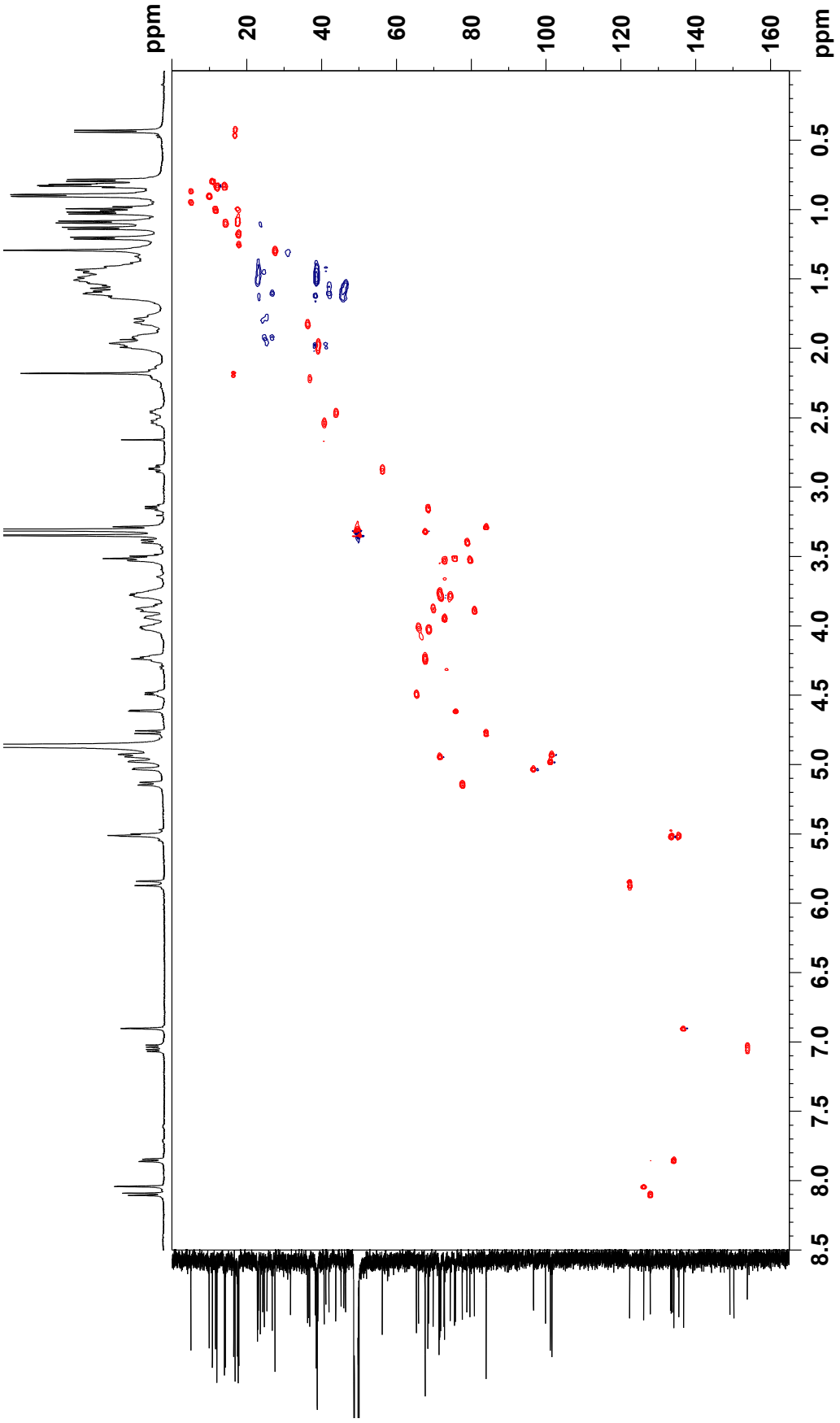

Figure S26. HMBC spectrum of **3** (500 MHz, CD_3OD).

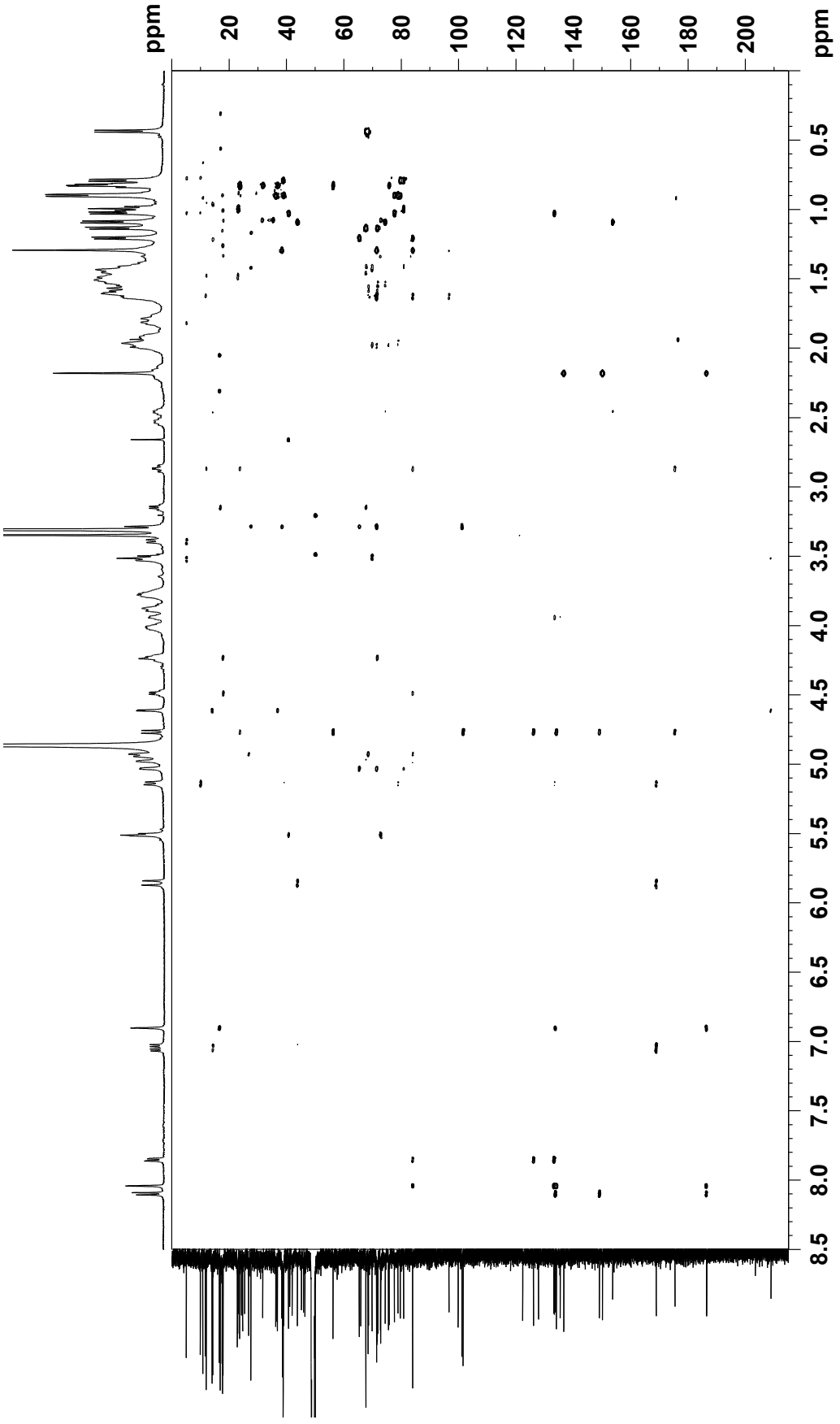

Figure S27. ROESY spectrum of **3** (500 MHz, CD_3OD).

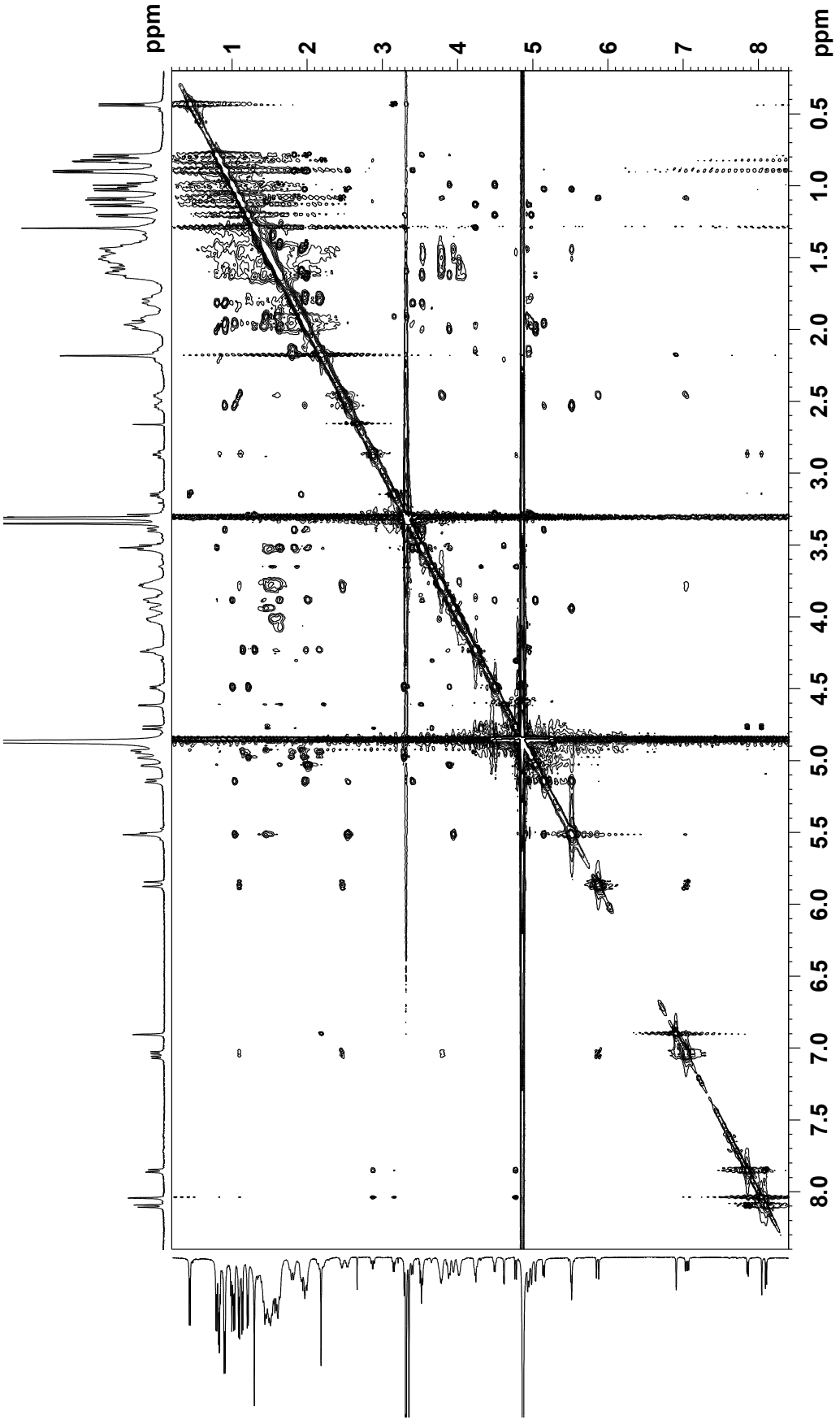

Figure S28. MS/MS spectra of **1**, **2**, and **3**. The numbers denote the *m/z* values of sodium adduct ions observed in the positive mode.

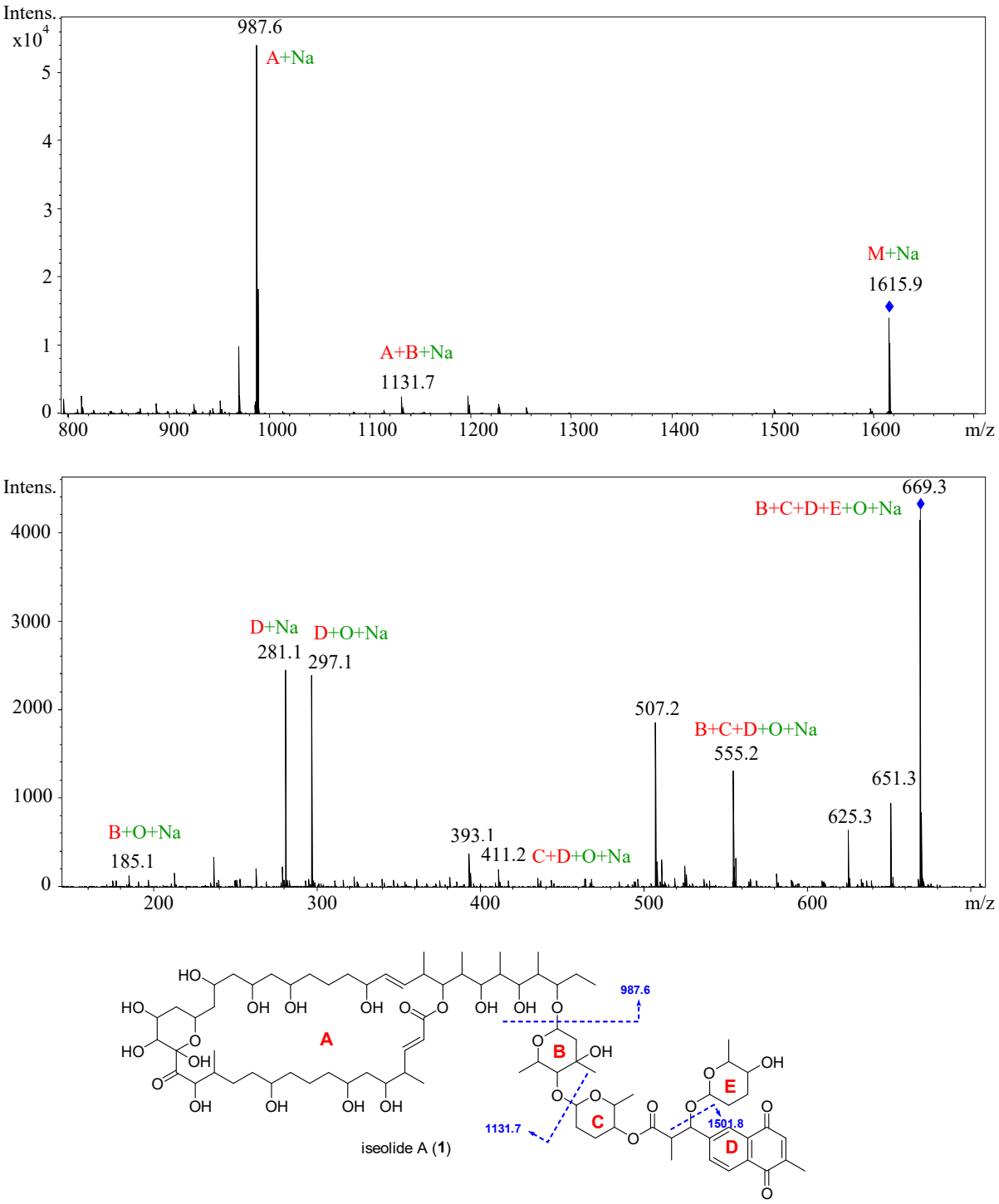

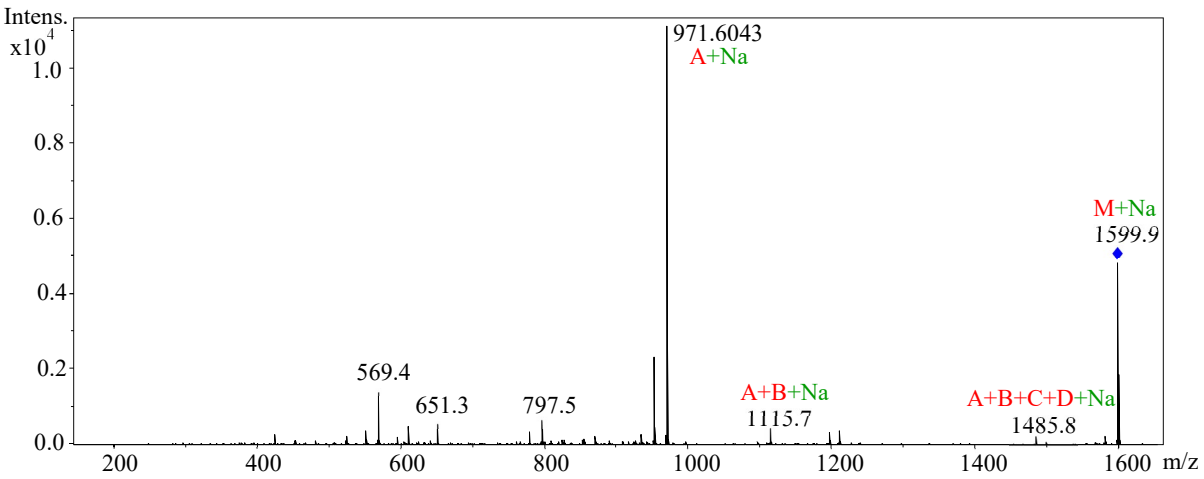

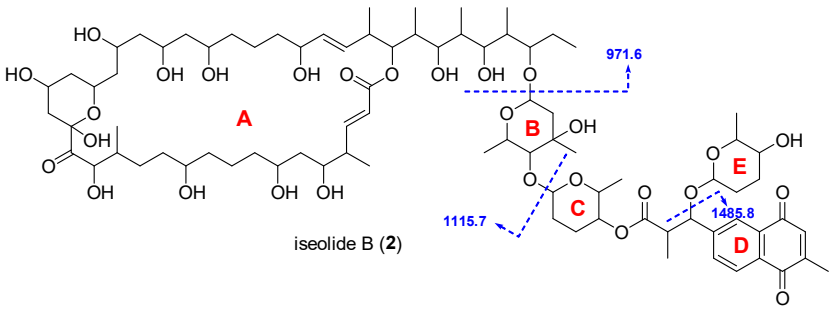

iseolide B (**2**)

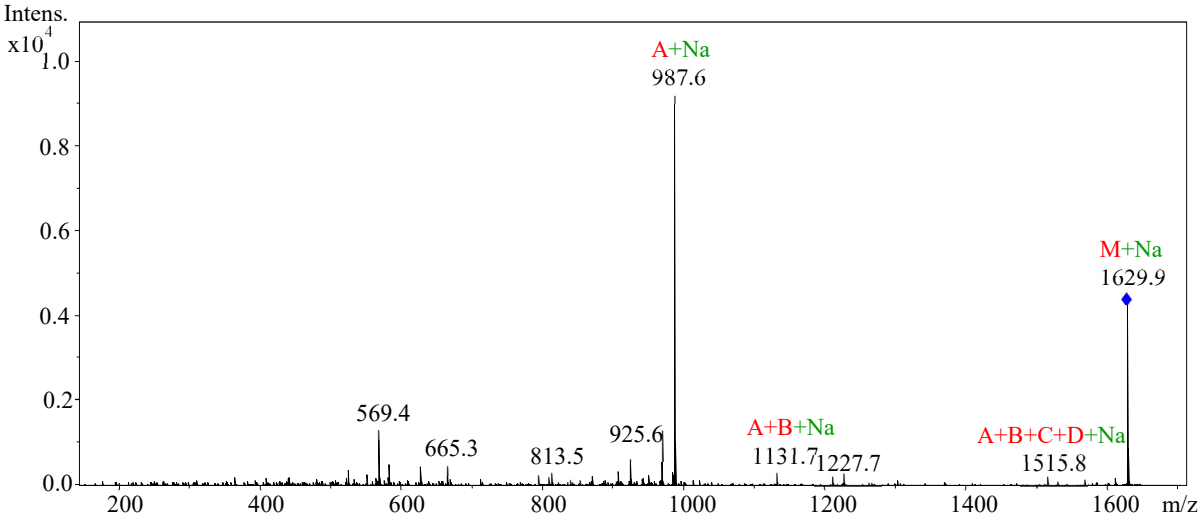

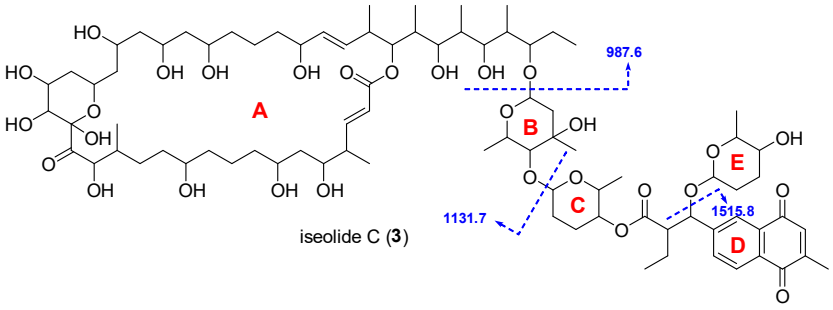

iseolide C (**3**)

Table S1. ^{1}H and ^{13}C NMR data for iseolides B (**2**) and C (**3**) in CD_3OD.

	2			**3**		
No.	δ_H, mult (*J* in Hz)[a]	δ_C[b]	HMBC[a,c]	δ_H, mult (*J* in Hz)[a]	δ_C[b]	HMBC[a,c]
1		168.9			168.9	
2	5.86, d (15.9)	112.4	1, 4	5.86, d (15.9)	122.4	1
3	7.05, dd (7.1, 15.9)	153.7	1, 2, 4, 5, 44	7.05, dd (7.1, 15.9)	153.7	1, 4, 5, 44
4	2.46, m	43.8	2, 3, 5, 44	2.46, m	43.8	3, 5, 44
5	3.78, m	74.5	3, 44	3.78, m	74.4	44
6	1.53, m; 1.61, m	41.9	5	1.55, m; 1.60, m	41.9	5
7	3.77, m	71.5		3.78, m	74.4	
8	1.37-1.56, m	38.7		1.55, m; 1.60, m	41.9	9
9	1.41, m	23.1		1.44, m	23.0	
10	1.37-1.56, m	38.8		1.35-1.56, m	38.8	9
11	3.51, m	73.1	10	3.53, m	72.8	
12	1.44, m; 1.56, m	36.6		1.44, m; 1.57, m	36.4	
13	1.32, m; 1.69, m	32.1	11	1.28, m; 1.62, m	31.7	
14	2.25, m	36.4	45	2.22, m	36.8	
15	4.69, d (2.5)	76.0	13, 14, 16, 45	4.61, d (3.2)	75.8	13, 14, 16, 45
16		210.8			208.9	
17		99.6			99.8	
18	1.34, m; 2.09, m	41.3	16, 17, 19, 20	3.51, m	75.5	15, 19
19	4.08, m	65.1		3.87, m	69.8	
20	1.23, m; 1.94, m	42.2	19, 21	1.42, m; 1.98, m	41.1	18, 19
21	4.20, m	68.0		4.22, m	67.6	
22	1.50-1.66, m	46.1	21	1.50-1.66, m	45.9	23
23	4.04, m	68.5		4.01, m	68.6	
24	1.50-1.66, m	46.3		1.50-1.66, m	46.4	23
25	4.08, m	65.7		4.03, m	65.9	
26	1.50-1.66, m	45.8		1.50-1.66, m	45.2	
27	3.79, m	72.0		3.79, m	71.8	
28	1.37-1.56, m	38.5		1.35-1.56, m	38.6	29
29	1.51, m	22.8		1.51, m	22.8	
30	1.37-1.56, m	38.6		1.35-1.56, m	38.6	29, 31
31	3.95, m	72.7	32, 33	3.94, m	72.7	32, 33
32	5.52, m	135.4	31, 34	5.52, m	135.4	31, 33, 34
33	5.52, m	133.3	31, 34, 46	5.52, m	133.4	31, 32, 34, 46
34	2.53, m	40.6	32, 33	2.53, m	40.7	32, 33
35	5.14, dbr (9.5)	77.6	1, 33, 34, 36, 37, 46, 47	5.14, dbr (9.5)	77.6	1, 33, 34, 36, 37, 46, 47
36	1.96, m	39.0	35, 37, 47	1.96, m	39.0	
37	3.39 dbr (9.5)	78.8	35, 36, 38, 48	3.39, bdr (9.5)	78.8	35, 36, 39, 48
38	1.82, m	36.2	48	1.82, m	36.2	
39	3.52, m	79.6	37, 40, 41, 48	3.52, m	79.6	37, 38, 41, 48, 49
40	2.00, m	39.0		2.01, m	38.8	
41	3.89, m	60.9	49	3.89, m	80.9	
42	1.42, m; 1.62, m	23.13	41, 43,	1.43, m; 1.62, m	23.1	43
43	0.99, t (7.2)	11.6	42	0.99, t (7.4)	11.6	41, 42
44	1.09, d (6.9)	14.3	3,5	1.09, d (6.9)	14.3	
45	0.79, d (6.9)	13.8	15	0.82, d (6.6)	14.0	13, 14, 15
46	1.03, d (6.9)	17.5	33, 35	1.03, d (6.8)	17.5	
47	0.90, m	9.9	35, 37	0.90, m	9.9	
48	0.90, m	5.0	37, 39	0.90, m	5.0	
49	0.79, d (6.9)	10.8	39, 41	0.79, d (7.4)	10.6	39, 40, 41
1′	5.03, dbr (3.5)	96.6	41, 3′, 5′	5.03, dbr (3.5)	96.6	41, 3′, 5′

2′	1.61, m; 1.97, m	38.3	1′, 4′, 7′	1.63, m; 1.99, m	38.3	1′, 4′, 7′
3′		71.4			71.4	
4′	3.28, sbr	83.9	2′, 3′, 5′, 7′, 1″	3.29, sbr	84.0	2′, 3′, 6′, 7′, 1″
5′	4.99, d (6.5)	65.3	1′, 4′, 6′	4.49, d (6.5)	65.3	1′, 4′, 6′
6′	1.20, d (6.7)	65.3	5′	1.21, d (6.6)	17.9	
7′	1.29, s	27.5	2′, 3′, 4′	1.29, s	27.5	2′, 3′, 4′
1″	4.96, m	101.2	3″, 5″, 4′	4.98, m	101.1	2″, 5″, 4′
2″	1.76, m; 2.14, m	24.1		1.77, m; 1.96, m	25.4	
3″	1.76, m; 1.94, m	25.4		1.76, m; 2.14, m	25.3	
4″	4.92, m	71.4	2″	4.24, m	71.6	50, 3″
5″	4.23, m	67.6	6″	4.25, m	67.7	4″, 6″
6″	1.12, d (6.6)	17.6		1.13, d (6.6)	17.7	5″
1‴	4.98, m	101.4	3‴, 52	4.93, m	101.6	2‴, 3‴, 5‴
2‴	1.45, m; 1.93, m	24.7	1‴	1.44, m; 1.92, m	24.7	
3‴	1.61, m; 1.93, m	26.8		1.60, m; 1.92, m	26.8	
4‴	3.33, m	67.6		3.32, m	67.7	
5‴	3.18, q (6.7)	68.4	4‴, 5‴	3.15, q (6.6)	68.4	1‴, 3‴, 4‴, 6‴
6‴	0.47, d (6.6)	16.9	4‴, 5‴	0.44, d (6.6)	16.8	4‴, 5‴
50		175.8			175.4	
51	2.99, dq (7.3, 9.8)	48.6	50, 52, 63	2.87, dt (3.8, 10.5)	56.2	50, 52
52	4.80 d, (9.8)	84.2	1‴, 50, 51, 53, 54, 62, 63	4.77, d (10.2)	84.0	50, 51, 53, 54, 63, 65, 1‴
53		148.8			149.1	
54	8.04， s	126.1	52, 56, 60, 62	8.04, s	126.1	52, 56, 61, 63
55		133.7			133.7	
56		186.3			186.3	
57	6.90, s	136.7	55, 59, 64	6.90, s	136.7	55, 60, 64
58		150.1			150.1	
59		186.4			186.4	
60		133.2			133.2	
61	8.10, d (7.9)	127.8	53, 55, 58	8.10, d (8.0)	127.9	
62	7.85, d (7.9)	134.1	52, 54, 60	7.85, d (8.0)	134.1	53, 55
63	0.92, m	14.7	52	0.83, m; 1.46, m	23.6	52, 54, 61
64	2.18, s	16.5	57, 58, 59	2.18, s	16.5	57, 58, 60
65				0.83, t (7.2)	12.0	50, 51, 53

[a] Recorded at 500 MHz.

[b] Recorded at 125 MHz.

[c] From proton to indicated carbons.

[d] Coupling constant could not be determined due to signal overlapping.

CHAPTER 3

TMKS8A, a Chlorinated α-Lapachone from a Sea Slug-Derived Actinomycete of the Genus *Streptomyces*

3-1 Background

As discussed in Chapters 1 and 2, marine microorganism is a rising star for the exploration of new natural products. Especially, marine invertebrates-derived actinomycetes are now attracting attention as one of the promising niches for the discovery of new secondary metabolites [1]. Marine microbial natural products from Indonesia are still under evaluated, although, as a maritime country in the tropical zone, Indonesia is blessed with abundant marine resources as a host of marine microbes [2]. According to the review by Hanif et al. [3], among 486 new marine natural products from Indonesia, published during January 1970 to December 2017, only 48 compounds (6.5%) are derived from microorganisms. This number is likely quite few, compared to the expected biodiversity in marine ecosystem of Indonesia [4].

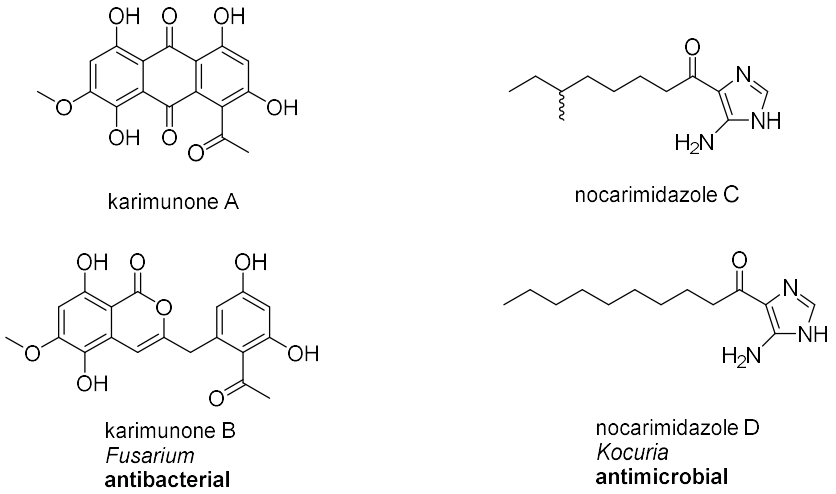

Figure 3-1. Chemical structures of karimunones A–B and nocarimidazoles C–D.

The marine microbes of Indonesia are one of the important sources of microorganisms in our laboratory, and some interesting secondary metabolites have been discovered. Karimunones A and B (Figure 3-1), two new aromatic polyketides were isolated from sponge-associated *Fusarium* sp. KJMT.FP.4.3 which was collected from an Indonesian sponge *Xestospongia*. Among them, karimunone B showed antibacterial activity against multidrug resistant *Salmonella enterica* ser. Typhi with a MIC of 125 μg/mL [5]. Nocarimidazoles C and D (Figure 3-1), two new alkanoylimidazoles were isolated from a marine-derived actinomycete strain of the genus *Kocuria*, isolated from a stony coral *Mycedium* sp., which were moderately antimicrobial against Gram-positive bacteria and fungi, with MIC ranges of 6.25–25 μg/mL [6].

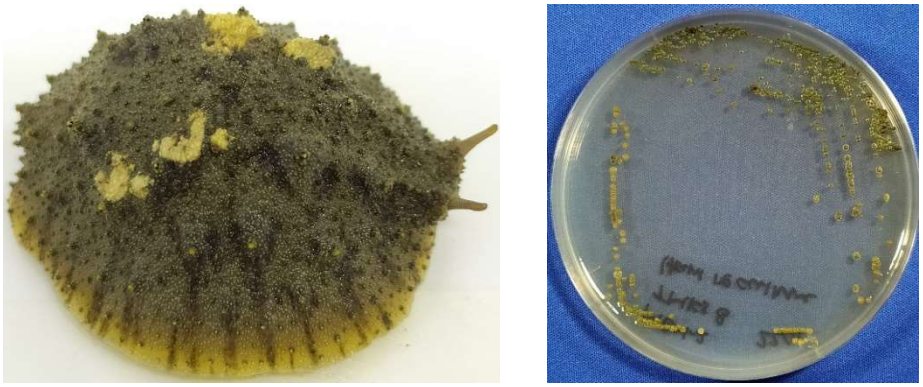

Figure 3-2. Slug *Paromoionchis tumidus* (left) and *Streptomyces* sp. TMKS8 on Bn-2 agar (right).

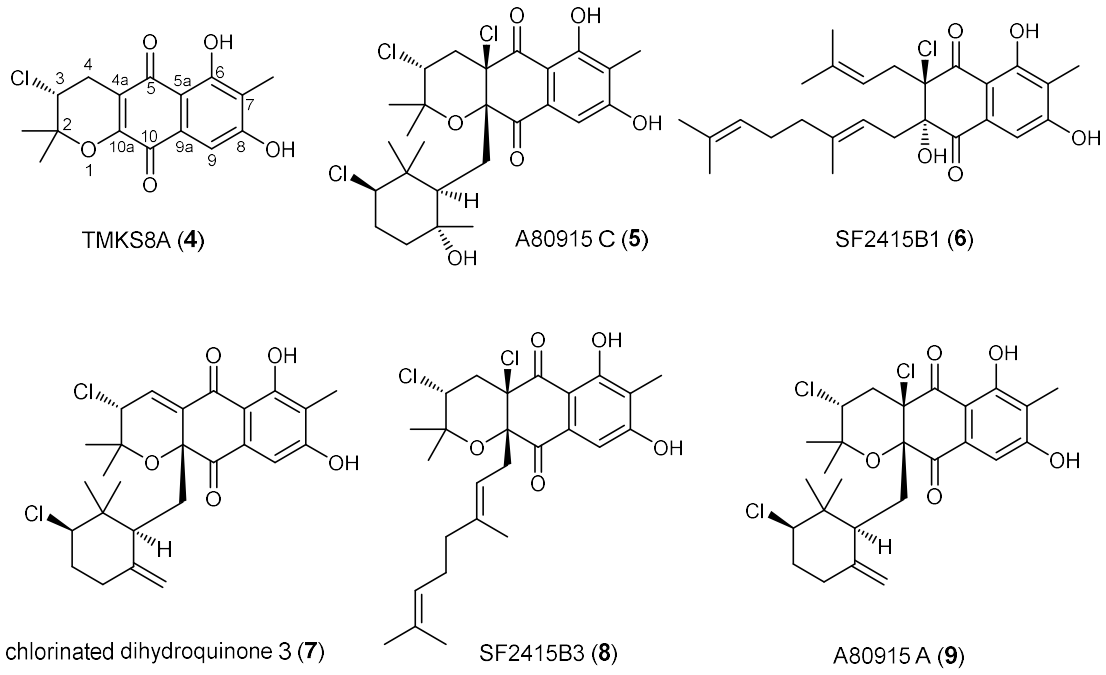

Figure 3-3. Secondary metabolites isolated from *Streptomyces* sp. TMKS8.

In my continuous investigation on marine microbes of Indonesia, *Streptomyces* sp. TMKS8 isolated from an air-breathing slug, *Paromoionchis tumidus*, collected at Mangkang mangrove forest, Semarang, Central Java, Indonesia, was found to produce TMKS8A (**4**), a new chlorinated α-lapachone derivative, along with five known related metabolites, A80915 C (**5**), SF2415B1 (**6**), chlorinated dihydroquinone 3 (**7**), SF2415B3 (**8**), and A80915 A (**9**) (Figure 3-3).

3-2 Results and discussion

3-2-1 Fermentation and isolation

The producing strain TMKS8 was isolated from a sea slug, *Paromoionchis tumidus*, collected at Mangkang mangrove forest, Indonesia. Strain TMKS8 was cultured in A3M liquid medium and the whole culture broth was extracted with 1-butanol. The extract was consecutively fractionated to silica gel and ODS column chromatography, and the final purification was accomplished by reverse-phase HPLC to give TMKS8A (**4**).

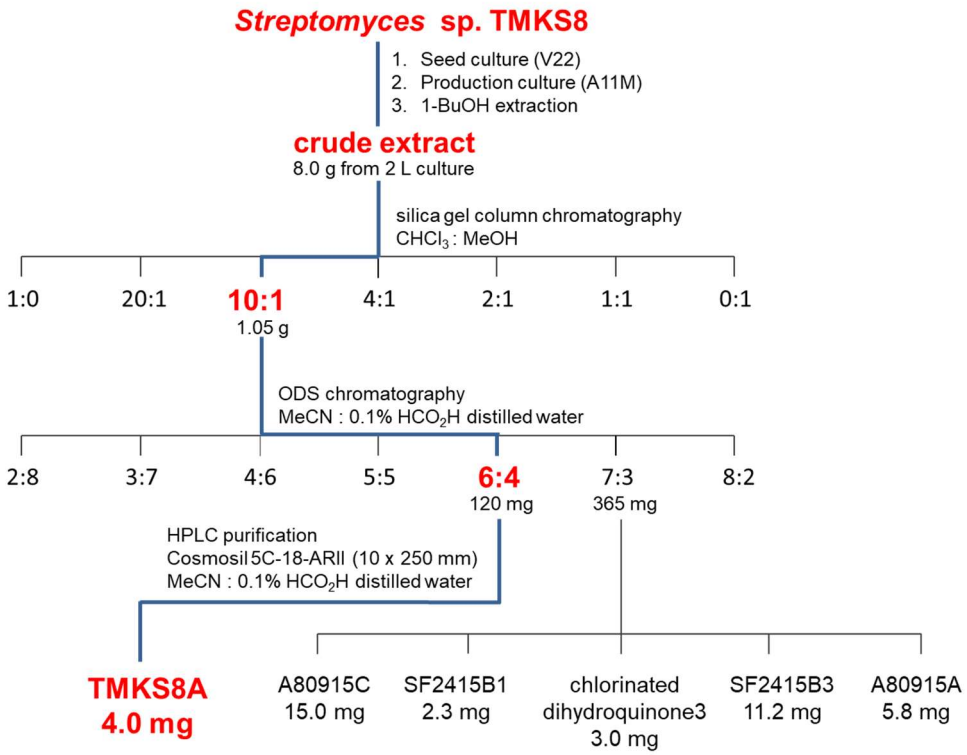

Scheme 3-1. Isolation of secondary metabolites isolated from *Streptomyces* sp. TMKS8.

3-2-2 Structure determination

Compound **4** was obtained as an orange powder. The IR spectrum indicated the presence of hydroxy (3417 cm^{-1}) and carbonyl (1655 cm^{-1}) groups. The characteristic UV spectrum with the absorption maxima at 215, 262, 309, and 419 nm was indicative of the naphthoquinone chromophore [7]. The molecular formula was determined as $C_{16}H_{15}ClO_5$, on the basis of the HRESITOFMS analysis which gave a deprotonated molecule $[M - H]^-$ at *m/z* 321.0517 (calcd for $C_{16}H_{14}{}^{35}ClO_5$, 321.0524) with a typical isotopic pattern of a compound containing one chlorine atom (Figure S10).

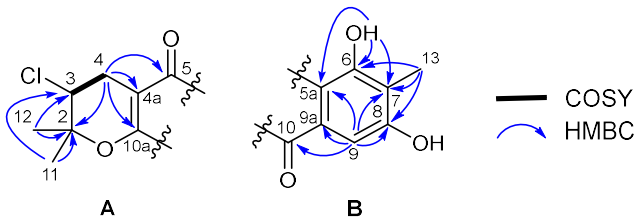

Figure 3-4. Partial structures A and B deduced from COSY and HMBC analyses.

Table 3-1. ^{1}H and ^{13}C NMR data for TMKS8A (**4**) in DMSO-d_6.

Position	δ_H,mult (*J* in Hz)[a]	δ_C[b]	HMBC[a,c]
2		79.6	
3	4.56, t (4.9)	58.0	4, 4a, 11, 12
4α	2.78, dd (4.7, 19.2)	26.6	2, 3, 4a, 5, 10a
4β	3.08, dd (5.0, 19.2)		2, 3, 4a, 5, 10a
4a		116.9	
5		188.0	
5a		106.5	
6		160.7	
6-OH	12.67		5a, 6, 7
7		117.5	
8		161.3	
9	7.06, s	107.1	5, 5a, 7, 8, 9a, 10
9a		129.2	
10		178.0	
10a		152.7	
2α-Me	1.45, s	23.6	2, 3, 2β-Me
2β-Me	1.39, s	24.5	2, 3, 2α-Me
7-Me	2.03, s	8.0	6, 7, 8

[a]Recorded at 500 MHz.
[b]Recorded at 125 MHz.
[c]From proton to indicated carbon(s).

Two singlet methyl protons at δ_H 1.45 and 1.39, which were mutually correlated in the HMBC spectrum, showed long-range correlations to an oxygenated carbon C2 (δ_C 79.6) and a methine carbon C3 (δ_C 58.0). The methine proton H3 (δ_H 4.56), in turn, displayed a COSY correlation with methylene protons H4 (δ_H 2.78, 3.08), which was further correlated with three sp^2 carbons, C4a (δ_C 116.9), C5 (δ_C 188.0), and C10a (δ_C 152.7). Chemical shifts suggested the oxygenation of C5 and C10a, and thus the linkages of C4/C4a, C4a/C5, and C4a/C10a were deduced as the only possible connectivity among these carbons. Meanwhile, the singlet methyl proton at δ_H 2.03 were correlated with C7 (δ_C 117.5) and two deshielded sp^2 carbons C6 (δ_C 160.7) and C8 (δ_C 161.3), whereas a hydroxy proton at δ_H 12.67 had correlations to C5a (δ_C 106.5), C6, and C7. In addition, H9 (δ_H 7.06, s) showed intense HMBC cross peaks to C5a and C7 and relatively weak cross peaks to C8 and C9a. These correlation data afforded a

penta-substituted benzene ring, comprising six carbons from C5a to C9a, with a hydroxy group at C6, a methyl group at C7, and an oxygen substitution at C8. Furthermore, the carbonyl carbon C10 (δ_C 178.0) was placed at C9a by an HMBC correlation from H9 to C10. To satisfy the molecular formula, the ether linkage between C2 and C10a, the attachment of a chlorine atom at C3, and the placement of a hydroxy group at C8 were deduced, providing two partial structures **A** and **B** (Figure 3-4). Connectivity between **A** and **B** was suggested by a four-bond correlation from H9 to C5, but two linkage patterns were possible (Figure 3-5). Of the two possible structures **I** and **II**, the former was likely more probable, because the sharp singlet resonance of the phenolic proton 6-OH (δ_H 12.67) implied the hydrogen bonding of this proton to an adjacent carbonyl oxygen.

Table 3-2. DFT-calculated NMR chemical shifts of two possible structures **I** and **II** for TMKS8A (**4**).

	TMKS8A (**4**)		structure **I**		structure **II**		structure **I**	structure **II**
Position	δ_C(exp)	δ_H(exp)	δ_C(calc)	δ_H(calc)	δ_C(calc)	δ_H(calc)	$\lvert\delta_C(exp)-\delta_C(calc)\rvert$	$\lvert\delta_C(exp)-\delta_C(calc)\rvert$
2	79.6		82.3		85.0		2.7	5.4
3	58.0	4.56	55.5[a]	4.36	55.8[a]	4.40	2.5	2.2
4	26.6	2.78	30.7	2.89	30.5	2.76	4.1	3.9
		3.08		3.01		2.93		
4a	116.9		117.7		108.9		0.8	8.0
5	188.0		185.8		174.2		2.2	13.8
5a	106.5		108.1		107.2		1.6	0.7
6	160.7		159.8		155.1		0.9	5.6
6-OH		12.67		13.11[b]		9.61[b]		
7	117.5		119.9		121.4		2.4	3.9
8	161.3		157.2		155.6		4.1	5.7
9	107.1	7.06	107.0	7.31	111.2	7.47	0.1	4.1
9a	129.2		128.9		129.5		0.3	0.3
10	178.0		177.6		177.7		0.4	0.3
10a	152.7		152.7		164.6		0.0	11.9
2α-Me	23.6	1.45	24.9	1.49	25.0	1.60	1.3	1.4
2β-Me	24.5	1.39	26.0	1.40	25.8	1.54	1.5	1.3
7-Me	8.0	2.03	10.7	2.30	11.0	2.28	2.7	3.0
		MAE[c]	1.74	0.14	4.48	0.18		

[a]The heavy-atom errors were corrected by empirical linear scaling. (see Experimental Section for details)
[b]Exchangeable signals are not included for MAEs evaluation.
[c] MAE = mean absolute error (ppm).

To validate this speculation, density functional theory (DFT)-based calculation of NMR chemical shifts for the structures **I** and **II** were conducted at the mPW1PW91/6-31+G(d,p) level of theory (Table 3-2) [8]. It is well known that calculated chemical shifts of carbons bonding to chlorine atoms show relatively large differences from the experimental values due to the heavy-atom effect [8]. Therefore, scaling correction, which was determined by a linear regression procedure using the data set for chlorinated compounds, was applied to the prediction of the ^{13}C chemical shift of C3 position (Figure S9).

The experimental ^{1}H and ^{13}C NMR data of **4** were much closer to those calculated for **I**, suggesting that the *p*-quinone structure was more probable for **4**. In structure **II**, specifically, three carbons, C4a, C5, and C10a, constructing the central quinone ring displayed large differences from the calculated chemical shifts (Figure 3-5). The mean absolute errors (MAEs) for ^{13}C NMR chemical shift prediction are significantly smaller for **I** than **II** (1.74 ppm for **I**, 4.48 ppm for **II**, Table 3-2), also supporting **I** to be the correct structure.

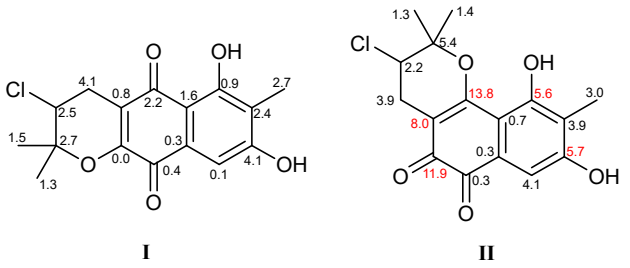

Figure 3-5. Two possible structures **I** and **II** for **4**. Absolute values of difference between the calculated and experimental ^{13}C NMR chemical shifts are indicated.

The conformation of the dihydropyran ring was elucidated from the coupling constants and NOESY analyses. Medium *J* values for H3/H4α and H3/H4β indicated the axial orientation of the chlorine atom at C3. NOESY correlations between H3 and 2β-Me and between H4β and 2β-Me differentiated the two methyl groups at C2. Because of the lack of functional groups for derivatization with chiral auxiliaries, theoretical calculations of electronic circular dichroism (ECD) spectrum using time-dependent density functional theory (TDDFT) were conducted to determine the absolute configuration. The ECD spectrum of **4** in MeOH displayed positive Cotton effects around 259, 305, and 458 nm and a negative one around 385 nm. This pattern was in agreement with the theoretical ECD spectrum for (*R*)-enantiomer (Figure 3-6), thereby establishing the absolute configuration of the chlorinated C3 carbon as *R*. The

absolute configuration of 3-chloro-6,8-dihydroxy-α-lapachone, the 7-demethyl congener of **4** [9], could be proposed as *R* on the basis of its specific rotation value $[\alpha]^{20}_{D}$ -22 (*c* 0.07, $CHCl_3$), which is nearly close to that of **4** with the same negative sign ($[\alpha]^{23}_{D}$ -26, *c* 0.07, $CHCl_3$).

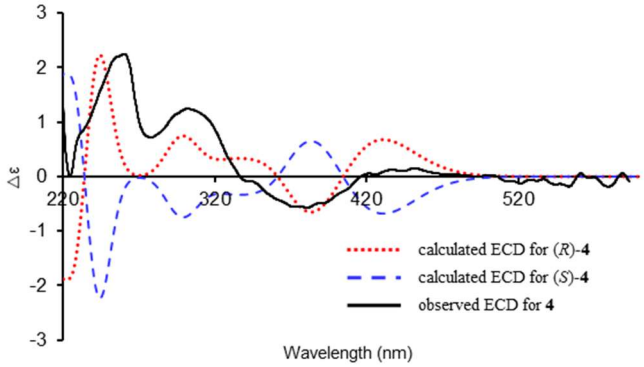

Figure 3-6. Experimental ECD spectrum of TMKS8A (**4**) in methanol, in comparison with the calculated ECD spectra of (*R*)- and (*S*)-**4**.

3-2-3 Bioactivity

Bioactivity of **4** was examined in antimicrobial and cytotoxicity assays. Compound **4** exhibited modest activity against Gram-positive bacteria, *Bacillus subtilis* PCI219, *Kocuria rhizophila* ATCC9341, *Staphylococcus aureus* FDA209P JC-1 with MIC values ranging from 6.25 to 12.5 μg/mL and weak activity against *Candida albicans* NBRC0197 while inactive against *Escherichia coli* NIHJ JC-2 (Table 3-3). Additionally, compound **4** exhibited cytotoxicity against P388 murine leukemia cells with IC_{50} of 9.8 μM.

Table 3-3. Antimicrobial activity of TMKS8A (**4**).

Microorganism	MIC (μg/mL)
Bacillus subtilis PCI219	6.25
Kocuria rhizophila ATCC9341	6.25
Staphylococcus aureus FDA209P JC-1	12.5
Escherichia coli NIHJ JC-2	> 100
Candida albicans NBRC0197	50

3-3 Conclusion

My screening of antimicrobial substances from marine actinomycetes of Indonesia led to the discovery of one new napyradiomyinc, TMKS8 A (**4**). Napyradiomycins,

possessing halogenated meroterpenoid structure are a large class of metabolites mainly produced by bacteria of the family streptomyces, over 50 members within this class [10]. However, (*R*)-3-chloro-6,8-dihydroxy-α-lapachone [9] and (*R*)-3-chloro-6-hydroxy-8-methoxy-α-lapachone [11] were reported as the smallest unit among them, only consisting of a semi-napthoquinone and a tetrahydropyran ring. Compound **4** is thus a new member of this class.

3-4 Experimental section

3-4-1 General experimental procedures

Optical rotation was measured using a JASCO P-1030 polarimeter. The CD spectra were recorded on a Jasco J-720W spectropolarimeter. ECD spectra were visualized using GaussView 6.0.16 and Microsoft Excel. UV and IR spectra were recorded on a Shimadzu UV-1800 spectrophotometer and a PerkinElmer Spectrum 100 spectrophotometer, respectively. NMR experiments were performed on a Bruker AVANCE 500 spectrometer in DMSO-d_6, using residual solvent signals (δ_H 2.50 for ^{1}H and δ_C 39.5 for ^{13}C) as internal references. HR-ESITOF mass spectrum was recorded on a Bruker micrOTOF focus mass spectrometer. An Agilent HP1200 system equipped with a diode array detector was used for analysis and purification. Conformational searches were performed with MacroModel implemented in the Maestro 12.3 software package [12]. All DFT-based calculations were performed with the Gaussian 16 Revision B.01 program [13]. Parts of these computations were conducted using the SuperComputer System, Institute for Chemical Research, Kyoto University.

3-4-2 Microorganism

Strepromyces sp. TMKS8 was isolated from an air-breathing slug, *Paromoionchis tumidus*, collected at Mangkang mangrove forest, Semarang, Central Java, Indonesia. After washing with sterilized sea water to remove mud and contaminants, the specimen was ground using mortar and the resultant paste was diluted in sterilized sea water to the concentrations of 10^0 to 10^{-3}. In total 100 μL from each dilution were spread onto ISP 4 agar medium supplemented with nalidixic acid (2 mg/L), cyclohexamide (2 mg/L), nystatin (3 mg/L), and humus fertilizer at 2% (purchased from a local store in Semarang, Indonesia). *Streptomyces* sp, TMKS8 was collected from the dilution of 10^{-1}. The isolate was identified as a member of *Streptomyces* on the basis of 96.7% similarity in

the 16S rRNA gene sequence (1087 bp, accession number MW048810) to *Streptomyces aculeolatus* NBRC 14824^T (accession number NR_041166).

3-4-3 Fermentation

Streptomyces sp. TMKS8 growing on ISP 4 agar was transferred into a 500 mL K-1 flask containing 100 mL of V22 seed culture [soluble starch 1%, glucose 0.5%, NZ-caze (Humco Scheffield Chemical Co.) 0.3%, yeast extract (Difco Laboratories) 0.2%, Tryptone (Difco Laboratories) 0.5%, K_2HPO_4 0.1%, $MgSO_4 \cdot 7H_2O$ 0.005%, and $CaCO_3$ 0.3% in distilled water (pH 7.0)]. The seed culture was cultivated on a rotary shaker (200 r.p.m.) at 30 ˚C for 8 days. Afterward, 5 mL aliquots of the seed culture were transferred into 20 500 mL K-1 flasks containing 100 mL of A11M medium [2% glucose, 2.5% soluble starch, 0.5% yeast extract, 0.5% polypeptone, 0.5% NZ- amine, 0.5% $CaCO_3$, and 1% Diaion HP-20 (Mitsubishi Chemical Co., Yokohama, Japan) in distilled water (pH 7.0)], which were cultivated on a rotary shaker (200 r.p.m.) at 30 ˚C for 8 days.

3-4-4 Extraction and isolation

At the end of the fermentation period, 100 mL of 1-butanol was added to each flask, and the flasks were shaken for one hour. The mixture was centrifuged at 6000 rpm for 10 min, and the organic layer was separated from the aqueous layer containing the mycelium. Evaporation of the solvent gave 8.0 g of extract from 2 L of culture. The extract was subjected to silica gel column chromatography with a step gradient of $CHCl_3$/MeOH (1:0, 20:1, 10:1, 4:1, 2:1, 1:1, and 0:1 v/v). Fraction 3 (10:1) was concentrated *in vacuo* to provide 1.05 g of brown solid, which was next subjected to ODS column chromatography with a step gradient of MeCN/0.1% HCO_2H aqueous solution (2:8, 3:7, 4:6, 5:5, 6:4, 7:3, and 8:2 v/v). Fraction 2-5 (6:4) was concentrated *in vacuo* to provide 0.12 g of semi-pure material. Final purification was achieved by preparative HPLC (Cosmosil 5C-18-ARII, 10 × 250 mm, 4 mL/min, UV detection at 254 nm) with 56% MeCN in 0.1% HCO_2H solution to yield TMKS8A (**4**, 4.0 mg, t_R 18.9 min). Similarly, from fraction 7, which gave 365 mg of dried material after concentration, preparative HPLC (Cosmosil 5C-18-ARII, 10 × 250 mm, 4 mL/min, UV detection at 254 nm) with a mixture of MeCN and 0.1% HCO_2H aqueous solution (76:24) yielded A80915 C (**5**, 15.0 mg, t_R 12.5 min), SF2415B1 (**6**, 2.3 mg, t_R 13.6 min), chlorinated hydroquinone 3 (**7**, 3.0 mg, t_R 15.7 min), SF2415B3 (**8**, 11.2 mg, t_R 23.1

min), and A80915 A (**9**, 5.8 mg, t_R 24.2 min).

TMKS8A (4): orange powder; $[\alpha]^{23}_D$ -26 (*c* 0.07, $CHCl_3$); ECD (2 × 10^{-5} M, MeOH) λ_{ext} ($\Delta\varepsilon$) 222 (0), 259 (+2.2), 305 (+1.2), 385 (-0.6), 458 (+0.1) nm; UV (MeOH) λ_{max} (log ε) 217 (4.21), 264 (4.04), 315 (3.74), 422 (3.34) nm; IR ν_{max} 3417, 2926, 2856, 1665, 1624, 1432, 1332, 1098, 848, 762 cm^{-1}; ^1H and ^{13}C NMR data, Table 1; HR-ESITOFMS *m/z* 321.0517 $[M - H]^-$ (calcd for $C_{16}H_{14}{}^{35}ClO_5$, 321.0524).

3-4-5 Biological assays

Antimicrobial assay and cytotoxic assay were carried out according to the procedures previously described [14].

3-4-6 Computational procedure

The conformational search of structures **I** began by applying 10,000 steps of the Monte Carlo multiple minimum (MCMM) method with PRCG energy minimization using the OPLS3e force field without solvation to obtain 8 conformers with energies within 30 kcal/mol of the minimum energy conformer. The next optimizations were performed at the B3LYP/6-31G(d) level of theory (gas phase). Frequency calculations were carried out at the same level of theory to confirm the absence of imaginary frequencies and to obtain thermal corrections to the Gibbs free energies. After single-point energies were calculated at the B3LYP-D3BJ/6-311+G(d,p) level of theory with solvation effects using the IEFPCM model of DMSO, the thermal corrections at the B3LYP/6-31G(d) level were added to obtain the Gibbs free energies. The shielding tensors were calculated by the GIAO method at the mPW1PW91/6-31+G(d,p)-IEFPCM(DMSO) level of theory. The chemical shifts (δ_{calc}) were calculated using tetramethylsilane (TMS) as a reference standard according to $\delta_{calc} = \sigma_0 - \sigma_x$, where σ_x is the Boltzmann-averaged shielding tensor of the low-lying 4 conformers within 3.0 kcal/mol, and σ_0 is the shielding tensor of TMS calculated at the same level of theory as σ_x. The chlorinated C3-chemical shift ($\delta_{calc(correct)}$) was corrected using the following formula, $\delta_{calc(correct)} = a \cdot \delta_{calc} + b$, where $a = 0.8498$ and $b = -1.2917$. Factors *a* and *b* were determined by a linear regression procedure using our own data set for Cl-substituted sp^3-carbon shifts of 10 compounds in the DMSO-d_6 solvent, (see Figure S9) [15-17]. The calculation of structure **II** was similarly performed using 8 conformers for the DFT optimization, 4 conformers for the chemical shifts calculation, respectively.

The C3-chemical shift was corrected by using the above scaling factors. For the ECD simulation of **4**, single-point energies of **I** were re-evaluated at the at the B3LYP-D3BJ/6-311+G(d,p)-IEFPCM level using methanol as the solvent, and the thermal corrections at the B3LYP/6-31G(d) level were added to afford 4 conformers within 3.0 kcal/mol from the minimum Gibbs free energy. The ECD spectra of the **4** structures were simulated by the calculation of 25 states using TD-DFT at the ωB97X-D/def2-TZVP-IEFPCM(MeOH) level of theory, and were averaged based on their Boltzmann distribution. The calculated ECD spectra were red-shifted by 10 nm.

References

1) Sayed, A. M.; Hassan, M. H. A.; Alhadrami, H. A.; Hassan, H. M.; Goodfellow, M.; Rateb, M. E. *J. Appl. Microbiol.* **2020,** *128,* 630-657.
2) Blunt, J. W.; Carroll, A. R.; Copp, B. R.; Davis, R. A.; Keyzers, R. A.; Prinsep, M. R. *Nat. Prod. Rep.* **2018**, *35*, 8-53.
3) Hanif, N.; Murni, A.; Tanaka, C.; Tanaka, J. *Mar. Drugs.* 2019, 17, 364.
4) Tanaka, J. *J. Phys. Conf. Ser.* **2020**, *1460*, 012079.
5) Sibero, M. T.; Zhou, T.; Fukaya, K.; Urabe, D.; Radjasa, O. K. K.; Sabdono, A. et al. *Beilstein. J. Org. Chem.* **2019**, *15*, 2941-2947.
6) Karim, M. R. U.; Harunari, E.; Sharma, A. R.; Oku, N.; Akasaka, K.; Urabe, D. et al. *Beilstein. J. Org. Chem.* **2020**, *16*, 2719-2727.
7) Motohashi, K.; Sue, M.; Furihata, K.; Ito, S.; Seto, H. *J. Nat. Prod.* **2008**, *71*, 595-601.
8) Lodewyk, M. W.; Siebert, M. R.; Tantillo, D. J. *Chem. Rev.* **2012**, *112*, 1839-1862.
9) Wu, Z. C.; Li, S.; Li, J.; Chen, Y.; Saurav, K.; Zhang, Q. et al. *Mar Drugs.* **2013**, *11*, 2113-2125.
10) Ahmadi, E. S.; Tajbakhsh, A.; Iranshahy, M.; Asili, J.; Kretschmer, N.; Shakeri, A.; *Mini. Rev. Med. Chem.* **2020**, *20*, 2019-2035.
11) Motohashi, K.; Sue, M.; Furihata, K.; Ito, S.; Seto, H. *J. Nat. Prod.* **2008**, *71*, 595–601.
12) MacroModel, Schrödinger, LLC: New York, NY, 2020.
13) Gaussian 16, Revision B.01; Gaussian, Inc.: Wallingford, CT, 2016.
14) Karim, M. R. U.; Harunari, E.; Oku, N.; Akasaka, K.; Igarashi, Y. *J. Nat. Prod*. **2020**, *83*, 1295−1299.
15) Sugimura, N.; Furuya, A.; Yatsu, T.; Shibue, T. *Bunseki Kagaku* **2015**, *64*,147-150.
16) Shepherd, E. D.; et al. *J. Org. Chem.* **2019**, *84*, 4971-4991.
17) Braddock, D. C.; Rzepa, H. S. *J. Nat. Prod.* **2008**, *71*, 728-730.

3-5 Spectral data

Table of contents

Figure S1. UV spectrum of TMKS8A (**4**).

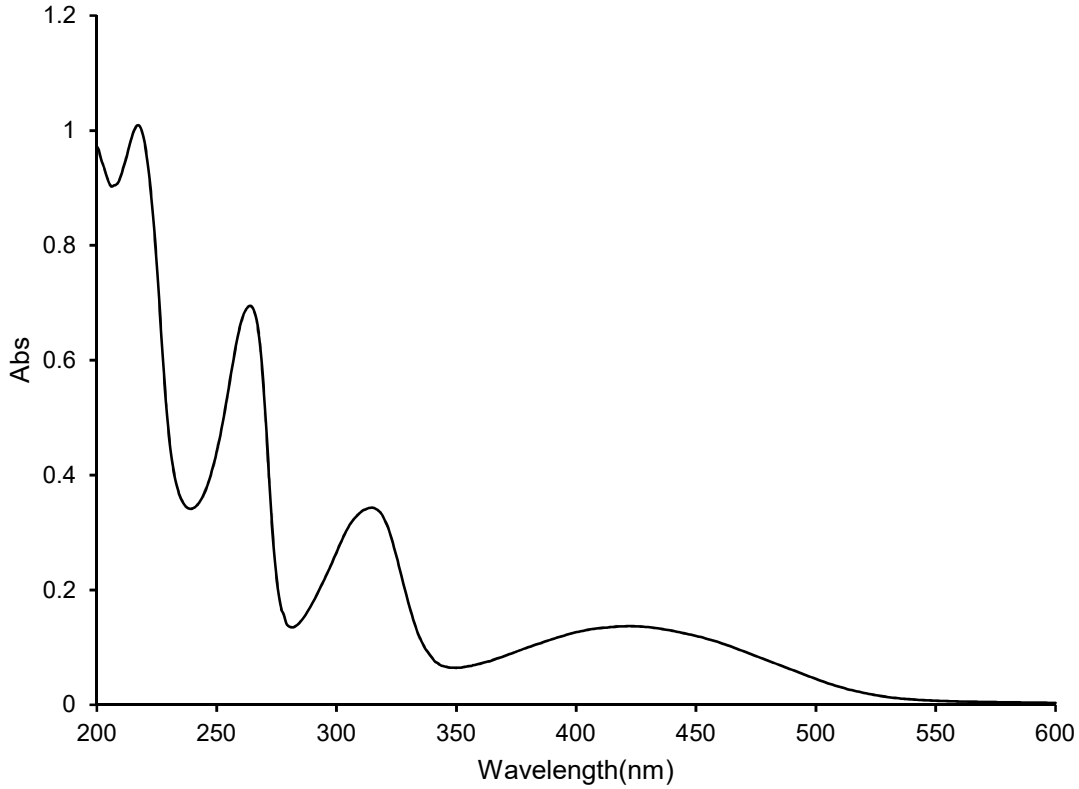

Figure S2. IR spectrum of **4**.

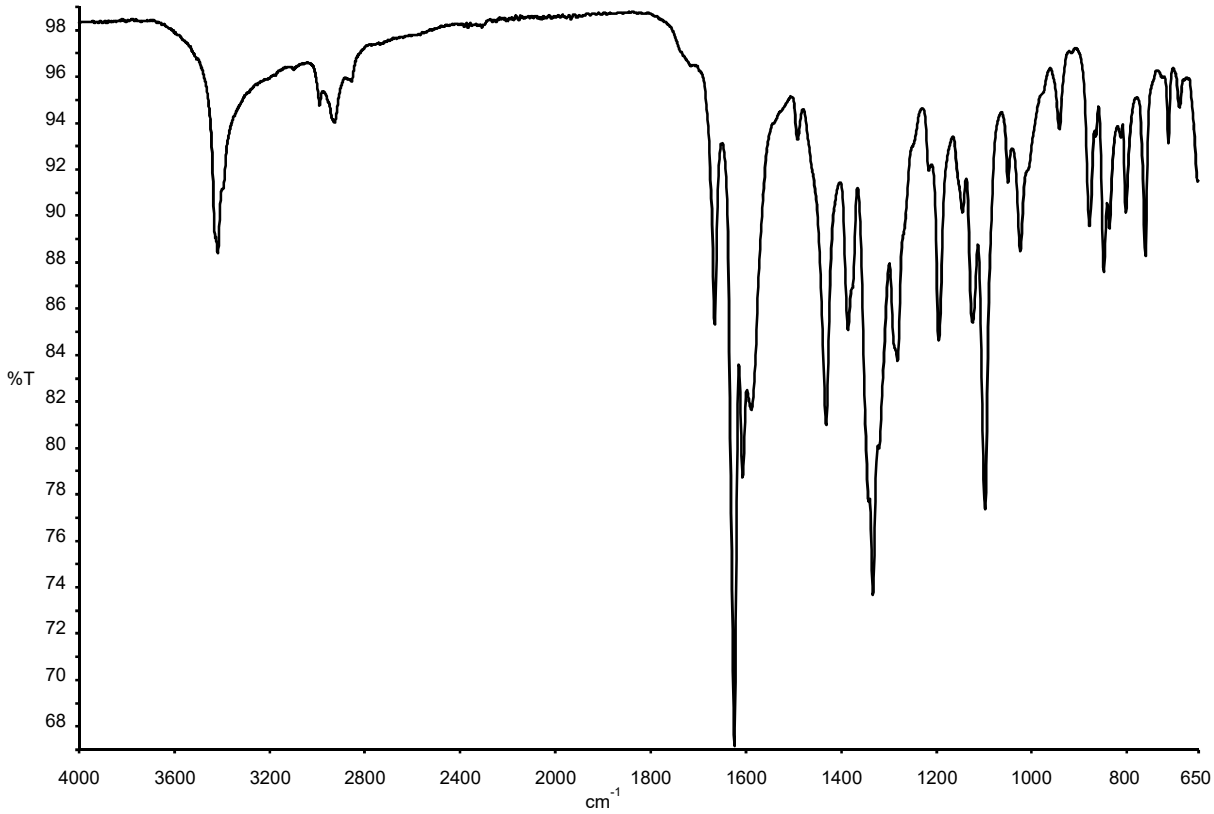

Figure S3. ^{1}H NMR spectrum of **4** (500 MHz, DMSO-d_6).

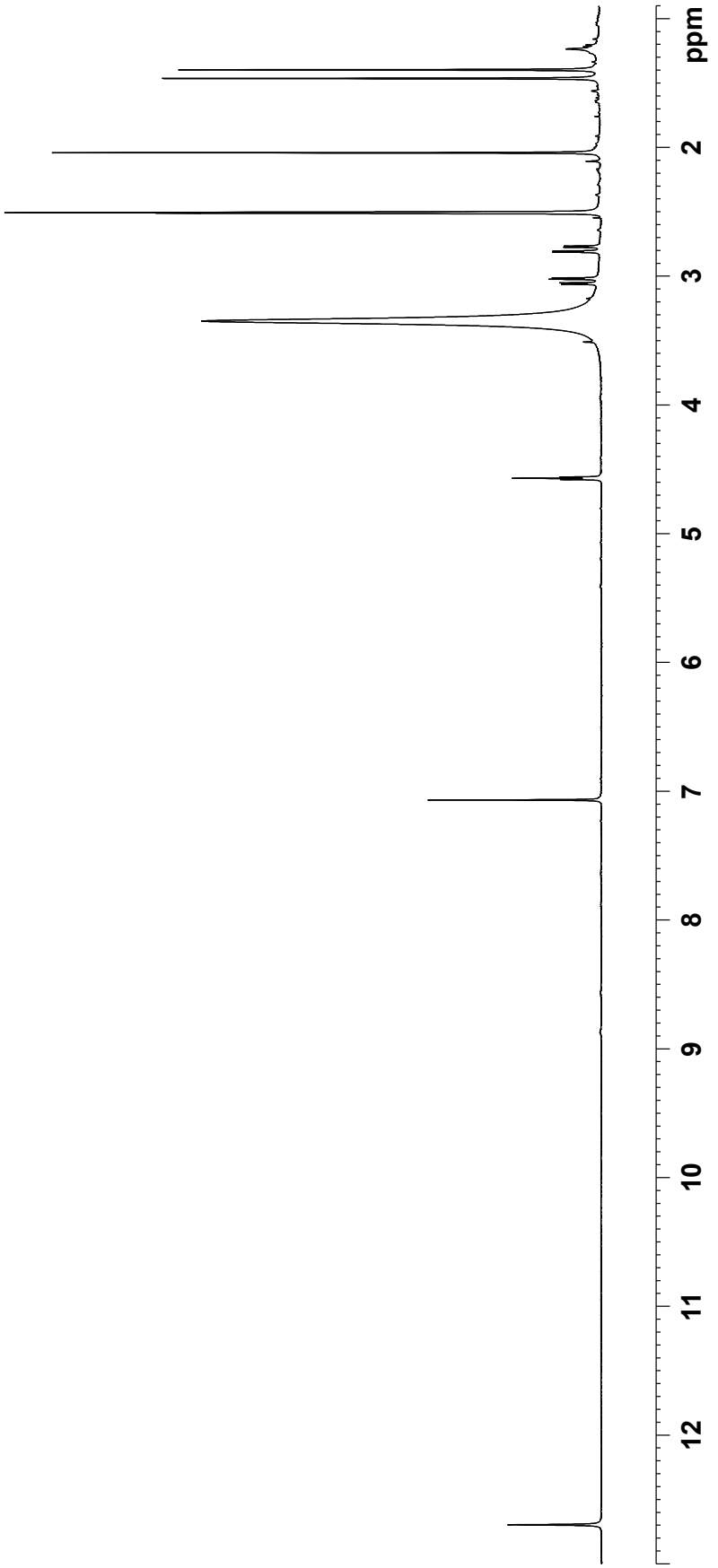

Figure S4. ^{13}C NMR spectrum of **4** (125 MHz, DMSO-d_6).

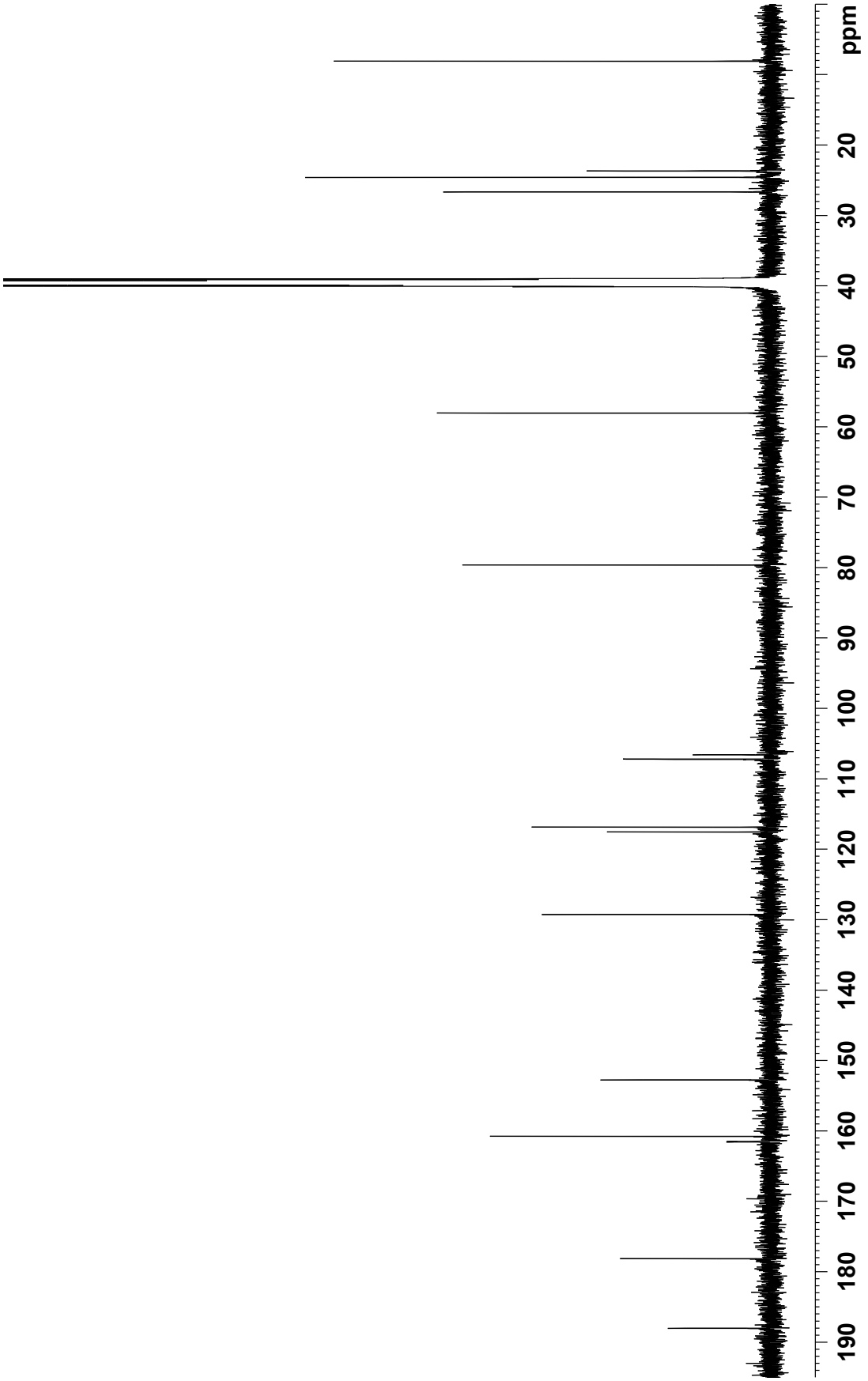

Figure S5. COSY spectrum of **4** (500 MHz, DMSO-d_6).

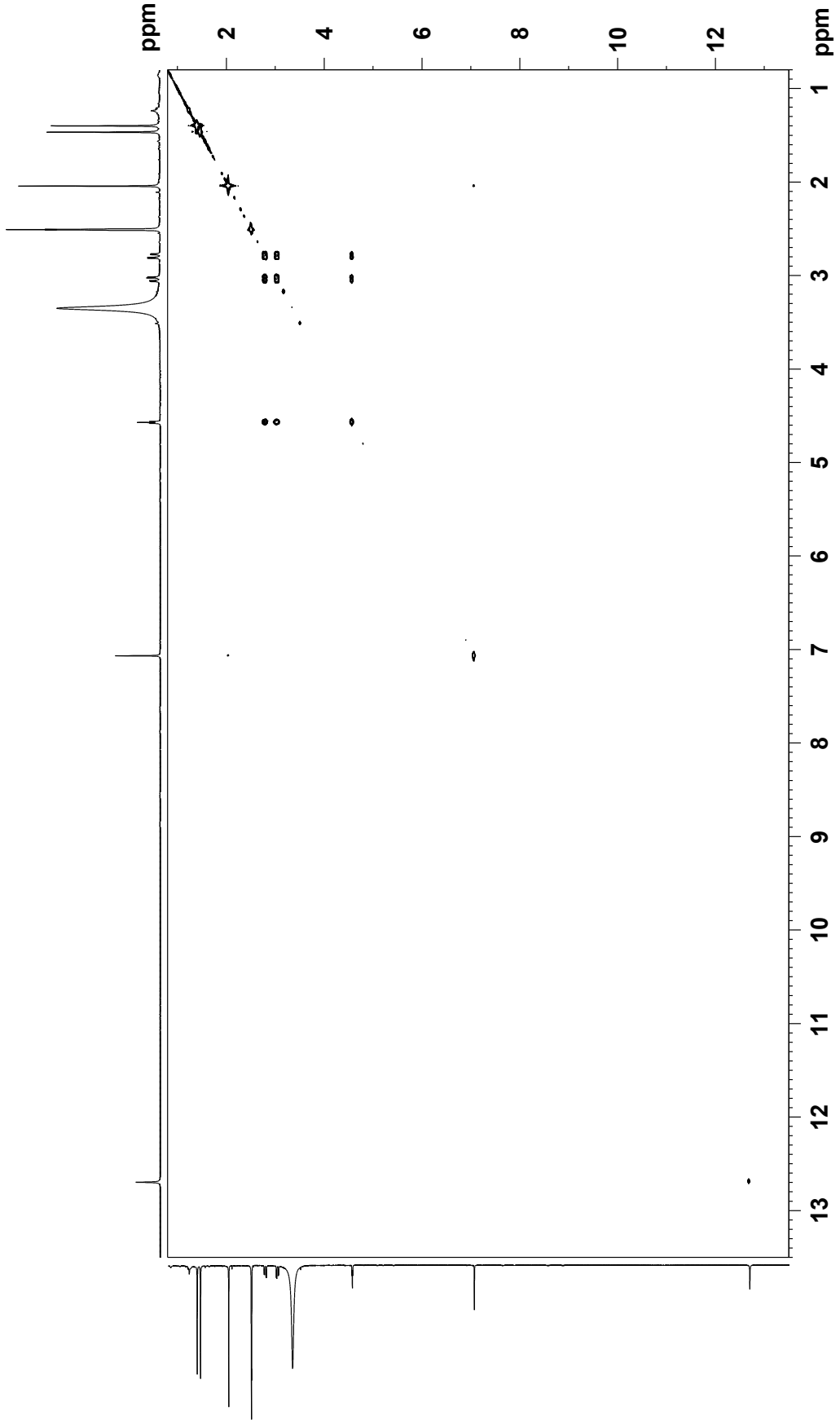

Figure S6. HSQC spectrum of **4** (500 MHz, DMSO-d_6).

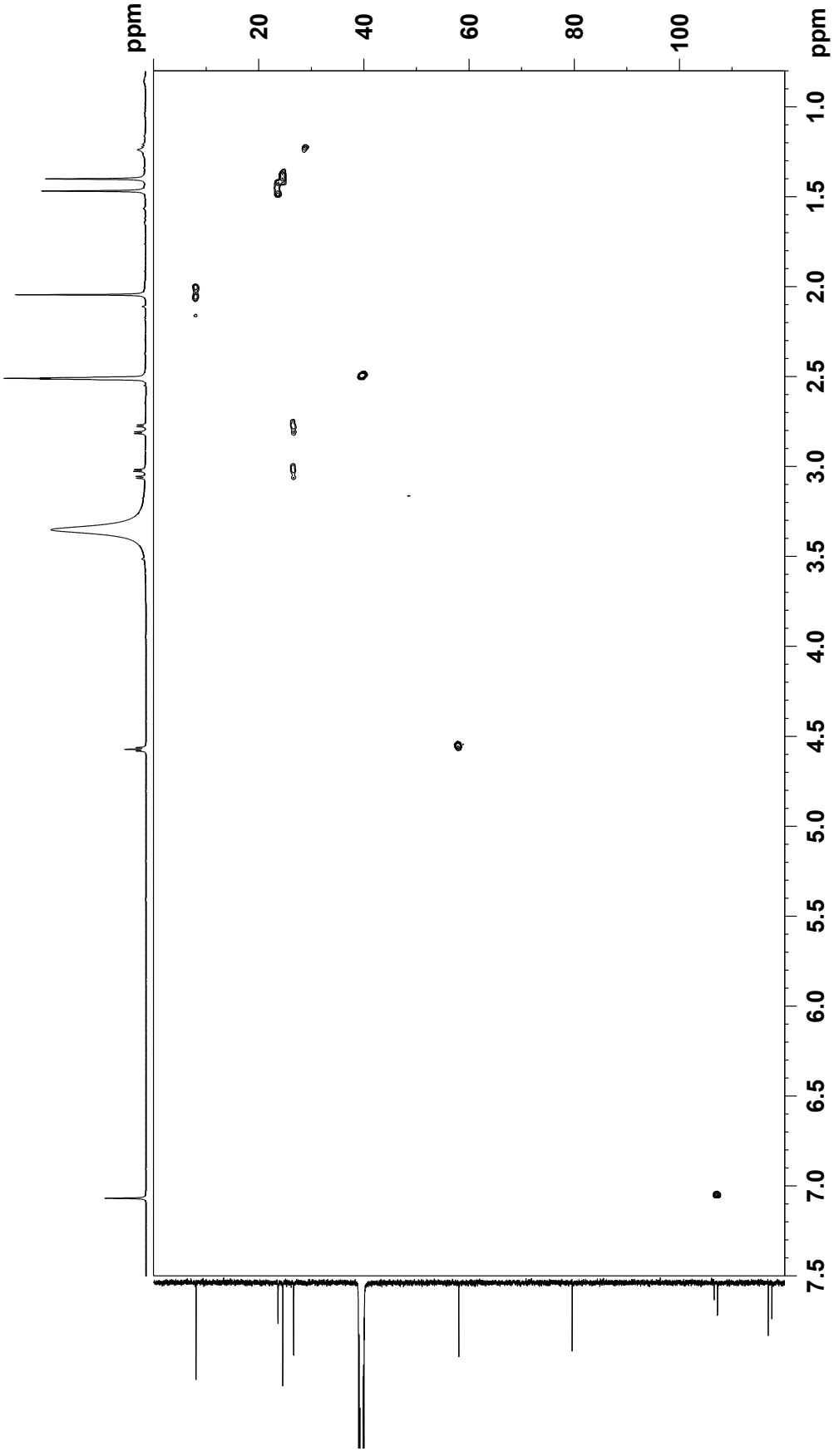

Figure S7. HMBC spectrum of **4** (500 MHz, DMSO-d_6).

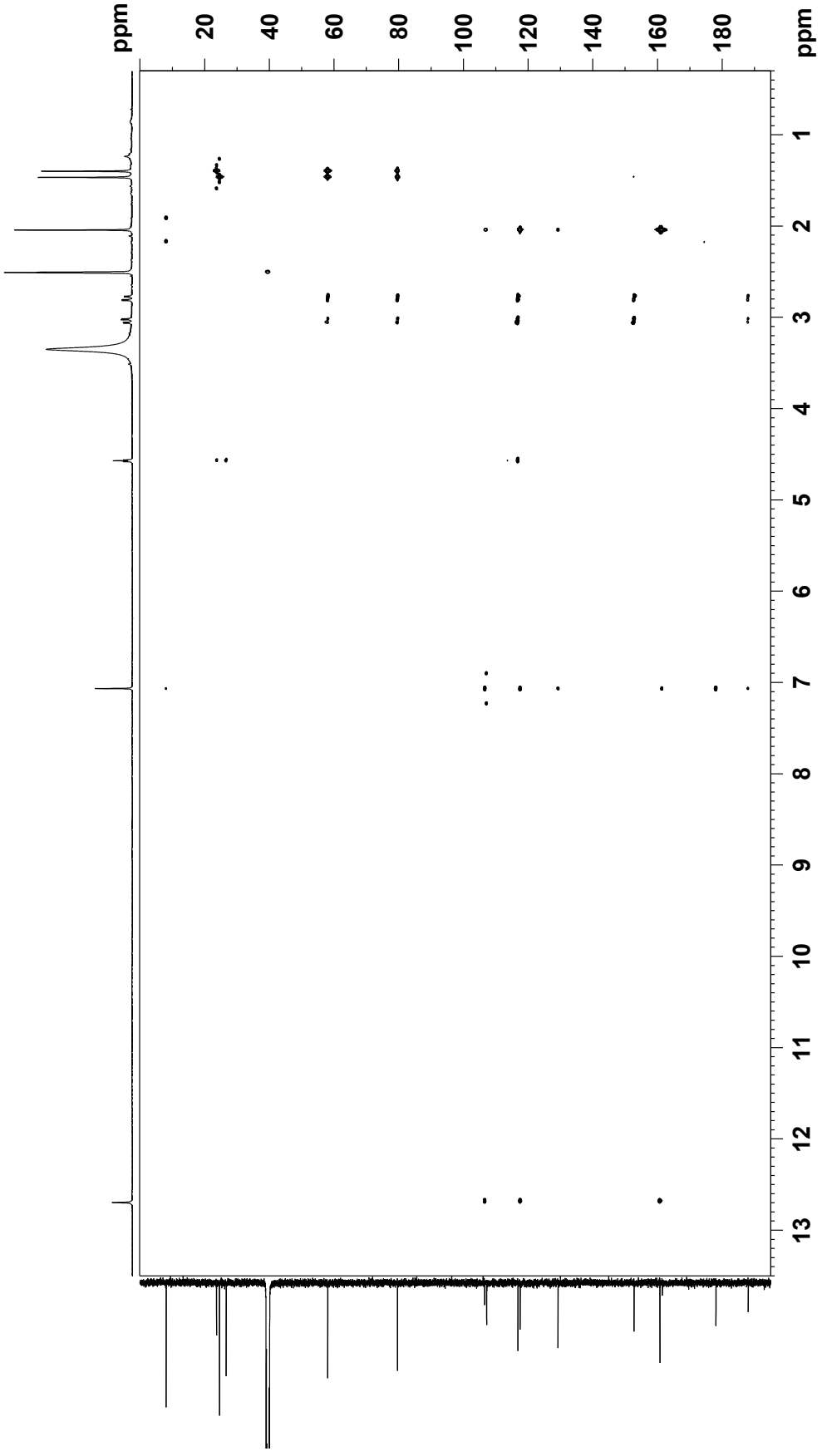

Figure S8. NOESY spectrum of **4** (500 MHz, DMSO-d_6).

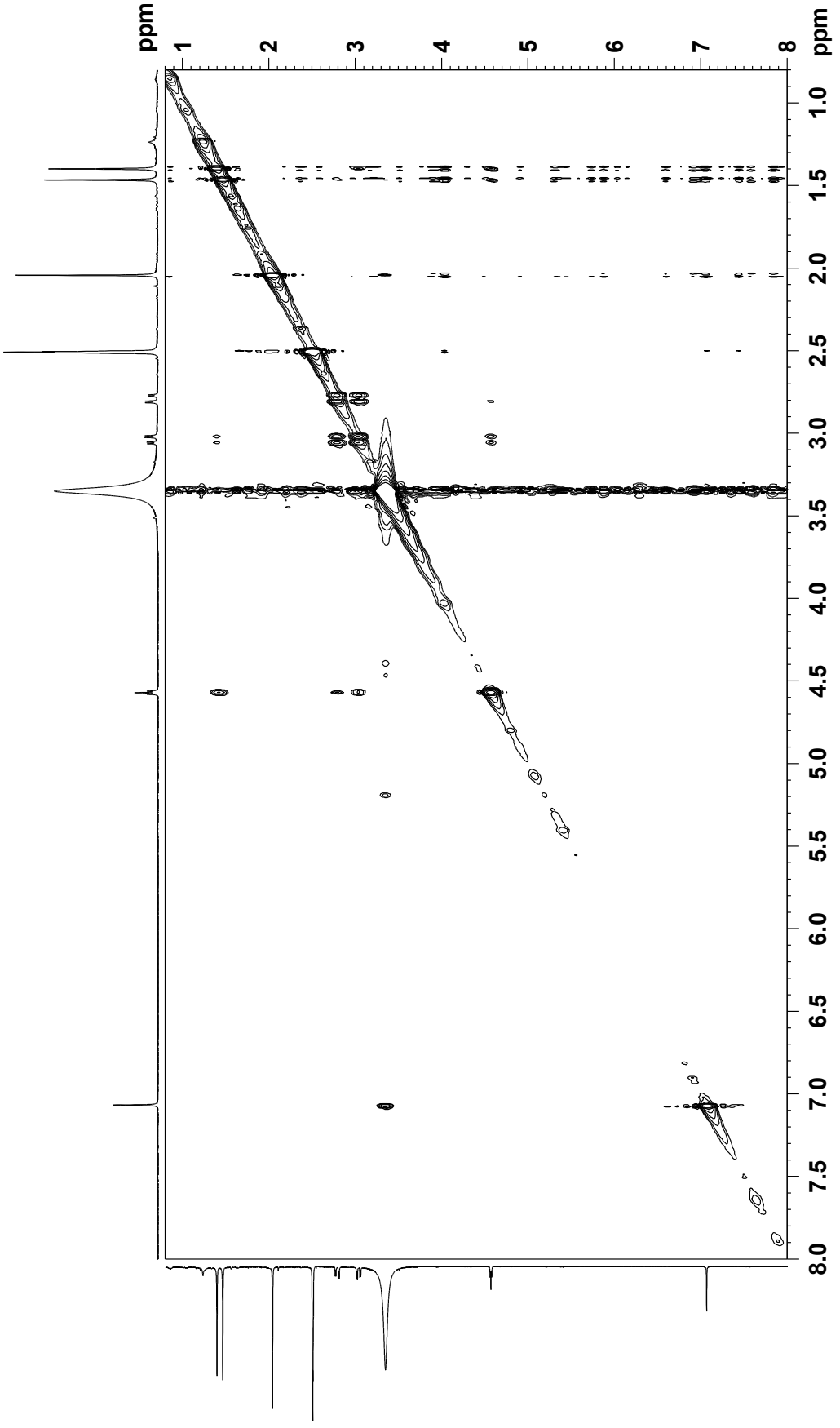

Figure S9. Determination of the scaling factors for the correction of Cl-substituted ^{13}C chemical shifts.

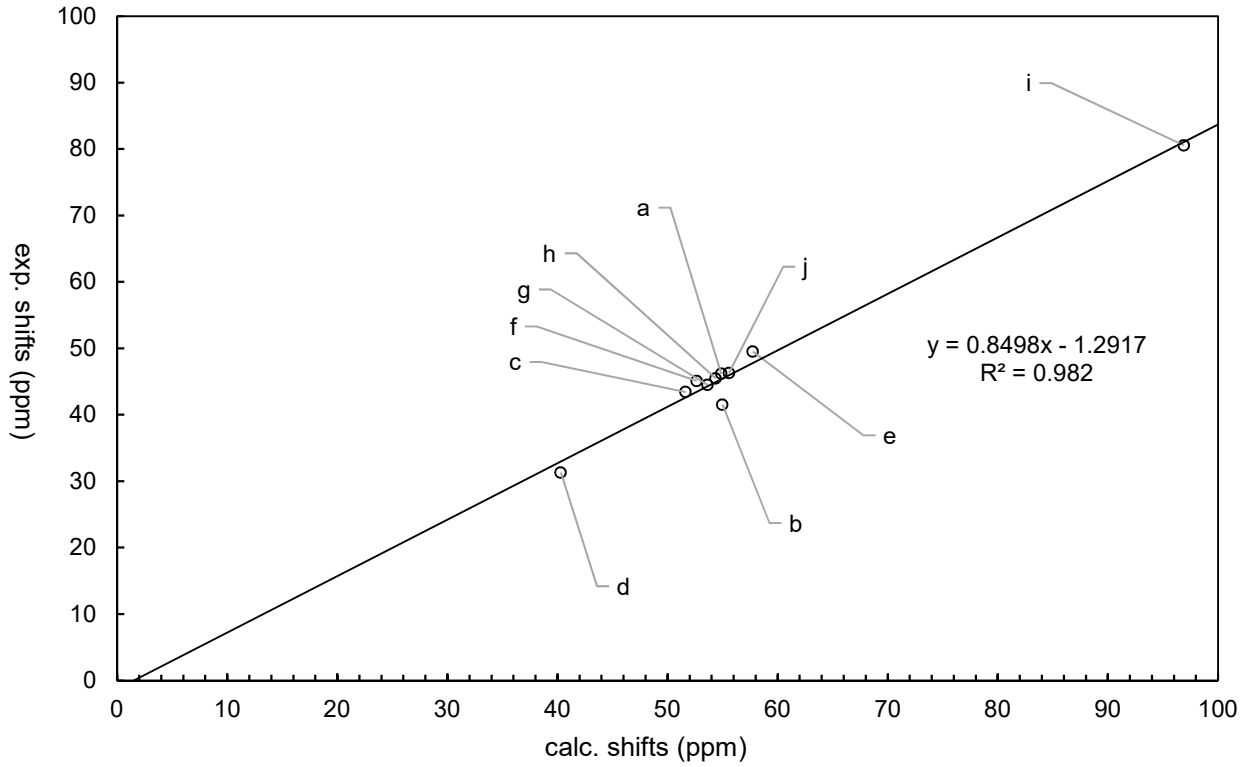

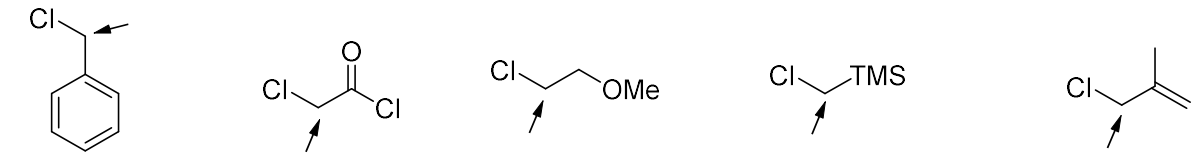

a
exp. 46.2
calc. 54.9

b
exp. 41.5
calc. 55.0

c
exp. 43.4
calc. 51.6

d
exp. 31.3
calc. 40.3

e
exp. 49.5
calc. 57.7

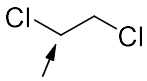

f
exp. 45.1
calc. 52.6

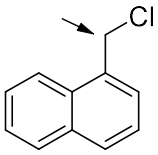

g
exp. 44.5
calc. 53.6

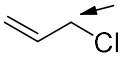

h
exp. 45.5
calc. 54.4

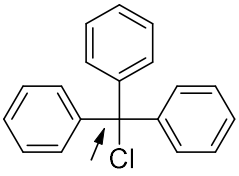

i
exp. 80.5
calc. 96.9

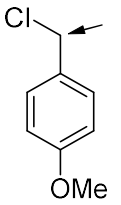

j
exp. 46.3
calc. 55.6

Exp. means experimental chemical shifts for the indicated carbon atoms in DMSO-d_6. The NMR spectra were recorded on a Bruker AVANCE 400 spectrometer, and tetramethylsilane was used as internal reference. Calc. means calculated chemical shifts for the indicated carbon atoms using the same procedure and level of theory as for the calculation of structures **I** and **II** as described in Experimental Section.

Table S1. Structure, energy and Cartesian coordinate of **structure I-1**.

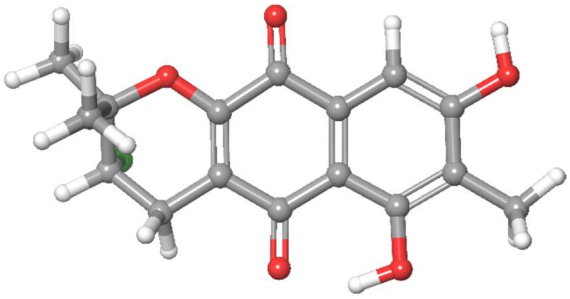

structure I-1 (Boltzmann population: 57%)

B3LYP-D3BJ/6-311+G(d,p)-IEFPCM(DMSO)//B3LYP/6-31G(d):			
Gibbs Free Energy (a.u.)	=	−1455.250610	
B3LYP-D3BJ/6-311+G(d,p)-IEFPCM(DMSO):			
Electronic energy (a.u.)	=	−1455.487910	
B3LYP/6-31G(d):			
Zero-point correction (a.u.)	=	0.285614	
Thermal correction to Energy (a.u.)	=	0.305529	
Thermal correction to Enthalpy (a.u.)	=	0.306473	
Thermal correction to Gibbs Free Energy (a.u.)	=	0.237300	

C	2.651600	−1.126892	−1.221340	C	2.856896	−2.499807	−1.444121
C	1.863176	−3.445832	−1.172755	C	0.631748	−2.979573	−0.663071
C	0.403374	−1.600973	−0.431671	C	1.437384	−0.685399	−0.721593
O	−0.309578	−3.900605	−0.409756	C	2.062292	−4.919131	−1.405057
O	4.043624	−2.957698	−1.935548	C	−0.882720	−1.134250	0.087147
C	−1.087245	0.302675	0.311959	C	−0.091713	1.191797	0.056683
C	1.244859	0.770863	−0.486535	O	−1.813062	−1.929567	0.344599
O	2.115402	1.598774	−0.708410	C	−2.432616	0.764917	0.802762
C	−2.604191	2.266044	0.567108	C	−1.330912	3.048999	0.957287
O	−0.179832	2.518889	0.240550	C	−1.378230	4.528624	0.585311
C	−1.061774	2.885714	2.464450	Cl	−3.051877	2.546297	−1.187622
H	3.429121	−0.397736	−1.433363	H	−1.103872	−3.405330	−0.068810
H	1.944123	−5.478318	−0.469439	H	1.305107	−5.306976	−2.096274
H	3.052351	−5.122710	−1.814532	H	4.634944	−2.203327	−2.084310
H	−3.225691	0.202762	0.303512	H	−2.548814	0.551808	1.874750
H	−3.450173	2.658306	1.134205	H	−2.214888	5.019687	1.093627
H	−0.448168	5.012673	0.897028	H	−1.495440	4.658558	−0.491471
H	−1.907558	3.262112	3.050125	H	−0.885433	1.842876	2.739979
H	−0.172214	3.461751	2.734598				

Table S2. Structure, energy and Cartesian coordinate of **structure I-2**:

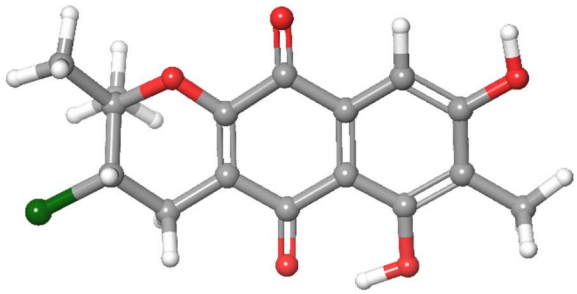

structure I-2 (Boltzmann population: 23%)

B3LYP-D3BJ/6-311+G(d,p)-IEFPCM(DMSO)//B3LYP/6-31G(d):		
Gibbs Free Energy (a.u.)	=	−1455.249758
B3LYP-D3BJ/6-311+G(d,p)-IEFPCM(DMSO):		
Electronic energy (a.u.)	=	−1455.486904
B3LYP/6-31G(d):		
Zero-point correction (a.u.)	=	0.285529
Thermal correction to Energy (a.u.)	=	0.305572
Thermal correction to Enthalpy (a.u.)	=	0.306516
Thermal correction to Gibbs Free Energy (a.u.)	=	0.237145

C	2.800070	−1.247256	−0.672195	C	2.958200	−2.590622	−1.056065
C	1.875601	−3.474948	−1.101545	C	0.602854	−2.976762	−0.746800
C	0.420675	−1.626691	−0.358422	C	1.544650	−0.773495	−0.327955
O	−0.422308	−3.839725	−0.793810	C	2.023521	−4.916003	−1.508385
O	4.183660	−3.078945	−1.400173	C	−0.904384	−1.130408	0.014847
C	−1.056087	0.276346	0.413274	C	0.014363	1.113077	0.424467
C	1.400700	0.652753	0.069242	O	−1.909470	−1.873695	0.006584
O	2.343398	1.428937	0.108073	C	−2.420341	0.762219	0.829008
C	−2.277193	2.076986	1.590000	C	−1.335002	3.074853	0.874266
O	−0.030740	2.411594	0.763173	C	−1.790393	3.451296	−0.538284
C	−1.045680	4.310289	1.722376	Cl	−3.920616	2.807762	1.885536
H	3.646089	−0.565826	−0.639827	H	−1.231757	−3.332900	−0.510923
H	1.677611	−5.580867	−0.708451	H	1.403287	−5.136268	−2.385129
H	3.061717	−5.154392	−1.742025	H	4.839471	−2.368377	−1.323345
H	−3.070325	0.892542	−0.045246	H	−2.908914	0.009355	1.454545
H	−1.870682	1.890312	2.587134	H	−2.759606	3.956225	−0.504792
H	−1.057171	4.127741	−0.986828	H	−1.880748	2.572278	−1.182995
H	−1.941688	4.927901	1.819661	H	−0.705701	4.022747	2.722420
H	−0.257061	4.901969	1.248589				

Table S3. Structure, energy and Cartesian coordinate of **structure I-3**:

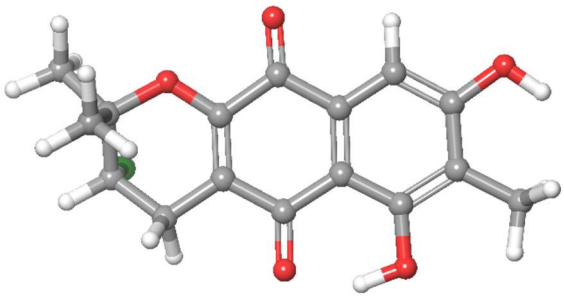

structure I-3 (Boltzmann population: 14%)

B3LYP-D3BJ/6-311+G(d,p)-IEFPCM(DMSO)//B3LYP/6-31G(d):			
Gibbs Free Energy (a.u.)	=	−1455.249321	
B3LYP-D3BJ/6-311+G(d,p)-IEFPCM(DMSO):			
Electronic energy (a.u.)	=	−1455.487466	
B3LYP/6-31G(d):			
Zero-point correction (a.u.)	=	0.285653	
Thermal correction to Energy (a.u.)	=	0.305419	
Thermal correction to Enthalpy (a.u.)	=	0.306364	
Thermal correction to Gibbs Free Energy (a.u.)	=	0.238145	

C	2.691270	−0.990731	−1.241475	C	2.932955	−2.356511	−1.466355
C	1.971731	−3.335730	−1.190772	C	0.726526	−2.917555	−0.671536
C	0.461544	−1.545739	−0.437459	C	1.466234	−0.595925	−0.733109
O	−0.191529	−3.860272	−0.409802	C	2.253369	−4.796400	−1.441190
O	4.156551	−2.675646	−1.967166	C	−0.834569	−1.121789	0.091322
C	−1.085616	0.305863	0.321085	C	−0.122368	1.228383	0.060549
C	1.224434	0.854344	−0.492510	O	−1.738122	−1.947660	0.354310
O	2.062577	1.712989	−0.716782	C	−2.442203	0.721528	0.822907
C	−2.666207	2.216408	0.591632	C	−1.417121	3.041239	0.973485
O	−0.254213	2.551071	0.247780	C	−1.516757	4.518904	0.604035
C	−1.131474	2.885270	2.478407	Cl	−3.137176	2.484299	−1.158963
H	3.456572	−0.256667	−1.464472	H	−0.995002	−3.379827	−0.062170
H	1.388231	−5.401901	−1.169076	H	2.473946	−4.993837	−2.500109
H	3.106910	−5.155294	−0.848204	H	4.218231	−3.636388	−2.085998
H	−3.219673	0.133909	0.328510	H	−2.542980	0.502823	1.895333
H	−3.520456	2.578861	1.166134	H	−2.365810	4.980989	1.118951
H	−0.601216	5.033435	0.909802	H	−1.645791	4.646117	−0.471717
H	−1.984757	3.233020	3.070895	H	−0.918765	1.848502	2.751188
H	−0.259277	3.489916	2.742537				

Table S4. Structure, energy and Cartesian coordinate of **structure I-4**:

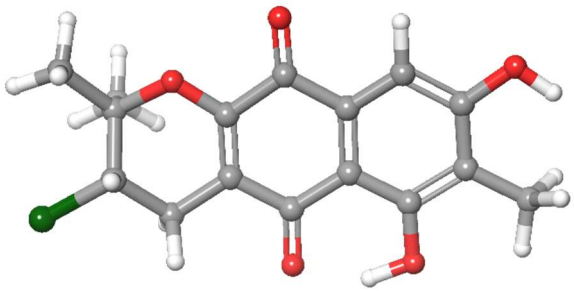

structure I-4 (Boltzmann population: 6%)

B3LYP-D3BJ/6-311+G(d,p)-IEFPCM(DMSO)//B3LYP/6-31G(d):		
Gibbs Free Energy (a.u.)	=	−1455.248472
B3LYP-D3BJ/6-311+G(d,p)-IEFPCM(DMSO):		
Electronic energy (a.u.)	=	−1455.486449
B3LYP/6-31G(d):		
Zero-point correction (a.u.)	=	0.285570
Thermal correction to Energy (a.u.)	=	0.305466
Thermal correction to Enthalpy (a.u.)	=	0.306410
Thermal correction to Gibbs Free Energy (a.u.)	=	0.237977

C	2.855320	−1.122685	−0.637975	C	3.046257	−2.458461	−1.030442
C	1.987359	−3.371119	−1.097073	C	0.694676	−2.915974	−0.754780
C	0.479285	−1.573071	−0.357786	C	1.583111	−0.690672	−0.306636
O	−0.315819	−3.795883	−0.817825	C	2.216401	−4.800748	−1.520397
O	4.320379	−2.815953	−1.343146	C	−0.861962	−1.114477	0.003090
C	−1.056882	0.282994	0.411342	C	−0.009782	1.148246	0.443003
C	1.393475	0.729346	0.101960	O	−1.848726	−1.883635	−0.023843
O	2.311458	1.531861	0.160702	C	−2.439034	0.727979	0.813967
C	−2.341150	2.039483	1.587608	C	−1.417733	3.068630	0.892131
O	−0.094877	2.441773	0.791847	C	−1.865666	3.444979	−0.522833
C	−1.172336	4.303997	1.754085	Cl	−4.007606	2.722675	1.868523
H	3.696057	−0.440219	−0.596980	H	−1.136913	−3.301355	−0.538260
H	2.914582	−5.318786	−0.847304	H	1.277727	−5.355587	−1.508029
H	2.623575	−4.864294	−2.539742	H	4.342049	−3.751157	−1.599929
H	−3.081529	0.848263	−0.067225	H	−2.914590	−0.043164	1.427121
H	−1.942124	1.855343	2.588223	H	−2.848278	3.923817	−0.497258
H	−1.145138	4.144313	−0.956570	H	−1.924665	2.569435	−1.175853
H	−2.085787	4.896509	1.845200	H	−0.837051	4.017013	2.755867
H	−0.394063	4.920583	1.295219				

Table S5. Structure, energy and Cartesian coordinate of **structure II-1**:

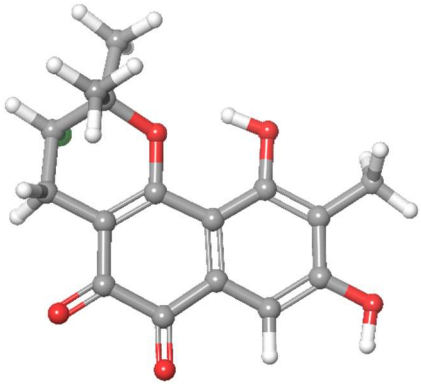

structure II-1 (Boltzmann population: 49%)

B3LYP-D3BJ/6-311+G(d,p)-IEFPCM(DMSO)//B3LYP/6-31G(d):		
Gibbs Free Energy (a.u.)	=	−1455.238363
B3LYP-D3BJ/6-311+G(d,p)-IEFPCM(DMSO):		
Electronic energy (a.u.)	=	−1455.475697
B3LYP/6-31G(d):		
Zero-point correction (a.u.)	=	0.285430
Thermal correction to Energy (a.u.)	=	0.305484
Thermal correction to Enthalpy (a.u.)	=	0.306428
Thermal correction to Gibbs Free Energy (a.u.)	=	0.237334

C	0.684893	1.140627	−3.245298	C	−0.105058	0.156002	−3.850366
C	−0.748142	−0.820410	−3.084509	C	−0.584720	−0.791100	−1.682744
C	0.207172	0.196155	−1.042757	C	0.840669	1.159161	−1.867891
O	−1.238372	−1.775568	−1.022537	C	−1.598677	−1.894425	−3.708599
O	−0.273942	0.113776	−5.203400	C	1.881154	2.236989	0.253492
C	1.197380	1.212770	1.026463	C	0.407035	0.284978	0.407765
C	1.690605	2.230646	−1.278962	O	−0.267216	−0.667548	1.122267
O	2.233429	3.083384	−1.958641	C	1.420100	1.212763	2.516030
C	0.973810	−0.100816	3.150883	C	−0.381012	−0.557472	2.576868
O	2.591358	3.092344	0.768616	C	−0.817415	−1.943136	3.044965
C	−1.469581	0.482799	2.890991	Cl	2.265557	−1.374310	2.894850
H	1.189294	1.904943	−3.830698	H	−1.053782	−1.676607	−0.068764
H	−2.625325	−1.848678	−3.326978	H	−1.621378	−1.792351	−4.794034
H	−1.216028	−2.889293	−3.453360	H	0.230239	0.838670	−5.604978
H	2.476012	1.401801	2.727229	H	0.875093	2.040977	2.991237
H	0.887453	−0.007709	4.235116	H	−0.914886	−1.953812	4.135500
H	−1.792493	−2.193334	2.614401	H	−0.093048	−2.705441	2.753737
H	−1.567350	0.617363	3.973523	H	−1.252307	1.452860	2.438402
H	−2.430521	0.133000	2.502183				

Table S6. Structure, energy and Cartesian coordinate of **structure II-2**:

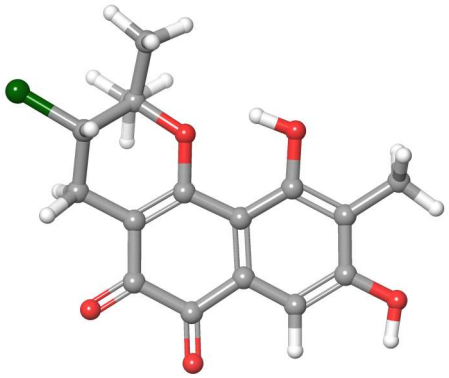

structure II-2 (Boltzmann population: 21%)

B3LYP-D3BJ/6-311+G(d,p)-IEFPCM(DMSO)//B3LYP/6-31G(d):		
Gibbs Free Energy (a.u.)	=	−1455.237564
B3LYP-D3BJ/6-311+G(d,p)-IEFPCM(DMSO):		
Electronic energy (a.u.)	=	−1455.474739
B3LYP/6-31G(d):		
Zero-point correction (a.u.)	=	0.285354
Thermal correction to Energy (a.u.)	=	0.305532
Thermal correction to Enthalpy (a.u.)	=	0.306476
Thermal correction to Gibbs Free Energy (a.u.)	=	0.237175

C	0.700076	1.126062	−3.260133	C	−0.273192	0.305543	−3.842982
C	−1.097238	−0.503190	−3.055150	C	−0.926181	−0.474516	−1.654353
C	0.050868	0.347443	−1.036845	C	0.858453	1.148348	−1.883165
O	−1.766589	−1.285630	−0.970334	C	−2.152446	−1.394128	−3.654435
O	−0.451335	0.265911	−5.194479	C	2.079683	2.070590	0.216546
C	1.208426	1.218427	1.011941	C	0.281269	0.414762	0.410364
C	1.912380	2.036188	−1.318993	O	−0.540461	−0.395940	1.146233
O	2.630144	2.727229	−2.019443	C	1.363829	1.279691	2.511479
C	0.148946	0.664072	3.190489	C	−0.238489	−0.691275	2.559752
O	2.922524	2.806835	0.713746	C	0.874127	−1.740262	2.597964
C	−1.553411	−1.236406	3.109710	Cl	0.440235	0.496639	4.982285
H	1.348000	1.756851	−3.863121	H	−1.568725	−1.193107	−0.018209
H	−3.144606	−1.136296	−3.266339	H	−2.165132	−1.307065	−4.741315
H	−1.975557	−2.441751	−3.384735	H	0.180514	0.871669	−5.612589
H	2.279724	0.765747	2.829485	H	1.486222	2.321790	2.822042
H	−0.712673	1.331075	3.106639	H	1.137003	−1.973223	3.633345
H	0.531451	−2.658198	2.110838	H	1.773683	−1.394578	2.081939
H	−1.436424	−1.516761	4.158969	H	−2.347829	−0.486885	3.035205
H	−1.857269	−2.125659	2.547649				

Table S7. Structure, energy and Cartesian coordinate of **structure II-3**:

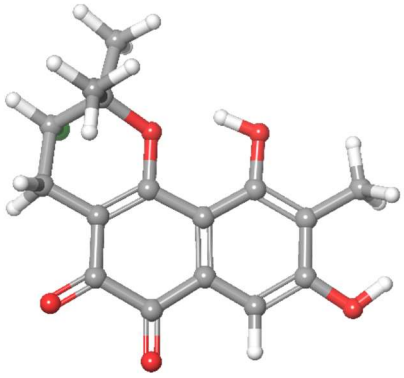

structure II-3 (Boltzmann population: 21%)

B3LYP-D3BJ/6-311+G(d,p)-IEFPCM(DMSO)//B3LYP/6-31G(d):		
Gibbs Free Energy (a.u.)	=	−1455.237563
B3LYP-D3BJ/6-311+G(d,p)-IEFPCM(DMSO):		
Electronic energy (a.u.)	=	−1455.474813
B3LYP/6-31G(d):		
Zero-point correction (a.u.)	=	0.285334
Thermal correction to Energy (a.u.)	=	0.305385
Thermal correction to Enthalpy (a.u.)	=	0.306329
Thermal correction to Gibbs Free Energy (a.u.)	=	0.237250

C	0.793193	1.253943	−3.196514	C	0.009675	0.288760	−3.838684
C	−0.657653	−0.703647	−3.113625	C	−0.530321	−0.717463	−1.706987
C	0.255096	0.249897	−1.029636	C	0.914560	1.230779	−1.817364
O	−1.201637	−1.709758	−1.074285	C	−1.493570	−1.739319	−3.825892
O	−0.066228	0.366359	−5.195130	C	1.918916	2.242648	0.356624
C	1.210089	1.204088	1.086472	C	0.424874	0.300837	0.426601
C	1.760170	2.280609	−1.178502	O	−0.273069	−0.662803	1.105013
O	2.322726	3.148378	−1.820256	C	1.401161	1.164184	2.579954
C	0.926073	−0.158279	3.173642	C	−0.420338	−0.584686	2.558477
O	2.625075	3.076453	0.911132	C	−0.883809	−1.975325	2.983949
C	−1.503603	0.461338	2.871777	Cl	2.208199	−1.441280	2.916324
H	1.305599	2.017674	−3.769770	H	−1.032114	−1.626604	−0.115678
H	−1.934858	−2.437044	−3.114770	H	−2.316889	−1.277315	−4.389546
H	−0.891971	−2.327273	−4.533937	H	−0.628063	−0.348815	−5.531731
H	2.454559	1.335262	2.817384	H	0.856434	1.987604	3.063745
H	0.816432	−0.089607	4.257603	H	−1.006969	−2.009799	4.071385
H	−1.851455	−2.203664	2.525301	H	−0.161641	−2.739509	2.692138
H	−1.624276	0.572677	3.954633	H	−1.264811	1.438592	2.446412
H	−2.459556	0.132108	2.453742				

Table S8. Structure, energy and Cartesian coordinate of **structure II-4**:

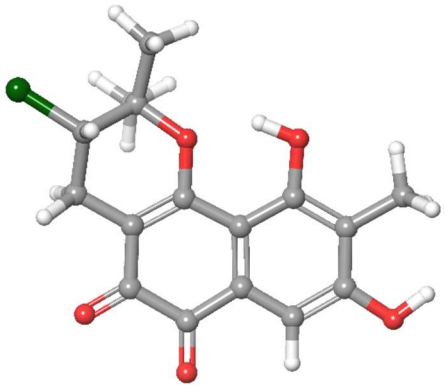

structure II-4 (Boltzmann population: 9%)

B3LYP-D3BJ/6-311+G(d,p)-IEFPCM(DMSO)//B3LYP/6-31G(d):		
Gibbs Free Energy (a.u.)	=	−1455.236733
B3LYP-D3BJ/6-311+G(d,p)-IEFPCM(DMSO):		
Electronic energy (a.u.)	=	−1455.473862
B3LYP/6-31G(d):		
Zero-point correction (a.u.)	=	0.285273
Thermal correction to Energy (a.u.)	=	0.305440
Thermal correction to Enthalpy (a.u.)	=	0.306384
Thermal correction to Gibbs Free Energy (a.u.)	=	0.237129

C	0.815170	1.228730	−3.214132	C	−0.147910	0.423876	−3.833160
C	−0.994610	−0.400231	−3.084815	C	−0.862818	−0.409306	−1.678637
C	0.103690	0.396816	−1.024616	C	0.935585	1.214965	−1.834879
O	−1.717316	−1.229610	−1.021130	C	−2.027745	−1.260189	−3.771614
O	−0.215196	0.485936	−5.190446	C	2.108859	2.084533	0.317429
C	1.214978	1.218070	1.070969	C	0.300338	0.431955	0.428735
C	1.979773	2.086190	−1.221704	O	−0.541342	−0.391263	1.129818
O	2.717790	2.790063	−1.885638	C	1.335550	1.245077	2.574807
C	0.105483	0.616319	3.212788	C	−0.269902	−0.722564	2.541358
O	2.941481	2.804982	0.853457	C	0.840260	−1.774187	2.578009
C	−1.597068	−1.278546	3.049530	Cl	0.357515	0.405279	5.006030
H	1.466866	1.861028	−3.805738	H	−1.533498	−1.151977	−0.064294
H	−2.599803	−1.834773	−3.043696	H	−2.741578	−0.653159	−4.346803
H	−1.562501	−1.975809	−4.464694	H	−0.911881	−0.107941	−5.510504
H	2.243723	0.722931	2.901474	H	1.452297	2.279771	2.911202
H	−0.753218	1.286728	3.126353	H	1.080925	−2.032078	3.612883
H	0.506786	−2.679777	2.062166	H	1.750927	−1.417977	2.089436
H	−1.503055	−1.584116	4.094046	H	−2.388777	−0.526059	2.976010
H	−1.889781	−2.153688	2.459999				

Table S9. DFT-calculated NMR chemical shifts of two possible structures **I** and **II** for TMKS8A (**4**).

	TMKS8A (**4**)		structure **I**		structure **II**		structure **I**	structure **II**
Position	δ_C(exp)	δ_H(exp)	δ_C(calc)	δ_H(calc)	δ_C(calc)	δ_H(calc)	$\lvert\delta_C(exp)-\delta_C(calc)\rvert$	$\lvert\delta_C(exp)-\delta_C(calc)\rvert$
2	79.6		82.3		85.0		2.7	5.4
3	58.0	4.56	55.5[a]	4.36	55.8[a]	4.40	2.5	2.2
4	26.6	2.78	30.7	2.89	30.5	2.76	4.1	3.9
		3.08		3.01		2.93		
4a	116.9		117.7		108.9		0.8	8.0
5	188.0		185.8		174.2		2.2	13.8
5a	106.5		108.1		107.2		1.6	0.7
6	160.7		159.8		155.1		0.9	5.6
6-OH		12.67		13.11[b]		9.61[b]		
7	117.5		119.9		121.4		2.4	3.9
8	161.3		157.2		155.6		4.1	5.7
9	107.1	7.06	107.0	7.31	111.2	7.47	0.1	4.1
9a	129.2		128.9		129.5		0.3	0.3
10	178.0		177.6		177.7		0.4	0.3
10a	152.7		152.7		164.6		0.0	11.9
2α-Me	23.6	1.45	24.9	1.49	25.0	1.60	1.3	1.4
2β-Me	24.5	1.39	26.0	1.40	25.8	1.54	1.5	1.3
7-Me	8.0	2.03	10.7	2.30	11.0	2.28	2.7	3.0
		MAE[c]	1.74	0.14	4.48	0.18		

[a]The heavy-atom errors were corrected by empirical linear scaling. (see Experimental Section for details)
[b]Exchangeable signals are not included for MAEs evaluation.
[c]MAE = mean absolute erro.

Figure S10. HRESITOFMS spectrum of **4**.

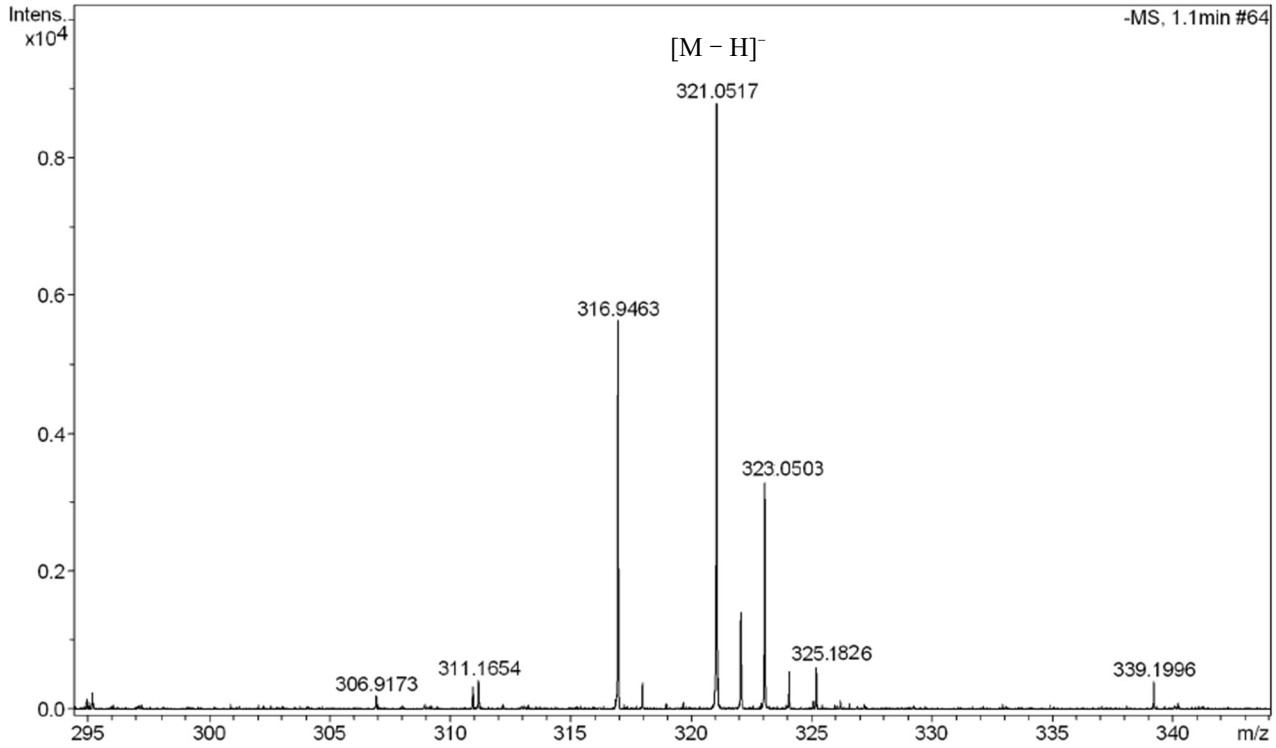

CHAPTER 4

Nomimicins B–D, Tetronate-class Polyketides from a Marine-Derived Actinomycete of the Genus *Actinomadura*

4-1 Background

Actinobacteria are well known for their ability to produce secondary metabolites belonging to the family Actinomycetaceae including the genera of *Streptomyces*, *Actinobaculum*, *Acanobacterium*, *Actinomadura* and several others, most of them are more active to fight against pathogenic organisms [1]. Among these, the genus *Actinomadura*, belonging to the family *Thermomonosporaceae* [2] within the class Actinobacteria, is known to produce interesting bioactive metabolites. So far, approximately 270 natural products were isolated and reported from *Actinomadura*. Among of them, marine *Actinomadura* plays a very important role to yield a number of unique chemical moieties: Halomadurones showed activity against neurodegenerative diseases [3]; Forazoline A showed antifungal activity [4].

In addition, in our laboratory several bioactive compounds, nomimicin with antimicrobial activity [5], nonthmicin with neuroprotective and antiinvasive activity were found from *Actinomadura* [6]. Among the various marine sources, our laboratory has been studying deep-sea water (DSW) as an unexplored source of actinomycetes for new bioactive compounds [7]. DSW is defined as seawater present below -200 m and is characterized by low temperature, rich inorganic nutrient, mineral abundance, and homeostasis [8].

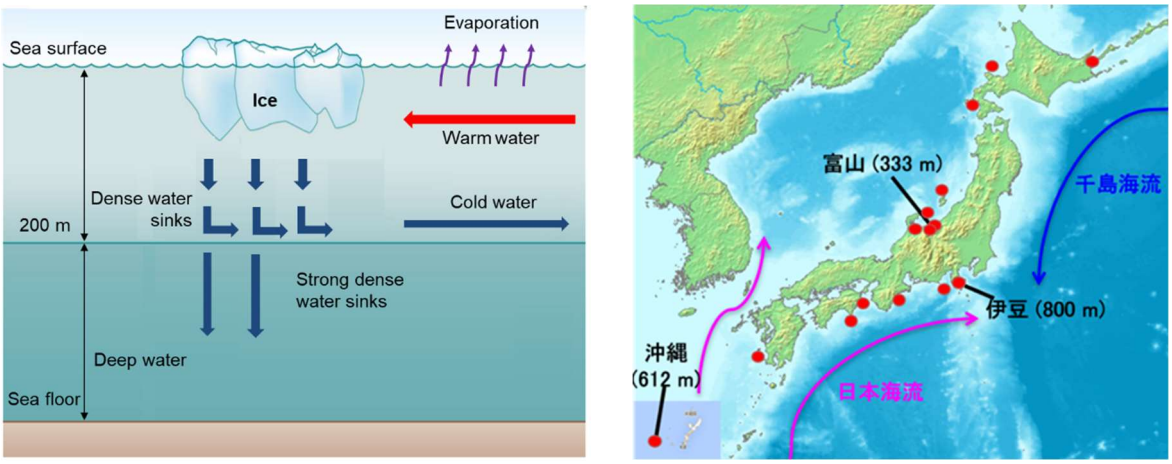

Figure 4-1. Schematic diagram of the formation of deep seawater (left) and geographical location of DSW pumping stations in Japan (right).

In general, the main reason for the formation of DSW is considered to be due to complicated factors such as air-sea fluxes or sea-ice fluxes, which increase the density of surface seawater and reduce buoyancy, convection forms dense water, and finally sinks dense water to form DSW [9]. Currently, 15 pumping facilities for DSW are in

operation at various geographical sites around Japan Islands for aquaculture, agriculture, food industry, power generation, and health care [10]. In the past 20 years, our group studied the actinomycetes collected from the DSW of the Sea of Japan.

This strategy has led to isolate some bioactive compounds such as TPU-0037-C, is a novel lydicamycin congener, isolated from *Streptomyces*. This compound showed antibiotic activity against MRSA [11]. Kosinostatin, a quinocycline antibiotic, was isolated from the culture broth of *Micromonospora* [12]. Nyuzenamide A, discovered from *Streptomyces*, displayed antifungal activity against pathogenic fungi and cytotoxicity [7]. Watasemycins A and B, isolated from *Streptomyces*, showed antibiotic activity against Gram-positive and negative bacteria and yeast [13] (Figure 4-2).

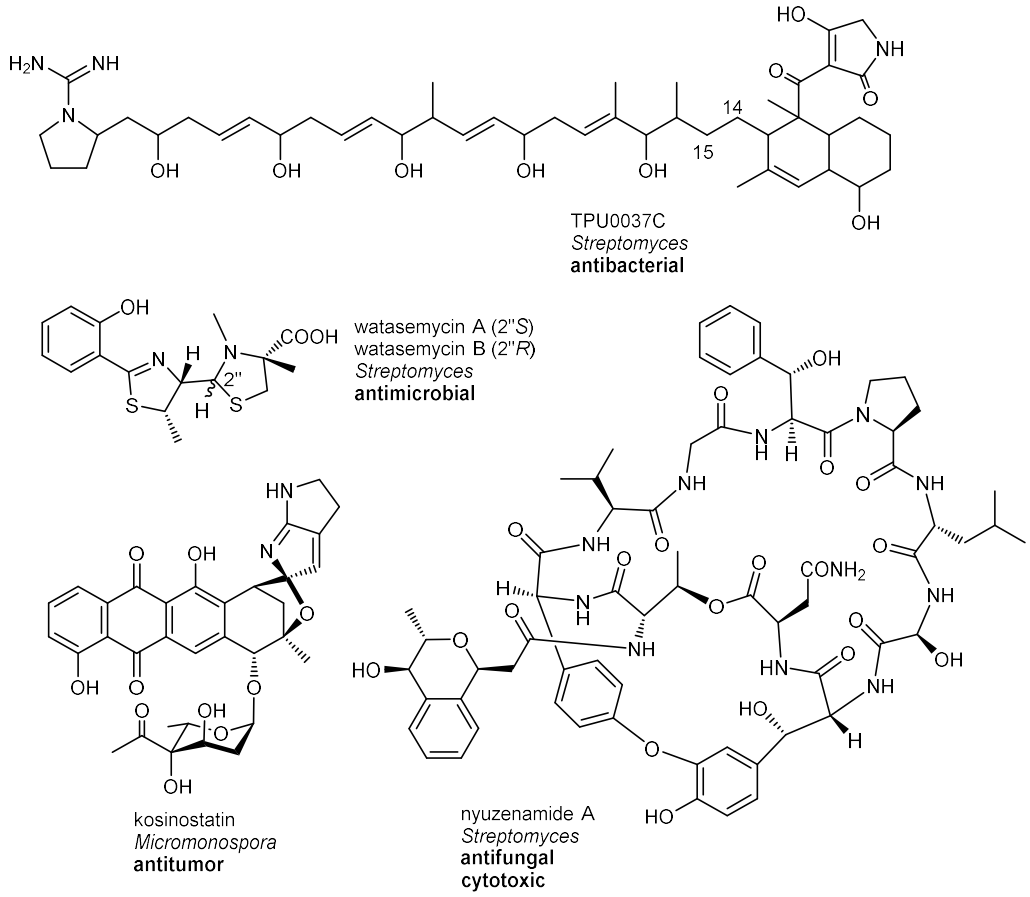

Figure 4-2. The structures of compounds from DSW actinomycetes collected in Toyama Bay.

We recently carried out metagenomic analysis of DSW using DGGE and pyrosequencing techniques and revealed that the bacterial community structure in DSW was varied depending on the collection sites [14]. Furthermore, we found that the DSW of Sagami Bay (Pacific Ocean side of Honshu Island, Japan) contained more unknown actinomycete species than other sea areas, which eventually led to the discovery of

akazamicin, a new cytotoxic aromatic polyketide from *Nonomuraea* [15] and akazaoxime, an antibacterial oxime derivative from *Micromonospora* [16] (Figure 4-3).

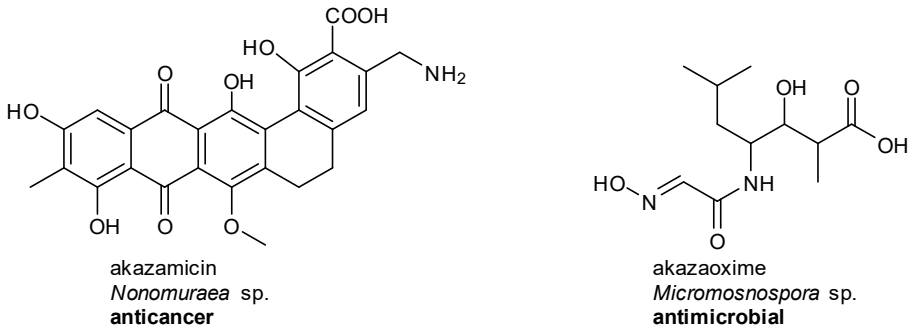

Figure 4-3. The structures of compounds from DSW actinomycetes collected in Sagami Bay.

Along the lines of these previous studies, metabolite analysis of actinomycetes from the DSW of Sagami Bay was further conducted, and three new tetronate-class polyketides, nomimicins B (**10**), C (**11**), and D (**12**), along with nomimicin A (**13**) were found from a rare actinomycete of the genus *Actinomadura*. I herein describe the isolation, structure determination, and biological activities of **10**–**12** (Figure 4-5).

Figure 4-4. *Actinomadura* sp. AKA43 on Bn-2 agar.

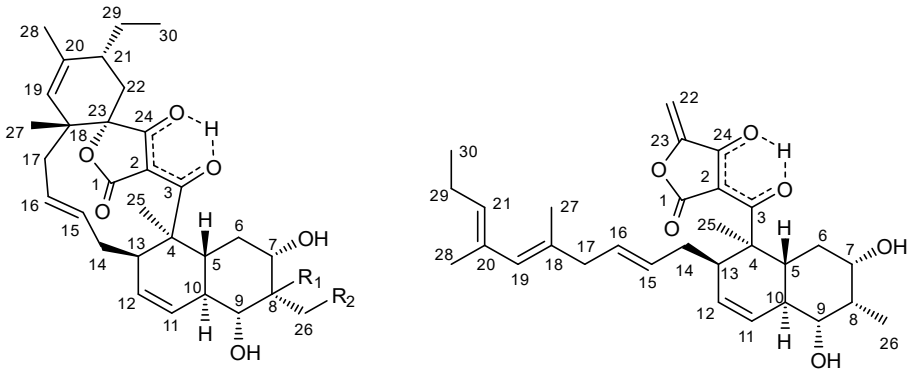

Figure 4-5. Structures of nomimicins A–D (**13, 10**–**12**).

4-2 Results and discussion

4-2-1 Fermentation and isolation

The producing strain *Actinomadura* sp. AKA43 was isolated from the DSW collected at a depth of -800 m in Sagami Bay, Japan. Strain AKA43 was cultured in A16 medium and the whole culture broth was extracted with 1-butanol. The extract was subjected to silica gel and ODS column chromatographies and the final purification was achieved by reverse-phase HPLC to yield two new spirotetronate polyketides nomimicins B (**10**) and C (**11**) along with a known compound nomimicin A (**13**) [5].

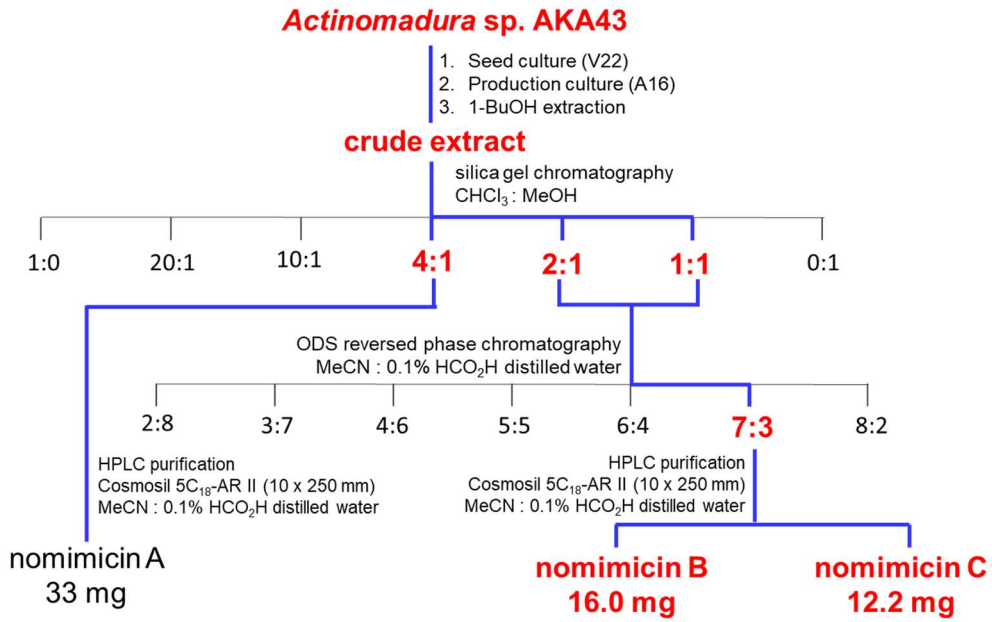

Scheme 4-1. Isolation of nomimicins A–C (**13, 10**, **11**).

From the extract of the fermentation broth cultured in A11M medium, an additional new tetronate polyketide, nomimicin D (**12**), was isolated.

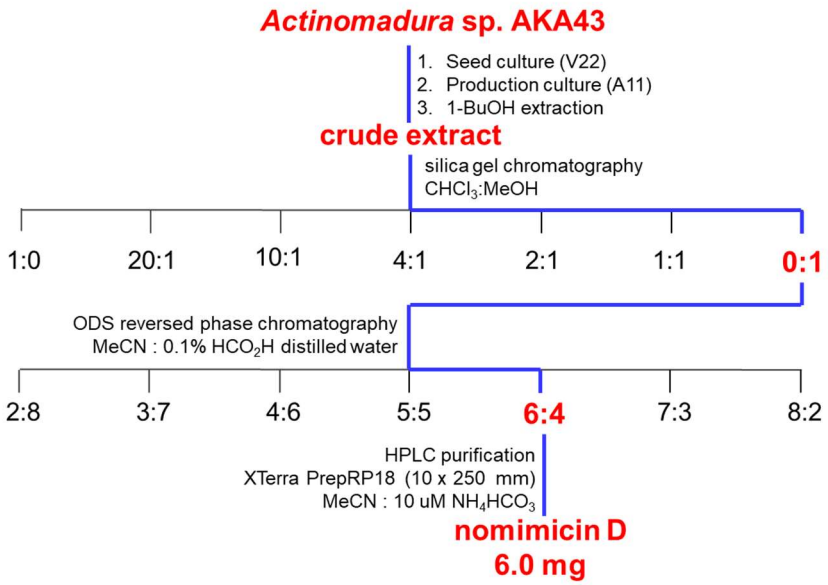

Scheme 4-2. Isolation of nomimicin D (**12**).

4-2-2 Structure determination

Nomimicin B (**10**) was obtained as a colorless amorphous solid. The molecular formula was determined to be $C_{30}H_{40}O_8$, based on the HR-ESITOFMS analysis ($[M + Na]^+$ *m/z* 551.2612, Δ -0.3 mmu). Structural analogy between **10** and **13** was suggested by the global similarity of UV and NMR spectra between them. In the ^{13}C NMR, four nonprotonated carbons assignable to the tetronic acid moiety were detected at δ_C 108.2, 170.4, 200.7, and 204.5. In addition, ^{13}C NMR and HSQC analyses revealed the presence of six sp^2 carbons (five are proton-bearing), two quaternary sp^3 carbons, two oxygen-bearing nonprotonated carbons, six sp^3 methines (two are oxygenated), six sp^3 methylenes, and four methyl groups (Table 4-1).

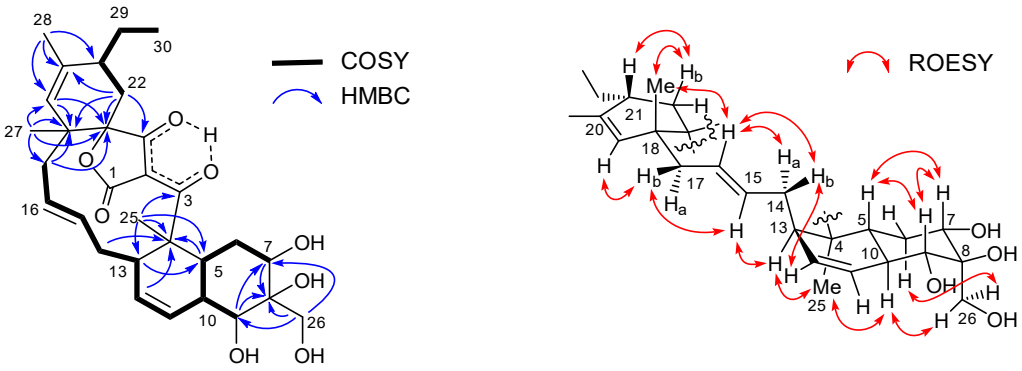

Figure 4-6. COSY and key HMBC correlations and relative correlations for **10** determined by ROESY analysis.

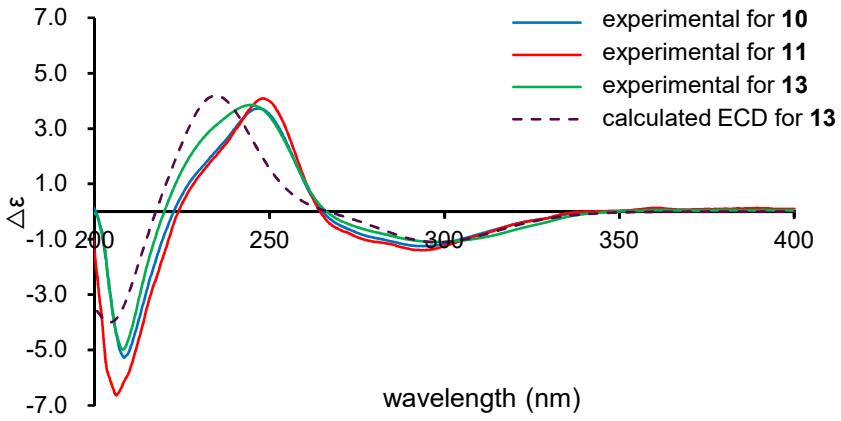

Figure 4-7. Comparison of ECD spectra of **10**, **11**, and **13**.

COSY analysis clarified two carbon chains (Figure 4-6). The first one starting from H7 and ending at H17 contained an oxymethine (H9) branching at C10, a *cis*-double bond between C11 and C12 ($^3J_{H11,H12}$ = 10.0 Hz), and a *trans*-double bond between C15 and C16 ($^3J_{H15,H16}$ = 14.8 Hz). Placement of the oxygenated carbon C8 between C7 and C9 and the attachment of the oxygenated methylene C26 to C8 were deduced from the HMBC correlations from H7 and H9 to C8 and C26 and from H26 to C7, C8, and C9, thereby establishing a highly oxygenated cyclohexane ring. This six-membered ring was fused with another six-membered ring to give a dehydrodecalin core by the correlations from a singlet methyl H25 to C4, C5, and C13. A series of HMBC correlations from two methyl singlets H27 and H28 elucidated the carbon connectivity of C23-C18-C19-C20-C21 (Figure 4-6), which was then coupled with the other COSY-defined fragment, C22/C21/C29/C30, by the correlations from H22 to C18 and C23, yielding a cyclohexene ring. This ring was joined together with the dehydrodecalin moiety at the quaternary carbon C18 by HMBC correlations from H17 to C18, C19, and C23. As for the remaining four sp^2 carbons, C1, C2, C3, and C24, although only limited HMBC correlations H22/C24 and H25/C3 were available, a spirotetronate structure was assembled in consideration of the high similarity of ^{13}C NMR chemical shifts of these carbons to those for the corresponding carbons in **13** as well as the closeness of UV spectral pattern between **10** and **13**. The remaining four protons were finally assigned to hydroxy protons at C7, C8, C9, and C26 to complete the planar structure of **10**. While **13** has an axial methyl group at C8 and equatorial hydroxy groups at C7 and C9, **10** has two additional hydroxy groups at C8 and C26. The axial orientation of the C26 hydroxymethyl group was supported by ROESY

correlations H26/H6ax and H26/H10 (Figure 4-6). Relative configuration of the remaining part was determined to be identical with **13** on the basis of ROESY correlations (Table S1) and $^{3}J_{HH}$ coupling constants [5].

Table 4-1. ^{1}H and ^{13}C NMR data for nomimicins B (**10**) and C (**11**).

	Nomimicin B (**10**)			Nomimicin C (**11**)		
no.	δ_C[b]	δ_H, mult (*J* in Hz)[a]	HMBC[a,c]	δ_C[b]	δ_H, mult (*J* in Hz)[a]	HMBC[a,c]
1	170.4			169.9		
2	108.2			108.4		
3	200.8			201.0		
4	51.0			51.0		
5	36.6	1.66[d]	4, 7, 9, 25	36.4	1.68[d]	4, 6, 7, 9, 10, 25
6ax	34.3	1.34, ddd (12.0, 12.0, 12.0)	5, 7, 10	34.1	1.20, ddd (11.9, 11.9, 11.9)	5, 7, 8, 10
6eq		2.41, brd (12.0)	7		2.35[d]	5, 7, 8, 10
7	77.4	3.74, dd (12.0, 4.3)	5, 6, 8, 26	76.8	3.62, dd (11.8, 4.2)	5, 6, 8, 26
8	77.4			79.1		
9	80.5	3.21, d (11.2)	5, 7, 8, 10, 11, 26	79.8	3.11, d (11.0)	5, 8, 10, 11, 26
10	41.8	2.02[d]		41.7	1.85[d]	
11	124.5	5.85, d (10.0)	5, 9, 13	124.8	5.84, d (10.0)	5, 9, 10, 13
12	132.0	5.61, ddd (10.0, 5.3, 2.6)	4, 10, 13	131.6	5.60, ddd (10.0, 5.1, 2.5)	4, 10, 13
13	39.4	2.81, m	4, 11, 12, 14, 25	39.4	2.79, m	4, 5, 11, 12, 14, 15, 25
14a	37.6	1.80[d]	4, 13, 15, 16	37.6	1.80[d]	4, 13, 15, 16
14b		1.98[d]	16		1.98[d]	15, 16
15	137.5	5.49, dd (14.7, 11.5)		137.6	5.48, dd (14.5, 11.9)	
16	124.8	5.12, dd (14.8, 11.3)		124.8	5.12, dd (14.8, 11.6)	
17a	44.1	1.95[d]	15, 16	44.0	1.95[d]	15, 16, 18, 19, 23
17b		2.32[d]	15, 16, 27		2.32[d]	15, 16, 19, 27
18	40.8			40.7		
19	130.8	5.00, s	17, 18, 23, 28	130.7	5.01, s	17, 18, 21, 23, 28
20	135.1			135.1		
21	40.5	2.00[d]		40.5	2.01[d]	
22a	30.7	1.78[d]	18, 20, 21, 23, 24, 29	30.7	1.79[d]	18, 21, 23, 24, 29
22b		2.34[d]	18, 21, 29		2.34[d]	21, 29
23	87.9			88.0		
24	204.6			204.7		
25	16.6	1.60, s	3, 4, 5, 13	16.6	1.59, s	3, 4, 5, 13
26	62.9	3.99, s	7, 8, 9	13.9	1.15, s	7, 8, 9
27	24.4	1.24, s	17, 18, 19, 23	24.3	1.25, s	17, 18, 19, 23
28	22.5	1.75, s	19, 20, 21	22.4	1.75, s	19, 20, 21
29a	26.4	1.58[d]	22, 30	26.4	1.62[d]	21, 22, 30
29b		1.72[d]	30		1.75[d]	20, 22, 30
30	13.2	0.93, t (7.4)	21, 29	13.1	0.93, t (7.4)	21, 29

[a]Recorded at 500 MHz.
[b]Recorded at 125 MHz.
[c]From proton to indicated carbon(s).
[d]Overlapping signals.

The absolute configuration of **10** was deduced to be the same as **13** in consideration of the overall similarity of ECD for **10** and **13** (Figure 4-7). This proposition was evidenced by the density functional theory (DFT) calculation of ECD spectrum for **13**

of which absolute configuration was established by the modified Mosher's method in our previous work [15]. Since the acyl tetronic acid exists as a mixture of keto-enol tautomeric isomers, the calculation was carried out using the four possible canonical structures of **13** (**13a**–**13d** in Figure 4-8). The calculated ECD spectra of **13a**–**13d** and the one for **13**, which include all contributions from each tautomer according to the energy distribution, are shown in Figure 5 and Figure 4, respectively. The experimental ECD spectrum of **13** with positive and negative Cotton effects at 244 and 298 nm matched well with the calculated one of **13**. To be noteworthy is that **13a** and **13b** have lower free energy than **13c** and **13d** and the calculated spectra for **13a** and **13b** are similar to the experimental one, indicating that **13a** and **13b** are the dominant tautomers in solution. This is the first validation to state that the keto carbonyl in the five-membered ring (C24 in Figure 4-8) and the acyl ketone connecting at C2 (C3 in Figure 4-8) are preferably enolized to form stable isomeric structures in spirotetronic acids.

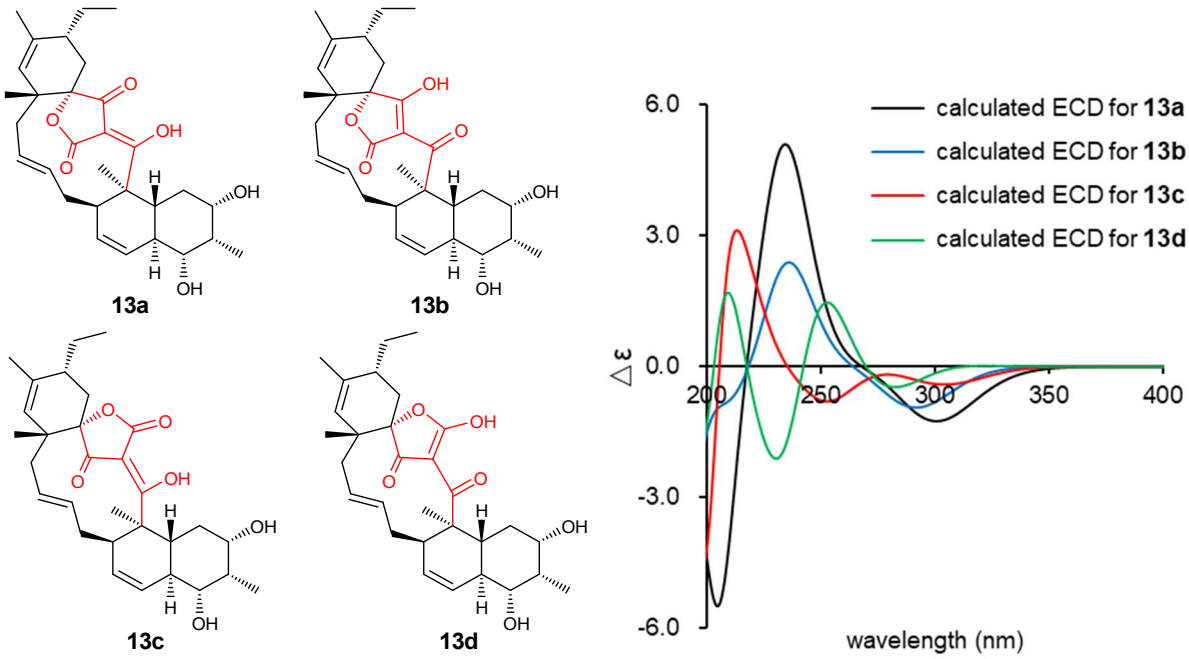

Figure 4-8. Four tautomers (**13a**–**13d**) of tetronic acid moiety of **13** and calculated ECD spectra.

The molecular formula of nomimicin C (**11**) was determined as $C_{30}H_{40}O_7$ on the basis of HR-ESITOFMS data (*m/z* 535.2665 $[M + Na]^+$, Δ -0.1 mmu), indicating that one oxygen (16 amu) less in **11** than **10**. This was consistent with the NMR spectra of **11** in which the resonances for the hydroxylated methylene H26/C26 (δ_H 3.99, δ_C 62.9) disappeared and those for a shielded methyl group (δ_H 1.15, δ_C 13.9) appeared instead, implying that the C26 hydroxymethyl group in **10** was replaced by a methyl group in

11. HMBC correlations from H26 to C7, C8, and C9 and ROESY correlation between H26 and H10 supported the presence of a methyl group at C8 and its axial orientation (Figure S36). The remaining part of **11** was constructed by COSY and HMBC analyses and the relative configuration was established by NOESY/ROESY analyses (Table S2). Close similarity of ECD spectra between **10** and **11** was also indicative of the same absolute configuration of **11** and **13** (Figure 4-7).

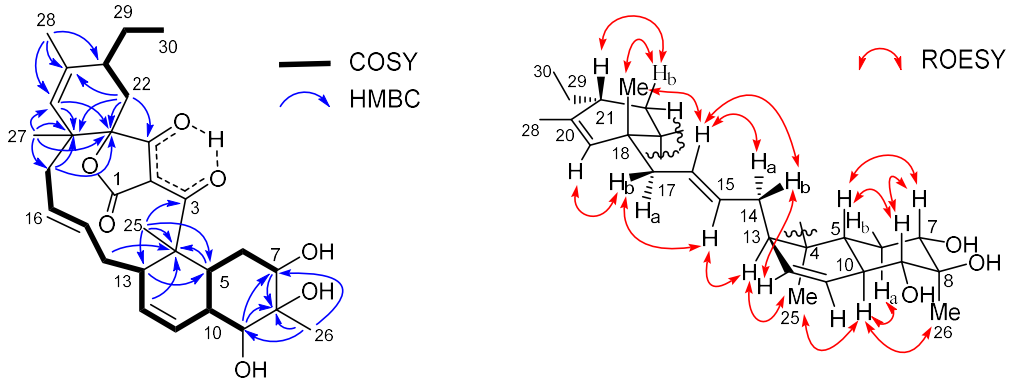

Figure 4-9. COSY and key HMBC correlations and relative correlations for **11** determined by ROESY analysis.

The molecular formula of nomimicin D (**12**) was determined to be $C_{30}H_{42}O_6$ through the HR-ESITOFMS analysis which gave a sodium adduct ion $[M + Na]^+$ at *m/z* 519.2717 (Δ 0.0 mmu). Analysis of ^1H, ^{13}C, and HSQC spectra revealed the presence of four oxygenated sp^2 carbons, three nonprotonated sp^2 carbons, six sp^2 methines, one sp^2 methylene, one quaternary carbon, six sp^3 methines (two are oxygenated), four sp^3 methylenes, and five sp^3 methyl groups (Table 4-2). A sequence of COSY correlations from the doublet methyl H26 to an oxymethine H7 via an oxymethine H9, together with HMBC correlations from H26 and H8 to C7 and H8 to C6, gave an oxygenated cyclohexane ring with a methyl substitution (Figure 4-9). COSY correlations were extended from H10 to a methylene H17, providing a carbon chain containing double bonds at C11/C12 and C15/C16. HMBC correlations from a singlet methyl H25 to C4, C5, and C13 closed another cyclohexane ring and thus a dehydrodecalin core with a side chain at C13 was established. The chain was further extended from H17 to the terminal methyl H30 by COSY correlations for H21/H29/H30 and a series of HMBC correlations from two allylic methyls H27 and H28 to the carbons within three-bond length (Figure 4-9). The remaining five nonprotontaed carbons, C1 (δ_C 174.5) , C2 (δ_C 99.5), C3 (δ_C 203.2), C23 (δ_C 155.7), and C24 (δ_C 180.7), and the *exo*-methylene group

(H22: δ_H 4.66/5.00; C22: δ_C 88.7) were assigned to the tetronic acid moiety based on the following considerations. First, the ^{13}C chemical shifts of these six carbons were closely similar to those for the tetronic acid bearing an *exo*-methylene substituent in the known natural products [17-19]. Secondly, the UV spectrum of **12** showing the absorption maxima at 243 and 302 nm was matched well with that for ecteinamycin which possesses the *exo*-methylene substituted tetronic acid moiety [6]. This assignment was supported by correlations from H22 to C23, C24, and C2 and from H25 to C3 though not all the carbon-carbon connectivities were proven by HMBC analysis.

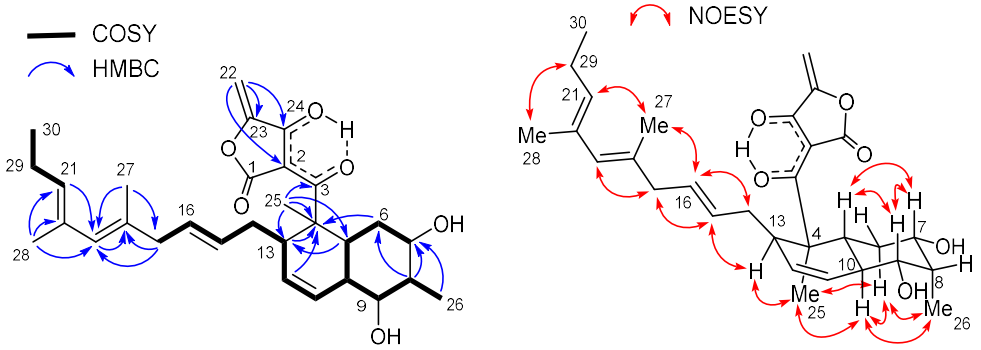

Figure 4-10. COSY and key HMBC correlations and relative configuration of **12** determined by NOESY analysis.

The relative configuration of **12** was elucidated by analyzing the NOESY spectrum (Table S2). Correlations for H5/H7, H5/H9 and H7/H9 and large scalar couplings ($^3J_{HH}$ > 10 Hz) for H5/H6ax, H6ax/H7 and H5/H9 established the *trans*-ring fusion of the dehydrodecalin moiety. The axial orientation of the methyl group at C8 was evidenced by NOESY correlations H26/H6ax and H26/H10. Correlations of H25/H10 and H25/H13 placed the H25 methyl and H13 on the same side of the dehydrodecalin ring at the H9 axial proton. The geometries of the double bonds at C15/C16, C18/C19, and C20/C21 were assigned all to be *E* based on the NOESY correlations H13/H15, H14/H16, H15/H17, H17/H19, and H28/H29 (Figure 4-10). The s-*cis* configuration of the diene moiety was indicated by a NOESY correlation between H21 and H27. The absolute configuration of the dehydrodecalin moiety of **12** was tentatively assigned to be identical with **13** because **12** was considered as a biosynthetic precursor of **13** [20].

Table 4-2. ^{1}H and ^{13}C NMR data for nomimicin D (**12**).

no.	δ_C[b]	δ_H, mult (*J* in Hz)[a]	HMBC[a,c]
1	174.5		
2	99.5		
3	203.2		
4	52.8		
5	36.5	1.72[d]	4, 7, 9, 11, 25
6ax	30.8	1.14, ddd (11.7, 11.7, 11.7)	4, 5, 7, 8, 10
6eq		1.80, brd (11.7)	7
7	72.3	3.83, ddd (11.6, 4.5, 4.5)	26
8	43.4	2.32, m	7, 9, 10, 26
9	75.5	3.40, dd (10.8, 4.7)	5, 10, 11, 26
10	38.9	1.94[d]	9, 11
11	125.8	5.85, d (10.2)	5, 9, 10, 12, 13
12	131.5	5.72, ddd (10.2, 4.8, 2.5)	4, 13, 14
13	41.5	3.32[d]	4, 5, 14
14a	38.7	1.75[d]	12, 13, 15, 16
14b		2.00[d]	12, 13, 15, 16
15	131.8	5.40, dt (15.0, 7.2)	14, 16, 17
16	130.7	5.26, dt (15.2, 7.0)	14, 15, 17
17	44.9	2.63, d (6.9)	15, 16, 18, 19, 27
18	135.6		
19	130.5	5.59, s	17, 21, 27, 28
20	133.5		
21	131.9	5.20, t (7.3)	19, 29, 26
22a	88.7	4.66, d (1.5)	
22b		5.00, d (1.5)	2, 23, 24
23	155.7		
24	180.7		
25	16.0	1.38, s	3, 4, 5, 13
26	6.1	0.92, d (6.9)	7, 8, 9
27	18.2	1.69, s	17, 18, 19
28	17.2	1.67, s	19, 20, 21
29	22.5	2.08, q (7.5)	20, 21, 30
30	14.8	0.98, t (7.5)	21, 29

[a]Recorded at 500 MHz.
[b]Recorded at 125 MHz.
[c]From proton to indicated carbon(s).
[d]Overlapping signals.

4-2-3 Bioactivity

Compounds **10**–**12** showed antimicrobial activity against *Kocuria rhizopila* with MIC of 6.5 μg/mL and **10** and **11** were also active against *Bacillus subtilis* with MIC of 12.5 μg/mL. Compounds **10**–**12** were inactive against *Staphylococcus aureus*, *Ralstonia solanacearum*, *Rhizobium radiobacter*, and *Candida albicans*. In addition, **10** and **11** exhibited cytotoxicity against P388 murine leukemia cells with IC_{50} of 33 and 89 μM, respectively.

Table 4-3. Antimicrobial activity of **10**–**12**.

	MIC, (μg/mL)		
Microorganisms	Nomimicin B	Nomimicin C	Nomimicin D
Kocuria rhizophila ATCC9341	6.25	6.25	＞100
Bacillus subtilis PCI219	12.5	12.5	＞100
Staphylococcus aureus FDA209P JC-1	＞100	＞100	＞100
Rhizobium radiobacter NBRC14554	＞100	＞100	＞100
Escherichia coli NIHJ JC-2	＞100	＞100	＞100
Ralstonia solanacearum SUPP1541	＞100	＞100	＞100
Candida albicans NBRC0197	＞100	＞100	＞100
Saccharomyces cerevisiae S100	＞100	＞100	＞100

4-3 Conclusion

In summary, UV-based chemical screening of bioactive compounds from deep seawater-derived actinomycetes led to the discovery of three new polyketides, nomimicins B (**10**), C (**11**), and D (**12**) along with a known congener nomimicin A (**13**) from *Actinomadura* sp. AKA43. Compounds **10** and **11** are the new members of spiroteronate-class antibiotics, characterized by a macrocyclic structure containing a *trans*-decalin unit and a tetronic acid moiety spiro-linked with a cyclohexene ring. To date, more than 100 compounds [21-22] including tetrocarcin [23] and kijanimicin [24] are known within spiroteronate-class. Of these, nomimicins A–C are featured by the smallest macrocyclic ring and highly oxygenated dehydrodecalin moiety. Spirotetronates are known to be constructed by the intramolecular Diels-Alder reaction [25]. Compound **12** is very likely to be a biosynthetic precursor of **13**. This is the first report on the isolation of a biosynthetic precursor of spirotetronate antibiotics as an innate metabolite from a wild-type strain while such an intermediate was obtained from a genetically engineered strain [26].

4-4 Experimental section

4-4-1 General experimental procedures

Optical rotations were measured using a JASCO P-1030 polarimeter. ECD spectra were recorded on a JASCO J-720W spectropolarimeter. UV and IR spectra were recorded on a Shimadzu UV-1800 spectrophotometer and a PerkinElmer Spectrum 100, respectively. All NMR experiments were performed on a Bruker AVANCE 500

spectrometer in CD_3OD using the residual solvent proton (δ_H 3.31) and carbon (δ_C 49.2) signals as internal standards. HR-ESITOFMS were recorded on a Bruker micrOTOF focus mass spectrometer. Agilent HP1200 system equipped with a diode array detector was used for analysis and purification. The computational study was performed using the MacroModel implemented in the Maestro 12.3 software package [27] and the Gaussian16 Rev C.01 program [28]. A part of these computations were conducted using the SuperComputer System, Institute for Chemical Research, Kyoto University. Molecular structures were visualized using Maestro 12.3 software package. ECD spectra were visualized using GaussView 6.0.16 and Microsoft Excel 2019.

4-4-2 Microorganism

Actinomadura sp. AKA43 was isolated from the sea water sample collected from Sagami Bay at a depth of -800 m at the Izu-Akazawa DSW pumping station in Shizuoka, Japan, as previously reported [15]. The isolated strain was identified as a member of the genus *Actinomadura* on the basis of 100% similarity in the 16s rRNA gene sequence (1397 nucleotides, DDBJ accession number LC498623) with *Actinomadura geliboluensis* A8036^T (accession number HQ157187).

4-4-3 Fermentation

Actinomadura sp. AKA43 cultured on Bn-2 agar medium [soluble starch 0.5%, glucose 0.5%, meat extract (Kyokuto Pharmaceutical Industrial Co., Ltd.) 0.1%, yeast extract (Difco Laboratories) 0.1%, NZ-case (Wako Chemicals USA, Inc.) 0.2%, NaCl 0.2%, $CaCO_3$ 0.1%, and agar 1.5% in distilled water] was inoculated into a 500 mL K-1 flask containing 100 mL of the V-22 seed medium [soluble starch 1%, glucose 0.5%, NZ-case 0.3%, yeast extract 0.2%, Tryptone (Difco Laboratories) 0.5%, K_2HPO_4 0.1%, $MgSO_4 \cdot 7H_2O$ 0.05%, and $CaCO_3$ 0.3% in distilled water (pH 7.0)]. The flask was shaken on a rotary shaker (200 rpm) at 30 °C for 4 days. For the production of nomimicins B (**10**) and C (**11**), the seed culture (3 mL) was transferred into 20 500 mL K-1 flasks each containing 100 mL of the A16 production medium [glucose 2%, Pharmamedia (Traders Protein, Memphis, TN, USA) 1%, $CaCO_3$ 0.5%, and Diaion HP-20 (Mitsubishi Chemical, Kanagawa, Japan) 1% in distilled water]. The inoculated flasks were placed on a rotary shaker (200 rpm) at 30 °C for 7 days. For the production of nomimicin D (**12**), the seed culture (3 mL) was transferred into 20 500 mL K-1 flasks each containing 100 mL of the A11M production medium [glucose 0.2%, soluble starch

2.5%, yeast extract 0.5%, polypeptone (Wako Pure Chemical Industries, Ltd.) 0.5%, NZ-amine (Wako Pure Chemical Industries, Ltd.) 0.5%, $CaCO_3$ 0.5%, and Diaion HP-20 1% in distilled water]. The inoculated flasks were placed on a rotary shaker (200 rpm) at 30 °C for 7 days.

4-4-4 Extraction and isolation

At the end of the fermentation period, 100 mL of 1-butanol was added to each flask and the flasks were agitated on a rotary shaker for 1 h. The mixture was centrifuged at 6000 rpm for 10 min and the organic layer was separated from the aqueous layer containing the mycelium. Evaporation of the solvent gave 3.8 g of extract from 2 L of A16 culture. The extract was subjected to silica gel column chromatography with a step gradient of $CHCl_3$/MeOH (1:0, 20:1, 10:1, 4:1, 2:1, 1:1, and 0:1 v/v). Fraction 4 (4:1) was concentrated to give 0.23 g of brown oil, which was further purified by preparative HPLC (Cosmosil 5C18-ARII, 10 × 250 mm, 4 mL/min, UV detection at 254 nm) with 73% MeCN in 0.1% HCO_2H solution to yield nomimicin A (**13**, 33 mg, t_R 21.5 min). Fractions 5 (2:1) and 6 (1:1) were combined and concentrated to provide 0.48 g of brown oil, which was then fractionated by ODS column chromatography with a gradient of MeCN-0.1% HCO_2H solution (2:8, 3:7, 4:6, 5:5, 6:4, 7:3, and 8:2 v/v). The ODS fraction 6 (7:3) was concentrated to afford 0.22 g of semipure material. Final purification was achieved by preparative HPLC (Cosmosil 5C18-ARII, 10 × 250 mm, 4 mL/min, UV detection at 254 nm) with 52% MeCN in 0.1% HCO_2H solution to yield nomimicin B (**10**, 16.1 mg, t_R 19.5 min) and nomimicin C (**11**, 12.2 mg, t_R 21.5 min). Similarly, evaporation of the solvent gave 3.0 g of extract from 2 L of A11M culture. The extract was subjected to silica gel column chromatography with a gradient of $CHCl_3$/MeOH (1:0, 20:1, 10:1, 4:1, 2:1, 1:1, and 0:1 v/v). Fraction 7 (0:1) was concentrated to give 0.37 g of brown oil, which was then fractionated by ODS column chromatography with a gradient of MeCN-0.1% HCO_2H solution (2:8, 3:7, 4:6, 5:5, 6:4, 7:3, and 8:2 v/v). The ODS fraction 5 (6:4) was concentrated to give 72.6 mg of semipure material. The final purification using preparative HPLC (Cosmosil XTerra Prep RP18, 10 × 250 mm, 4 mL/min, UV detection at 254 nm) with 38% MeCN in 10 mM NH_4HCO_3 solution yielded nomimicin D (**12**, 6.0 mg, t_R 30.5 min).

Nomimicin B (**10**): colorless amorphous solid; $[\alpha]_D^{23}$ -29 (*c* 0.10, MeOH); UV (MeOH) λ_{max} (log ε) 246 (3.83), 293 (3.71) nm; ECD (9.5 × 10^{-5} M, MeOH) λ_{ext} (Δε)

208 (-5.27), 247 (+3.72), 294 (-1.24) nm; IR ν_{max} 3360, 2965, 1755, 1619, 1408, 1088, 998 cm^{-1}; ^{1}H and ^{13}C NMR data, see Table 1; HR-ESITOFMS *m/z* 551.2612 $[M + Na]^+$ (calcd for $C_{30}H_{40}O_8Na$, 551.2615).

Nomimicin C (**11**): colorless amorphous solid; $[\alpha]_D^{23}$ -12 (*c* 0.10, MeOH); UV (MeOH) λ_{max} (log ε) 246 (3.93), 292 (3.78) nm; ECD (9.7×10^{-5} M, MeOH) λ_{ext} (Δε) 208 (-6.63), 246 (+4.08), 298 (-1.39) nm; IR ν_{max} 3380, 2963, 1744, 1618, 1404, 1097, 1007 cm^{-1}; ^{1}H and ^{13}C NMR data, see Table 1; HR-ESITOFMS *m/z* 535.2665 $[M + Na]^+$ (calcd for $C_{30}H_{40}O_7Na$, 535.2666).

Nomimicin D (**12**): colorless amorphous solid; $[\alpha]_D^{23}$ -70 (*c* 0.10. MeOH); UV (MeOH) λ_{max} (log ε) 243 (3.99), 302 (3.54) nm; ECD (5×10^{-5} M, MeCN) λ_{ext} (Δε) 205 (-10.19), 295 (−1.71), 331.6 (+1.09) nm; IR ν_{max} 3380, 2963, 1723, 1619, 1413, 1258, 1010 cm^{-1}; ^{1}H and ^{13}C NMR data, see Table 2; HR-ESITOFMS *m/z* 519.2717 $[M + Na]^+$ (calcd for $C_{30}H_{40}O_6Na$, 519.2717).

Nomimicin A (**13**): colorless amorphous solid; $[\alpha]_D^{23}$ -78 (*c* 0.10, MeOH) {lit. $[\alpha]_D^{23}$ -87.3 (*c* 0.10. $CHCl_3$)}; UV (MeOH) λ_{max} (log ε) 242 (3.73), 298 (3.59) nm; ECD (1.0×10^{-5} M, MeOH) λ_{ext} (Δε) 208 (-4.98), 244 (+3.85), 298 (-1.09) nm; IR ν_{max} 3348, 2938, 1735, 1620, 1435, 997 cm^{-1}; HR-ESITOFMS *m/z* 519.2722 $[M + Na]^+$ (calcd for $C_{30}H_{40}O_6Na$, 519.2717).

4-4-5 Biological assays

Antimicrobial assay and cytotoxic assay were carried out according to the procedures previously described [29].

References

1) Bérdy, J. *J. Antibiot*. **2005,** *58,* 1-26.
2) Lam, K. S. *Curr. Opin. Microbiol*. **2006,** *9,* 245-251.
3) Wyche, T. P.; Standiford, M.; Hou, Y.; Braun, D.; Johnson, D. A.; Johnson, J. A.; Bugni, T. S. *Mar. Drugs.* **2013**, *11*, 5089–5099.
4) Wyche, T. P.; Piotrowski, J. S.; Hou, Y.; Braun, D.; Deshpande, R.; McIlwain, S. et al. *Angew. Chem. Int. Ed.* **2014**, *53*, 11583–11586.
5) Igarashi, Y.; Iida, T.; Oku, N.; Watanabe, H.; Furihata, K.; Miyanouchi. K. *J. Antibiot.* **2012,** *65,* 355–359.
6) Igarashi, Y.; Matsuoka, N.; In, Y.; Kataura, T.; Tashiro, E.; Saiki, I.; et al. *Org. Lett.* **2017**, *19*, 1406–1409.

7) Karim, M. R. U.; In, Y.; Zhou, T.; Harunari, E.; Oku, N.; Igarashi, Y. *Org. Lett*. **2021**, *23,* 2109–2113.
8) Imada, C. *Deep Ocean Water Res.* **2012**, *13*, 33–40.
9) Nakasone, T.; Akeda, S. *UJNR Technical Report* **1999**, *28*, 69–75.
10) Yang, T.; Yamada, K.; Nakayama, J.; Igarashi, Y.; Terahara, T.; Kobayashi, T.; Imada, C. *Deep Ocean Water Research* **2019,** *19,* 137-146.
11) Furumai, T.; Eto, K.; Sasaki, T.; Higuchi, H.; Onaka, H.; Saito, N.; Fujita, T.; Naoki, H.; Igarashi, Y. *J. Antibiot*. **2002**, *55*, 873–880.
12) Furumai, T.; Igarashi, Y.; Higuchi, H.; Saito, N.; Oki, T. *J. Antibiot.* **2002**, 55, 128–133.
13) Igarashi. Y.; Ikeda. M.; Miyanaga, S.; Kasai, H.; Shizuru, Y.; Matsuura, N. *J. Antibiot.* **2015,** *68,* 345–347.
14) Terahara, T.; Yamada, K.; Nakayama, J.; Igarashi, Y.; Kobayashi, T.; Imada, C. *Gene* **2015**, *576*, 696–700.
15) Yang, T.; Yamada, K.; Zhou, T.; Harunari, E.; Igarashi, Y.; Terahara, T.;.Kobayashi, T.; Imada, C. *J. Antibiot.* **2019,** *72,* 202-209.
16) Igarashi, Y.; Matsuyuki, Y.; Yamada, M.; Fujihara, N.; Harunari, E.; Oku, N.; Karim, M. R. U.; Yang, T.; Yamada, K.; Imada, C.; Fukaya, K.; Urabe, D. *J. Org. Chem.* **2021,** *86,* 6528–6537.
17) Terui, Y.; Sakazaki, R.; Shoji, J. *J. Antibiot.* **1990,** *43,* 1245−1253.
18) Keller-Juslén, C.; King, H. D.; Kuhn, M.; Loosli, H. R.; Pache, W.; Petcher, T. J.; Weber, H. P.; von Wartburg, A. *J. Antibiot.* **1982,** *35,* 142−150.
19) Hatsu, M.; Sasaki, T.; Miyadoh, S.; Watabe, H.; Takeuchi, Y.; Kodama, Y.; Orikasa, Y.; Kajii, K.; Shomura, T.; Yamamoto, H.; Sezaki, M.; Inouye, S.; Kondo, S. *J. Antibiot.* **1990,** *43,* 259−266.
20) Hashimoto, T.; Hashimoto, J.; Teruya, K.; Hirano, T.; Shin-ya, K.; Ikeda, H.; Liu, H. W.; Nishiyama, M.; Kuzuyama, T. *J. Am. Chem. Soc.* **2015,** *137*, 572−575.
21) Lacoske, M. H.; Theodorakis, E. A. *J. Nat. Prod*. **2015,** *78,* 562–575.
22) Braddock, A. A.; Theodorakis, E. A.; *Mar. Drugs.* **2019,** *17,* 232.
23) Tomita, F.; Tamaoki, T.; Shirahata, K.; Kasai, M.; Morimoto, M.; Ohkubo, S.; Mineura, K.; Ishii, S. *J. Antibiot.* **1980,** *33,* 668-670.
24) Mallams, A. K.; Puar, M. S.; Rossman, R. R.; McPhail, A. T.; Macfarlane, R. D. *J. Am. Chem. Soc.* **1981,** *103*, 3940–3943.
25) Zhang, H.; White-Phillip, J. A.; Melançon, III, C. E.; Kwon, H. J.; Yu, W. L.; Liu, H. W. *J. Am. Chem. Soc.* **2007,** *129*, 14670-14683.
26) Jeon, B. S.; Wang, S. A.; Ruszczycky, M. W.; Liu, H. W.; *Chem. Rev.* **2017,** *117*, 5367−5388.
27) *MacroModel;* Schrödinger, LLC: New York, NY, 2020.
28) *Gaussian 16,* Revision C.01; Gaussian, Inc.: Wallingford, CT, 2016.
29) Karim, M. R. U.; Harunari, E.; Oku, N.; Akasaka, K.; Igarashi, Y. *J. Nat. Prod.* **2020,** *83*, 1295−1299.

4-5 Spectral data

Table of contents

Figure S1. UV spectra of nomimicin B (**10**).

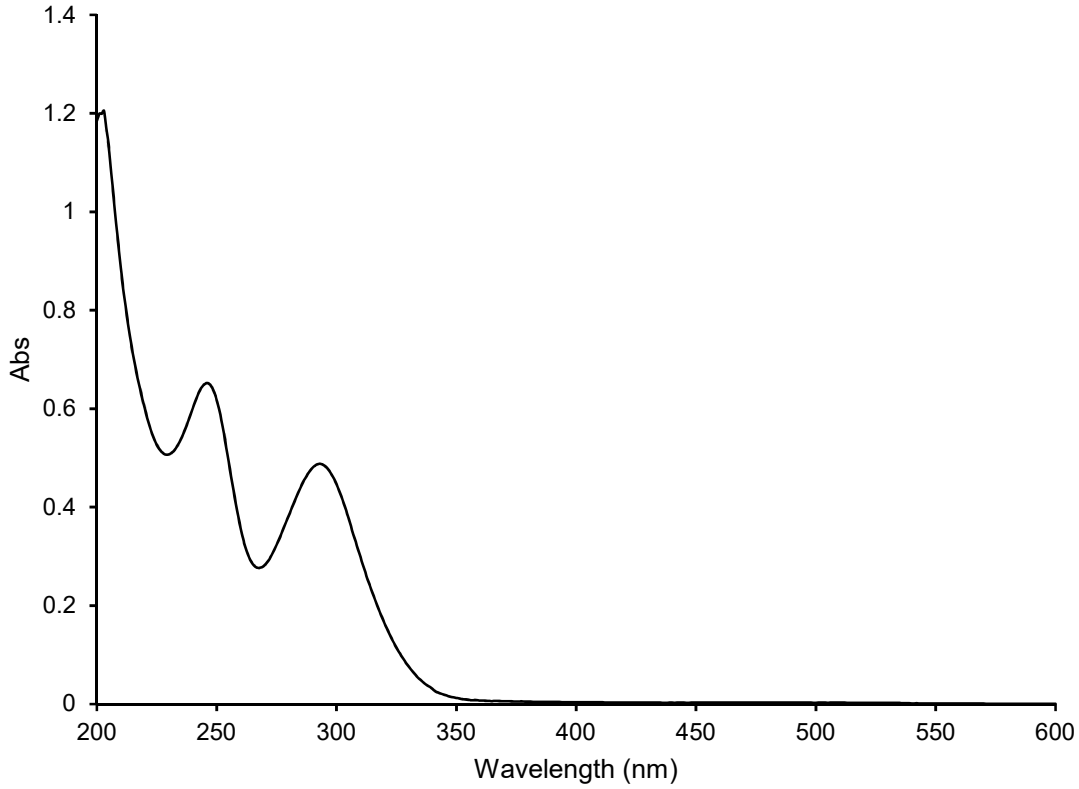

Figure S2. IR spectrum of **10**.

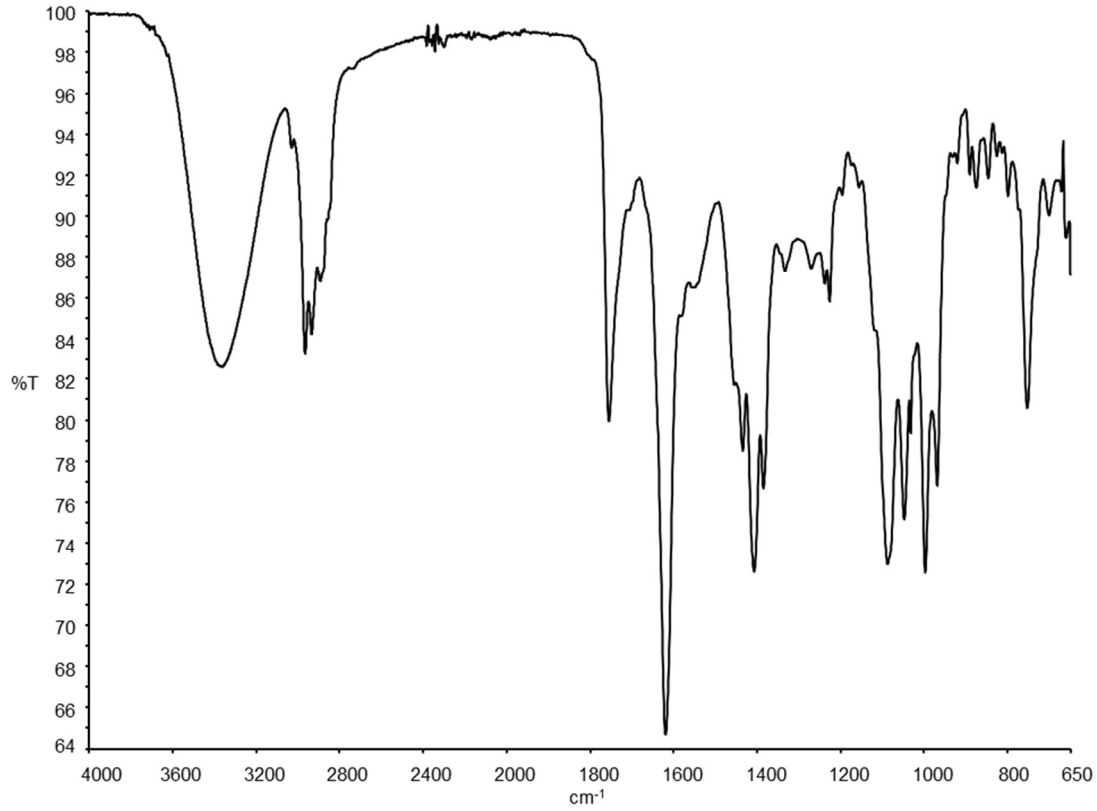

Figure S3. ^{1}H NMR spectrum of **10** (500 MHz, CD_3OD).

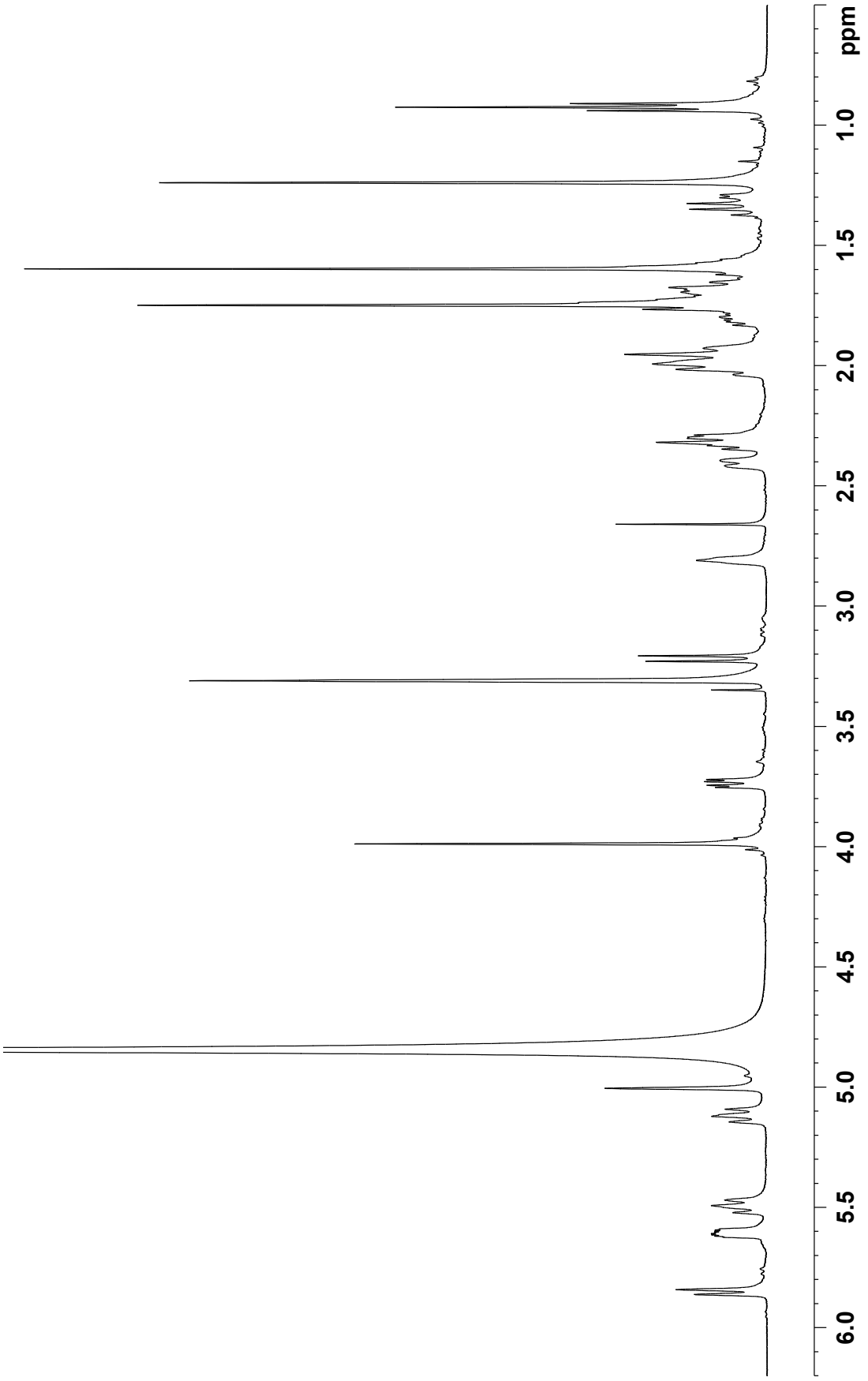

Figure S4. ^{13}C NMR spectrum of **10** (125 MHz, CD_3OD).

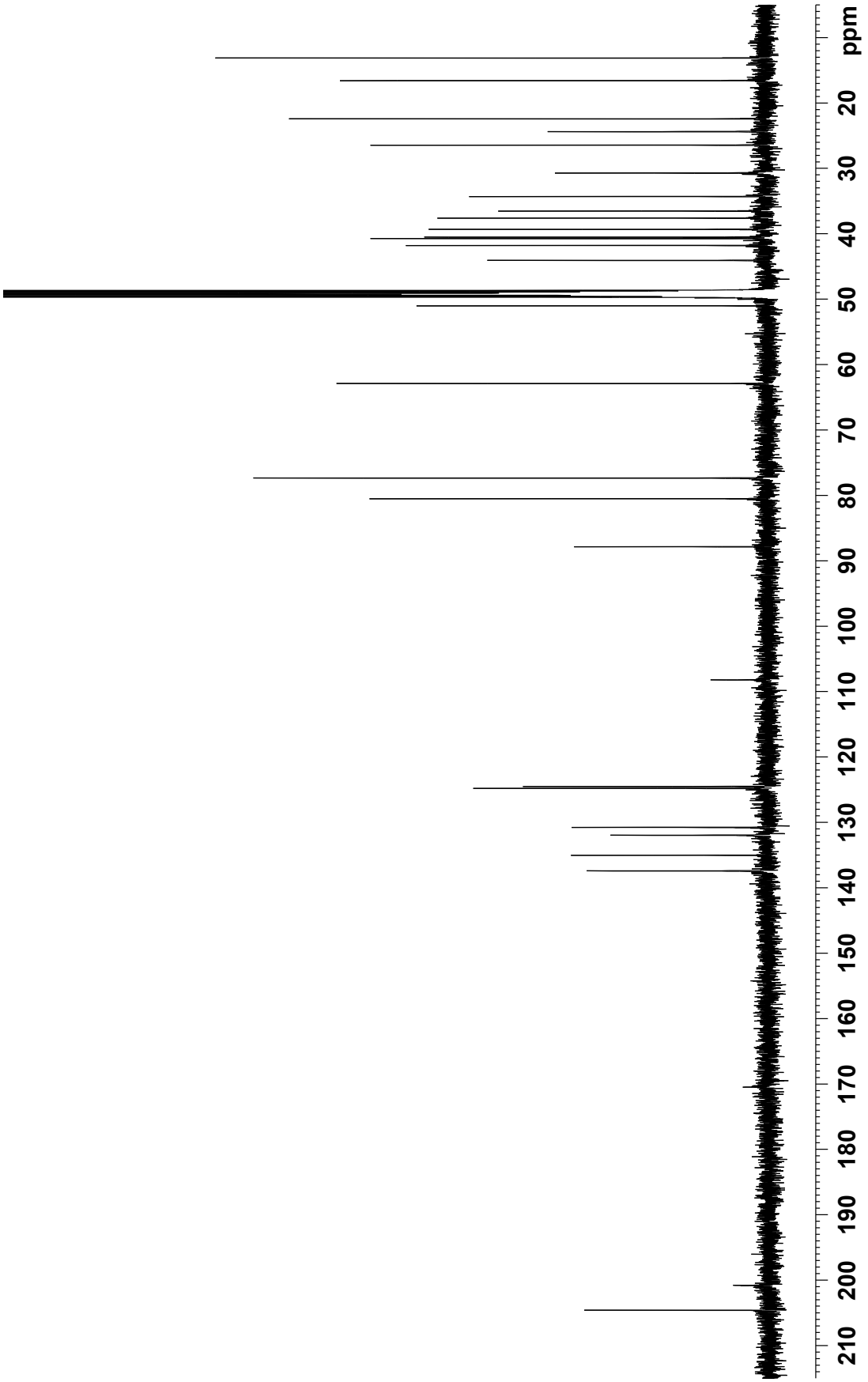

Figure S5. COSY spectrum of **10** (500 MHz, CD_3OD).

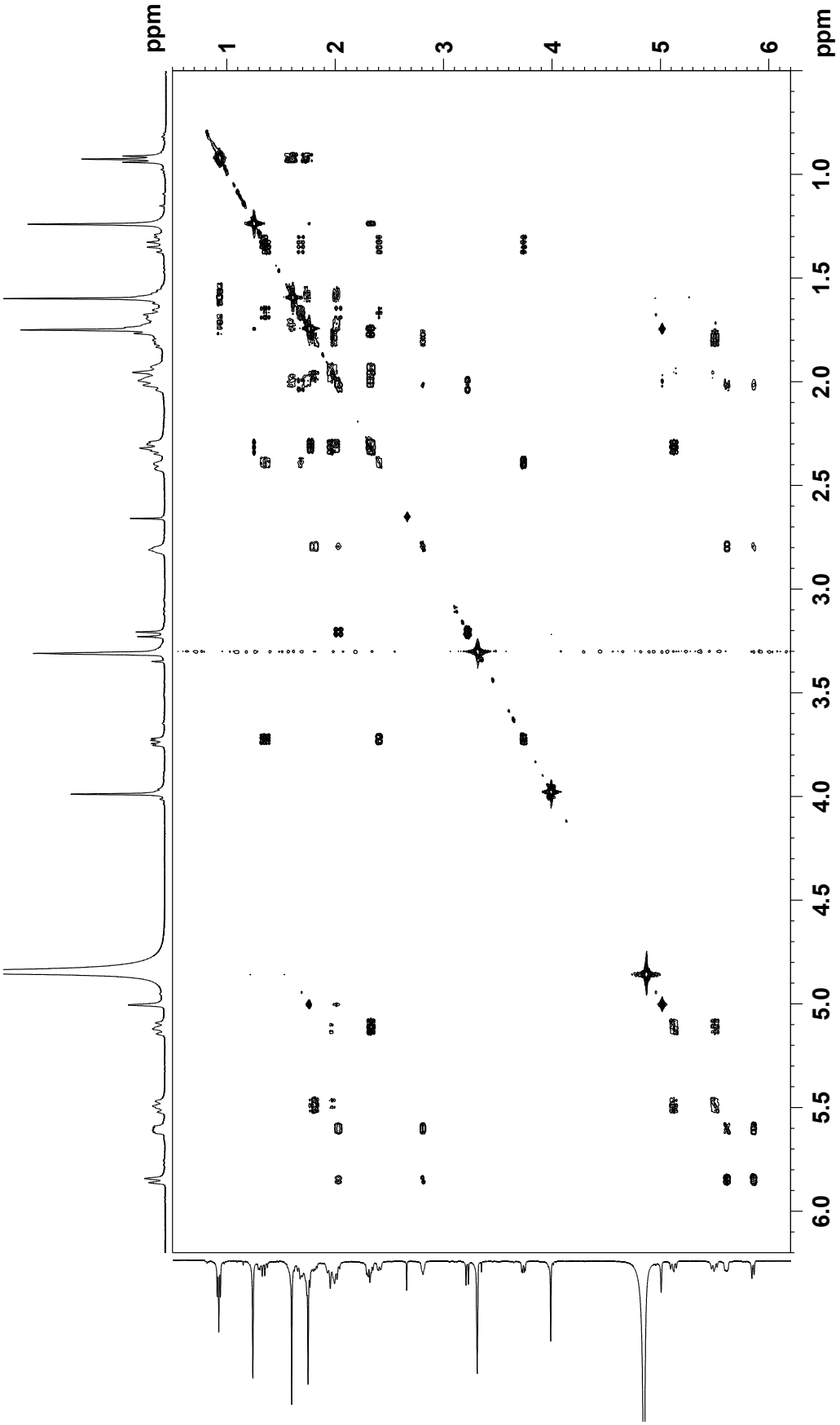

Figure S6. HSQC spectrum of **10** (500 MHz, CD_3OD).

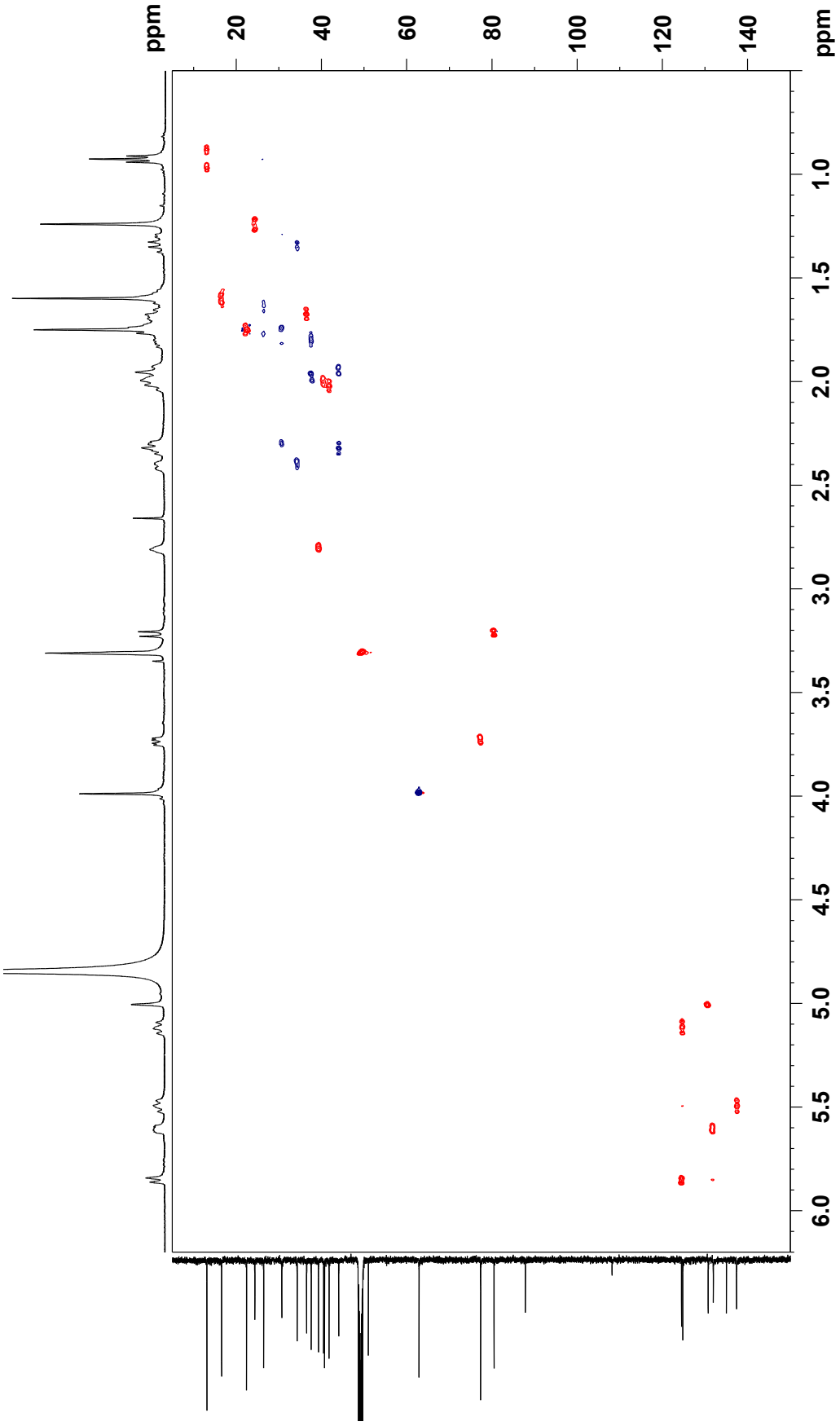

Figure S7. HMBC spectrum of **10** (500 MHz, CD_3OD).

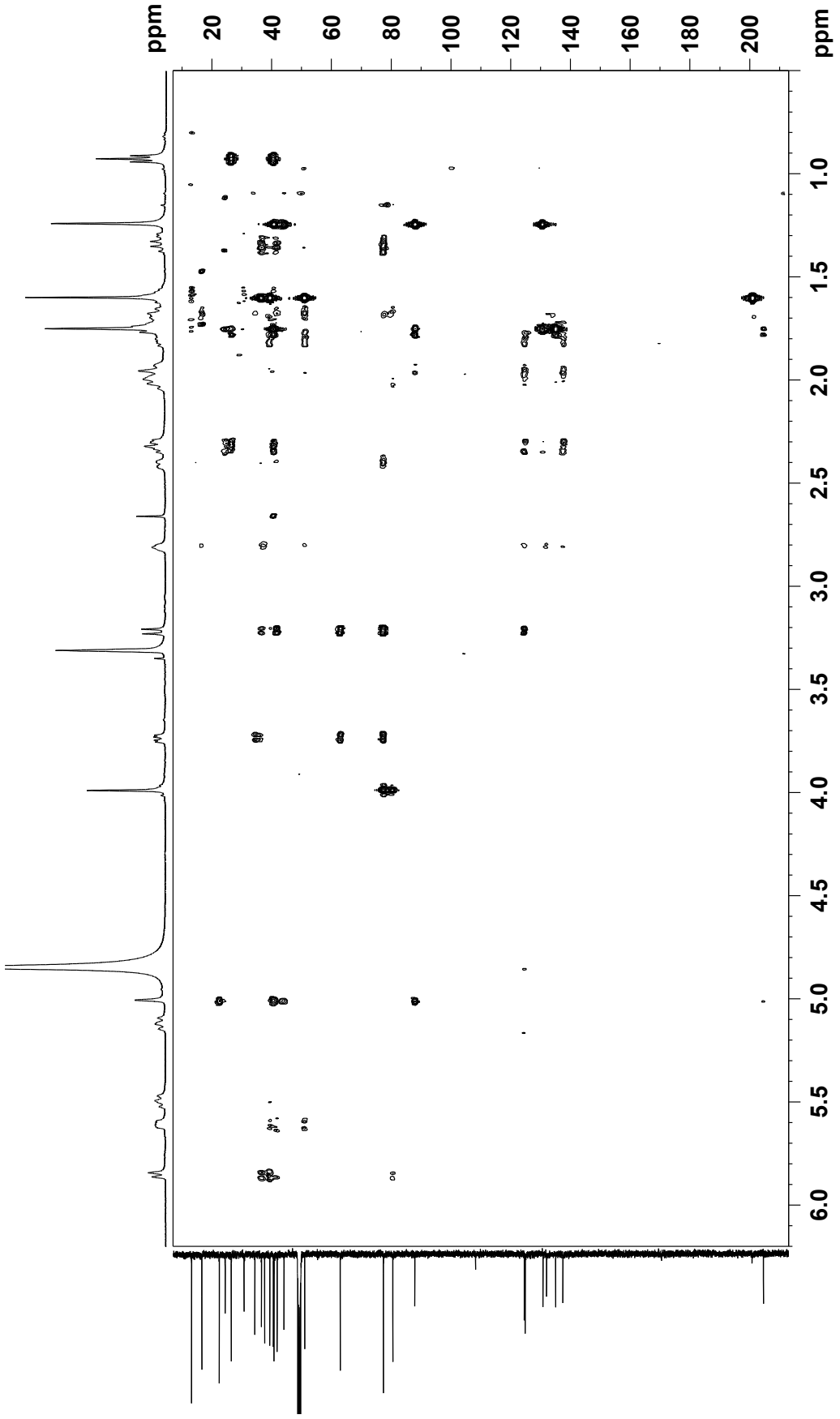

Figure S8. NOESY spectrum of **10** (500 MHz, CD_3OD).

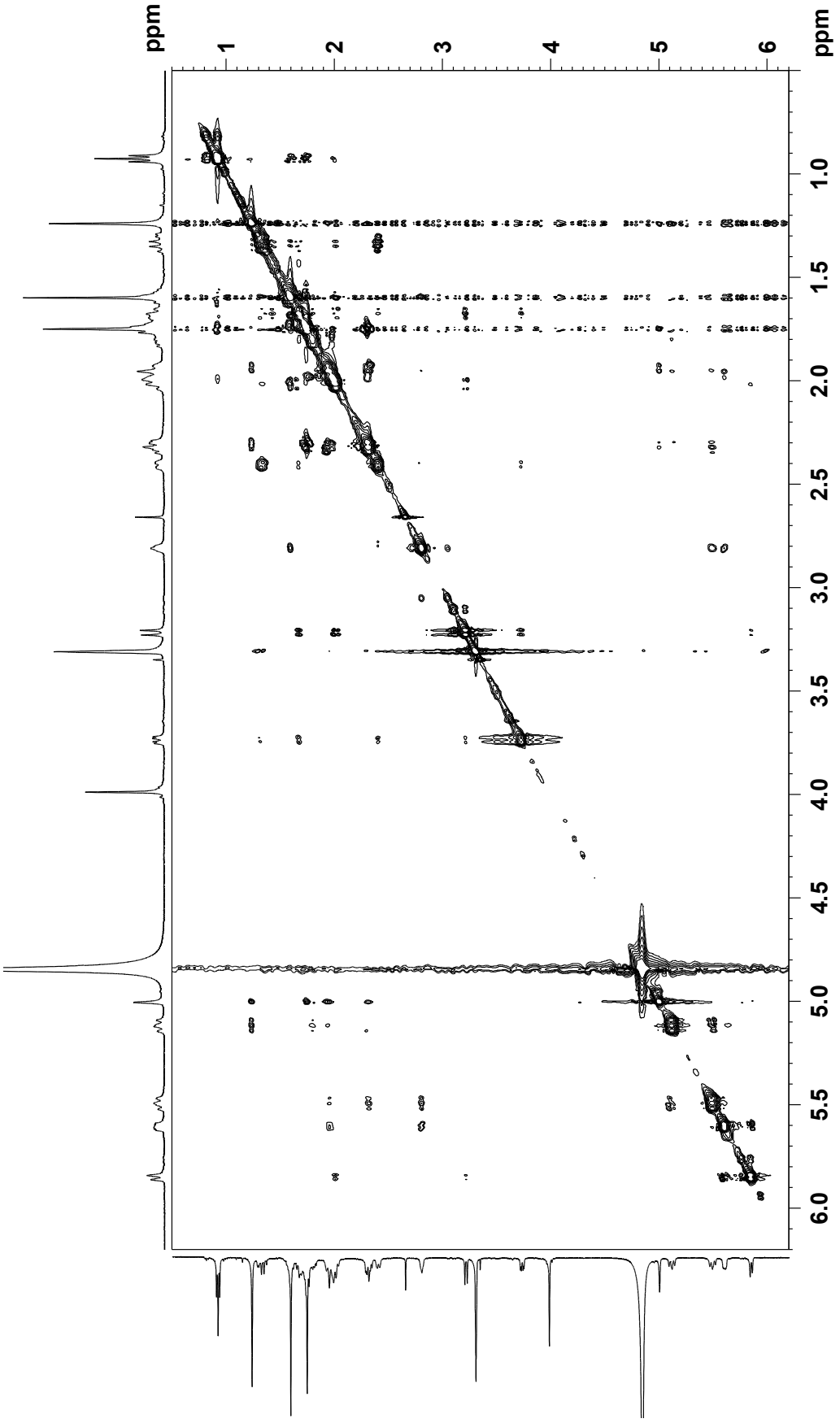

Figure S9. ROESY spectrum of **10** (500 MHz, CD_3OD).

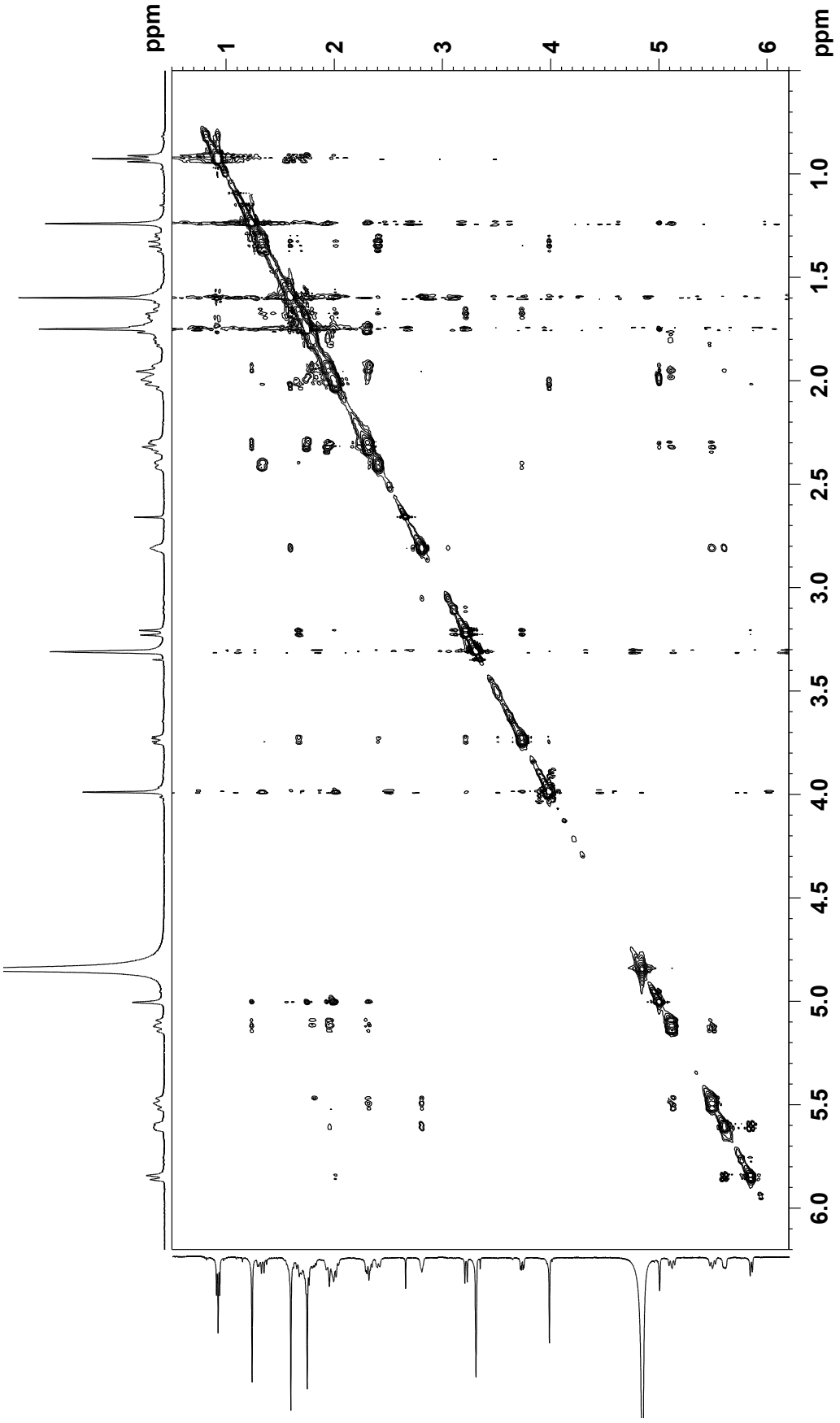

Figure S10. UV spectra of nomimicin C (**11**).

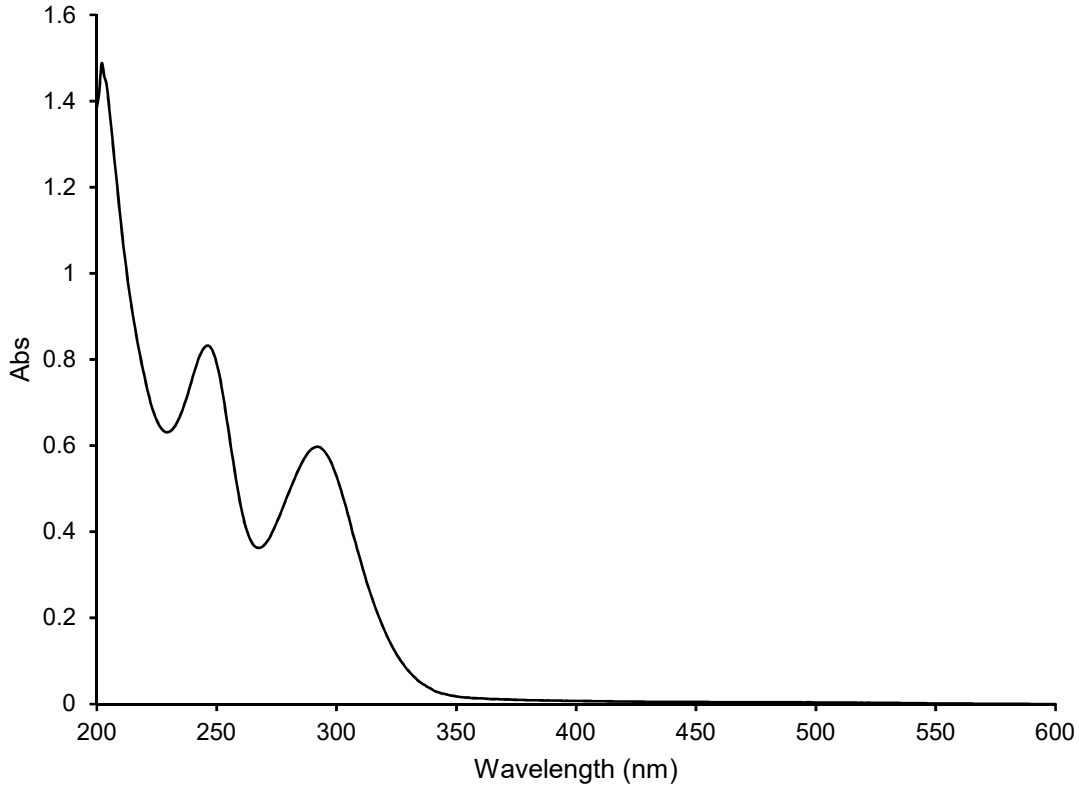

Figure S11. IR spectrum of **11**.

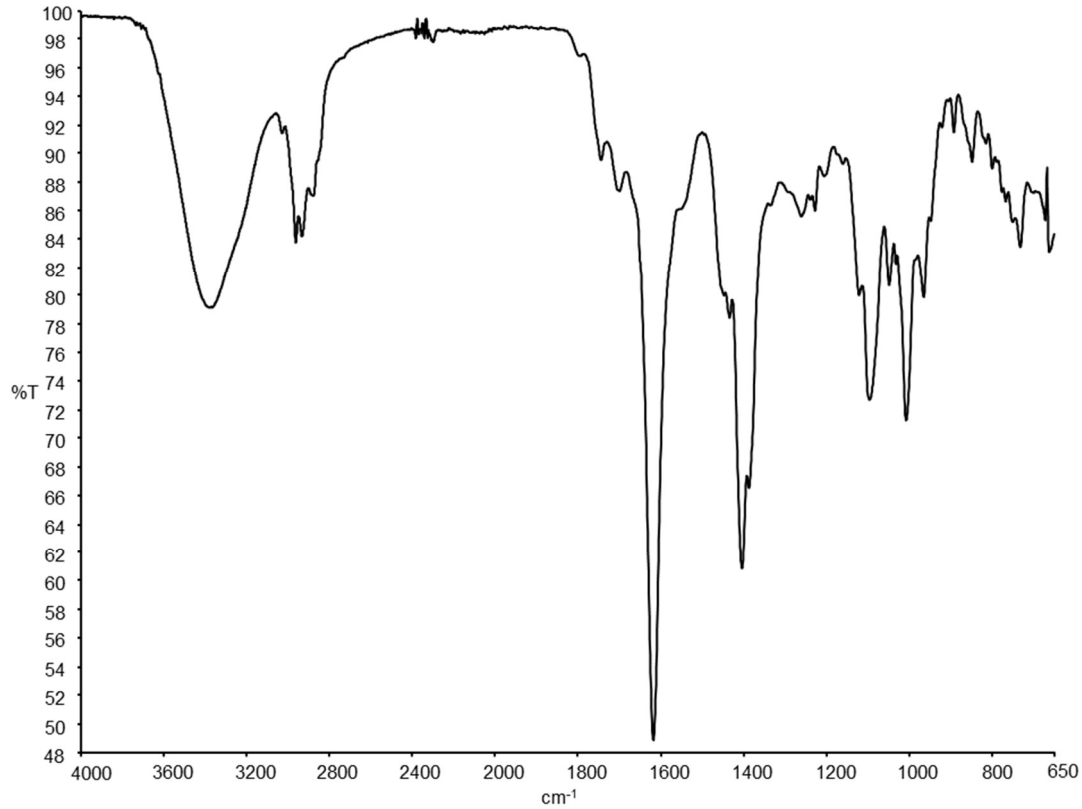

Figure S12. ^{1}H NMR spectrum of **11** (500 MHz, CD_3OD).

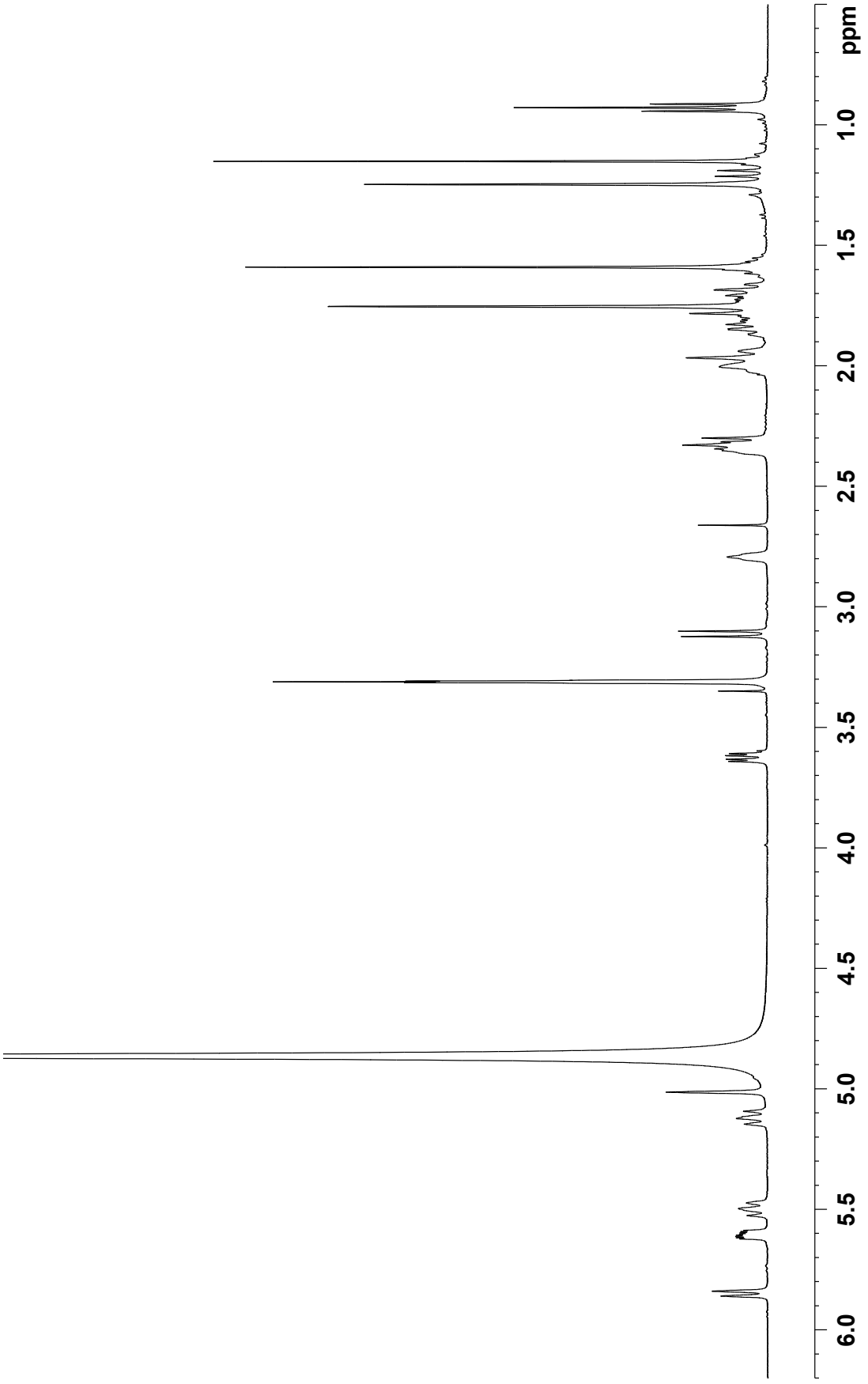

Figure S13. ^{13}C NMR spectrum of **11** (125 MHz, CD_3OD).

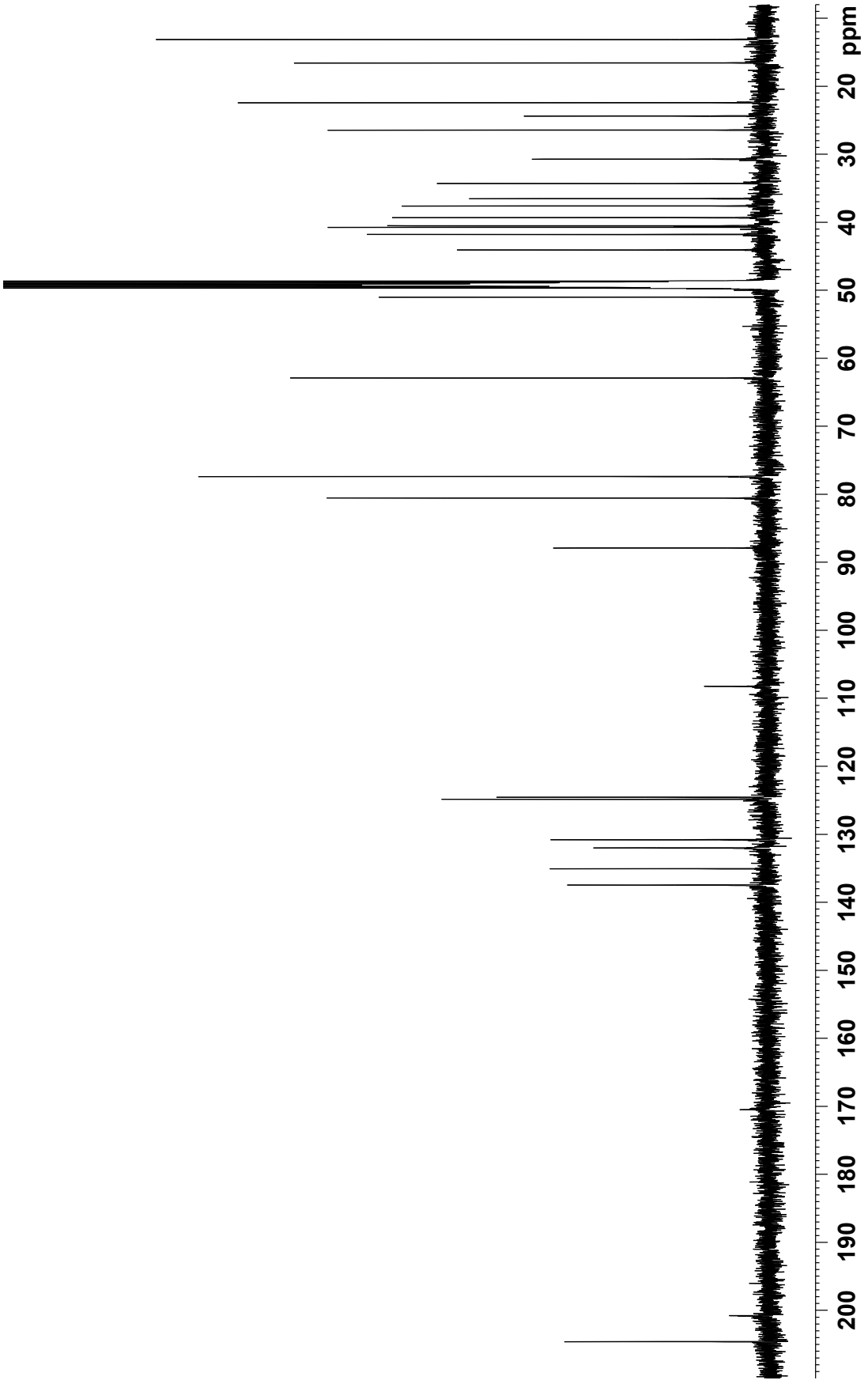

Figure S14. COSY spectrum of **11** (500 MHz, CD_3OD).

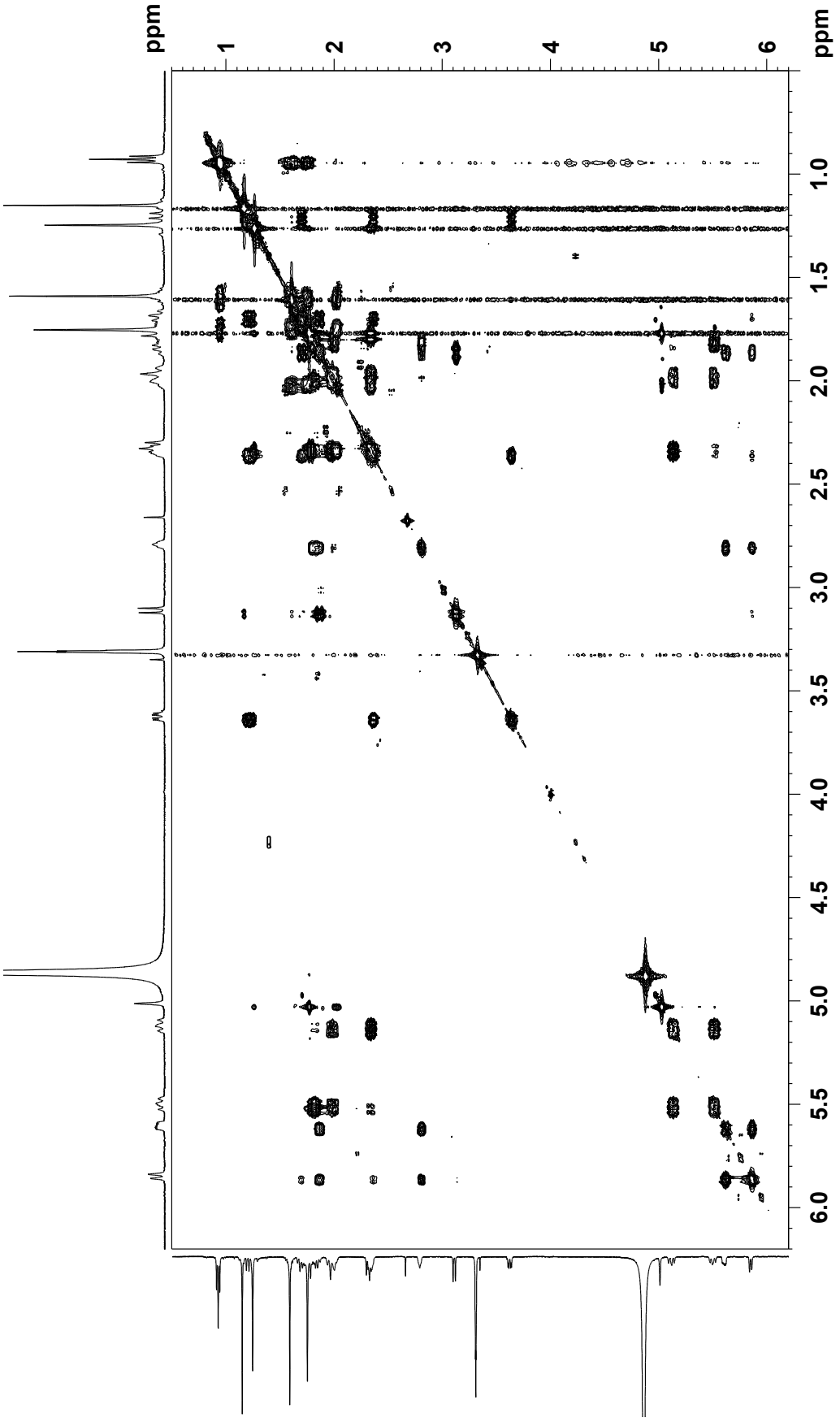

Figure S15. HSQC spectrum of **11** (500 MHz, CD_3OD).

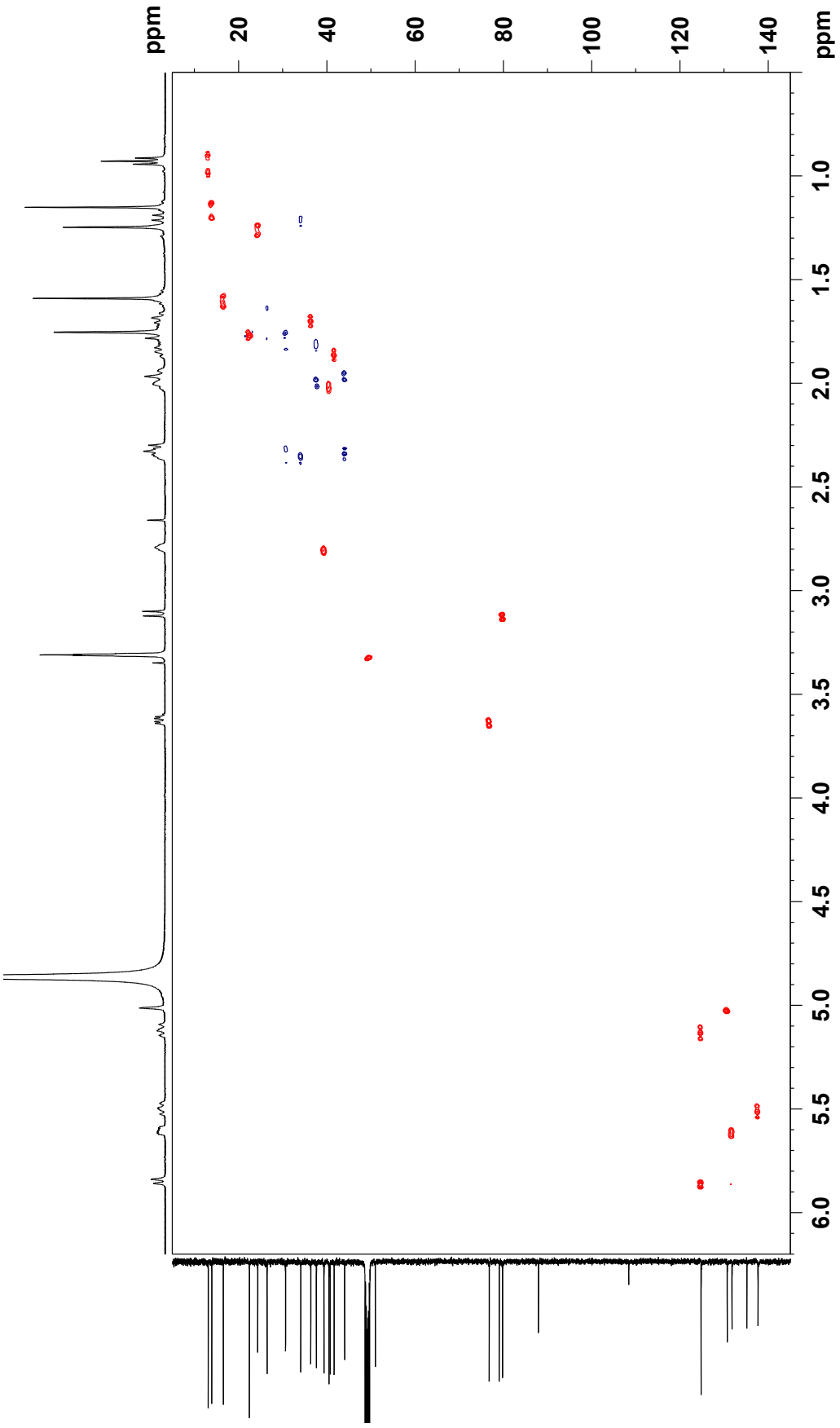

Figure S16. HMBC spectrum of **11** (500 MHz, CD_3OD).

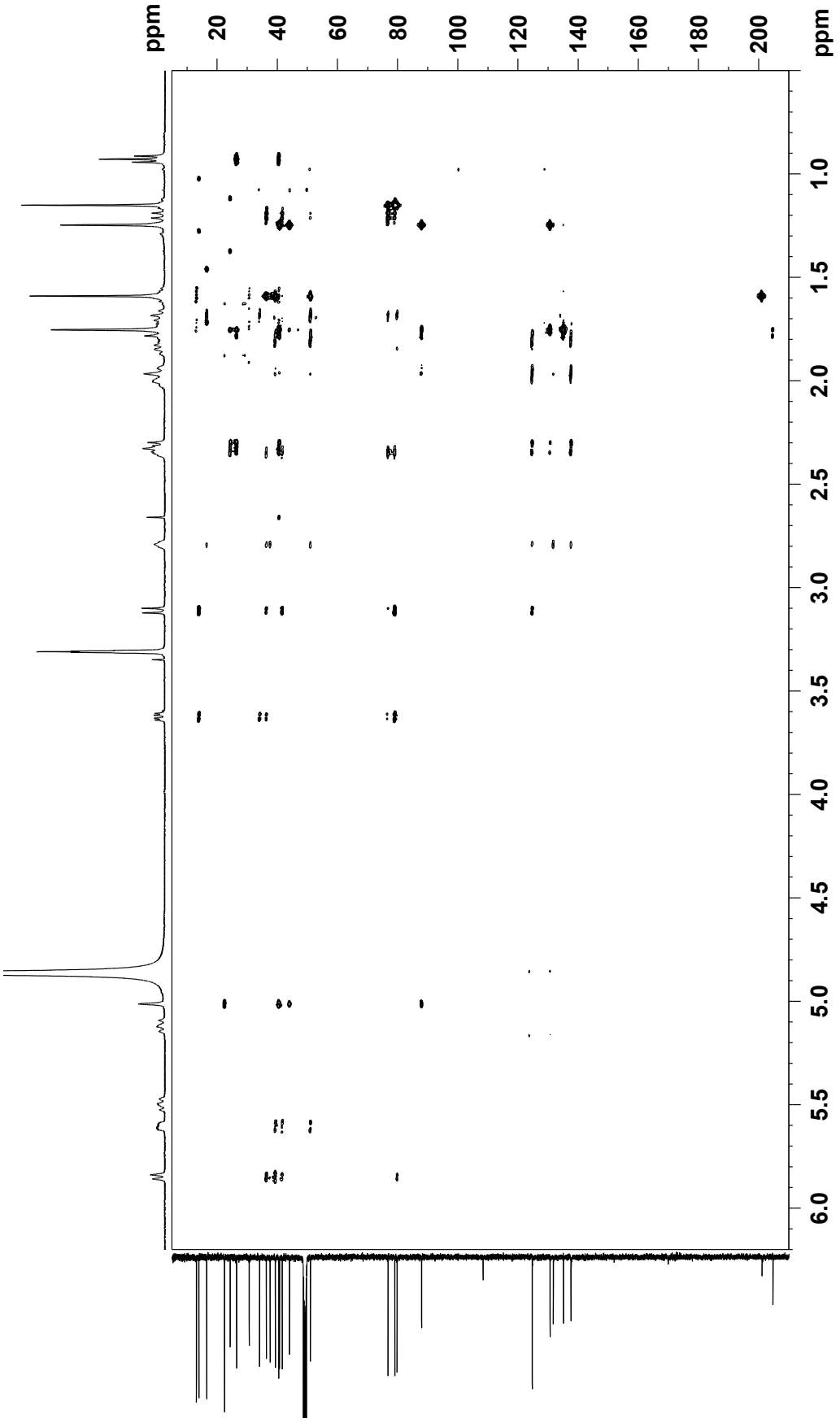

Figure S17. NOESY spectrum of **11** (500 MHz, CD_3OD).

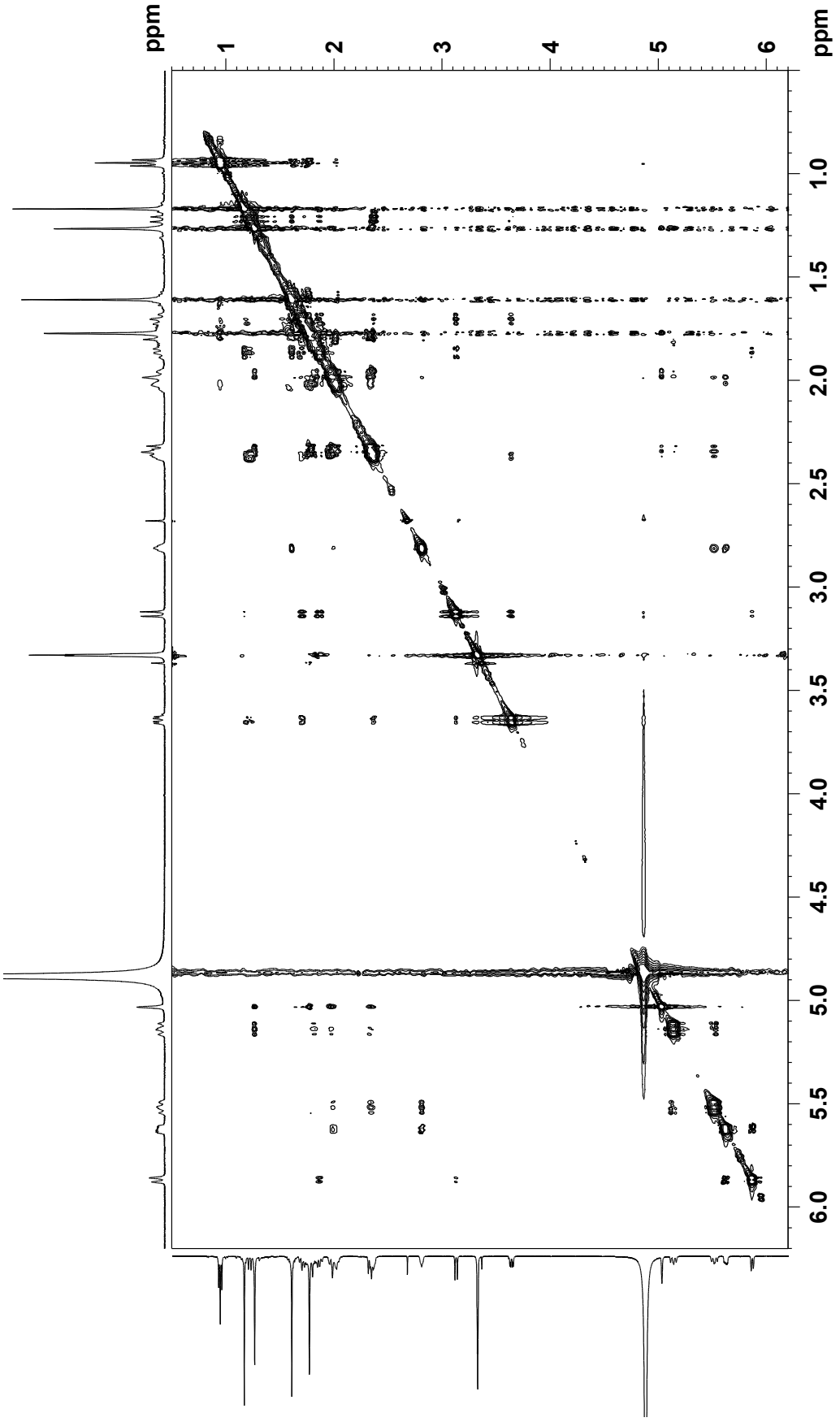

Figure S18. ROESY spectrum of **11** (500 MHz, CD_3OD).

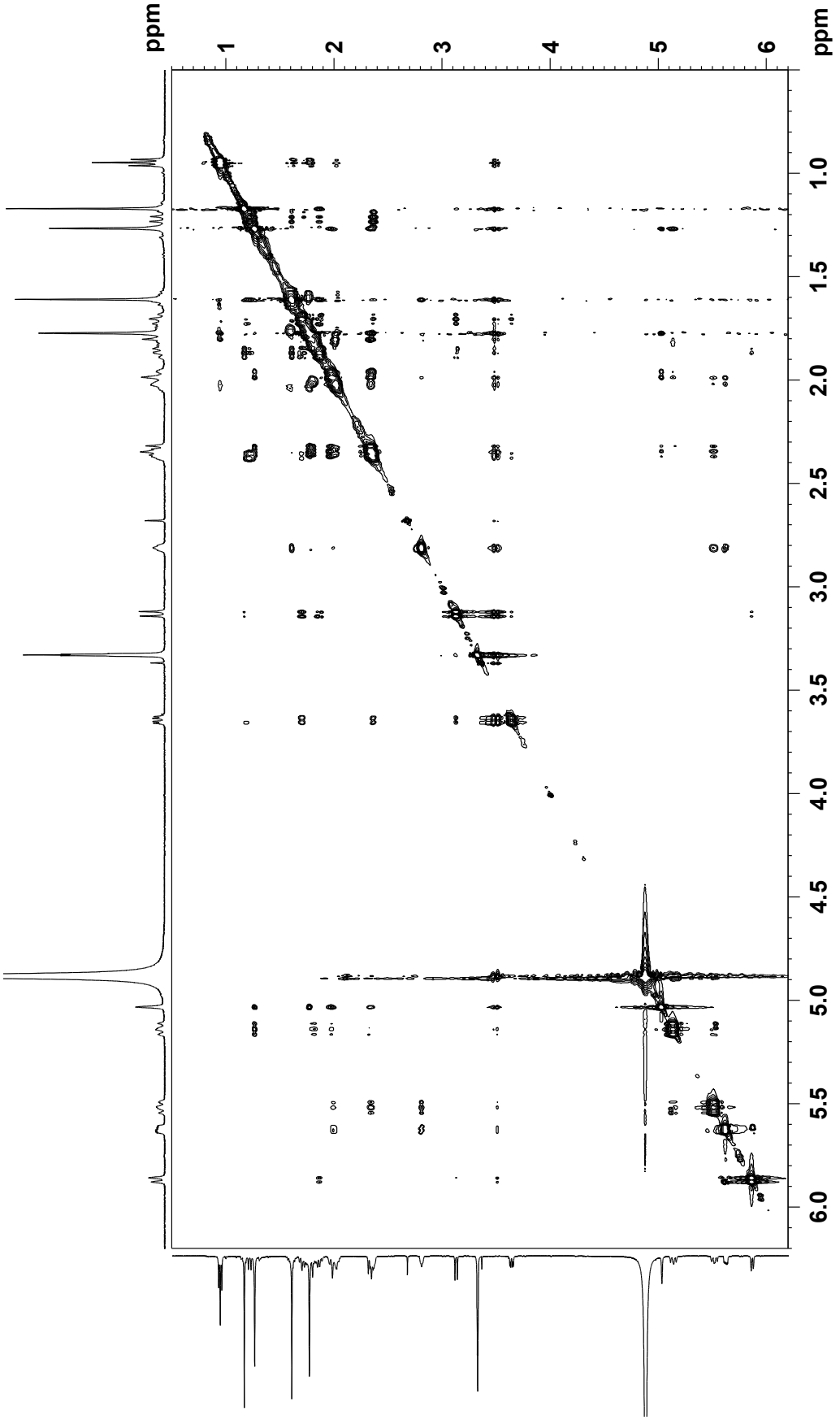

Figure S19. UV spectra of nomimicin D (**12**).

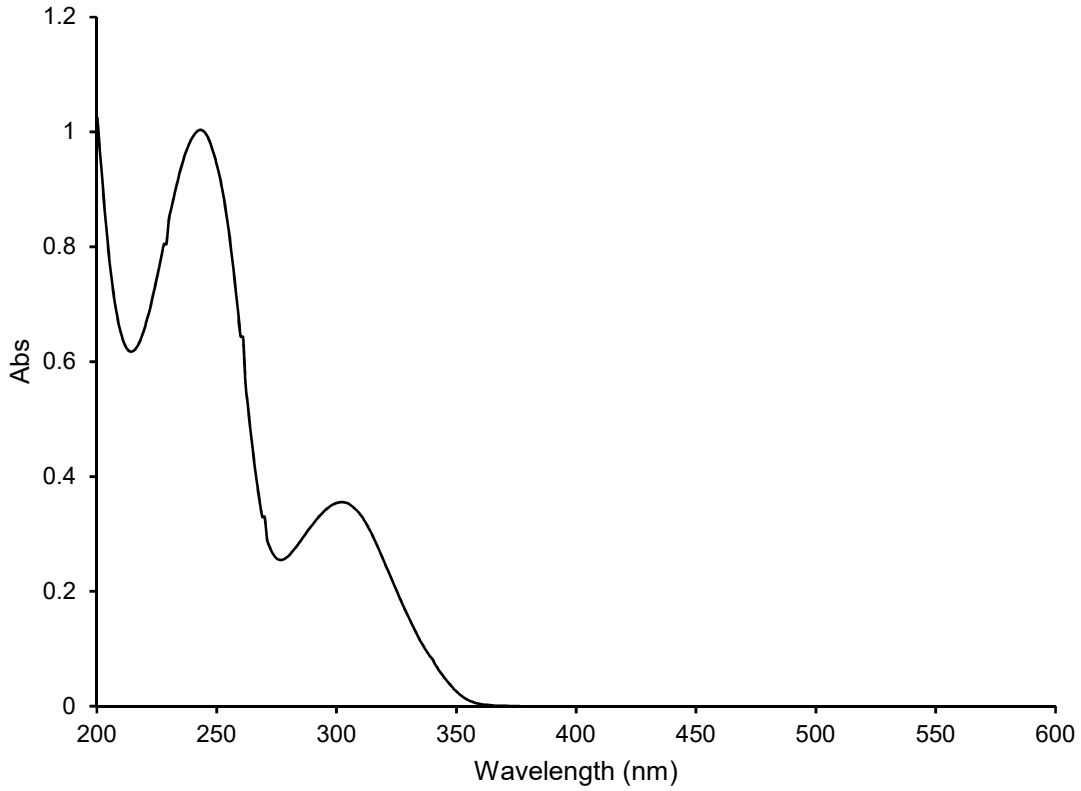

Figure S20. IR spectrum of **12**.

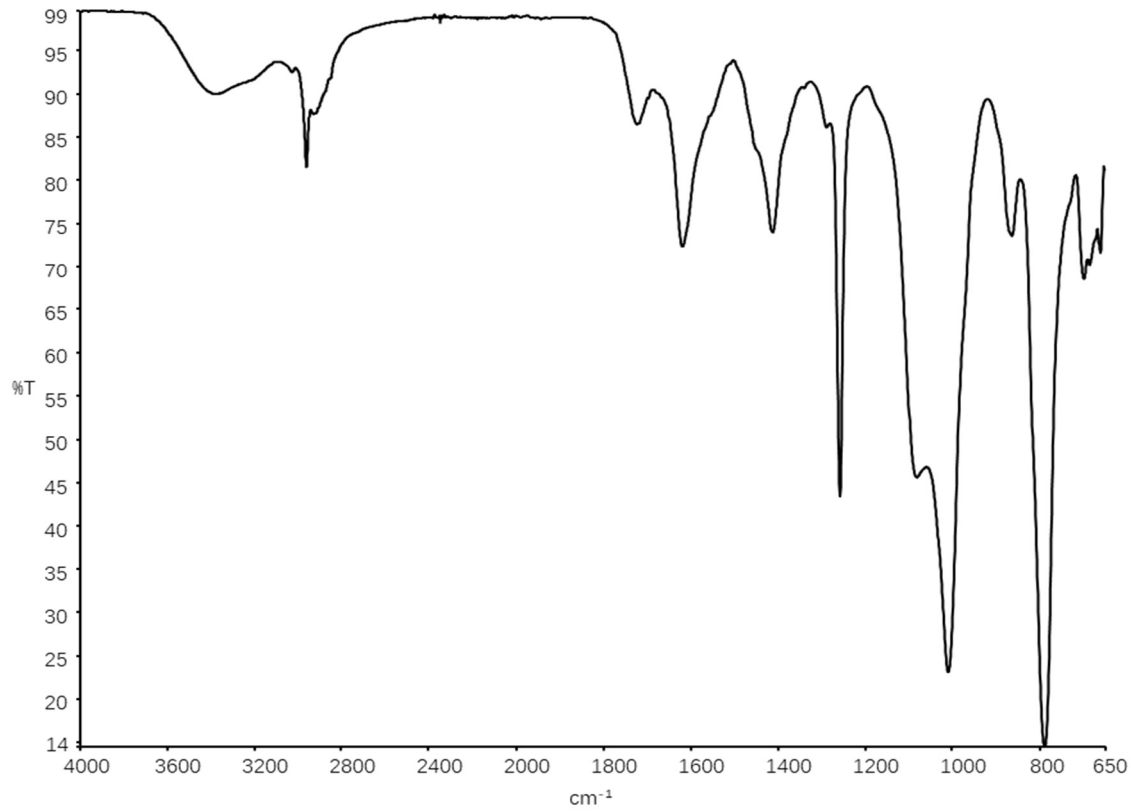

Figure S21. ^{1}H NMR spectrum of **12** (500 MHz, CD_3OD).

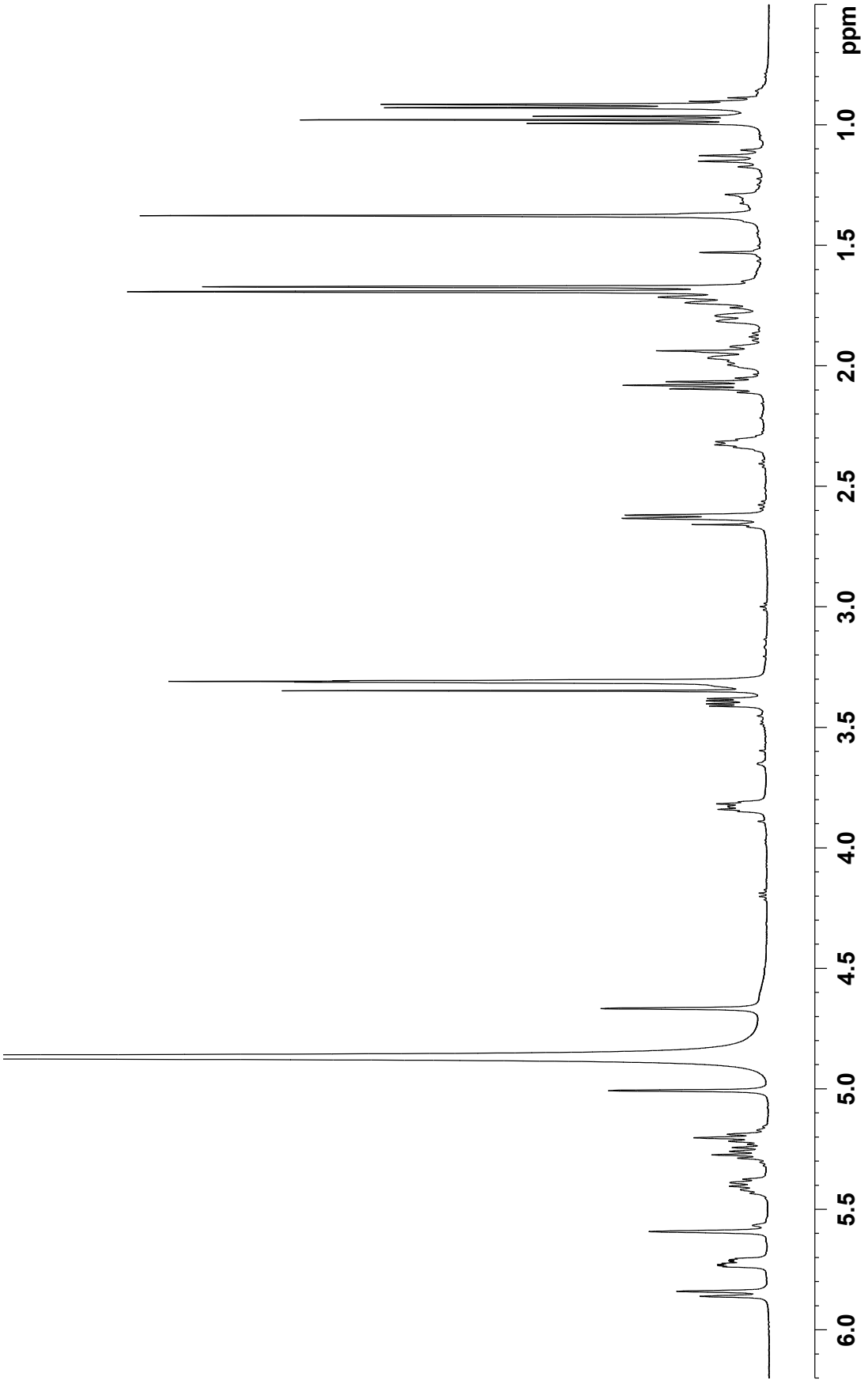

Figure S22. ^{13}C NMR spectrum of **12** (125 MHz, CD_3OD).

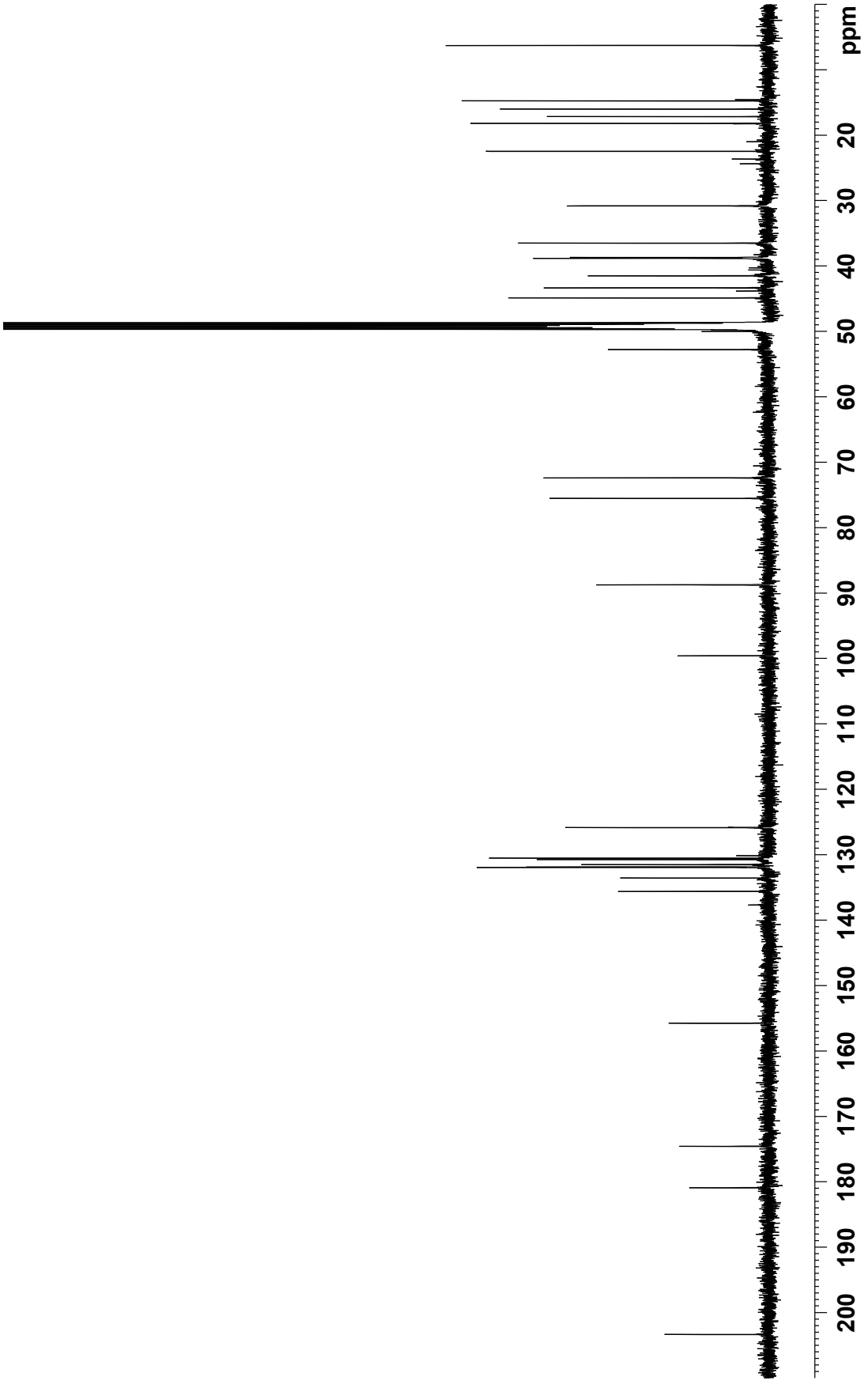

Figure S23. COSY spectrum of **12** (500 MHz, CD_3OD).

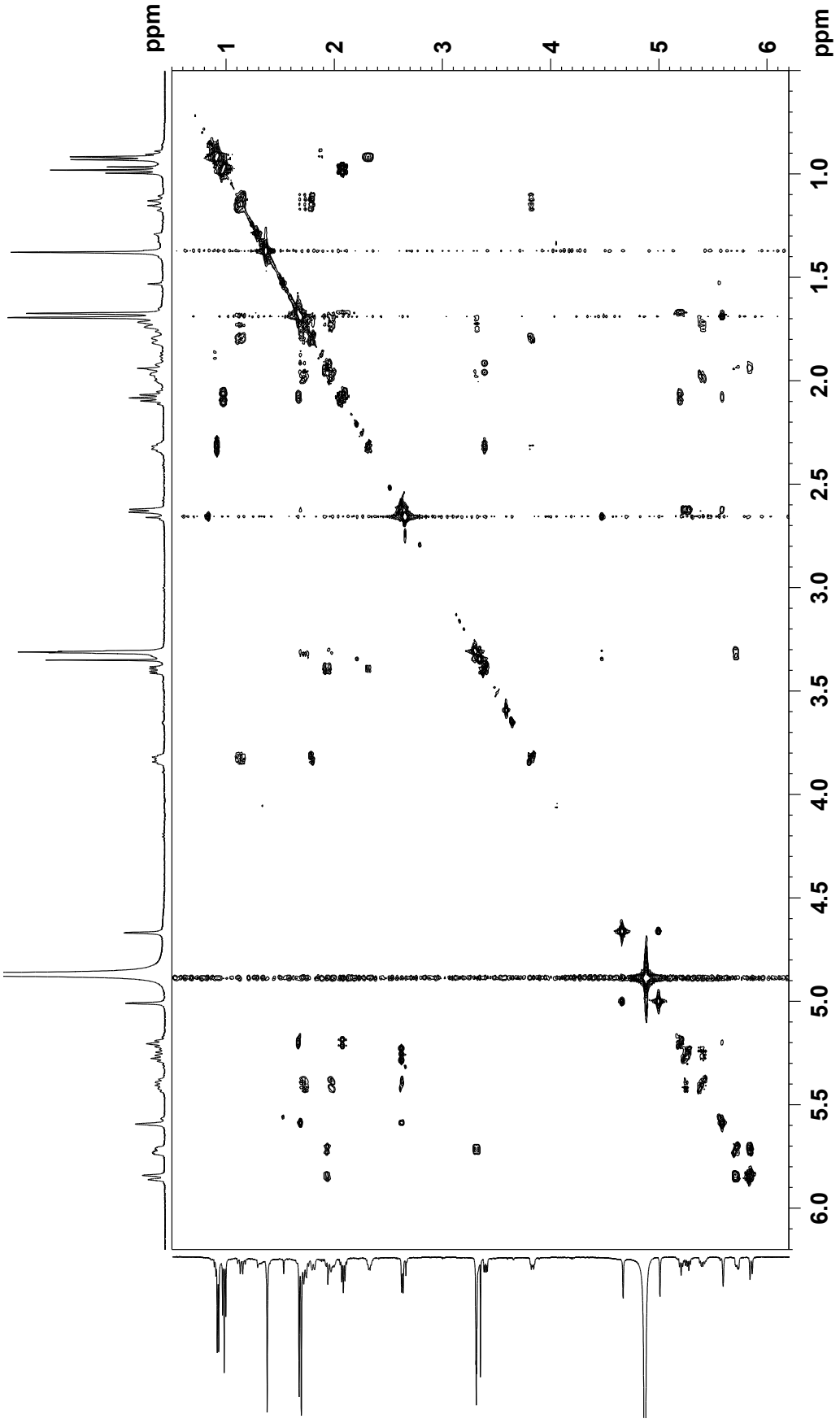

Figure S24. HSQC spectrum of **12** (500 MHz, CD_3OD).

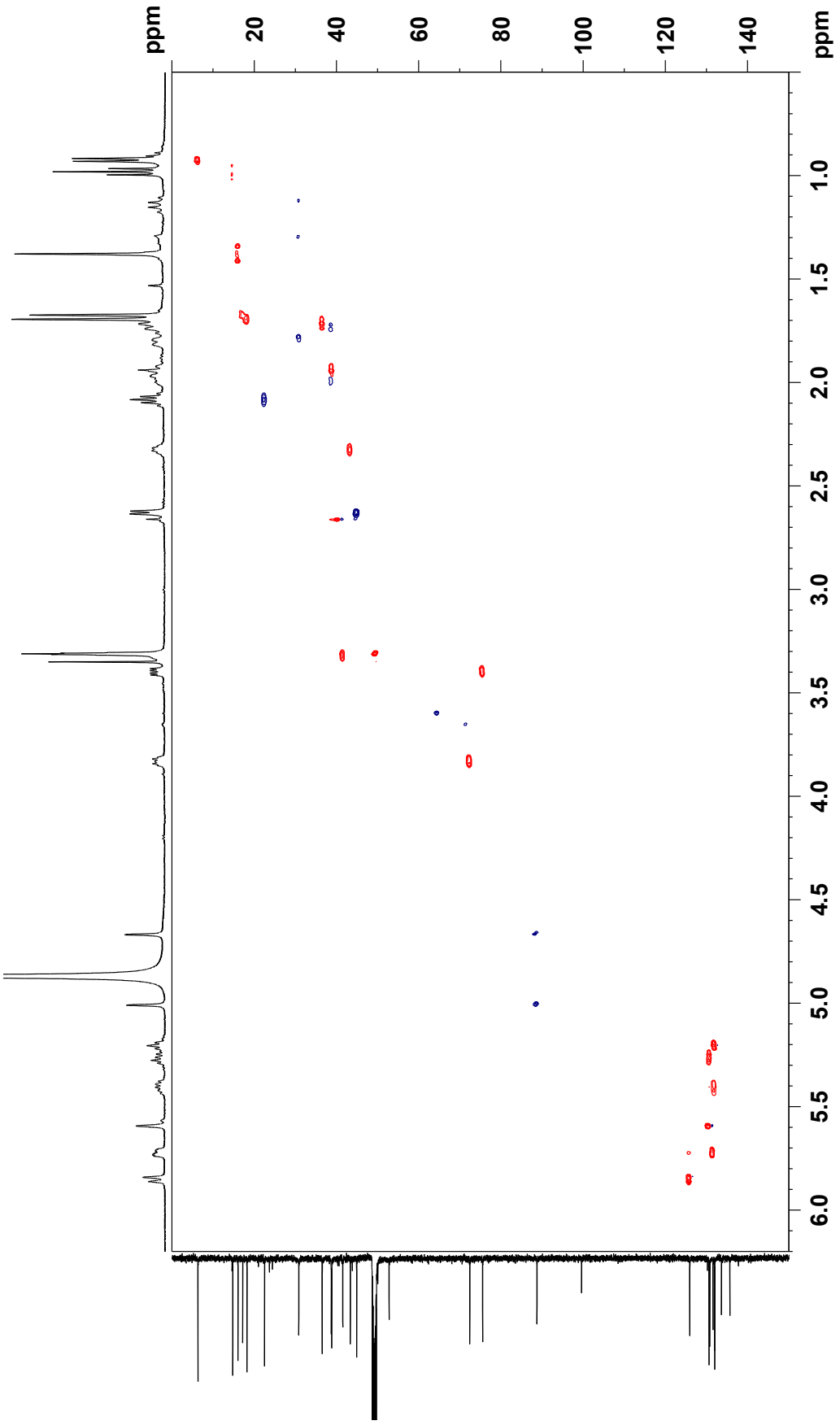

Figure S25. HMBC spectrum of **12** (500 MHz, CD_3OD).

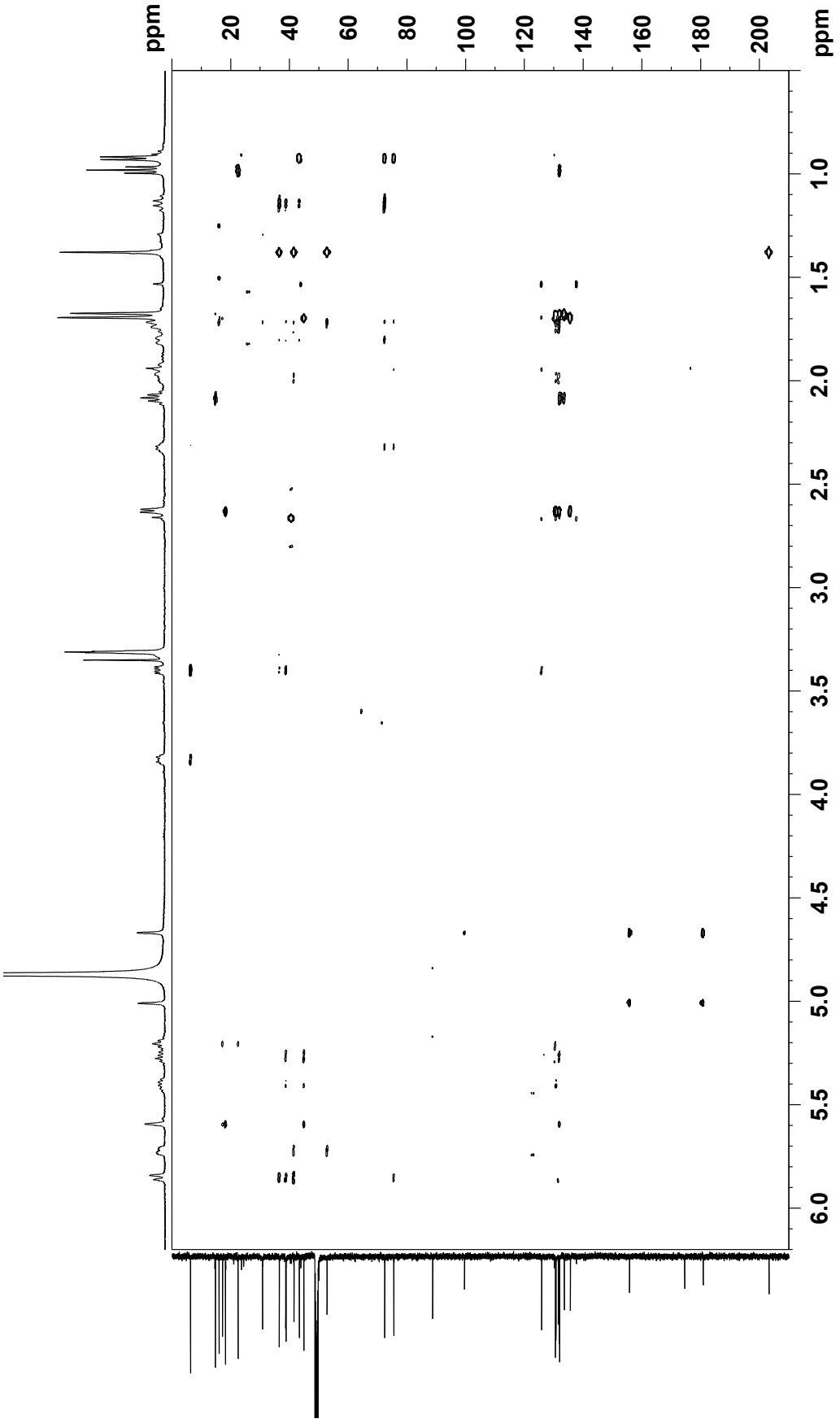

Figure S26. NOESY spectrum of **12** (500 MHz, CD_3OD).

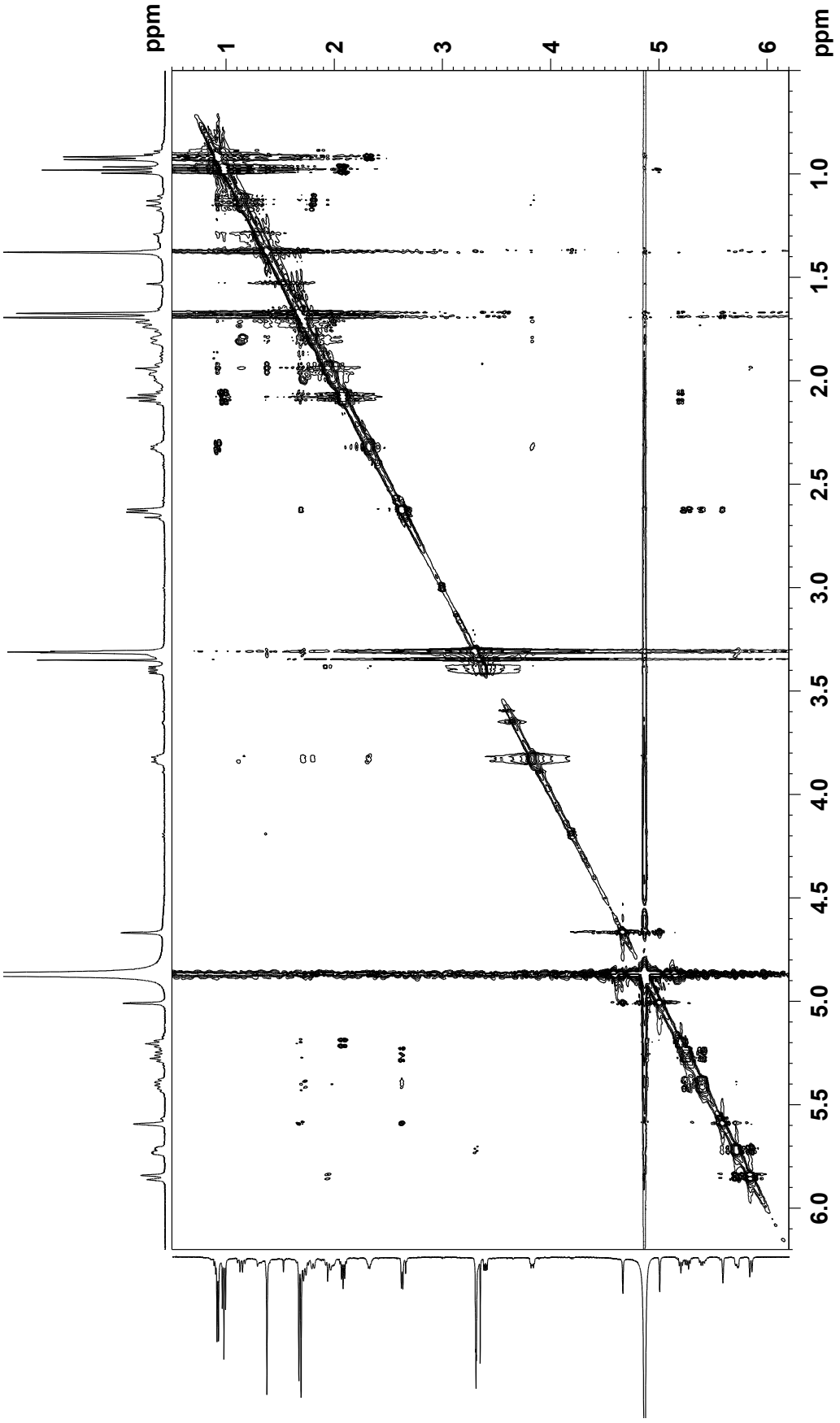

Figure S27. ROESY spectrum of **12** (500 MHz, CD_3OD).

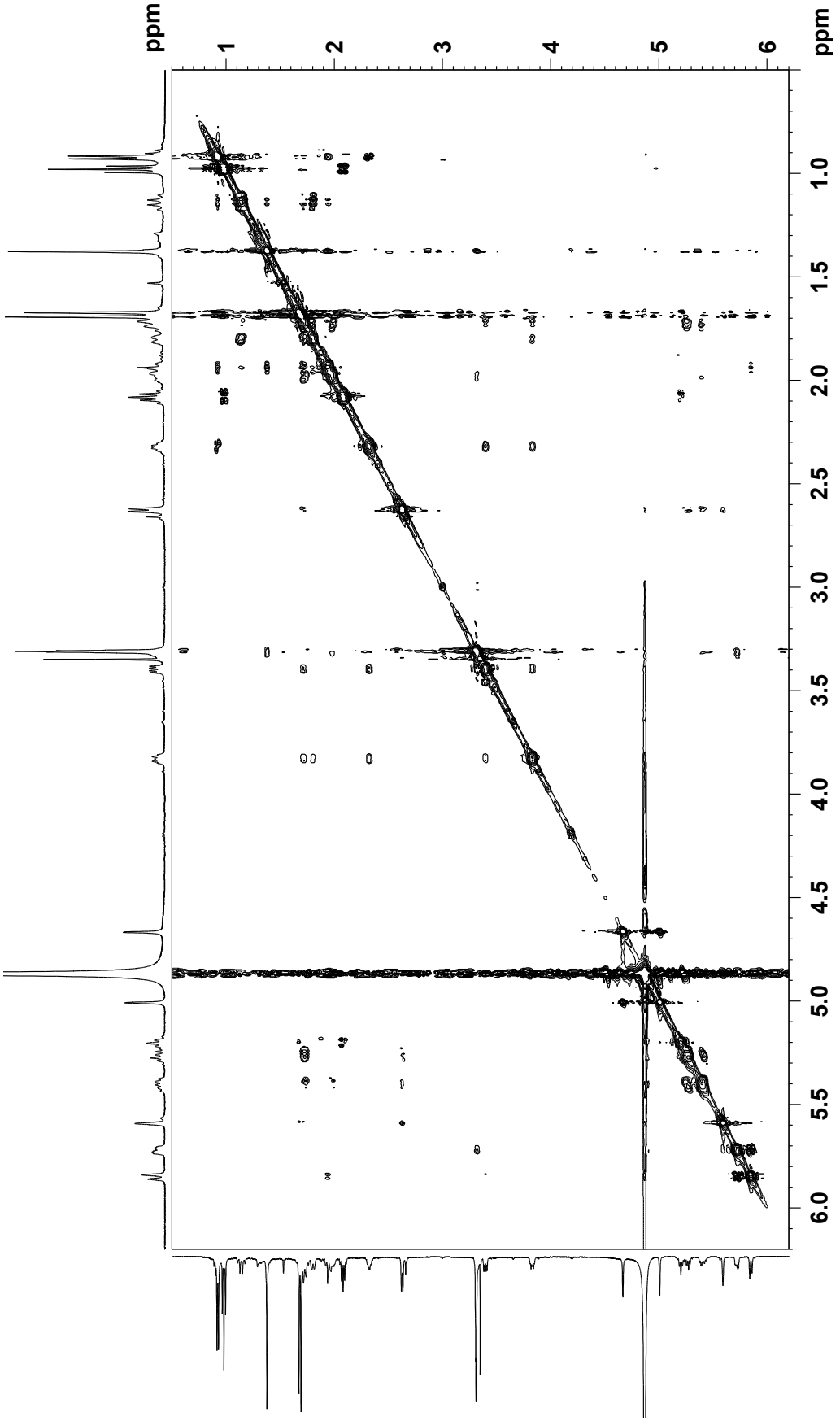

Figure S28. UV spectra of nomimicin A (**13**).

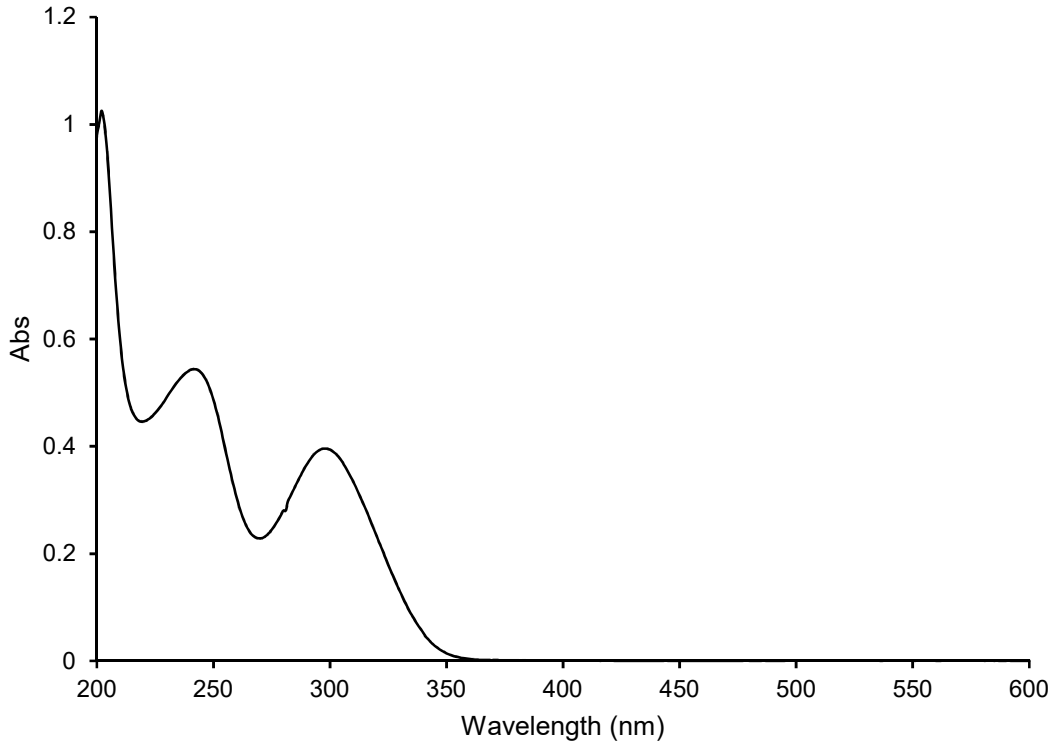

Figure S29. IR spectrum of **13**.

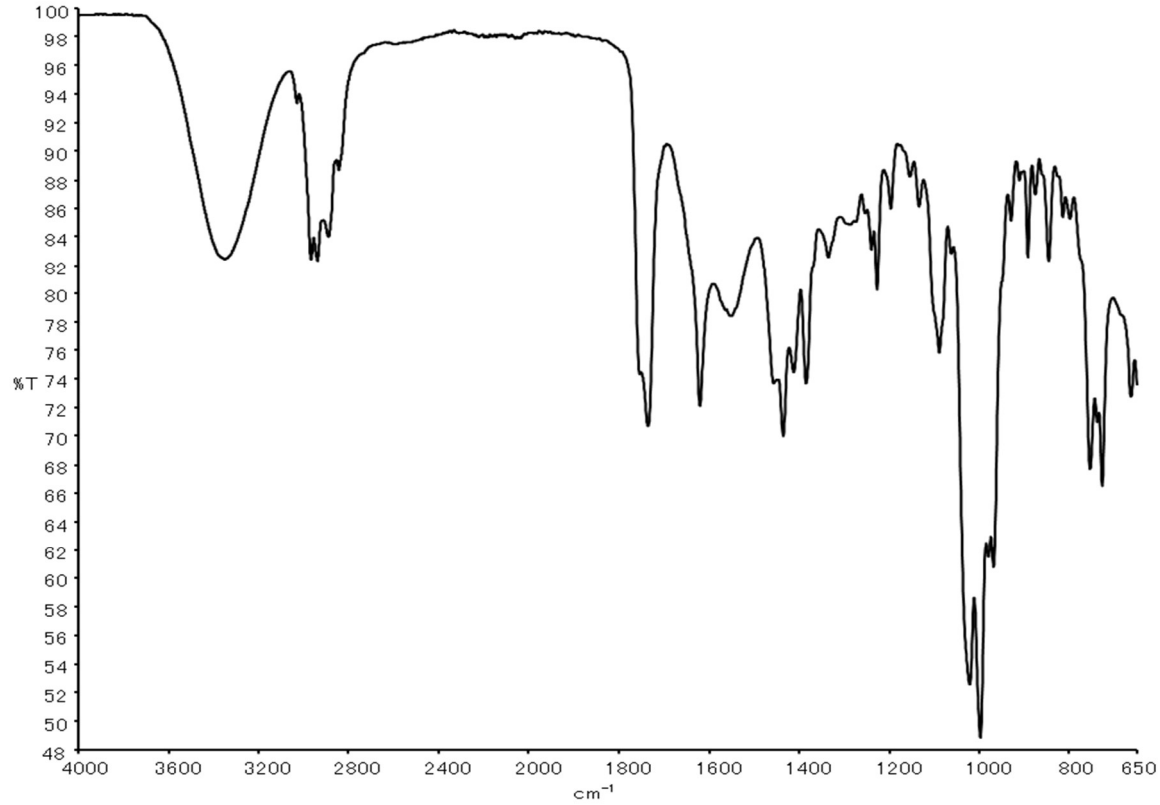

Figure S30. ^{1}H NMR spectrum of **13** (500 MHz, CD_3OD).

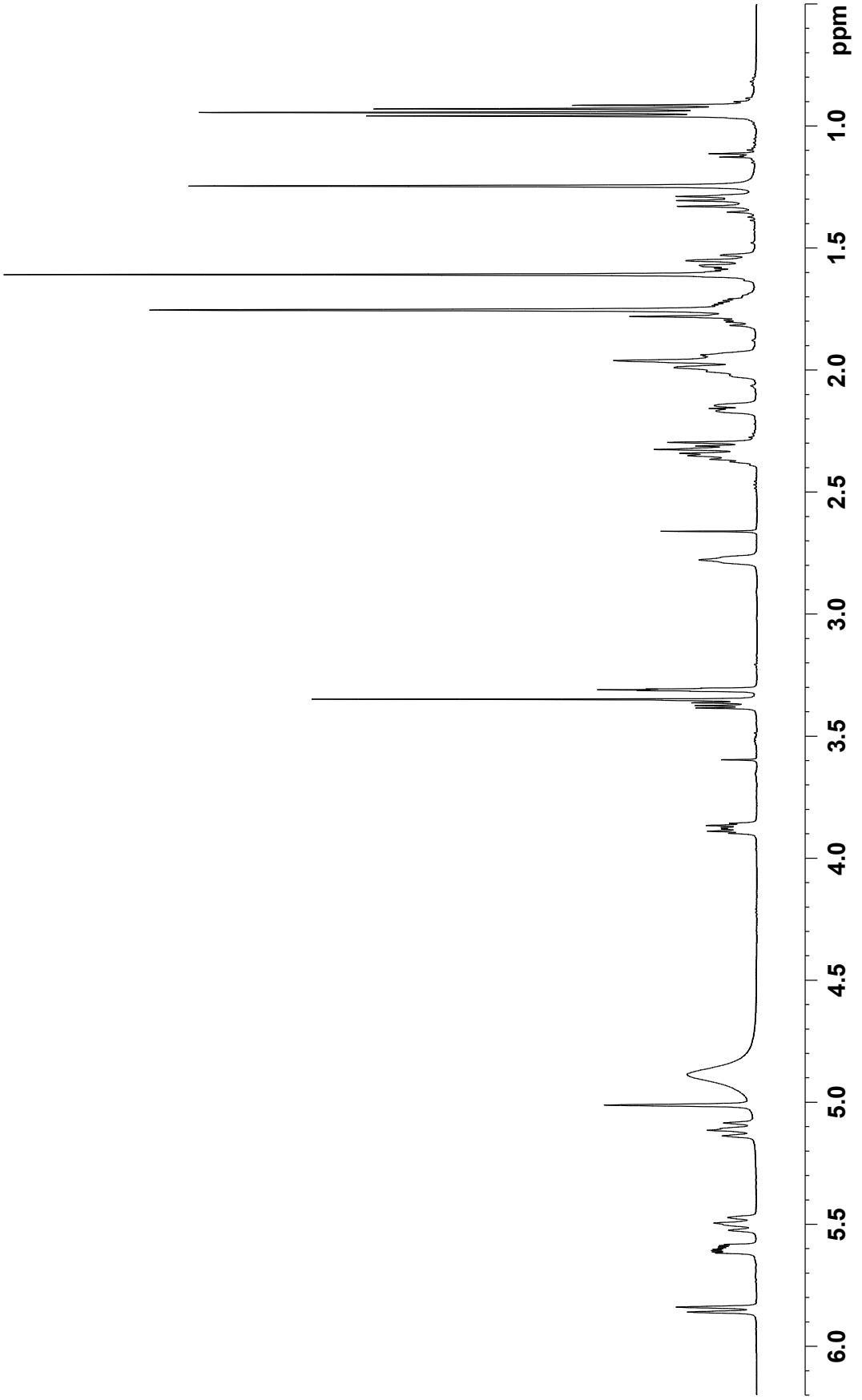

Figure S31. ^{13}C NMR spectrum of **13** (125 MHz, CD_3OD).

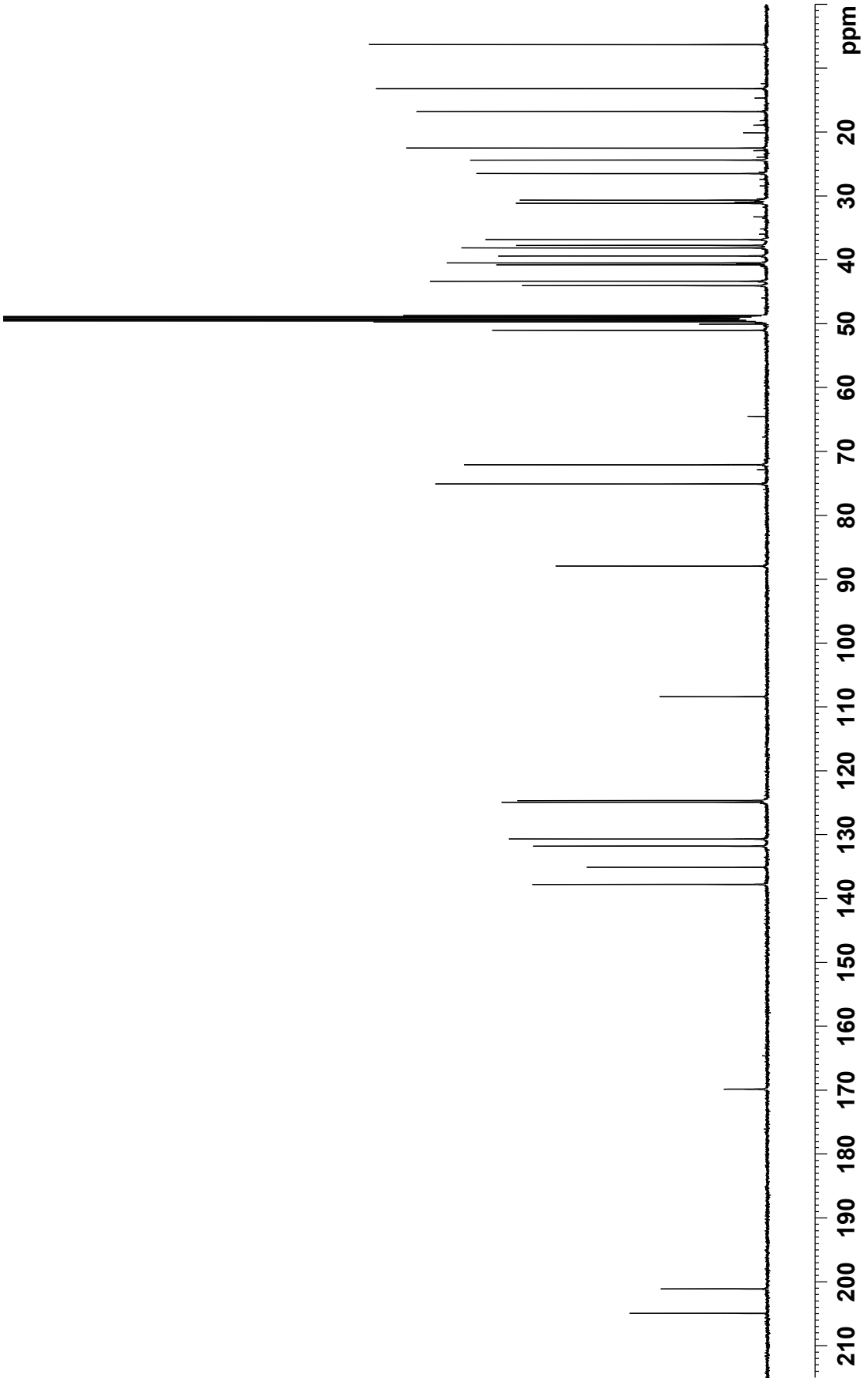

Figure S32. COSY spectrum of **13** (500 MHz, CD_3OD).

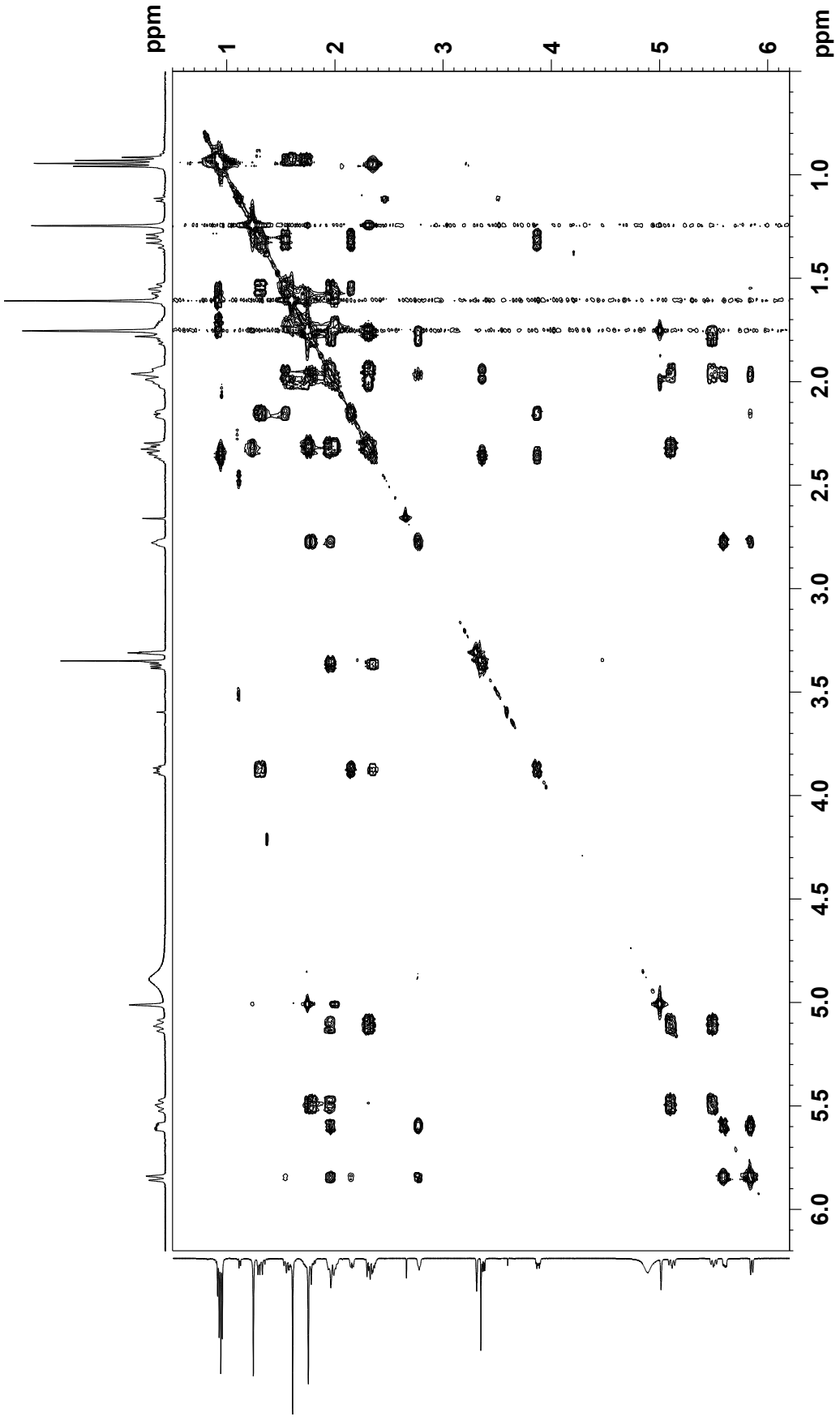

Figure S33. HSQC spectrum of **13** (500 MHz, CD_3OD).

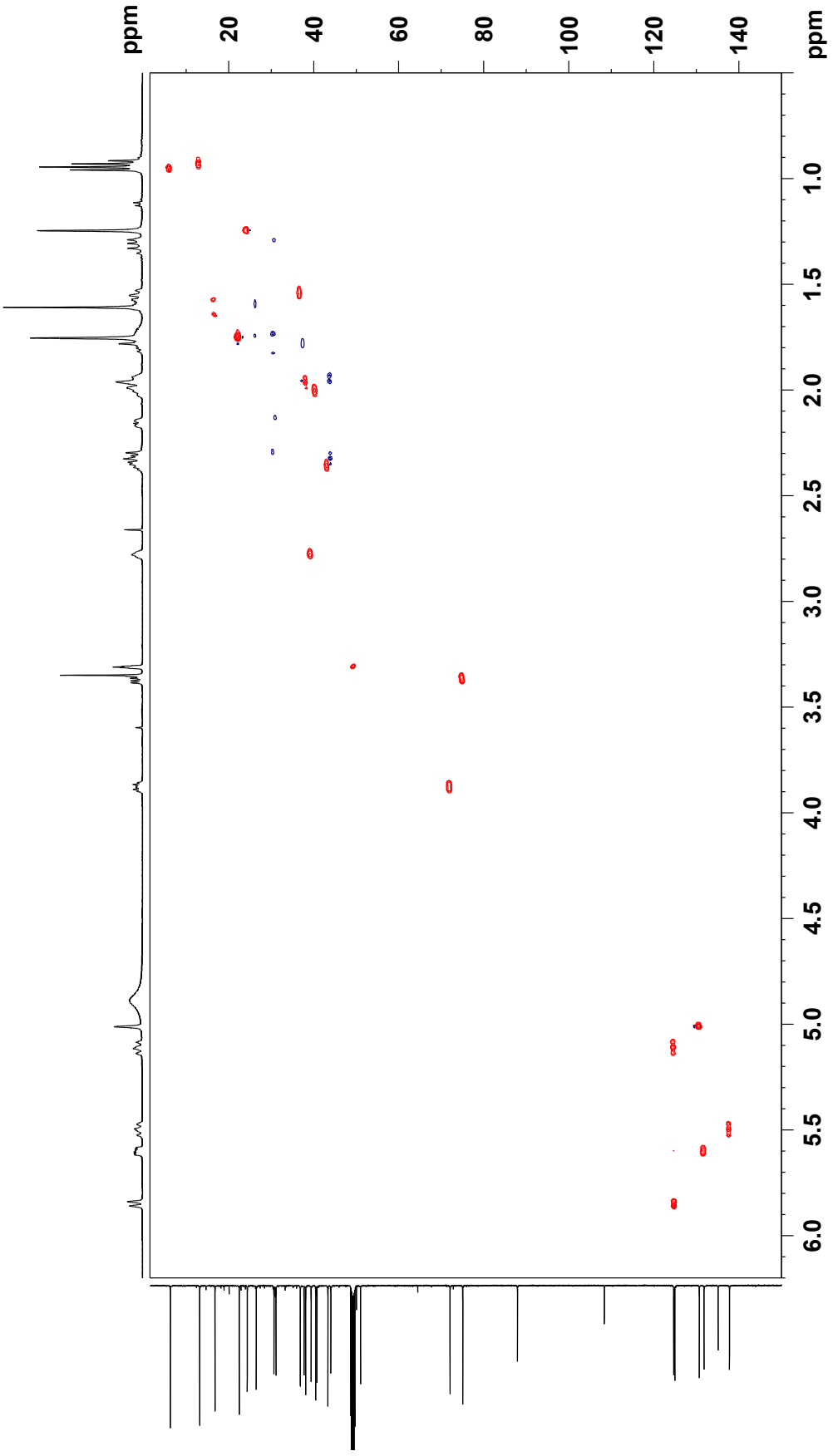

Figure S34. HMBC spectrum of **13** (500 MHz, CD_3OD).

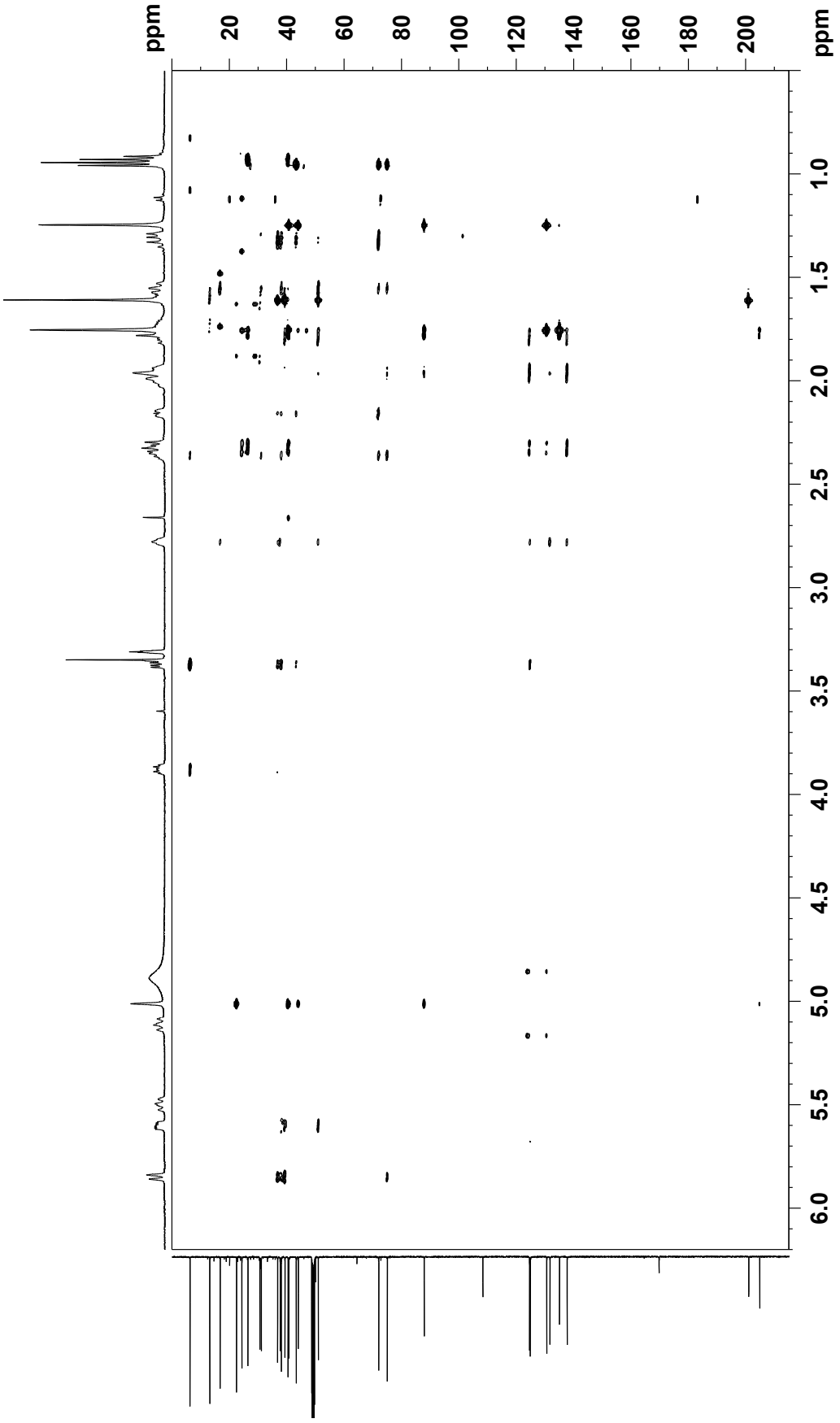

Table S1. NOESY and ROESY correlations of nomimicins B–C (**10**–**11**).

	10				**11**		
no.	δ_H,mult, (*J* in Hz)[a]	NOESY [a]	ROESY [a]	no.	δ_H,mult, (*J* in Hz)[a]	NOESY [a]	ROESY [a]
5	1.66, m	6b, 7, 9, 10	6b, 7, 9, 10	5	1.67, m	6b, 7, 9	6b, 7, 9
6a	1.34, m	6b, 10, 25,	6b, 10, 25, 26	6a	1.20, m	6b, 10, 25	6b, 10, 25
6b	2.41, br.d (11.1)	5, 6a, 7	5, 6a, 7	6b	2.33, m	5, 6a, 7	5, 6a, 7
7	3.73, dd (4.3, 11.9)	5, 6a, 9	5, 6a, 9	7	3.62, dd (4.2, 11.8)	5, 6a, 6b, 9	5, 6a, 6b, 9
9	3.21, d (11.2)	5, 7	5, 7	9	3.1, d (11.2)	5, 7, 10	5, 7, 10
10	2.02, m	6a, 11, 25	6a, 11, 25, 26	10	1.83, m	6a, 9, 11, 25, 26	6a, 9, 11, 25, 26
11	5.85, d (10.1)	9, 10, 12	9, 10, 12	11	5.84, d (10.1)	9, 10, 12	9, 10, 12
12	5.60, ddd (9.8, 5.0, 2.2)	11, 13, 14b	11, 13, 14b	12	5.60, ddd (10.1, 5.1, 2.6)	11, 13, 14b	11, 13, 14b
13	2.81, m	12, 15, 25	12, 15, 23	13	2.79, m	12, 14a, 14b, 15, 25	12, 14a, 14b, 15, 25
14a	1.79, m	15, 16	15, 16	14a	1.78, m	13, 16	13, 16
14b	1.98, m	12, 15, 16	12, 13, 15, 16	14b	1.95, m	12, 13, 15, 16	12, 13, 15, 16
15	5.49, m	13, 14a, 14b, 16, 17b	13, 14a, 14b, 16, 17b	15	5.48, m	13, 14b, 16, 17b	13, 14b, 16, 17b
16	5.12, dd (11.3, 14.8)	14a, 15, 17a, 17b, 27	14a, 14b, 15 17b, 27	16	5.12, dd (11.3, 14.8)	14a, 14b, 15, 17b, 27	14a, 14b, 17b, 27
17a	1.94, m	27, 17b, 19	27, 17b, 19	17a	1.95, m	16, 19, 17b, 27	16, 19, 17b, 27
17b	2.32, m	15, 16, 17a, 19	17a, 19, 16, 15	17b	2.31, m	15, 19, 17a, 27	15, 16, 17b, 19, 27
19	5.00, s	17a, 17b, 27, 28	27, 28, 17a, 17b	19	5.01, s	17b, 21, 27, 28	17b, 21, 27, 28
21	1.99, m	22b, 30	22b, 30	21	1.99, m	22b, 28, 30	22b, 28, 30
22a	1.74, m	30	30	22a	1.73, m	30	30
22b	2.29, m	21, 27, 29b	21, 27, 29b	22b	2.29, m	21, 22a, 27, 29b	21, 22a, 27, 29b
25	1.59, s	10, 13	10, 13	25	1.59, s	6b, 10, 13	6b, 10, 13
26	3.98, s		6b, 10	26	1.15, s	10	10
27	1.24, s		16, 17b, 19, 22b	27	1.24, s	16, 17b, 19, 22b	16, 7b, 19, 22b
28	1.74, s	19, 22a, 29b, 30	19	28	1.75, s	19, 21, 30	19, 21, 30
29a	1.62, m	30	22b, 30	29a	1.60, m	30	30
29b	1.77, m	21	21, 22b	29b	1.76, m	21, 22b, 30	21, 22b, 30
30	0.92, t (7.4)	21, 22a, 29a, 29b	21, 22a, 29a, 29b	30	0.92, t (7.4)	21, 22a, 28, 29a, 29b	21, 22a, 28, 29a, 29b

[a]Recorded at 500 MHz.

Table S2. ROESY and NOESY correlations of nomimicin D (**12**).

N	δ_H,mult, (*J* in Hz)[a]	NOESY [a]	ROESY [a]
1a	4.66, d (1.50)	1b	1b
1b	5.00, d (1.50)	1a	1a
8	1.71, m	10	10, 12
9a	1.13, q (11.6)	9b, 13, 27, 28	9b, 13, 27, 28
9b	1.79, d (11.6)	9a, 10	9a, 10
10	3.82, m	8, 9a, 9b, 11	8, 9b, 11, 12
11	2.31, d (6.8)	12, 28	10, 12, 28
12	3.39, dd (4.8, 6.1)	8, 11, 13	8, 9b, 10, 11
13	1.93, m	9a,12, 14, 27, 28	9a, 14, 27, 28
14	5.85, d (10.2)	13, 15	12, 13, 15
15	5.72, m	14, 16	14, 16
16	3.32, m	15, 17b, 18, 27	15, 17b, 18, 27
17a	1.73, m	17b, 18	17b, 18, 19
17b	1.99, m	16, 17a, 18	16, 17a, 18, 19
18	5.4, m	16, 17a, 17b, 20	17a, 17b, 20
19	5.26, m	20	17a, 17b, 20
20	2.62, d (6.8)	18, 19, 22, 29	18, 19, 22, 29
22	5.59, s	20, 29, 30	20, 29, 30
24	5.20, t (7.4)	25, 30	25, 30
25	2.08, q (7.6)	24, 26	24, 26
26	0.98, t (7.6)	25	25
27	1.37, s	9a, 13, 16	9a, 13, 16
28	0.92, d (6.9)	9a, 11, 13	9a, 11, 13
29	1.69, s	20, 22	20, 22
30	1.67, s	22, 24	22, 24

[a]Recorded at 500 MHz.

Table S3. Cartesian coordinates and energies of the most stable conformer of **13a**.

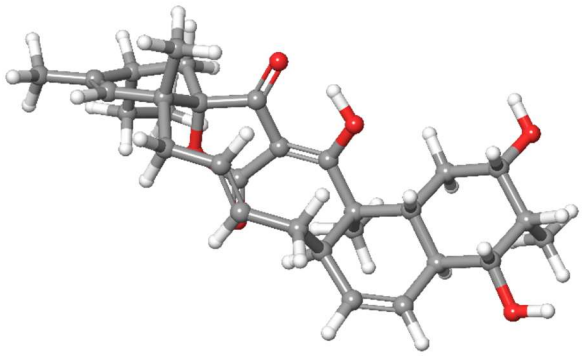

13a (ΔG = 0.0 kcal/mol)

M06-2X/def2-TZVP-SMD(MeOH)//M06-2X/6-31G(d)-SMD(MeOH):		
Gibbs Free Energy (a.u.)	=	−1617.990463
M06-2X/def2-TZVP-SMD(MeOH):		
Electronic energy (a.u.)	=	−1618.593138
M06-2X/6-31G(d)-SMD(MeOH):		
Zero-point correction (a.u.)	=	0.663531
Thermal correction to Energy (a.u.)	=	0.697126
Thermal correction to Enthalpy (a.u.)	=	0.698070
Thermal correction to Gibbs Free Energy (a.u.)	=	0.602675

C	−3.503719	−2.346714	2.018768	C	−3.645152	−0.928348	2.483653
C	−2.842684	0.059614	1.614795	C	−1.406663	−0.467423	1.327473
C	−1.478556	−1.858223	0.592342	C	−2.535046	−2.744197	1.197996
C	−5.114423	−0.482563	2.517646	C	−5.279711	0.929994	3.107325
C	−4.385326	1.900074	2.329127	C	−2.928249	1.436913	2.295338
H	−3.357511	0.126062	0.644467	H	−3.275366	−0.872508	3.519517
C	−5.025003	0.971896	4.615534	O	−5.838844	−1.443966	3.275191
O	−4.511032	3.183884	2.931226	C	−0.628314	−0.610233	2.647818
C	−0.659504	0.477094	0.398921	C	0.661656	0.373915	−0.030811
O	−1.393789	1.424828	−0.127383	C	1.639477	−0.706686	0.113186
O	2.586816	−0.577666	−0.849731	C	2.365451	0.552627	−1.719717
C	1.091115	1.157639	−1.160964	O	0.536366	2.160395	−1.624592
C	3.524265	1.533137	−1.535198	O	1.725959	−1.631641	0.893988
C	−1.689680	−1.808606	−0.957891	C	−0.406444	−1.965046	−1.729979
C	0.043227	−1.135931	−2.672441	C	1.404868	−1.243425	−3.302139

C	2.266578	0.047683	−3.188329	C	1.683546	1.118875	−4.130266
C	3.662248	−0.283699	−3.677645	C	4.821642	0.087611	−3.125828
C	4.887106	0.905325	−1.852568	C	6.139258	−0.320159	−3.729921
C	5.512444	0.066671	−0.711618	C	5.437464	0.718326	0.666353
H	−4.220916	−3.069641	2.399844	H	−0.513522	−2.347953	0.765753
H	−2.480596	−3.789269	0.893961	H	−5.489581	−0.477409	1.481599
H	−6.322708	1.233321	2.937115	H	−4.751292	1.947582	1.290979
H	−2.550962	1.377486	3.322789	H	−2.335827	2.192927	1.774845
H	−3.989715	0.728106	4.874078	H	−5.241348	1.967971	5.010081
H	−5.672929	0.256624	5.129063	H	−6.770566	−1.171176	3.284207
H	−3.988011	3.806797	2.401920	H	−1.108293	−1.368329	3.274221
H	0.400098	−0.923285	2.472441	H	−0.614276	0.335119	3.197890
H	−0.845789	1.972098	−0.768030	H	3.343562	2.379927	−2.204942
H	3.499613	1.926940	−0.514148	H	−2.362498	−2.633450	−1.225418
H	−2.207474	−0.885844	−1.250439	H	0.219027	−2.810432	−1.431182
H	−0.577815	−0.283741	−2.958990	H	1.944444	−2.082350	−2.849352
H	1.318885	−1.457654	−4.376482	H	2.210249	2.072954	−4.037394
H	0.619692	1.297559	−3.956449	H	1.805293	0.771193	−5.161667
H	3.681631	−0.872176	−4.596844	H	5.577214	1.743265	−2.030130
H	5.999076	−0.804052	−4.700691	H	6.791306	0.551283	−3.866927
H	6.676972	−1.020392	−3.079586	H	5.039526	−0.920376	−0.677361
H	6.565455	−0.099793	−0.966336	H	6.060169	0.172370	1.382180
H	5.792408	1.755548	0.637118	H	4.415026	0.722727	1.058638

Table S4. Cartesian coordinates and energies of the most stable conformer of **13b**.

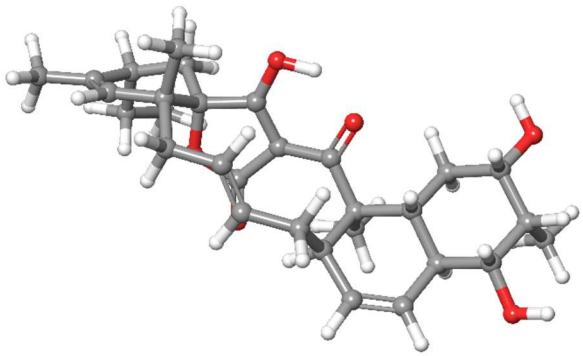

13b (ΔG = 0.4 kcal/mol)

M06-2X/def2-TZVP-SMD(MeOH)//M06-2X/6-31G(d)-SMD(MeOH):		
Gibbs Free Energy (a.u.)	=	−1617.989748
M06-2X/def2-TZVP-SMD(MeOH):		
Electronic energy (a.u.)	=	−1618.592155
M06-2X/6-31G(d)-SMD(MeOH):		
Zero-point correction (a.u.)	=	0.663404
Thermal correction to Energy (a.u.)	=	0.697073
Thermal correction to Enthalpy (a.u.)	=	0.698017
Thermal correction to Gibbs Free Energy (a.u.)	=	0.602407

C	3.618438	−2.909456	−0.579758	C	3.596050	−2.596963	0.886760
C	2.246516	−2.007607	1.341583	C	1.744913	−0.909585	0.363405
C	1.574001	−1.515065	−1.078718	C	2.729540	−2.413072	−1.436418
C	3.919407	−3.832798	1.738119	C	4.018140	−3.495126	3.236562
C	2.724025	−2.801589	3.672159	C	2.405109	−1.579392	2.810437
H	1.506189	−2.821987	1.306460	H	4.389366	−1.859668	1.088091
C	5.268592	−2.681520	3.576455	O	5.138024	−4.385086	1.254332
O	2.861065	−2.450254	5.045375	C	2.738885	0.264248	0.324390
C	0.375484	−0.398696	0.810911	C	−0.358178	0.669337	0.118117
O	−0.219862	−0.956279	1.743585	C	−0.133183	1.376208	−1.147617
O	−1.298307	1.950198	−1.549630	C	−2.383160	1.661905	−0.649570
C	−1.691651	0.841546	0.399706	O	−2.367565	0.368997	1.407338
C	−2.894037	2.981673	−0.067781	O	0.855282	1.518871	−1.836063
C	0.236993	−2.284458	−1.351032	C	−0.766837	−1.451250	−2.103366
C	−2.006901	−1.178225	−1.698225	C	−2.919243	−0.192170	−2.376254

C	−3.499885	0.907016	−1.437439	C	−4.542970	0.261648	−0.504280
C	−4.225278	1.915965	−2.305660	C	−4.198722	3.247720	−2.196414
C	−3.363629	3.958870	−1.152301	C	−4.980385	4.122875	−3.139989
C	−2.242858	4.779816	−1.835195	C	−1.211742	5.364777	−0.874187
H	4.416873	−3.553661	−0.940213	H	1.602124	−0.670138	−1.775574
H	2.794035	−2.675314	−2.492315	H	3.106877	−4.563318	1.595092
H	4.082399	−4.448033	3.781395	H	1.896101	−3.520285	3.561892
H	3.219561	−0.852265	2.910908	H	1.498088	−1.110394	3.197653
H	5.263195	−1.689580	3.113726	H	5.350434	−2.544297	4.657764
H	6.165481	−3.203811	3.232878	H	5.332275	−5.177042	1.781278
H	2.022055	−2.053943	5.329490	H	3.690265	−0.070811	−0.101061
H	2.368992	1.081147	−0.295383	H	2.929024	0.652284	1.329640
H	−1.734714	−0.221670	1.908174	H	−3.727638	2.745672	0.601172
H	−2.106467	3.424195	0.549511	H	0.479290	−3.173280	−1.947303
H	−0.195437	−2.653647	−0.411959	H	−0.396145	−0.983866	−3.019317
H	−2.362485	−1.633739	−0.770359	H	−2.383595	0.282214	−3.205743
H	−3.789946	−0.705525	−2.807762	H	−4.919434	0.969573	0.239730
H	−4.154491	−0.614174	0.020779	H	−5.393040	−0.060747	−1.114758
H	−4.847764	1.463781	−3.079838	H	−4.013156	4.688077	−0.646375
H	−5.641434	3.529251	−3.777741	H	−5.590130	4.846452	−2.585113
H	−4.314530	4.701212	−3.791520	H	−1.737548	4.161791	−2.584728
H	−2.723787	5.600685	−2.379436	H	−0.568568	6.082041	−1.393859
H	−1.694869	5.890488	−0.041819	H	−0.563519	4.589250	−0.452792

Table S5. Cartesian coordinates and energies of the most stable conformer of **13c**.

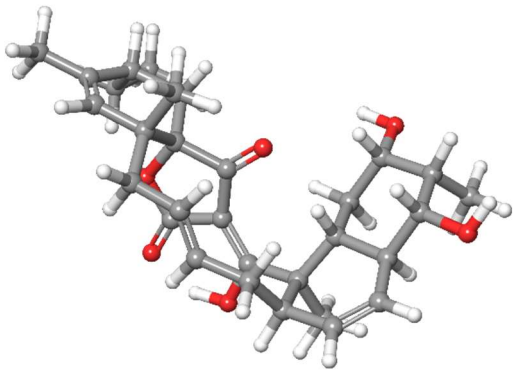

13c (ΔG = 3.5 kcal/mol)

M06-2X/def2-TZVP-SMD(MeOH)//M06-2X/6-31G(d)-SMD(MeOH):		
Gibbs Free Energy (a.u.)	=	−1617.984871
M06-2X/def2-TZVP-SMD(MeOH):		
Electronic energy (a.u.)	=	−1618.586628
M06-2X/6-31G(d)-SMD(MeOH):		
Zero-point correction (a.u.)	=	0.663069
Thermal correction to Energy (a.u.)	=	0.696797
Thermal correction to Enthalpy (a.u.)	=	0.697741
Thermal correction to Gibbs Free Energy (a.u.)	=	0.601757

C	1.860459	−3.459310	−2.831985	C	2.192833	−1.993084	−2.859413
C	1.197889	−1.132826	−2.052228	C	−0.251763	−1.602591	−2.299214
C	−0.397974	−3.086560	−1.796580	C	0.682014	−3.934794	−2.429161
C	3.612081	−1.676168	−2.374454	C	3.961273	−0.191477	−2.601203
C	2.903567	0.685037	−1.919253	C	1.480742	0.340058	−2.363188
H	1.415731	−1.295168	−0.991161	H	2.161243	−1.680349	−3.914794
C	4.147735	0.154664	−4.080021	O	4.512152	−2.530782	−3.068664
O	3.221913	2.045455	−2.197232	C	−0.570394	−1.573346	−3.814119
C	−1.344627	−0.781702	−1.620529	C	−1.334381	0.041244	−0.494802
O	−2.502099	−0.999269	−2.203615	C	−2.617691	0.454941	0.056409
O	−2.496049	0.957098	1.285166	C	−1.117345	0.929387	1.731912
C	−0.347569	0.355626	0.533365	O	0.868793	0.270088	0.544045
C	−0.695930	2.371282	2.000210	O	−3.731874	0.363810	−0.458461
C	−0.295529	−3.391619	−0.274381	C	−1.229319	−2.685563	0.669919
C	−0.820582	−2.195345	1.841232	C	−1.643751	−1.358336	2.779778

C	−1.054727	0.061423	3.016344	C	0.384052	−0.061543	3.556985
C	−1.876495	0.775743	4.069110	C	−2.106078	2.091865	4.110946
C	−1.571302	3.060906	3.068040	C	−2.898741	2.695141	5.243048
C	−2.699898	3.912004	2.446892	C	−2.190515	5.107404	1.644890
H	2.611150	−4.140192	−3.226940	H	−1.381654	−3.435593	−2.136929
H	0.488758	−5.006254	−2.460316	H	3.665526	−1.890851	−1.295217
H	4.918040	−0.003764	−2.092933	H	2.965445	0.510769	−0.835070
H	1.373687	0.533681	−3.438007	H	0.781958	1.002806	−1.841389
H	3.214072	0.091985	−4.647964	H	4.531124	1.173008	−4.184646
H	4.867138	−0.526239	−4.542819	H	5.409371	−2.331953	−2.755270
H	2.599991	2.595456	−1.694684	H	0.201758	−2.095590	−4.377998
H	−1.522805	−2.061216	−4.026022	H	−0.627951	−0.542631	−4.178704
H	−3.234325	−0.509748	−1.722967	H	0.356037	2.356798	2.297764
H	−0.745179	2.919170	1.052934	H	−0.457608	−4.476815	−0.198116
H	0.735084	−3.218691	0.057057	H	−2.268453	−2.554477	0.356545
H	0.222227	−2.350860	2.121294	H	−2.673820	−1.276961	2.412699
H	−1.692504	−1.838057	3.766809	H	0.769758	0.911027	3.873369
H	1.077931	−0.486199	2.829223	H	0.368726	−0.711604	4.439169
H	−2.256280	0.143831	4.873184	H	−0.924534	3.766509	3.612048
H	−3.013864	1.981457	6.063707	H	−2.404578	3.593578	5.632692
H	−3.902115	2.996720	4.921281	H	−3.333373	3.274692	1.818785
H	−3.336836	4.291939	3.252575	H	−3.027840	5.713157	1.283832
H	−1.556937	5.749962	2.267190	H	−1.604970	4.807807	0.770002

Table S5. Cartesian coordinates and energies of the most stable conformer of **13d**.

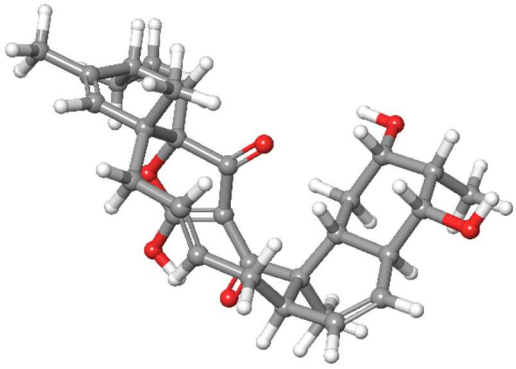

13d (ΔG = 6.6 kcal/mol)

M06-2X/def2-TZVP-SMD(MeOH)//M06-2X/6-31G(d)-SMD(MeOH):		
Gibbs Free Energy (a.u.)	=	−1617.979974
M06-2X/def2-TZVP-SMD(MeOH):		
Electronic energy (a.u.)	=	−1618.580947
M06-2X/6-31G(d)-SMD(MeOH):		
Zero-point correction (a.u.)	=	0.662219
Thermal correction to Energy (a.u.)	=	0.695993
Thermal correction to Enthalpy (a.u.)	=	0.696937
Thermal correction to Gibbs Free Energy (a.u.)	=	0.600973

C	4.798129	0.356612	−0.661757	C	3.865655	−0.611239	−1.337749
C	2.478207	−0.672378	−0.665771	C	2.621313	−0.693659	0.870177
C	3.296870	0.647454	1.332342	C	4.576705	0.857650	0.553923
C	3.674606	−0.330715	−2.832130	C	2.852422	−1.444172	−3.511003
C	1.516062	−1.602040	−2.775862	C	1.697146	−1.840457	−1.275720
H	1.948008	0.249241	−0.931338	H	4.335913	−1.605337	−1.274884
C	3.620670	−2.762442	−3.625970	O	4.962624	−0.206470	−3.423002
O	0.804306	−2.670629	−3.393564	C	3.534305	−1.859581	1.311313
C	1.320249	−0.869455	1.671112	C	−0.037871	−0.515583	1.282252
O	1.468333	−1.303555	2.834544	C	−1.001361	−0.508034	2.302151
O	−2.154086	0.042689	2.009603	C	−2.081994	0.579029	0.653163
C	−0.683430	0.158578	0.171270	O	−0.316574	0.384584	−0.973036
C	−3.177513	−0.099993	−0.157614	O	−0.880587	−0.951894	3.507228
C	2.526872	1.990994	1.182403	C	1.173362	2.120588	1.823974
C	0.151547	2.728125	1.218604	C	−1.265044	2.772635	1.720726

C	−2.290452	2.111794	0.754683	C	−2.204751	2.786596	−0.629176
C	−3.693033	2.329702	1.282666	C	−4.714940	1.480821	1.134440
C	−4.589757	0.146532	0.414789	C	−6.084489	1.833650	1.657514
C	−5.076852	−1.025825	1.293403	C	−5.283535	−2.323622	0.515721
H	5.721491	0.596044	−1.184682	H	3.532826	0.523239	2.397973
H	5.303092	1.534682	1.001980	H	3.132288	0.622443	−2.938194
H	2.625469	−1.101816	−4.531012	H	0.948354	−0.667932	−2.898276
H	2.229221	−2.786784	−1.115883	H	0.706718	−1.942932	−0.817550
H	3.807702	−3.226634	−2.652466	H	3.057212	−3.477479	−4.231171
H	4.587486	−2.598744	−4.109578	H	4.837256	−0.014227	−4.366424
H	−0.071990	−2.711056	−2.978506	H	3.068909	−2.824437	1.084137
H	4.498901	−1.813103	0.805816	H	3.717337	−1.820720	2.385965
H	0.094087	−1.261776	3.549185	H	−3.093032	0.265730	−1.184575
H	−2.957884	−1.172475	−0.189347	H	3.202828	2.748388	1.605874
H	2.433893	2.234842	0.117487	H	1.030825	1.666621	2.808126
H	0.331531	3.174889	0.239878	H	−1.331710	2.305737	2.711026
H	−1.588853	3.815716	1.838684	H	−3.014094	2.448215	−1.281310
H	−1.255279	2.601946	−1.134733	H	−2.320806	3.867898	−0.494541
H	−3.864129	3.288546	1.773680	H	−5.283593	0.195608	−0.438423
H	−6.142328	2.894263	1.917785	H	−6.857140	1.618341	0.909306
H	−6.338219	1.256490	2.553936	H	−4.367923	−1.183707	2.114935
H	−6.032211	−0.749527	1.751485	H	−5.687249	−3.103498	1.169287
H	−5.994464	−2.174091	−0.305060	H	−4.353556	−2.708892	0.085761

CHAPTER 5

Kumemicinones A–G, Cytotoxic Angucyclinone-class Polyketides from a Marine-Derived Actinomycete of the Genus *Actinomadura*

5-1 Background

In Chapter 4, three new tetronate-class polyketides nomimicins B–D were isolated from the culture extract of *Actinomadura* sp. AKA43 collected from the floating particles in the deep-sea water (DSW) of Sagami Bay, Japan. the results substantiated the validity of the actinomycetes collected from DSW for prospecting new bioactive molecules. To gain further support to this strategy, *Actinomadura* sp. KD439 isolated from suspended matter of DSW collected at Kumejima Island, Okinawa, Japan, was studies in this chapter.

The potential of microbes in deep-sea ecosystems as a source of new drug leads has not yet been fully understood, due to the limited accessibility of microbial sample collection. Deep-sea natural products represent just a fraction (<2%) of marine natural products reported, coupled with the high hit rates from screening programs [1]. Deep-sea environment is now attracting attention as one of the promising niches for discovering new secondary metabolites. There are 15 pumping stations for DSW in various geographical locations around Japan. During the search for new compounds from marine-derived actinomycetes, our laboratory reported the discovery of new secondary metabolites of different classes including polyketides and nonribosomal peptides from actinomycetes isolated from DSW collected from the Japan Sea (Toyama Bay) and Pacific Ocean (Sagami Bay) [2-3]. The metagenomic analysis of DSW using DGGE and pyrosequencing technology demonstrated that the bacterial community structure in DSW differs depending on the collection site, which prompted me to investigate DSW from Kumejima Island, Okinawa, Japan. [4]

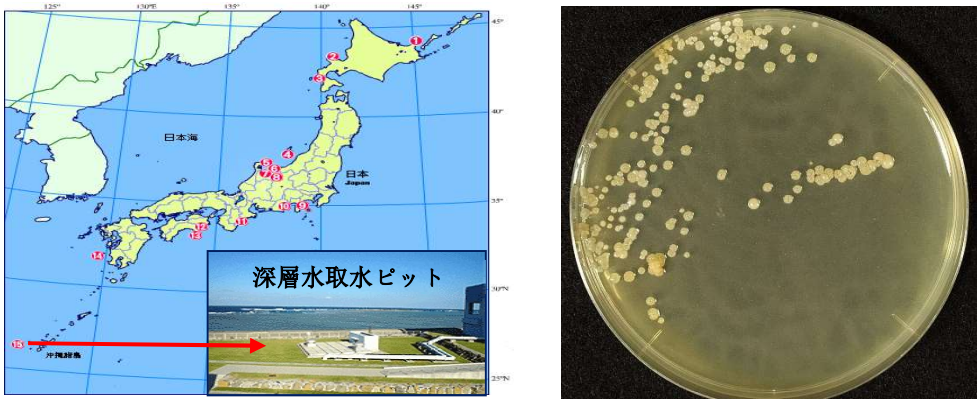

Figure 5-1. The deep seawater was collected at the Kumejima in Okinawa, Japan (right), and *Actinomadura* sp. KD439 on Bn-2 agar (left).

During the course of my continuing investigation on DSW-derived actinomycetes for new natural products, *Actinomadura* sp. KD439 isolated from suspended matter of DSW collected in Okinawa was found to produce eight new angucyclinone-class metabolites, kumemicinones A–G (**14**–**20**), along with two known congeners miaosporone E (**21**) and SF2315B (**22**) (Figure 5-2).

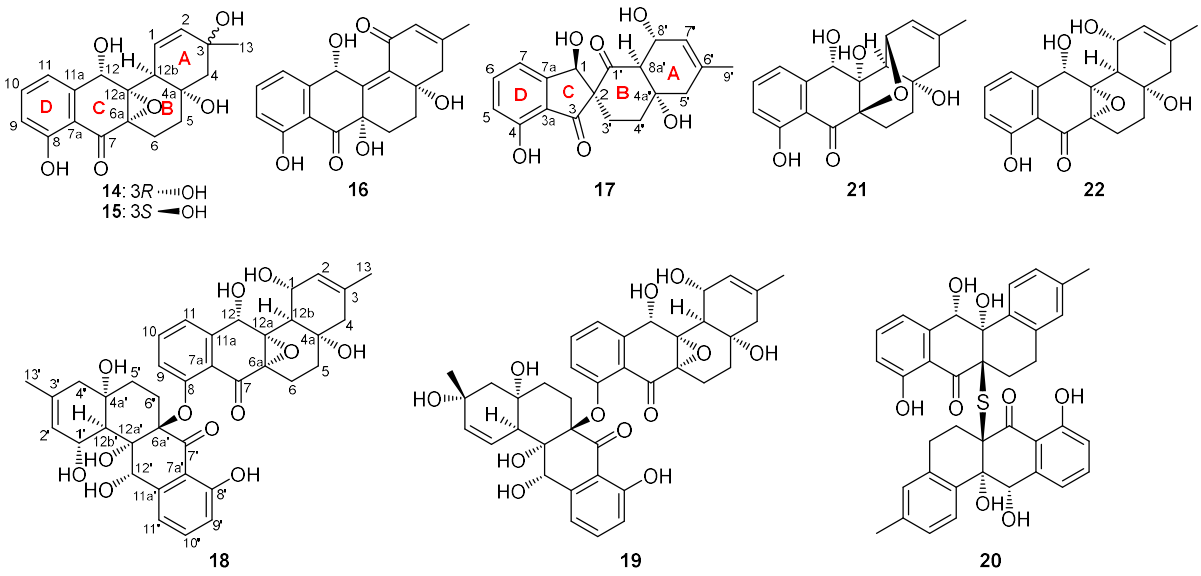

Figure 5-2. Structures of kumemicinones A–G (**14**–**20**), miaosporone E (**21**) and SF3215B (**22**).

5-2 Results and discussion

5-2-1 Fermentation and isolation

The producing strain KD439 was isolated from suspended matter in sea water collected at -612 m near the coast of Kumejima Island, Okinawa, Japan. Strain KD439 was cultured in A16 medium and the whole culture broth was extracted with 1-butanol. The extract was subjected to consecutive fractionation using silica gel and ODS column chromatography and the final purification was performed by reverse-phase HPLC to give eight new aromatic polyketides of angucycline family, which we designated as Kumemicinons A–G (**14**–**20**), along with miaosporone E (**21**) and SF2315B (**22**).

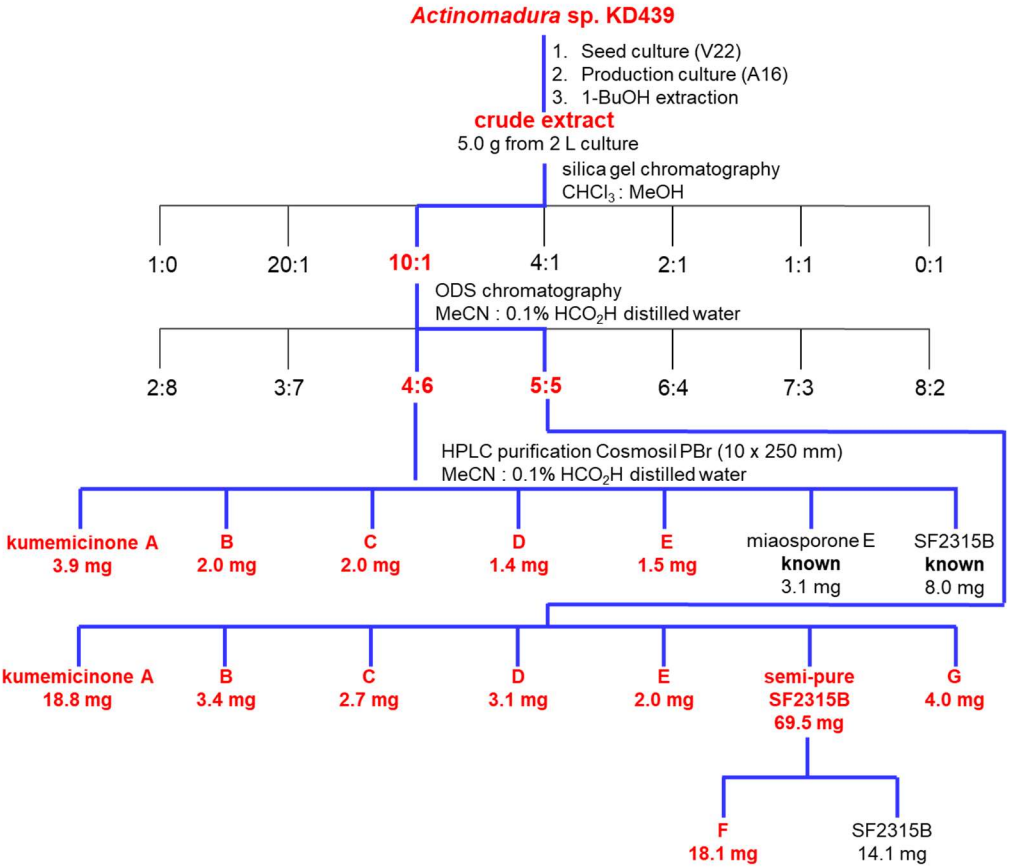

Scheme 5-1. Isolation of kumemicinones A–H (**14**–**20**), miaosporone E (**21**) and SF2315B (**22**).

5-2-2 Structure determination

Kumemicinone A (**14**) was obtained as a pale yellow crystalline solid. Its molecular formula was determined to be $C_{19}H_{20}O_6$ by HRESITOFMS analysis that gave a sodium adduct ion $[M + Na]^+$ at *m/z* 367.1152 (Δ 0.0 mmu). The IR spectrum indicated the presence of hydroxy (3345 cm^{-1}) and carbonyl groups (1639 cm^{-1}). Analysis of $^1H/^{13}C$ NMR and HSQC spectra allowed the assignment of 19 carbon resonances for one carbonyl carbon (δ_C 200.9), three nonprotonated sp^2 carbons (δ_C 162.9, 145.5, 113.9), five sp^2 methines (δ_C 137.9, 137.0, 125.9, 119.6, 117.4), four oxygenated sp^3 carbons (δ_C 70.9, 69.5, 67.1, 64.1), one sp^3 oxymethine (δ_C 68.4), one sp^3 methine (δ_C 46.8), three sp^3 methylenes (δ_C 42.6, 33.0, 21.1), and one methyl group (δ_C 29.3) (Table 5-1). D-ring was established by COSY correlations among H9/H10/H11 showing a doublet-triplet-doublet coupling typical for 1, 2, 3-trisubstituted benzene protons, together with HMBC correlations from H9 and H11 to C7a and H10 to C8 and C11a. B-ring was assembled from HMBC correlations from H5 and H6 to the neighboring carbons C4a and C6a and from H12b to C4a, C5, C6a, and

C12a. A-ring was constructed from a COSY fragment H12b/H1/H2 and a three-carbon fragment C13/C3/C4 based on HMBC correlations from methyl protons H13 to C2, C3 and C4 and from H4 to C2. Further HMBC correlations from H4, H5, and H12b to C4a confirmed the connectivity between A-ring and B-ring. Finally, assembly of C-ring by HMBC correlations from H12 to C7a, C11, C11a, and C12a and from H6 and H9 to C7 (δ_C 200.9) afforded the tetracyclic framework of **14**. The epoxide ring in positions C6a (δ_C 64.1) and C12a (δ_C 67.1) was inferred by ^{13}C chemical shift values of the corresponding epoxy carbons in SF2315B [5] and EI-1507-1 and -2 [6].

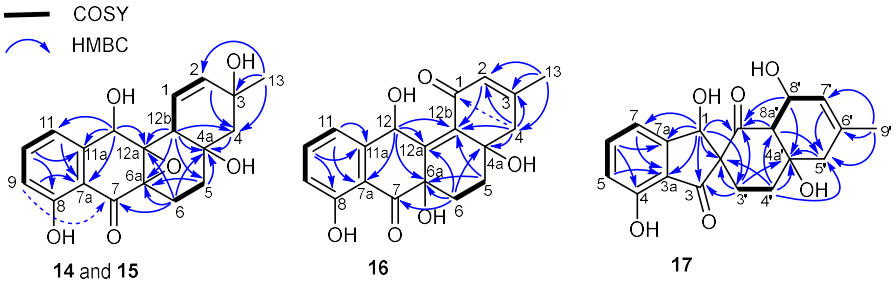

Figure 5-3. COSY and key HMBC correlations for **14**–**17**.

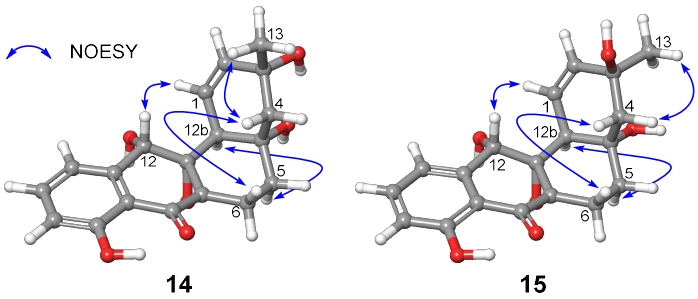

Figure 5-4. NOESY correlations supporting the relative configurations of **14** and **15**.

NOESY correlations for H12b/H5α and H4β/H6β suggested *cis*-fusion between A-ring and B-ring as well as α-orientation of H12b and 4a-OH (Figure 5-4). In addition, NOESY correlations for H4β/H13 and H1/H12 implied β-orientation of H12 and H13. This stereochemical assigment was consequently proven by X-ray crystallographic analysis which also established the absolute configuration (Figure 5-5).

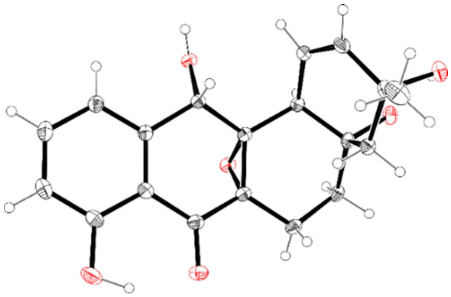

Figure 5-5. ORTEP drawing of **14**.

Table 5-1. ^{1}H and ^{13}C NMR data for kumemicinones A (**14**) and B (**15**) in CD_3OD.

	14			**15**		
no.	δ_C[b]	δ_H, mult (*J* in Hz)[a]	HMBC[a,c]	δ_C[b]	δ_H, mult, (*J* in Hz)[a]	HMBC[a,c]
1	125.9	6.37, dd (10.2, 5.3)	3, 4a, 12b	125.1	6.22, dd (10.3, 4.9)	3, 4a, 12b
2	137.0	5.94, dt (10.2, 1.7)	4, 12b, 13	137.5	5.80, d (10.4)	4, 12b, 13
3	69.5			70.2		
4α	42.6	1.59[d]	2, 3, 4a, 5, 12b	45.8	1.67[d]	2, 3, 4a, 5, 12b, 13
4β		1.90, d (14.2)	3, 13		1.90, d (13.9)	3, 12b, 13
4a	70.9			70.7		
5α	33.0	1.78, td (13.2, 5.3)	4a, 6, 6a, 12b	32.9	1.68[d]	4, 6, 4a, 12b
5β		1.60[d]	4, 4a, 6		1.68[d]	4, 6, 4a, 12b
6α	21.1	2.41, ddd (2.2, 5.2, 15.8)	5	20.8	2.31[d]	5, 4a, 6a, 12a
6β		2.15, ddd (5.4, 13.3, 15.8)	5, 4a, 6a, 12a		2.31[d]	5, 4a, 6a, 12a
6a	64.1			64.2		
7	200.9			200.9		
7a	113.9			113.8		
8	162.9			163.0		
9	117.4	6.83, brd (8.3)	7a, 8, 11	117.4	6.86, brd (8.3)	7a, 8, 11
10	137.9	7.52, t (8.0)	8, 11a	138.0	7.55, t (7.9)	8, 11a
11	119.6	7.16, brd (7.7)	7a, 9, 12	119.5	7.19, brd (7.7)	7a, 9, 12
11a	145.5			145.5		
12	68.4	4.90, s	7a, 11, 11a, 12a, 12b	68.2[e]	5.11, s	7a, 11, 11a, 12a
12a	67.1			68.2[e]		
12b	46.8	2.89, dd (5.3, 1.7)	1, 2, 4, 4a, 6a, 12a	45.2	2.85, brd (4.9)	1, 2, 4, 4a, 5, 6a, 12a
13	29.3	1.24, s	2, 3, 4	30.2	1.39, s	2, 3, 4

[a] Recorded at 500 MHz

[b] Recorded at 125 MHz

[c] Proton showing HMBC correlations to indicated carbons.

[d] Coupling constants not assignable due to signal overlapping.

[e] Signal overlapped.

Kumemicinone B (**15**) was obtained as a colorless amorphous solid with the same molecular formula as **14**. ^{1}H and ^{13}C NMR spectral data of **15** were similar to those for **14** in overall (Table 5-1) and the same planar structure was deduced from the comparison of 2D NMR data (Figure 5-3). NOESY correlations for H5α/H12b, H4β/H6β, and H1/H12 indicated the same relative configurations for the A/B-ring juncture and C12 as **14**, whereas a NOESY correlation detected for H4β/H13 inferred the inversion of configuration at C3 (Figure 5-4). Compound **15** was thus assigned to be a diastereomer of **14** with 3*S*-configuration. The absolute configuration was deduced

to be identical with **14**, except for C3, in consideration of the overall resemblance of ECD spectra for **14** and **15** (Figure 5-6).

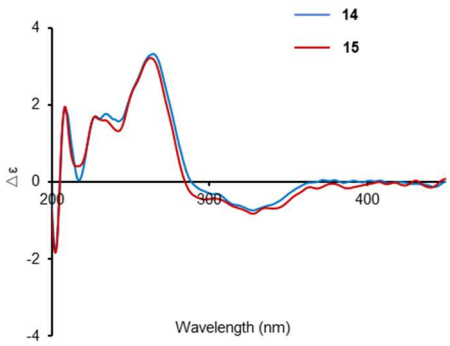

Figure 5-6. Experimental ECD spectra of **14** and **15**.

Table 5-2. ^{1}H and ^{13}C NMR data for kumemicinones C (**16**) and D (**17**) in CD_3OD.

	16				**17**		
no.	δ_C[b]	δ_H, mult (*J* in Hz)[a]	HMBC[a,c]	no.	δ_C[b]	δ_H, mult (*J* in Hz)[a]	HMBC[a,c]
1	192.8			1	78.3	5.27, s	2, 3, 3', 3a, 7, 7a
2	127.9	5.96, dd (2.5, 1.3)	4, 12b, 13	2	68.6		
3	161.7			3	205.5		
4α	46.4	2.39, d (18.6)	1, 2, 3, 4a, 5,12b, 13	3a	122.7		
4β		2.67, m	2, 3	4	157.8		
4a	73.0			5	117.2	6.85, d, (8.2)	3, 3a, 4, 7
5α	34.6	2.09[d]	4, 6,4a, 6a, 12b	6	139.2	7.59, t (7.9)	4, 7a
5β		1.75, ddd(13.7, 9.3, 3.4)	4, 6,4a, 6a, 12b	7	118.2	7.15, d (7.5)	1, 3a, 5, 6
6α	27.9	2.14[d]	4a, 5, 6a, 7, 12a	7a	155.8		
6β		2.20[d]	4a, 5, 6a, 7, 12a	1'	206.3		
6a	74.7			3'α	31.6	2.20, td (14.1, 4.5)	1, 2, 3, 4', 4a'
7	202.5			3'β		1.85, ddd (14.4, 4.7, 2.7)	1', 1, 2, 4', 4a'
7a	115.2			4'α	36.1	2.04, ddd (13.2, 4.5, 2.8)	2, 3', 4a', 5', 8a'
8	163.9			4'β		2.31[d]	2, 3', 4a', 5', 8a'
9	118.7	6.91, dd (0.9, 8.4)	7, 7a, 8, 11	4a'	74.6		
10	138.6	7.53, dd (7.5, 8.4)	8, 11a	5'α	39.4	2.32[d]	4a', 6', 7', 8a', 9'
11	121.6	6.94, d (8.4)	7a, 9, 11a, 12	5'β		1.96, d (18.3);	4a', 6', 8a'
11a	145.4			6'	134.8		
12	68.5	5.89, s	6a, 7a, 11, 11a, 12a, 12b	7'	122.8	5.61, m	5', 8', 8a', 9'
12a	141.7			8'	65.2	4.58, d (4.4)	1', 4a', 6', 7', 8a'
12b	141.1			8a'	62.4	3.34, m	1',4', 4a', 5', 7', 8'
13	24.4	1.94, s	2, 3, 4	9'	24.0	1.74, s	5', 6', 7'

[a] Recorded at 500 MHz
[b] Recorded at 125 MHz
[c] Proton showing HMBC correlations to indicated carbons.
[d] Coupling constants not assignable due to signal overlapping.

The molecular formula of Kumemicinone C (**16**) was determined to be $C_{19}H_{18}O_6$ based on the HR-ESITOFMS analysis that gave a sodium adduct ion $[M + Na]^+$ at *m/z*

365.0994 (Δ -0.2 mmu). Comparison of 1D/2D NMR spectra with those for **14** and **15** suggested the presence of the same C/D-ring system in **16**, but lacking of the epoxide moiety at C6a/C12a was evident from the absence of epoxide carbons (Table 5-2). HMBC correlations from H12 to C12a (δ_C 141.7) and C12b (δ_C 141.1) and from H5, H6, and H12 to C6a (δ_C 74.7) respectively indicated a double bond in positions C12a and C12b and an oxygen substitution at C6a. An α,β-enone structure in ring-A was evidenced by HMBC correlations from H13 to C2, C3, and C4, H2 to C12b, H4 to C2, C3, C4a, and C12b, and a four-bond correlation from H4 to C1 (Figure 5-3).

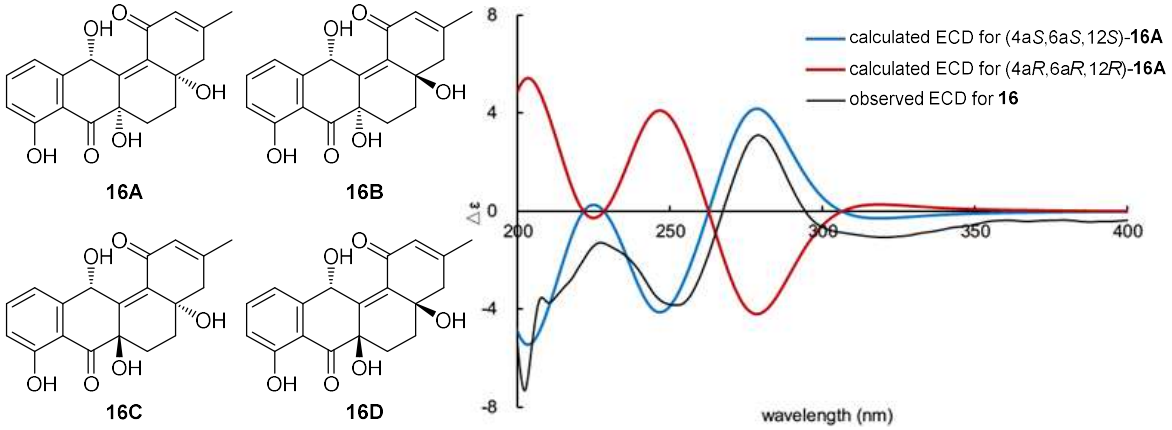

Figure 5-7. Four possible relative configurations for **16** (stereoisomers **16A**–**16D**) and experimental ECD spectrum of **16** in comparison with the calculated ECD spectra of (4a*S*,6a*S*,12*S*)-**16A** and (4a*R*,6a*R*,12*R*)-**16A**.

NOESY correlations for H4β/H5β and H4β/H6β inferred the opposite orientation of 4a-OH to these protons, however further diagnostic NOESY/ROESY correlations to assign the relative configuration of C6a and C12a were not detected (Figure S61). Then, the density functional theory (DFT)-based calculation of NMR chemical shifts was performed for four possible stereoisomers **16A**–**16D** at mPW1PW91/6-31G+(d,p)/PCM level of theory (Figure 5-7, Table S1). Calculated ^{1}H and ^{13}C chemical shifts of **16A** were most fitted with the experimental data with the smallest MAEs (mean absolute errors), thereby eliminating **16B**–**16C** from candidates (Table S1, Figure S68). The absolute configuration was determined to be 4a*S*,6a*S*,12*S* based on the comparison of calculated ECD spectra of enantiomers of **16A** with the experimental spectrum of **16** (Figure 5-7).

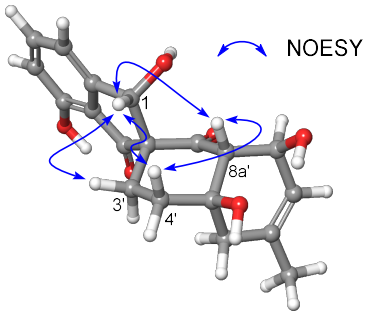

Figure 5-8. NOESY correlations supporting the relative configuration of **17**.

Kumemicinone D (**17**) was obtained as a yellow amorphous solid with a molecular formula of $C_{19}H_{20}O_6$. A trisubstituted benzene ring (D-ring) was confirmed by COSY correlations among H5, H6, and H7 and HMBC correlations from these protons to C3a, C4, and C7a (Figure 5-3). Another six-membered ring (A-ring) was assembled from COSY fragment H7'/H8'/H8a' and a three-carbon fragment C5'/C6'/C9', together with C4a', based on HMBC correlations from H9' to C5', C6', and C7' and from H5' and H8' to C4a'. A-ring was expanded to include a carbonyl carbon C1' connecting at C8a' and C3'/C4' fragment adjacent to C4a' by a series of HMBC correlations (Figure 5-3, Table 5-3). C1' and C3' were connected through a quaternary sp^3 carbon C2 based on HMBC correlations from H3' to C1' and C2 to furnish B-ring fused with A-ring. Finally, an oxymethine H1 and a keto carbon C3 were placed between B-ring and D-ring, assembling a spiro-fused tetracyclic structure of **17**.

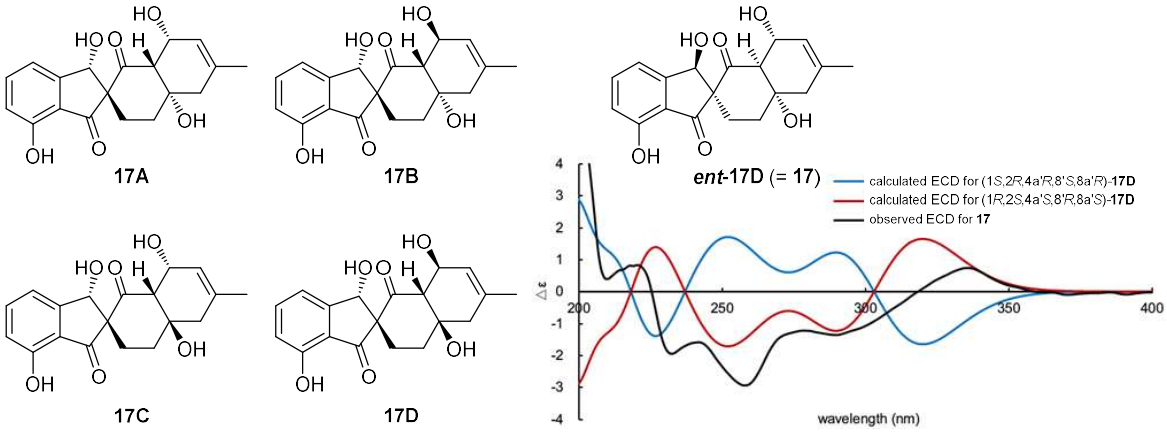

Figure 5-9. Four possible relative configurations for **17** (**17A**, **17B**, **17C**, and **17D**) and experimental ECD spectrum of **17** in methanol, in comparison with the calculated ECD spectra of (1*R*, 2*S*, 4a'*S*, 8'*R*, 8a'*S*)-**17D** and its antipode.

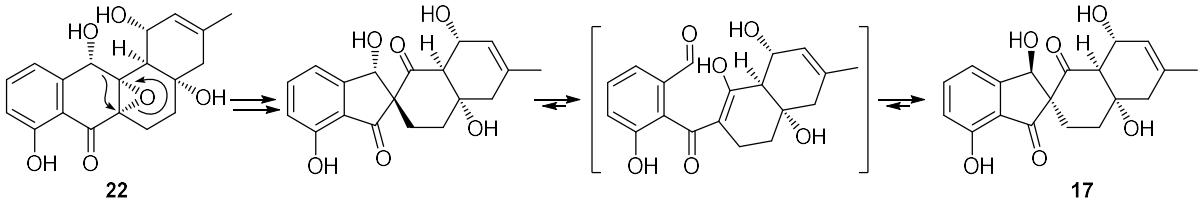

Figure 5-10. A plausible biogenesis of **17** from **22**.

NOESY correlations detected among H1, H3'β, H4'β, and H8a' inferred spatial proximity of these protons and their placement on the same side of the ring system (Figure 5-8), while relative configurations of C4'a and C8' were unable to be assigned due to signal overlapping of H4' and H5'. Since the relarive configurations at C1, C2, and C8a' are fixed, NMR chemical shift caluculation was conducted for the four possible stereoisomers **17A**–**17D** at mPW1PW91/6-31G+(d,p)/PCM level of theory (Figure 5-9, Tables S2). Calculated ^{1}H and ^{13}C chemical shifts of **17D** were matched most well with the experimental data with the smallest MAEs (Table S2).

No	**22**	Conditions	Results **22** : **17** : **a** : **b** : **c** : **d**
1	1.4 mg (4.1 mmol)	HCOOH (40 eq), MeOH (0.03 M), rt, 52 h	No reaction
2	1.1 mg (3.2 mmol)	HCl (5 eq), MeOH (0.03 M), 0 °C, 1.5 h	3.7 : 0 : 0 : 0 : 1.0 : 2.5
3	0.7 mg (2.0 mmol)	BF_3OEt_2(20 eq), DMSO (0.03 M), rt, 5.5 h	1.0 : 0 : 1.0 : 0 : 0 : 0
4	1.0 mg (2.9 mmol)	$Sc(OTf)_3$ (1 eq), MeOH (0.03 M), rt, 15.5 h	1.7 : 0 : 0 : 0 : 1.7 : 1.0
5	1.7 mg (4.9 mmol)	$TiCl_4$ (5 eq), DMSO (0.03 M), rt, 1.5 h	6.9 : 0 : 0 : 1.0 : 1.7 : 0

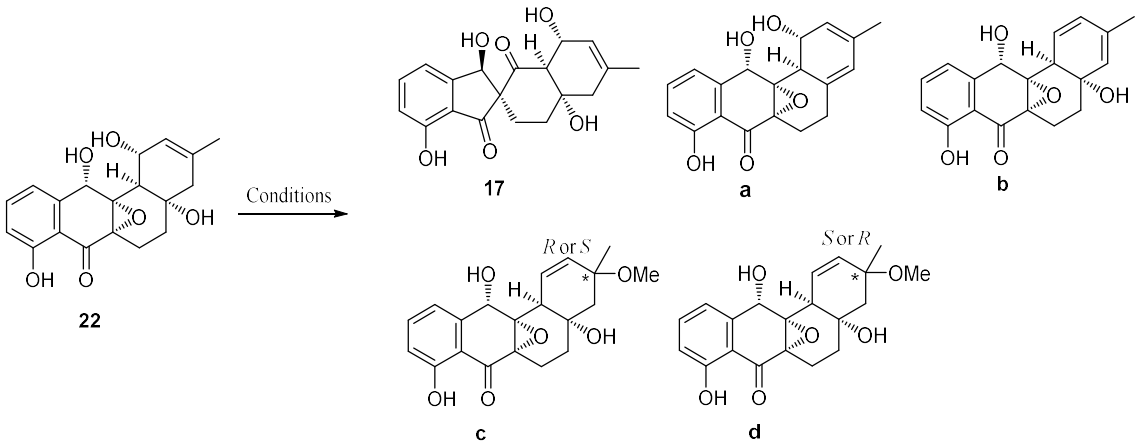

Figure 5-11. The results of the reaction of **22** under acidic conditions.

Absolute configuration of **17** was inferred using ECD calculation which displayed a good agreement with (1*R*,2*S*,4a'*S*,8'*R*,8a'*S*)-isomer (Figure 5-9). Contrary to our expectation, (*R*)-configuration at C1 was opposite to those for **14**–**17** with (1*S*)-

configuration. Given that **17** was derived from **22**, A rearrangement of the epoxy alcohol followed by a retroaldol-type cleavage of the C1-C2 bond gives an aldehyde-enol intermediate, which recyclizes by an aldol reaction to give **17**. Inversion of the C1 absolute configuration could be explained by cleavage of a C-C bond between C12 and C12a, followed by C-C bond formation between C6a and C12, leaving the absolute configurations at C4a', C8', and C8a' unchanged (Figure 5-10). Considering the acidic conditions in the purification process, there is a high possibility that the epoxy rearrangement will be promoted to form **17**. In order to test this speculation, the main product **22** under five different reaction conditions, through the determination of the products after the reaction, it is proved that **17** is not caused by acidic conditions (Figure 5-11). In addition, because silica may provide an acidic condition during the fractionation process. So we used 22 to mix with silica and tested it at different times from 1 to 7 days. The HPLC results were found to be the same as the results without the addition of silica In addition, because silica may provide an acidic condition during the fractionation process. So we used **22** to mix with silica and tested it at different times from 1 to 7 days. The HPLC results were found to be the same as the results without the addition of silica (Figure S65).

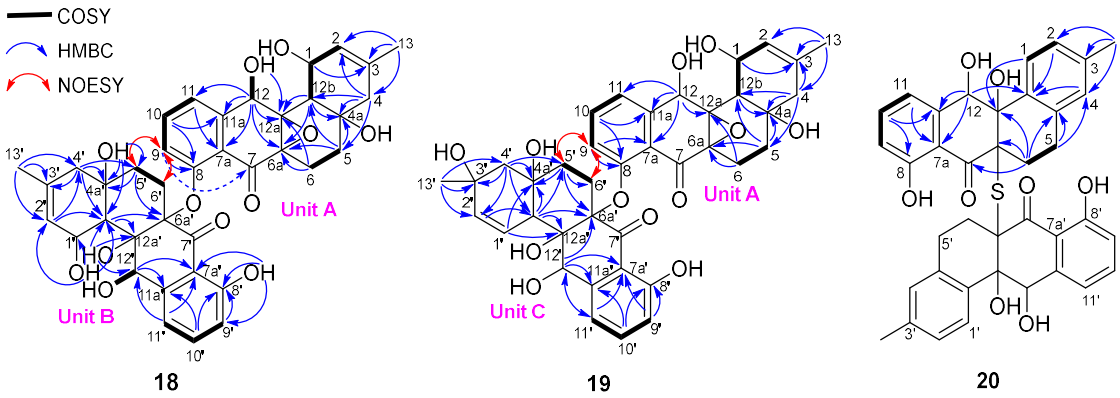

Figure 5-12. COSY, key HMBC and selected NOESY correlations for **18**–**20**.

Kumemicinone E (**18**) was obtained as a pale yellow crystallin solid with a molecular formula of $C_{38}H_{40}O_{12}$. In its ^{1}H and ^{13}C NMR spectra, resonances for two sets of a tetracyclic angucycline flamework were recognized (Table 5-3). 2D NMR analysis clarified that a half unit of **18** was identical with **22** (unit A, Figure 5-12). Another unit was almost the same as **22** while the more deshielded carbon resonances for C6a' (δ_C 87.3) and C12a' (δ_C 78.8) implied the cleavage of the epoxide ring at these

carbons (unit B, Figure 5-12). This was supported by HMBC correlations from an exchangeable proton at δ_H 6.28 (12a'-OH) to C12', C12a', and C12b'. Connectivity between the two units was not directly proven by HMBC analysis but an ether linkage between C8 and C6a' was inferred by NOESY correlations H9/ H5' and H9/ H6'. Thus, **18** was established as a dimer of **22** bridged through an ether oxygen. The relative and absolute configurations were confirmed by a single-crystal X-ray diffraction analysis (Figure 5-13).

Kumemicinone F (**19**) was obtained as a colorless amorphous solid with the same molecular formula as **18**. Comprehensive analysis of 1D/2D NMR data clarified that a half unit (unit A) was identical with that of **19** and another unit (unit C) possessed A-ring identical with that for **14** (Table 5-4, Figure 5-12). Connectivity between the two units in the positions C8 and C6a' via an ether bridge was also inferred by NOESY correlations for H9/H5' and H9/H6'. Relative configurations of units A and C were determined to be identical with those for **22** and **14**, respectively, based on NOESY correlations as illustrated. Compound **19** was presumably generated the coupling of **14** and **22** and thus the absolute configuration of **19** was proposed to be the same as **18**, which could be supported by the specific rotations with the same positive and similar absolute values for **18** ($[\alpha]_D^{23}$ +93, *c* 0.10 in MeOH) and **19** ($[\alpha]_D^{23}$ +53, *c* 0.10 in MeOH).

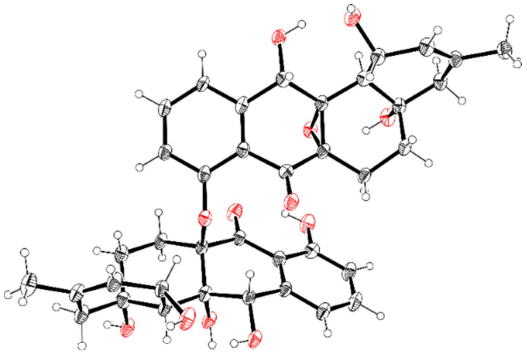

Figure 5-13. ORTEP drawing of **18**.

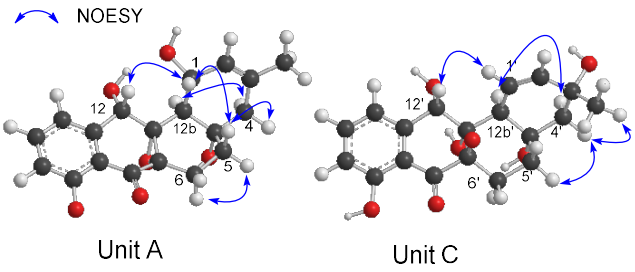

Figure 5-14. Key NOESY correlations supporting the relative configuration of units A and C in **20**.

Kumemicinone G (**20**) was obtained as a pale brown amorphous solid. HR-ESITOFMS showed a sodium adduct ion $[M+Na]^+$ at *m*/*z* 673.1862, which established a molecular formula $C_{38}H_{34}O_8S$ (Δ – 0.5 mmu). Interpretation of ^{13}C NMR and HSQC spectra confirmed 19 carbon resonances corresponding to a half of the carbon number inferred by the molecular formula, suggesting a symmetrical dimeric structure for **20** (Table 5-5). A tricyclic system comprising B/C/D-rings was evidenced by COSY correlations for H5/H6 and H9/H10/H11 and a series of HMBC correlations shown in Figure 5-14. A-ring was identified as a trisubstituted benzene with a methyl substitution by HMBC correlations from a methyl proton H13 to C2, C3, and C4, H2 and H4 to C12b, and H1 to C4a. Positions of hydroxy groups were confirmed by comparing the ^{13}C NMR data obtained in CD_3OD and CD_3OH (Figure S64). Chemical shifts for C8, C12, and C12a were shifted in CD_3OH are slightly larger than CD_3OD which established that hydroxy groups were attached on C8, C12, and C12a. Therefore, the remaining sulfur atom was between C6a and C6a' (δ_C 63.2) to link the same monomer units. This was supported by the chemical shift of C6a similar to those for the corresponding carbons in previously reported S-bridged dimers, naquihexcin A [7] and hypogeamicin A [8]. Compound **20** was likely produced from **22** via aromatization of A-ring and opening of the epoxide ring by nucleophilic attack of a sulfur compound (formally S^{2-}) shown in Figure 5-14. While a syn-relationship of 12-OH and 12a-OH was verified by a NOESY correlation between H1 and H12, a trans-fusion of the B- and C-rings, but not a *cis*-fusion, was compatible with the dimeric structure. The absolute configuration was deduced by calculation of ECD spectra (Table S15). Although the calculated ECD curves for a (6a*S*,12*S*,12a*S*)-isomer **20** and the antipode *ent*-**20** were rather simpler in shapes than the experimental curve and hypsochromically shifted at the longer wave length region, two major Cotton effects were reproducibly placed near 280 nm (Figure 5-16). Because a theoretical spectrum of the enantiomer **7**, having the same (12*S*)-configuration as **14**–**16**, **18**, **19**, and SF2315B, agreed with the experimental curve, a (6a*S*,12*S*,12a*S*)-configuration was assigned.

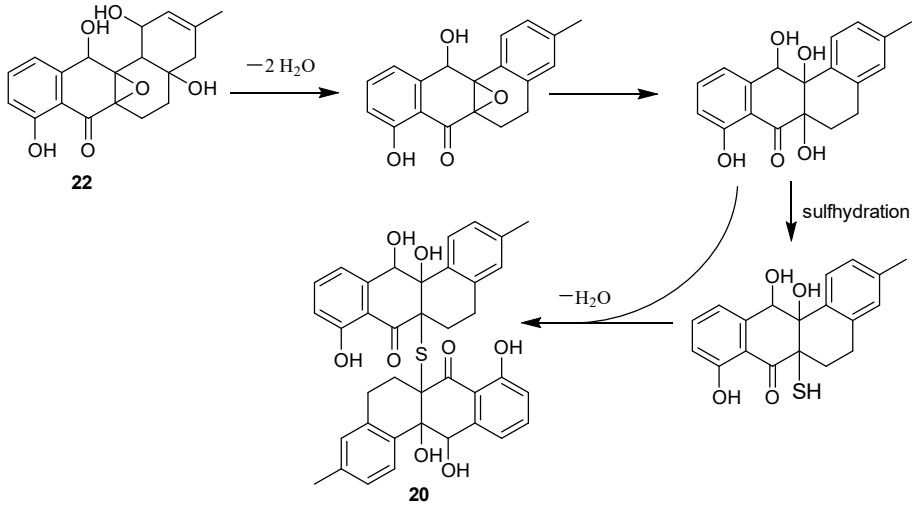

Figure 5-15. Plausible biogenetic pathway of **20** from **22**.

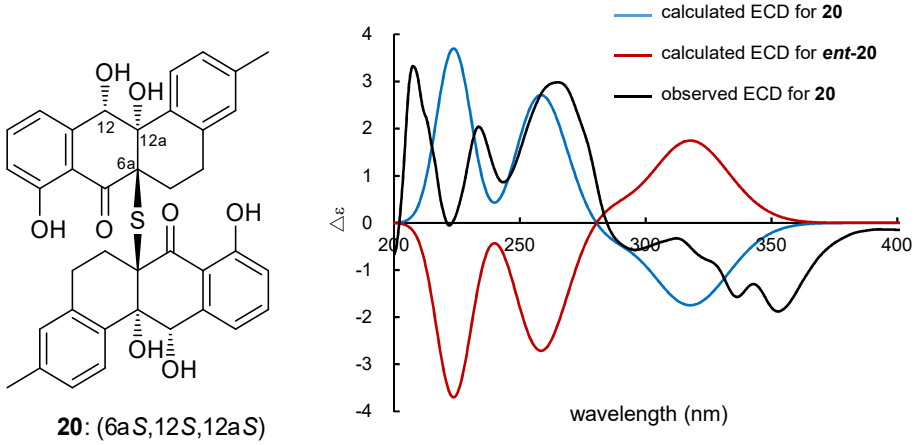

Figure 5-16. Experimental ECD spectrum of **20** (black) in comparison with the calculated ECD spectra of **20** (blue) and (6a*S*,12*S*,12a*S*)-**20** (red).

Table 5-3. ^{1}H and ^{13}C NMR data for kumemicinone E (**18**) in DMSO-d_6.

no.	δ_C[b]	δ_H, mult (*J* in Hz)[a]	HMBC[a,c]	no.	δ_C[b]	δ_H, mult (*J* in Hz)[a]	HMBC[a,c]
1	67.8	4.05, m	3, 4a, 12b	1’	65.7[d]	5.06, d (6.1)	3’
2	122.9	5.23, s	4, 12b, 13	2’	122.9	5.33, s	4’, 13’, 12b’
3	132.6			3’	132.2		
4α	43.5	1.80, d (17.6)	2, 3, 4a, 5, 12b, 13	4’α	45.0	1.96, d (16.7)	2’, 3’, 4a’, 5’, 12b’, 13’
4β		2.13[d]	2, 3, 4a, 5	4’β		2.47[d]	2’, 3’, 4a’, 5’
4a	70.5			4’a	72.7		
5α	27.5	1.09, m	4a, 6, 6a, 12b	5’α	28.6	1.59[d]	4a’, 6a’, 12b’
5β		1.31, m	4a, 6, 6a, 7	5’β		2.13[d]	7’
6α	13.9	0.88, m	5, 6a, 12a	6’α	19.6	2.13[d]	

6β		2.19[d]	4a, 5, 6a	6'β		2.41[d]	
6a	63.1			6a'	87.3		
7	192.4			7'	198.7		
7a	124.7			7a'	114.0		
8	151.6			8'	161.9		
9	122.7	7.09, d (8.2)	7, 7a, 8, 11	9'	115.2	6.73, d (8.3)	7', 7a', 8', 11'
10	132.5	7.50, t (8.0)	8, 11a	10'	136.8	7.53, t (8.0)	8', 11a'
11	122.0	7.38, d (7.8)	7a, 8, 9, 12	11'	117.2	7.20, d (7.6)	7a', 9', 12'
11a	142.1			11a'	145.9		
12	65.7[d]	5.06, d (6.1)	7a, 11, 11a, 12a	12'	67.6	5.72, d (5.1)	7a', 11', 11a'
12a	68.9			12a'	78.8		
12b	44.5	2.41[d]	1, 4a, 5, 6a, 12a	12b'	50.7	2.17[d]	1', 4a', 5', 6a', 12a'
13	22.6	1.62, s	2, 3, 4	13'	22.9	1.70, s	2', 3', 4'
1-OH		5.61, d (5.3)	1, 12b	1'-OH		5.83, d (4.4)	1', 2', 12b'
12-OH		5.69, d (6.2)	12, 12a	4a'-OH		6.18, s	4', 4a', 5', 12b'
4a-OH		4.06, s	4, 4a	8'-OH		11.48, s	7a', 8', 9'
				12'-OH		5.43, d (5.4)	11a', 12'
				12a'-OH		6.28, s	12', 12a', 12b'

[a] Recorded at 500 MHz

[b] Recorded at 125 MHz

[c] Proton showing HMBC correlations to indicated carbons.

[d] Coupling constant not assignable due to signal overlapping.

Table 5-4. ^{1}H and ^{13}C NMR data for kumemicinone F (**19**) in CD_3OD.

no.	δ_C[b]	δ_H,mult (*J* in Hz)[a]	HMBC[a,c]	no.	δ_C[b]	δ_H,mult (*J* in Hz)[a]	HMBC[a,c]
1	70.3	4.11, d (8.0)	3	1'	127.8	6.20, dd (10.4, 1.7)	2', 3', 4a', 12b'
2	123.6	5.31, s	4, 12b, 13	2'	131.4	5.57, dd (10.4, 1.9)	3', 4', 12b', 13'
3	135.3			3'	70.3		
4α	44.8	1.88, d (17.4)	2, 3, 4a, 5, 12b, 13	4'α	52.4	1.96, d (13.9)	3', 4a', 5', 12b', 13'
4β		2.29[d]		4'β		2.03, d (14.0)	2', 3', 4a', 12b', 5'
4a	73.0			4'a	73.4		
5α	28.8	1.18, m	4a, 6, 6a, 12b	5'α	29.2	1.62, d (14.5)	
5β		1.45, m	6	5'β		3.05, td (14.3, 3.6)	6', 4a', 6a'
6α	15.4	0.94, m	4a, 5, 6a	6'α	21.5	2.16, td (15.7, 3.8)	5'
6β		2.32[d]	4a, 5, 12a	6'β		2.48, dt (15.8, 3.4)	4a', 6a', 12a'
6a	65.1			6a'	88.4		
7	194.4			7'	199.9		
7a	126.9			7a'	115.8		
8	154.1			8'	164.4		
9	125.1	7.16, d (8.0)	7, 7a, 8, 11	9'	117.3	6.78, d (8.3)	7', 7a', 8', 11'

10	133.7	7.47[d]	8, 11a	10’	138.3	7.54, t (7.9)	8’, 11a’
11	123.3	7.46[d]	7a, 9, 12	11’	118.6	7.27, d (7.6)	7a’, 9’, 12’
11a	142.9			11a’	148.4		
12	67.8	5.18, s	6a, 7a, 11, 11a, 12a	12’	68.5	6.20, s	7a’, 11’, 11a’, 12a’, 12b’
12a	71.1			12a’	80.7		
12b	46.1	2.58, d (8.2)	1, 4, 4a, 5, 6a, 12a	12b’	47.2	2.86, s	1’, 2, 4a’, 5’, 6a’, 12a’
13	23.3	1.71, s	2, 3, 4	13’	32.7	1.34, s	2’, 3’, 4’

[a] Recorded at 500 MHz

[b] Recorded at 125 MHz

[c] Proton showing HMBC correlations to indicated carbons.

[d] Coupling constant not assignable due to signal overlapping.

Table 5-5. ^{1}H and ^{13}C NMR data for kumemicinone G (**20**) in CD_3OD.

no.	δ_C[b]	δ_H,mult (*J* in Hz)[a]	HMBC[a,c]
1/1’	130.2	8.23, d (8.3)	3, 4a, 12b
2/2’	127.9	6.85, d (8.3)	4, 12b, 13
3/3’	139.2		
4/4’	130.4	6.56, s	2, 5, 12b, 13
4a/4a’	138.0		
5α/5α’	25.9	1.69, m	6, 4a
5β/5β’		2.28d	4, 4a, 6, 6a, 12b
6α/6α’	22.5	1.92, dd (6.3, 13.4)	4a, 5, 6a, 7, 12a
6β/6β’		2.27d	4a, 5, 6a
6a/6a’	63.2		
7/7’	201.9		
7a/7a’	116.7		
8/8’	161.5		
9/9’	117.4	6.99, d (8.2)	7a, 8, 11
10/10’	137.7	7.64, t (8.0)	8, 11a
11/11’	120.8	7.24, d (7.7)	7a, 9, 12
11a/11a	146.3		
12/12’	72.0	5.23, s	7a, 11, 11a, 12b
12a/12a’	77.7		
12b/12b’	135.8		
13/13’	21.2	2.19, s	2, 3, 4

[a] Recorded at 500 MHz

[b] Recorded at 125 MHz

[c] Proton showing HMBC correlations to indicated carbons.

[d] Coupling constant not assignable due to signal overlapping.

5-2-3 Bioactivity

Bioactivity of **14**–**20** were evaluated in antimicrobial and cytotoxicity assays. All compounds were inactive against Gram-positive bacteria *Kocuria rhizophila* and *Staphylococcus aureus*, Gram-negative bacteria *Escherichia coli*, *Rhizobium radiobacter*, and *Tenacibaculum maritimum*, and a yeast *Candida albicans* (MIC > 100 μg/mL). Compound **14** showed the most potent cytotoxicity against P388 murine leukemia cells with an IC_{50} of 1.8 μM (Table 5-6). Its diastereomer (**15**) and the congeners lacking an expoxide ring **16** was less potent. A spirocyclic congener (**17**) was weakly active with an IC_{50} of 53 μM. Dimers (**18**–**20**) showed moderate active with an IC_{50} of 6.1–10.7 μM.

Table 5-6. Cytotoxicity of **14**–**22** against P388 murine leukemia cell.

	IC_{50} (μM)								
cell	**14**	**15**	**16**	**17**	**18**	**19**	**20**	**21**	**22**
P388	1.8	7.6	12.0	53.3	9.7	10.7	6.1	28.6	1.7

5-3 Conclusion

In conclusion, chemical screening from marine-derived *Actinomadura* sp. KD439 led to the discovery of eight new aromatic polyketides, Kumemicinones A–G (**14**–**20**), along with miaosporone E (**21**) and SF2315B (**22**). Kumemicinones belong to the angucycline-class polyketides of actinomycete origin which includes more than a hundred of compounds as represented by tetrangomycin [9], landomycins [10], and kanamycin [11]. More specifically, **14**–**16** are classified into the family of SF2315B characterized by the reduction of one of the quinone carbonyl groups to a hydroxy group. Compound **16** would be derived from **22** via oxidation of C1-hydroxy group and epoxide ring opening. Compound **17** was presumably generated from **22** by a cleavage and a formation of C-C bond. Skeletal reconstruction via C-C bond cleavage is known for some angucyclines and angucyclinones such as jadomycin [12], glivocarcin [13], and emycin [14], but a spirocyclic framework found in **17** is unprecedented in natural products. Ether-bridged dimeric structures of **18** and **19** are also unreported. One known example of angucyclinone dimers is hatomarubigin D in which two monomeric units are linked through a methylene group [15]. Thioether-bridged dimers of aromatic

polyketides like **20** are also uncommon. Only two examples, donghaesulfins [16] and BE-41926 [17], are known from *Streptomyces*. Discovery of Kumemicinones is an additional evidence supporting the idea that actinomycetes collectable from DSW could be a prolific source of novel scaffolds of bioactive natural products.

5-4 Experimental section

5-4-1 General experimental procedures

Optical rotations were measured using a JASCO DIP-3000 polarimeter. ECD spectra were recorded on a Jasco J-720W spectropolarimeter. UV and IR spectra were recorded on a Shimadzu UV-1800 spectrophotometer and a PerkinElmer Spectrum 100 spectrophotometer, respectively. NMR experiments were performed on a Bruker AVANCE 500 spectrometer using the signals of residual solvent protons (CD_3OD: δ_H 3.31; DMSO-d_6: δ_H 2.50) and carbons (CD_3OD: δ_C 49.2; DMSO-d_6: δ_C 39.5) HR-ESITOFMS were recorded on a Bruker micrOTOF focus mass spectrometer. Agilent HP1200 system equipped with a diode array detector was used for analysis and purification.

5-4-2 Microorganism

Deep-sea water (DSW) was collected at DSW pumping station of Okinawa Prefectural Government Deep Sea Water Research Center. In Kumejima Town, Shimajiri District, Okinawa Prefecture, Japan, as previously reported [18]. The isolated strain KD439 was identified as a member of the genus *Actinomadura* on the basis of 100% similarity in the 16S rRNA gene sequence (1277 nucleotides; DDBJ accession number LC648321) to *Actinomadura* sp. TF1, KC529344.1 (accession number KC529344).

5-4-3 Fermentation

Actinomadura sp. KD439 was maintained on Bn-2 agar medium [soluble starch 0.5%, glucose 0.5%, meat extract (Kyokuto Pharmaceutical Industrial Co., Ltd.) 0.1%, yeast extract (Difco Laboratories) 0.1%, NZ-case (Wako Chemicals USA, Inc.) 0.2%, NaCl 0.2%, $CaCO_3$ 0.1%, and agar 1.5% in distilled water (pH 7.0)]. Strain KD439 was inoculated into a 500 mL K-1 flask containing 100 mL of V-22 seed medium [soluble

starch 1%, glucose 0.5%, NZ-case 0.3%, yeast extract 0.2%, Tryptone (Difco Laboratories) 0.5%, K_2HPO_4 0.1%, $MgSO_4 \cdot 7H_2O$ 0.05%, and $CaCO_3$ 0.3% in distilled water (pH 7.0)]. The flask was shaken on a rotary shaker (200 rpm) at 30 °C for 4 days. The seed culture (3 mL) was transferred into 20 500 mL K-1 flasks each containing 100 mL of A16 production medium [glucose 2%, Pharmamedia (Traders Protein, Memphis, TN, USA) 1%, $CaCO_3$ 0.5%, and Diaion HP-20 (Mitsubishi Chemical, Kanagawa, Japan) 1% in distilled water]. The inoculated flasks were shaken on a rotary shaker (200 rpm) at 30 ˚C for 7 days.

5-4-4 Extraction and isolation

At the end of the fermentation period, 100 mL of 1-butanol was added to each flask, and the flasks were agitated on a rotary shaker for 1 h. The mixture was centrifuged at 6000 rpm for 10 min, and the organic layer was separated from the aqueous layer containing the mycelium. Evaporation of the solvent gave 5.0 g of extract from 2 L of culture. The extract was subjected to silica gel column chromatography with a step gradient of $CHCl_3$/MeOH (1:0, 20:1, 10:1, 4:1, 2:1, 1:1, and 0:1 v/v). Fraction 3 (10:1) was concentrated to provide 1.2 g of dark brown oil, which was then fractionated by ODS column chromatography with a step gradient of MeCN-0.1% HCO_2H aqueous solution (2:8, 3:7, 4:6, 5:5, 6:4, 7:3, and 8:2 v/v). ODS fraction 3 (4:6) was concentrated to provide 138 mg of semi-pure material, which was then purified by preparative HPLC (Nacalai Tesque, Cosmosil PBr, 10 x 250 mm, 4 mL/min, UV detection at 254 nm) with 36% MeCN in 0.1% HCO_2H solution to yield Kumemicinone A (**14**, 3.9 mg, t_R 32.7 min), Kumemicinone B (**15**, 2.0 mg, t_R 16.7min), Kumemicinone C (**16**, 2.0 mg, t_R 31.9 min) , Kumemicinone E (**17**, 1.5 mg, t_R 13.5 min), Kumemicinone H (**20**, 3.1 mg, t_R 48.2 min), miaosporone E (**21**, 1.4 mg, t_R 19.1 min) and SF2315B (**22**, 8.0 mg, t_R 44.5 min). ODS fraction 4 (5:5) (265 mg) was similarly purified by preparative HPLC (Nacalai Tesque, Cosmosil PBr, 10 x 250 mm, 4 mL/min, UV detection at 254 nm) with 38% MeCN in 0.1% HCO_2H solution to yield **14** (18.8 mg, t_R 30.6 min), **15** (3.4 mg, t_R 15.6 min), **16** (2.7 mg, t_R 28.7 min), **17** (2.0 mg, t_R 12.5 min), Kumemicinone G (**19**, 4.0 mg, t_R 38.5 min), and semi-pure Kumemicinone F (**18**, 69.5 mg, t_R 35.0 min). Compound **18** was further purified by preparative HPLC (Nacalai Tesque, Cosmosil PBr, 10 x 250 mm, 4 mL/min, UV detection at 254 nm)

with 30% MeCN in 0.1% HCO_2H solution to yield **20** (18.1 mg, t_R 24.5 min) and **22** (14.1 mg, t_R 15.1 min).

Kumemicinone A (**14**): pale yellow prism; mp 157~160°C; $[\alpha]_D^{23}$ +177 (*c* 0.10, MeOH); UV (MeOH) λ_{max} (log ε) 214 (4.53), 256 (4.20), 318 (3.78) nm; ECD (7.3×10^{-5} M, MeOH) λ_{ext} (Δε) 208 (+1.88), 217 (+0.04), 264 (+3.32), 327 (-0.74) nm; IR (ATR) ν_{max} 3345, 2934, 1639, 1455, 1258, 1134, 813, 760 cm^{-1}; ^1H and ^{13}C NMR data, Table 1; HR-ESITOFMS *m/z* 367.1152 $[M + Na]^+$ (calcd for $C_{19}H_{20}NaO_6$, 367.1152).

Kumemicinone B (**15**): yellow amorphous solid; $[\alpha]_D^{23}$ +85 (*c* 0.10, MeOH); UV (MeOH) λ_{max} (log ε) 214 (4.36), 263 (4.03), 335 (3.58) nm; ECD (7.3×10^{-5} M, MeOH) λ_{ext} (Δε) 208 (+1.95), 215 (+0.41), 262 (+3.21), 327 (-0.82) nm; IR (ATR) ν_{max} 3353, 2934, 1639, 1613, 1455, 1249, 1137, 812, 724 cm^{-1}; ^1H and ^{13}C NMR data, Table 1; HR-ESITOFMS *m/z* 367.1144 $[M + Na]^+$ (calcd for $C_{19}H_{20}NaO_6$, 367.1152).

Kumemicinone C (**16**): yellow amorphous solid; $[\alpha]_D^{23}$ -41 (*c* 0.10, MeOH); ECD (7.3×10^{-5} M, MeOH) λ_{ext} (Δε) 252 (-3.84), 279 (+3.10), 320 (-1.07) nm; UV (MeOH) λ_{max} (log ε) 264 (4.20), 336 (3.61) nm; IR (ATR) ν_{max} 3344, 2932, 1632, 1631, 1454, 1240, 1164, 1025, 821 cm^{-1}; ^1H and ^{13}C NMR data, Table 2; HR-ESITOFMS *m/z* 365.0994 $[M + Na]^+$ (calcd for $C_{19}H_{18}NaO_6$, 365.0996).

Kumemicinone D (**17**): yellow amorphous solid; $[\alpha]_D^{23}$ -129 (*c* 0.10, MeOH); UV (MeOH) λ_{max} (log ε) 247 (3.79), 293 (3.67) nm; ECD (7.3×10^{-5} M, MeOH) λ_{ext} (Δε) 258 (-2.93), 290 (-1.35), 336 (+0.74) nm; IR (ATR) ν_{max} 3354, 2932, 1709, 1682, 1602, 1467, 1291, 991 cm^{-1}; ^1H and ^{13}C NMR data, Table 3; HR-ESITOFMS *m/z* 367.1146 $[M + Na]^+$ (calcd for $C_{19}H_{20}NaO_6$, 367.1152).

Kumemicinone E (**18**): pale white plates; mp 198~200°C; $[\alpha]_D^{23}$ +93 (*c* 0.10, MeOH); UV (MeOH) λ_{max} (log ε) 260 (3.69), 302 (3.12), 340 (3.21) nm; ECD (7.3×10^{-5} M, MeOH) λ_{ext} (Δε) 205 (+2.98), 227 (-0.89), 261 (+2.65), 347 (-0.67) nm; IR (ATR) ν_{max} 3322, 2925, 1637, 1455, 1242, 991 cm^{-1}; ^1H and ^{13}C NMR data, Table 4; HR-ESITOFMS *m/z* 711.2406 $[M + Na]^+$ (calcd for $C_{38}H_{40}NaO_{12}$, 711.2412).

Kumemicinone F (**19**): yellow amorphous solid; $[\alpha]_D^{23}$ +53 (*c* 0.10, MeOH); UV (MeOH) λ_{max} (log ε) 210 (3.97), 261 (3.68), 305 (3.11), 342 (3.19) nm; ECD (7.3×10^{-5} M, MeOH) λ_{ext} (Δε) 205 (+0.91), 226 (-0.58), 261 (+2.37), 348 (-0.51) nm; IR (ATR)

ν_{max} 3347, 2929, 1686, 1596, 1454, 1241, 970, 724 cm^{-1}; ^{1}H and ^{13}C NMR data, Table 5; HR-ESITOFMS *m/z* 711.2409 $[M + Na]^+$ (calcd for $C_{38}H_{40}NaO_{12}$, 711.2412).

Kumemicinone G (**20**): brown amorphous solid; $[\alpha]_D^{23}$ -37 (*c* 0.10, MeOH); UV (MeOH) λ_{max} (log ε) 261 (3.46), 337 (3.32) nm; ECD (7.7×10^{-5} M, MeOH) λ_{ext} (Δε) 210 (+1.97), 222 (+0.12), 233 (+1.29), 243 (+0.69), 263 (+2.01), 352 (-1.24) nm; IR (ATR) ν_{max} 3411, 2924, 1646, 1613, 1455, 1328, 1250, 964, 760 cm^{-1}; ^{1}H and ^{13}C NMR data, Table 6; HR-ESITOFMS *m/z* 673.1862 $[M + Na]^+$ (calcd for $C_{38}H_{34}SNaO_8$, 673.1867).

Miaosporone E (**21**): colorless prism; mp 267~270°C; $[\alpha]_D^{23}$ +160 (*c* 0.10, MeOH); UV (MeOH) λ_{max} (log ε) 269 (3.54), 345 (3.17) nm; ECD (7.3×10^{-5} M, MeOH) λ_{ext} (Δε) 252 (-3.84), 279 (+3.10), 320 (-1.07) nm; IR (ATR) ν_{max} 3350, 2933, 1633, 1454, 1242, 968, 874, 771 cm^{-1}; ^{1}H and ^{13}C NMR data, Table 2; HR-ESITOFMS *m/z* 367.1155 $[M + Na]^+$ (calcd for $C_{19}H_{20}NaO_6$, 367.1152).

SF2315B (**22**): brown amorphous solid; $[\alpha]_D^{23}$ +81 (*c* 0.10, MeOH) (lit. $[\alpha]_D^{25}$ +103 (*c* 0.10. MeOH) [5]); ^{1}H and ^{13}C NMR data, Table S3; HR-ESITOFMS *m/z* 367.1145 $[M + Na]^+$ (calcd for $C_{19}H_{20}NaO_6$, 367.1152).

5-4-5 Generation of the global minimum conformers of 14 and 15

The conformational sampling of structure **14** was performed by applying 100 000 steps of the Monte-Carlo Multiple Minimum (MCMM) method with PRCG energy minimization by the OPLS3e force field to obtain 81 conformational isomers within 10.0 kcal/mol from the minimum energy conformer. The structures were then optimized at the M06-2X/6-31G(d,p) level of theory with the SMD solvation model. Frequency calculations were carried out at the same level of theory to confirm the absence of imaginary frequencies and obtain thermal corrections to the Gibbs free energies. After the single-point energies were calculated at the M06-2X/def2-TZVP-SMD level of theory, the thermal corrections were added to obtain the Gibbs free energies. The conformer having the minimum energy was determined as the global minimum conformer of **14**. The global minimum conformer of **15** was similarly calculated using 120 OPLS3e-minimized structures. The computational study was performed using the MacroModel implemented in the Maestro 12.3 or 12.8 software package and the

Gaussian16 Rev C.01 program. A part of these computations were conducted using the SuperComputer System, Institute for Chemical Research, Kyoto University. Molecular structures were visualized using Maestro 12.3 or 12.8 software package. ECD spectra were visualized using GaussView 6.0.16 and Microsoft Excel 2019.

5-4-6 NMR and ECD calculations of 16 and 17

The conformational sampling of structure **16A** was performed by applying 100 000 steps of the Monte-Carlo Multiple Minimum (MCMM) method with PRCG energy minimization by the OPLS3e force field to obtain 48 conformational isomers within 10.0 kcal/mol from the minimum energy conformer. The geometries were then optimized at the M06-2X/6-31G(d,p) level of theory with the SMD solvation model. Frequency calculations were carried out at the same level of theory to confirm the absence of imaginary frequencies and obtain thermal corrections to the Gibbs free energies. After eliminating duplicated structures with the threshold of 0.01 Å RMSD, the single-point energies were calculated at the M06-2X/def2-TZVP-SMD level of theory, affording 30 conformers within 3.0 kcal/mol from the minimum Gibbs free energy. The shielding tensors of the conformers were evaluated by the GIAO method at the mPW1PW91/6-31G+(d,p)-IEFPCM level of theory. Then, the chemical shifts (δ_{calc}) were calculated using tetramethylsilane (TMS) as a reference standard according to $\delta_{calc} = \sigma_0 - \sigma_x$, where σ_x is the Boltzmann-averaged shielding tensor of the low-lying conformers and σ_0 is the shielding tensor of TMS calculated at the same level of theory as σ_x. ECD spectra of the 30 low-lying conformers were calculated by the TDDFT of 25 excited states at the ωB97X-D/def2-TZVP-IEFPCM level of theory. The spectrum of **16A** was created by the weighted average of the above-obtained spectra (half-width: 0.24 eV) according to the Boltzmann distribution, corrected by a red-shift of 15 nm, and scaled to adjust the strength of the vertical axis. The chemical shifts of **16B**, **16C**, **16D**, **17A**, **17B**, **17C**, **17D** were similarly simulated using 20, 20, 63, 35, 66, 102 and 143 OPLS3e-minimized structures and 16, 13, 23, 11, 26, 19 and 35 DFT-optimized low-lying conformers, respectively. The ECD spectrum of **17D** was similarly created using the 35 DFT-optimized conformers.

5-4-7 ECD calculations of 20

The conformational sampling of structure **20** was performed by applying 100 000 steps of the Monte-Carlo Multiple Minimum (MCMM) method with PRCG energy minimization by the OPLS4 force field to obtain 105 conformational isomers within 5.0 kcal/mol from the minimum energy conformer. The geometries were then optimized at the B3LYP-D3BJ/6-31G(d) level of theory with the IEF-PCM solvation model. Frequency calculations were carried out at the same level of theory to confirm the absence of imaginary frequencies and obtain thermal corrections to the Gibbs free energies. After eliminating duplicated structures with the threshold of 0.01 Å RMSD, the single-point energies were calculated at the B3LYP-D3BJ/6-311+G(d,p) level of theory, affording 8 conformers within 2.5 kcal/mol from the minimum Gibbs free energy. The ECD spectrum of each conformer was simulated by the TDDFT calculation of 25 excited states at the ωB97X-D/def2-TZVP-IEFPCM level of theory. The spectrum of structure **20** was created by the weighted average of the above-obtained spectra (half-width: 0.24 eV) according to the Boltzmann distribution, corrected by a red-shift of 15 nm, and scaled to adjust the strength of the vertical axis.

5-4-8 Antimicrobial and cytotoxicity assay

Antimicrobial assay and cytotoxic assay were carried out according to the procedures previously described. [19]

References

1) Sogin, M. L.; Morrison, H. G.; Huber. Ja.; Welch, D.; Huse, S. M.; Neal, P. R. et al. *Proc. Natl. Acad. Sci. USA.* **2006**, 1*03*, 12115-12120.
2) Igarashi, Y.; Matsuyuki, Y.; Yamada, M.; Fujihara, N.; Harunari, E.; Oku, N.; Karim, M. R. U.; Yang, T.; Yamada, K.; Imada, C.; Fukaya, K.; Urabe, D. *J. Org. Chem.* **2021**, *86*, 6528–6537.
3) Karim, M. R. U.; In, Y.; Zhou, T.; Harunari, E.; Oku, N.; Igarashi, Y. *Org. Lett*. **2021**, *23,* 2109–2113.
4) Terahara, T.; Yamada, K.; Nakayama, J.; Igarashi, Y.; Kobayashi, T.; Imada, C. *Gene* **2015**, *576*, 696–700.
5) Sasaki, T.; Gomi, S.; Sezaki, M.; Takeuchi, Y.; Kodama, Y.; Kawamura, K. *J. Antibiot.* **1988**, *41*, 843-848.
6) Tsukuda, E.; Tanaka, T.; Ochiai, K.; Kondo, H.; Yoshida, M.; Agatsuma, T.; Saitoh, Y.; Teshiba, S.; Matsuda, Y. *J. Antibiot.* **1996**, *49*, 333-339.
7) Che, Q.; Tan, H.; Han, X.; Zhang, X.; Gu, Q.; Zhu, T.; Li, D. (2016). *Org. Lett*. **2016**, *18,* 3358–3361.
8) Derewacz, D. K.; Mcnees, C. R.; Scalmani, G.; Covington, C. L.; Shanmugam, G.; Marnett, L. J.; Polavarapu, P. L.; Bachmann, B. O. *J. Nat. Prod.* **2014**, *77*, 1759−1763.
9) Kharel, M. K.; Pahari, P.; Shepherd, M. D.; Tibrewal, N.; Rohr, J.; *Nat. Prod. Rep.* **2011**, *29*, 264-325.
10) Shaaban, K. A.; Srinivasan, S.; Kumar, R.; Damodaran, C.; Rohr, J. *J. Nat. Prod.* **2011**, *74*, 2−11.
11) Omura, S.; Nakagawa, A.; Yamada, H.; Hata, T.; Furusaki, A.; Watanabe, T. *Chem. Pharm. Bull.* **1973**, *21*, 931-940.
12) Martinez-Farina, C. F.; Robertson, A. W.; Yin, H.; Monro, S.; McFarland, S. A.; Syvitski, R. T.; Jakeman, D. L. *J. Nat. Prod.* **2015**, *78*, 1208– 1214.
13) Takahashi, K.; Yoshida, M.; Tomita, F.; Shirahata, K. *J. Antibiot.* **1981**, *34*, 271-275.
14) Gerlitz, M.; Udvarnoki, G.; Rohr, J. *Angew. Chem., Int. Ed. Engl.* **1995**, *34*, 1617– 1621.
15) Hayakawa, Y.; Ha, S.-C.; Kim, Y. J.; Furihata, K.; Seto, H. *J. Antibiot.* **1991**, *44*, 1179-1186.
16) Bae, M.; An, J. S.; Bae, E. S.; Oh, J.; Park, S. H.; Lim, Y.; Ban, Y. H.; Kwon, Y.; Cho, J.-C.; Yoon, Y. J.; Lee, S. K.; Shin, J.; Oh, D.-C. *Org. Lett.* **2019**, *21*, 3635– 3639.
17) Nishioka, H.; Nakase, K.; Nakajima, S.; Nagashima, M.; Kojiri, K.; Suda, H. Jpn. Kokai Tokkyo Koho. JP 10168054 A, Jun 23, 1998.
18) Yang, T.; Yamada, K.; Zhou, T.; Harunari, E.; Igarashi, Y.; Terahara, T.;.Kobayashi, T.; Imada, C. *J. Antibiot.* **2019,** *72,* 202-209.
19) Karim, M. R. U.; Harunari, E.; Oku, N.; Akasaka, K.; Igarashi, Y. *J. Nat. Prod.* **2020**, *83*, 1295−1299.

5-5 Spectral Data

Table of contents

Figure S1. UV spectrum of kumemicinone A (**14**).

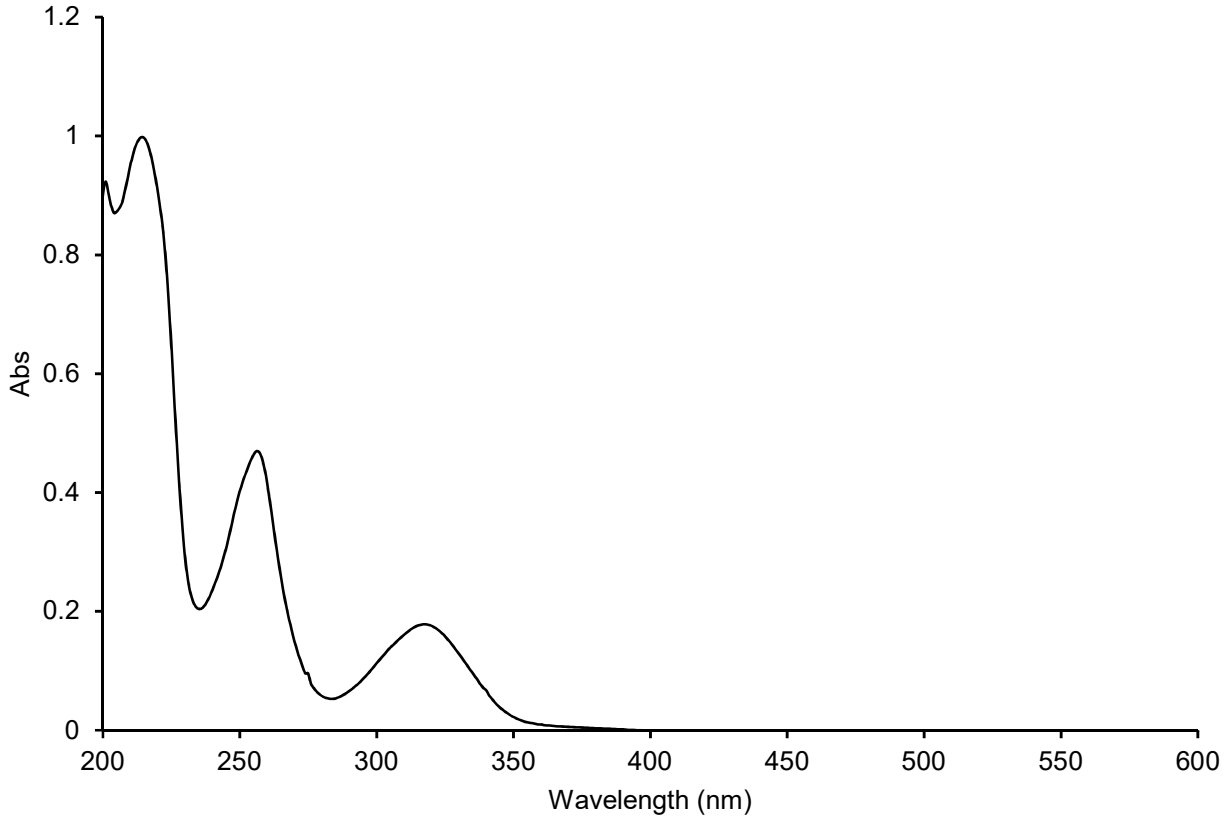

Figure S2. IR spectrum of **14**.

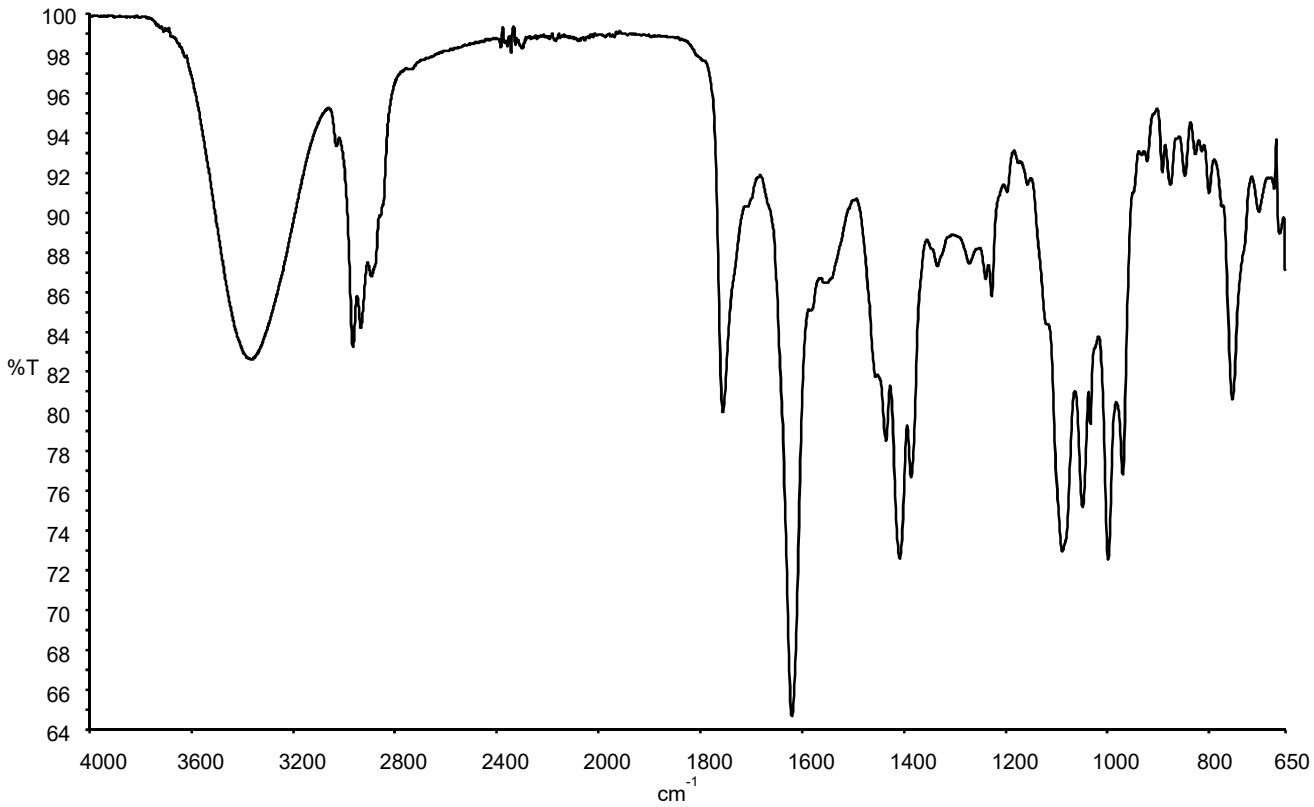

Figure S3. ^{1}H NMR spectrum of **14** (500 MHz, CD_3OD).

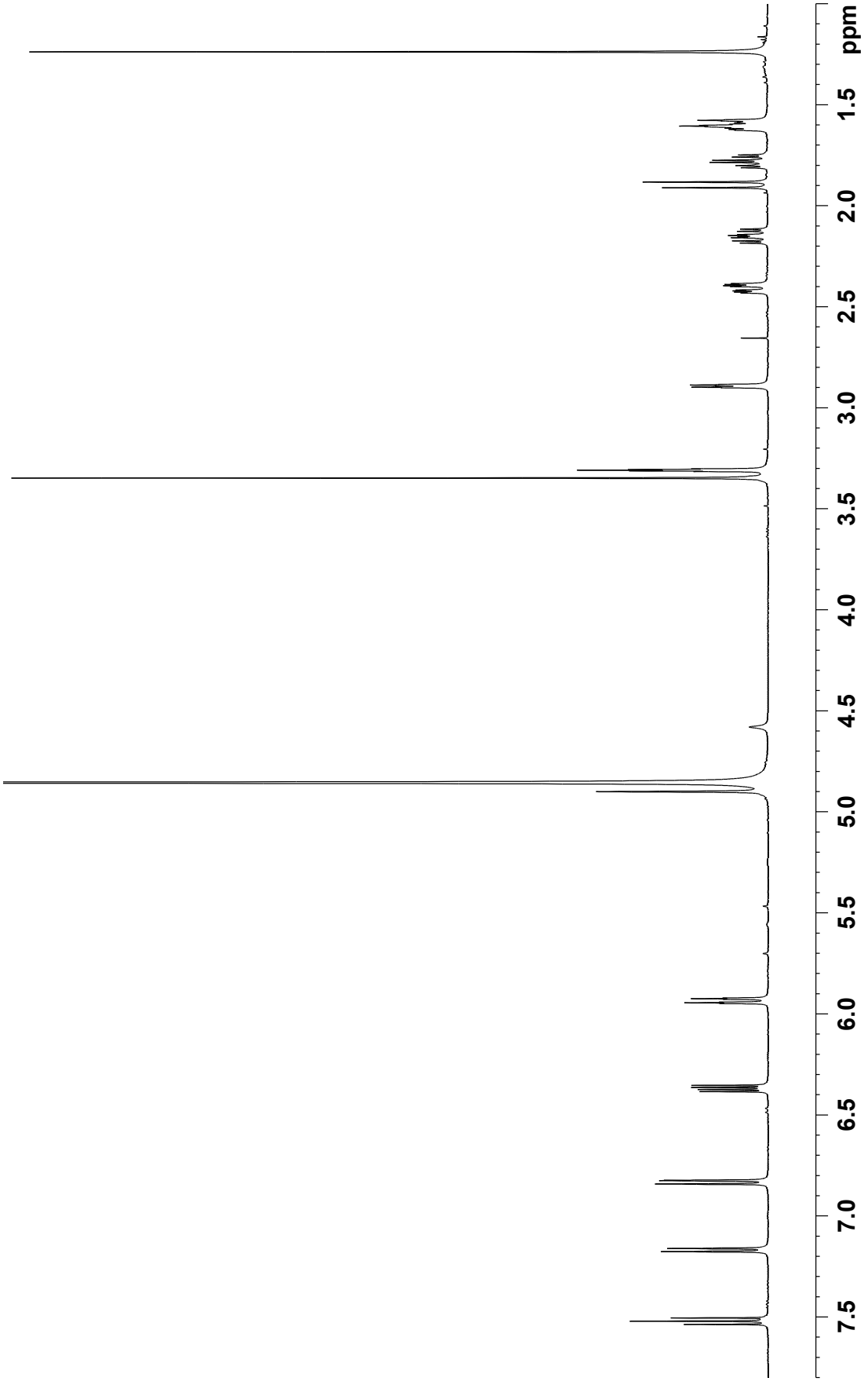

Figure S4. ^{13}C NMR spectrum of **14** (125 MHz, CD_3OD).

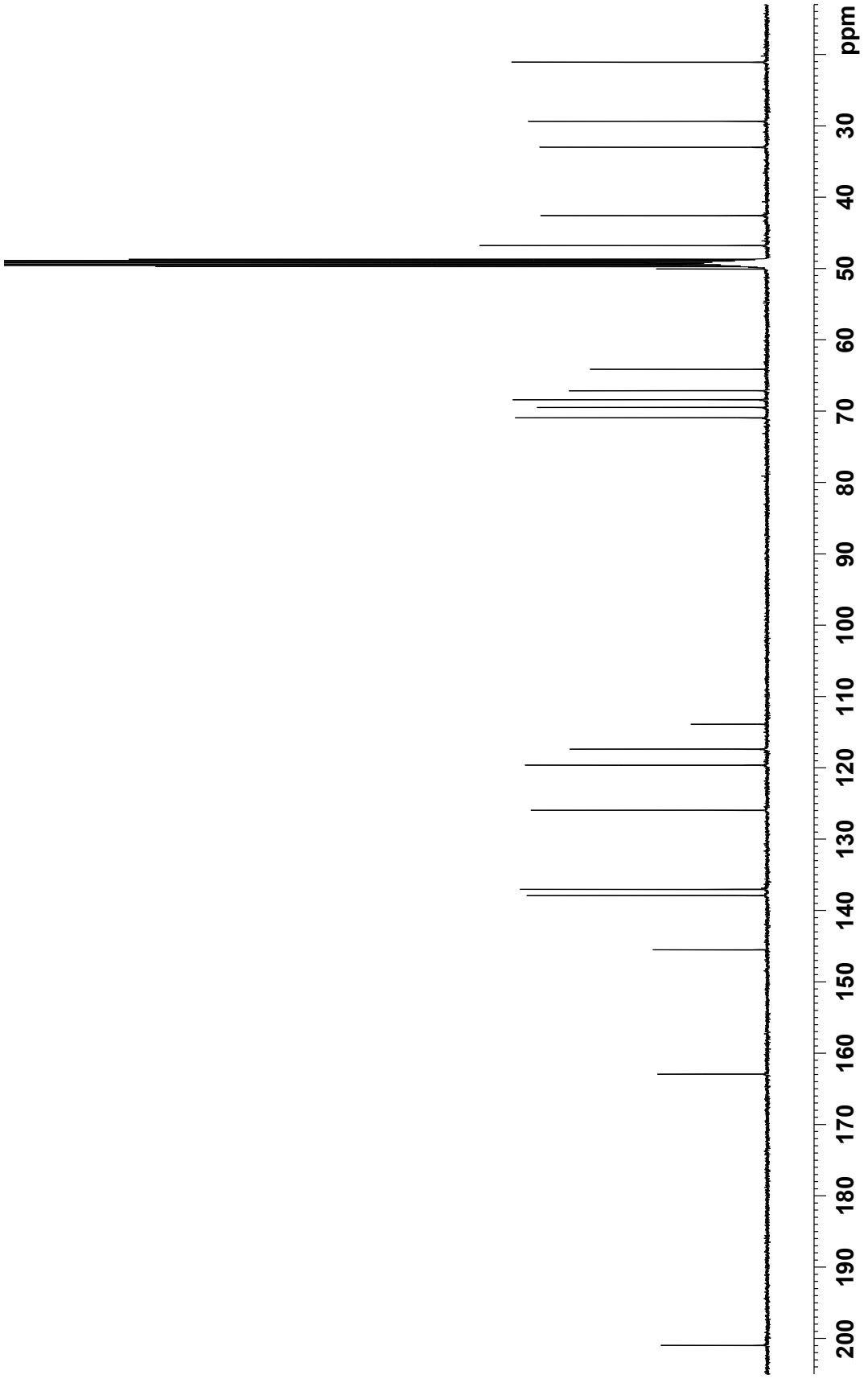

Figure S5. COSY spectrum of **14** (500 MHz, CD_3OD).

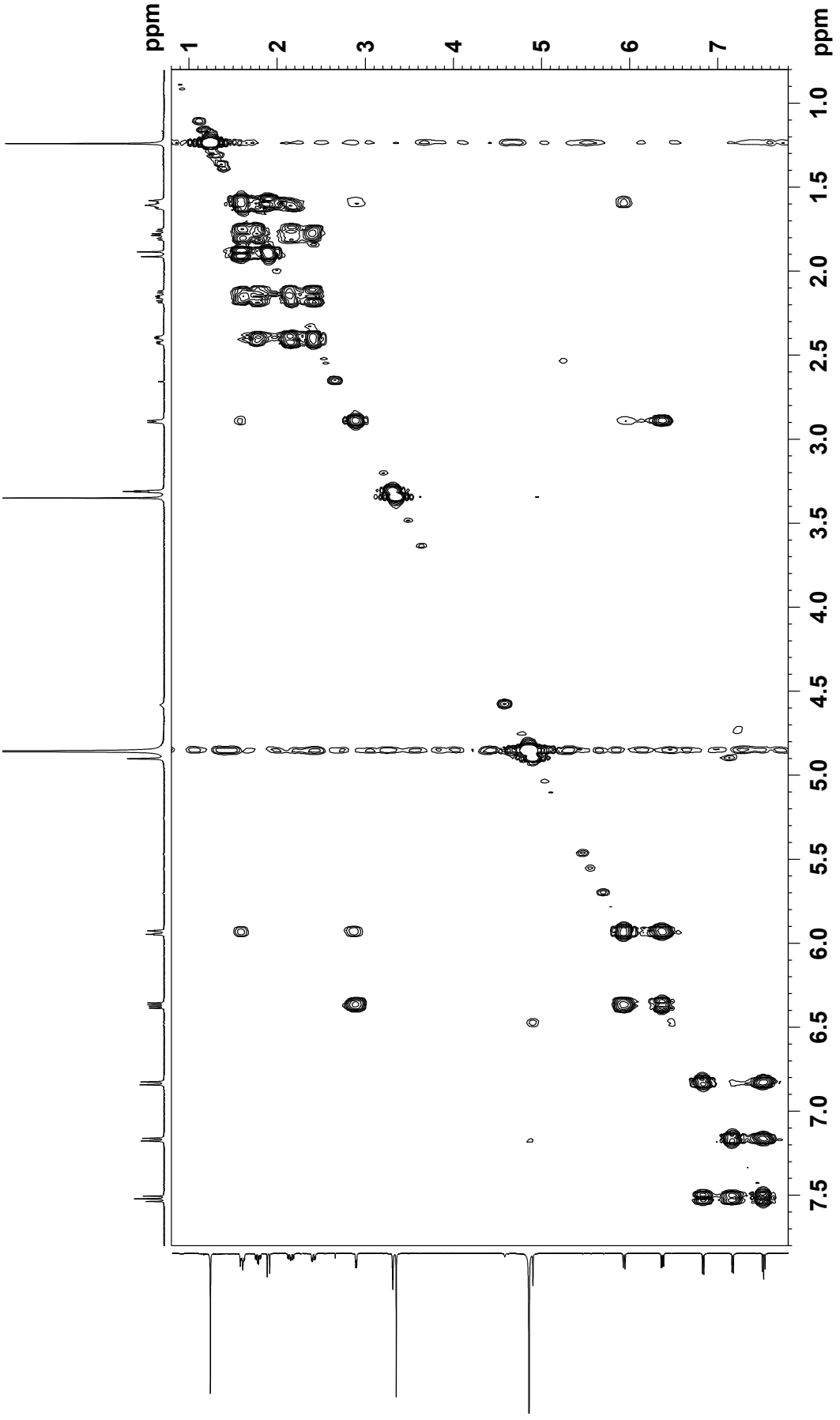

Figure S6. HSQC spectrum of **14** (500 MHz, CD_3OD).

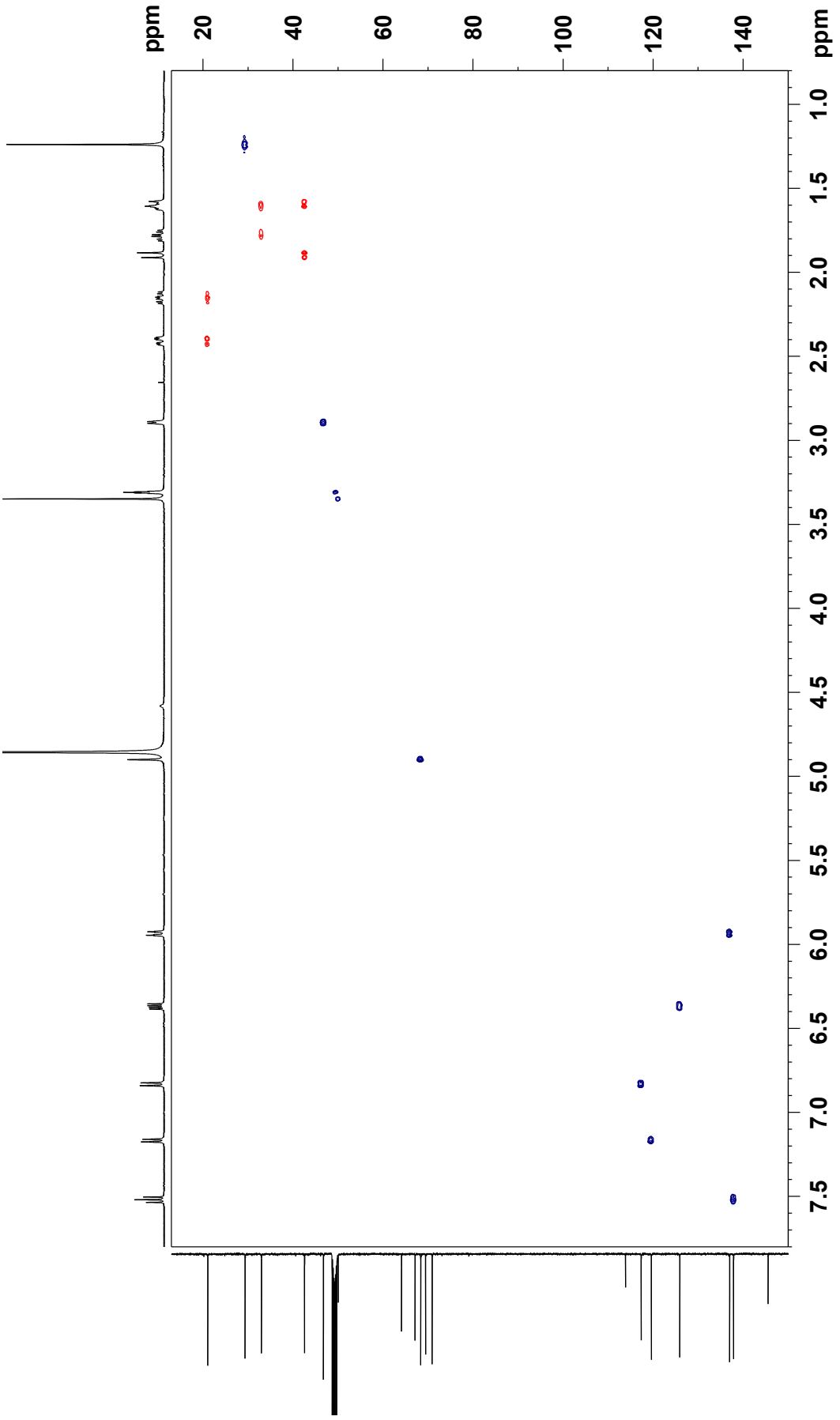

Figure S7. HMBC spectrum of **14** (500 MHz, CD_3OD).

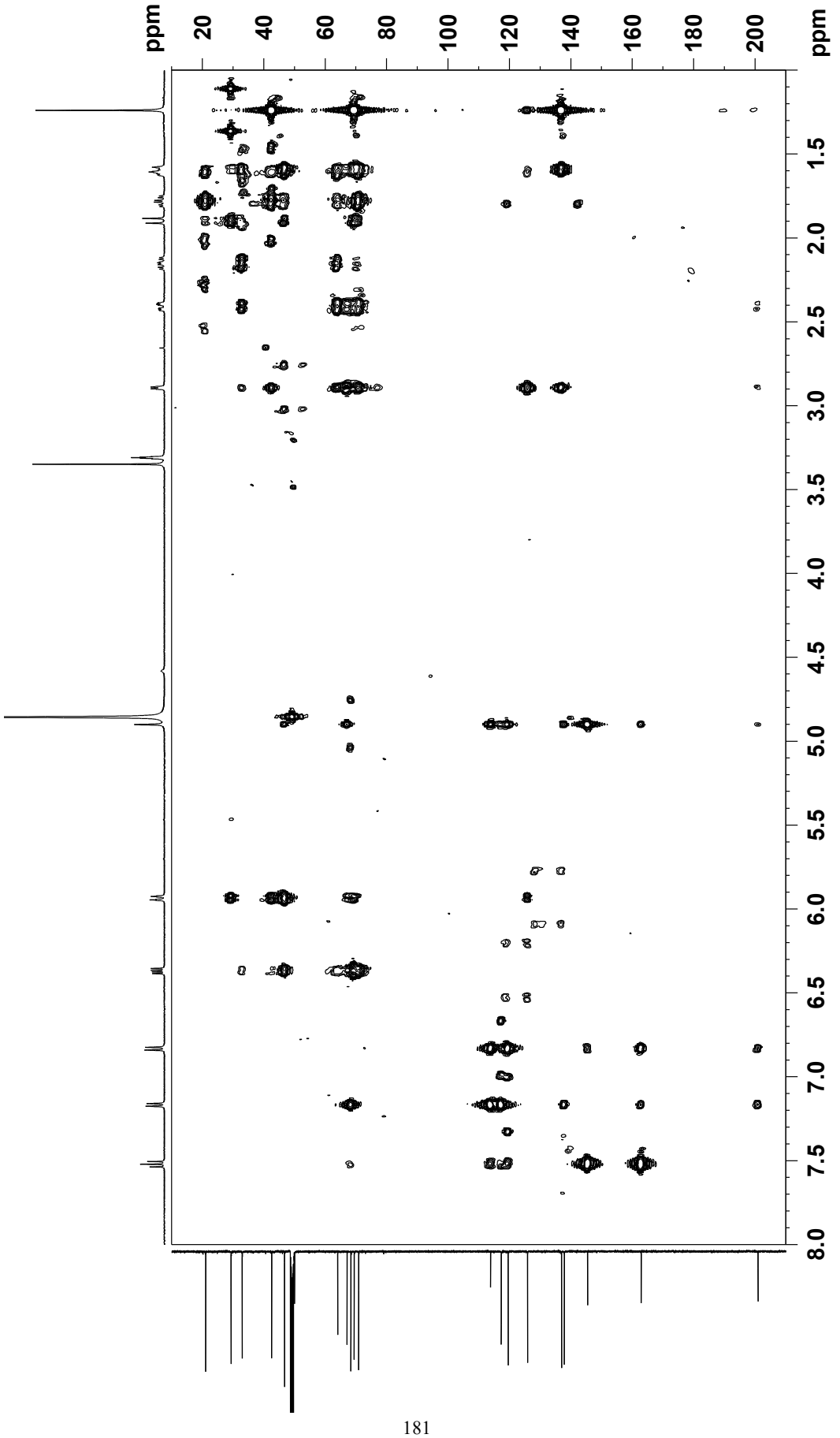

Figure S8. NOESY spectrum of **14** (500 MHz, CD_3OD).

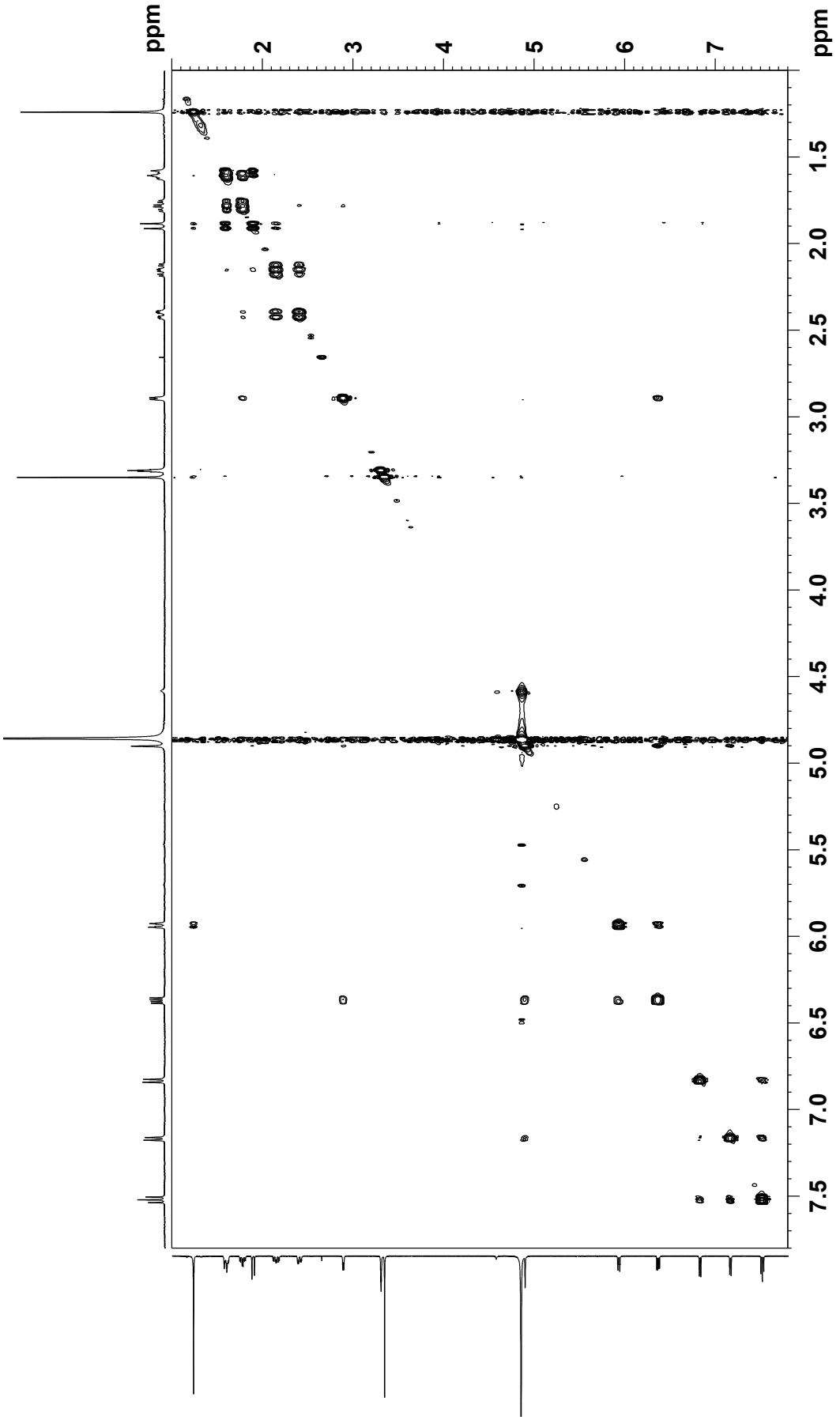

Figure S9. UV spectrum of kumemicinone B (**15**).

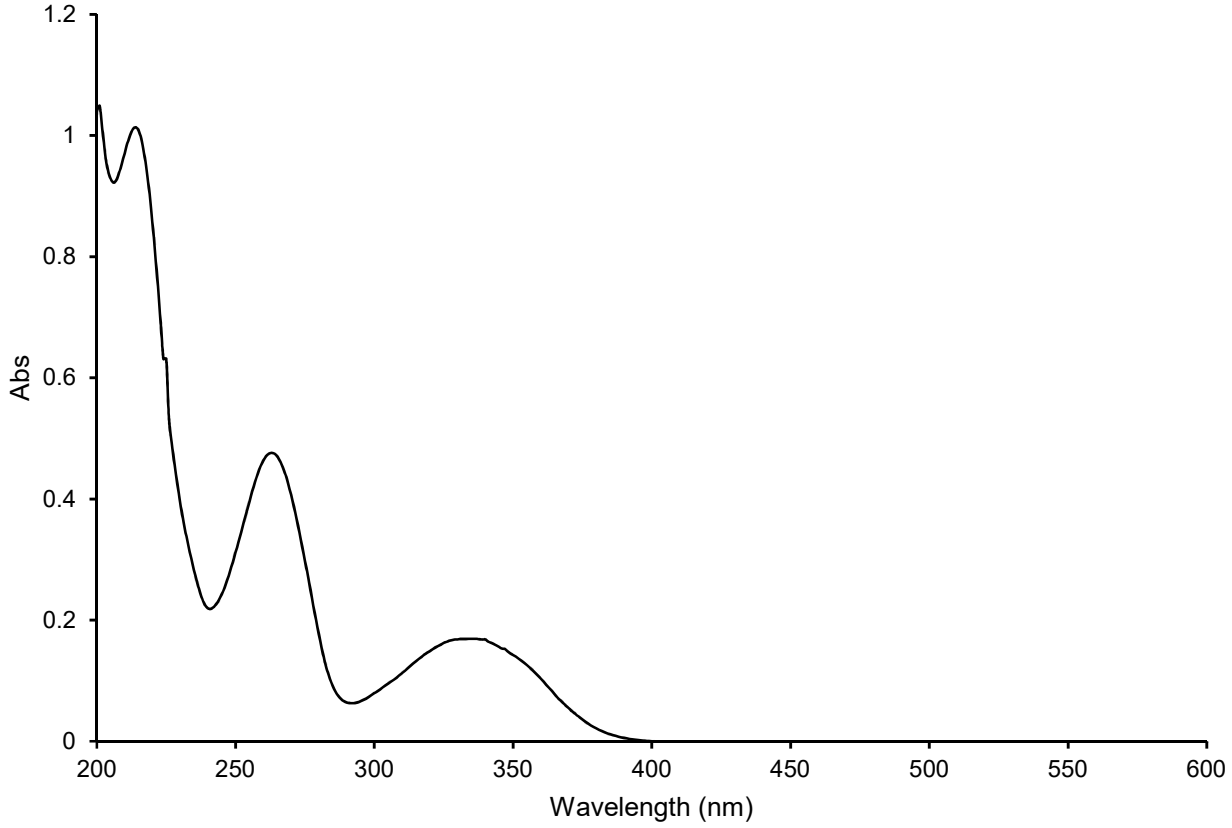

Figure S10. IR spectrum of **15**.

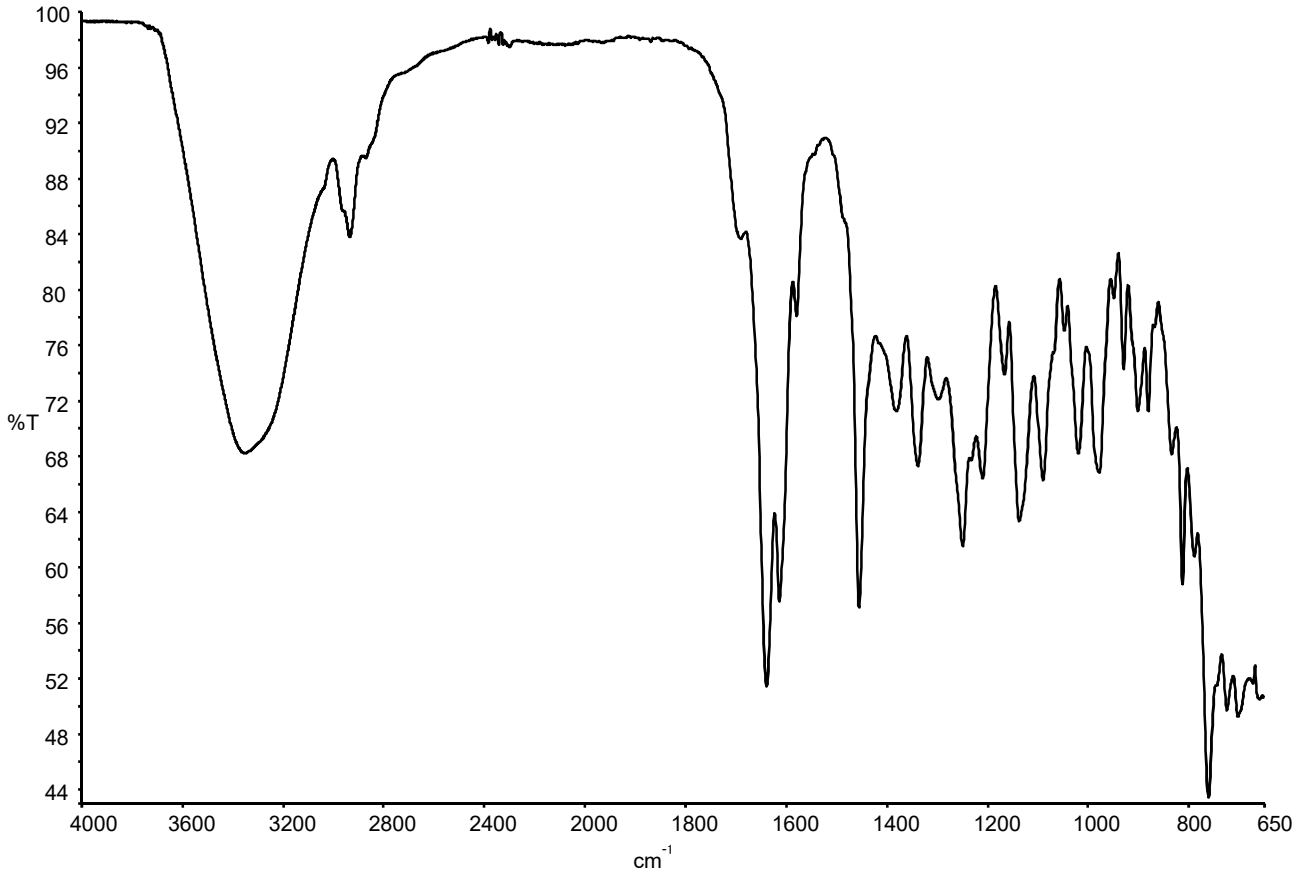

Figure S11. ^{1}H NMR spectrum of **15** (500 MHz, CD_3OD).

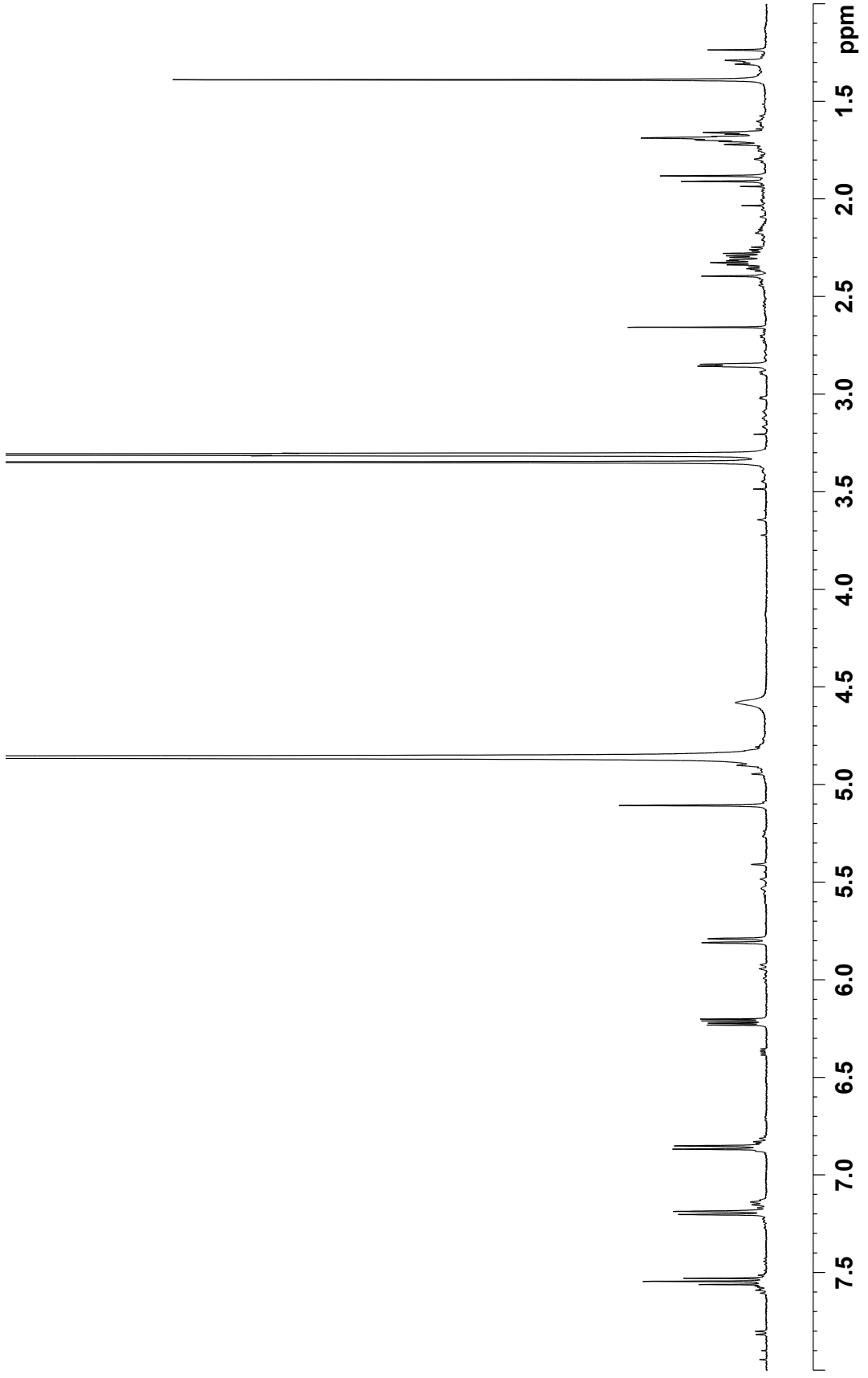

Figure S12. ^{13}C NMR spectrum of **15** (125 MHz, CD_3OD).

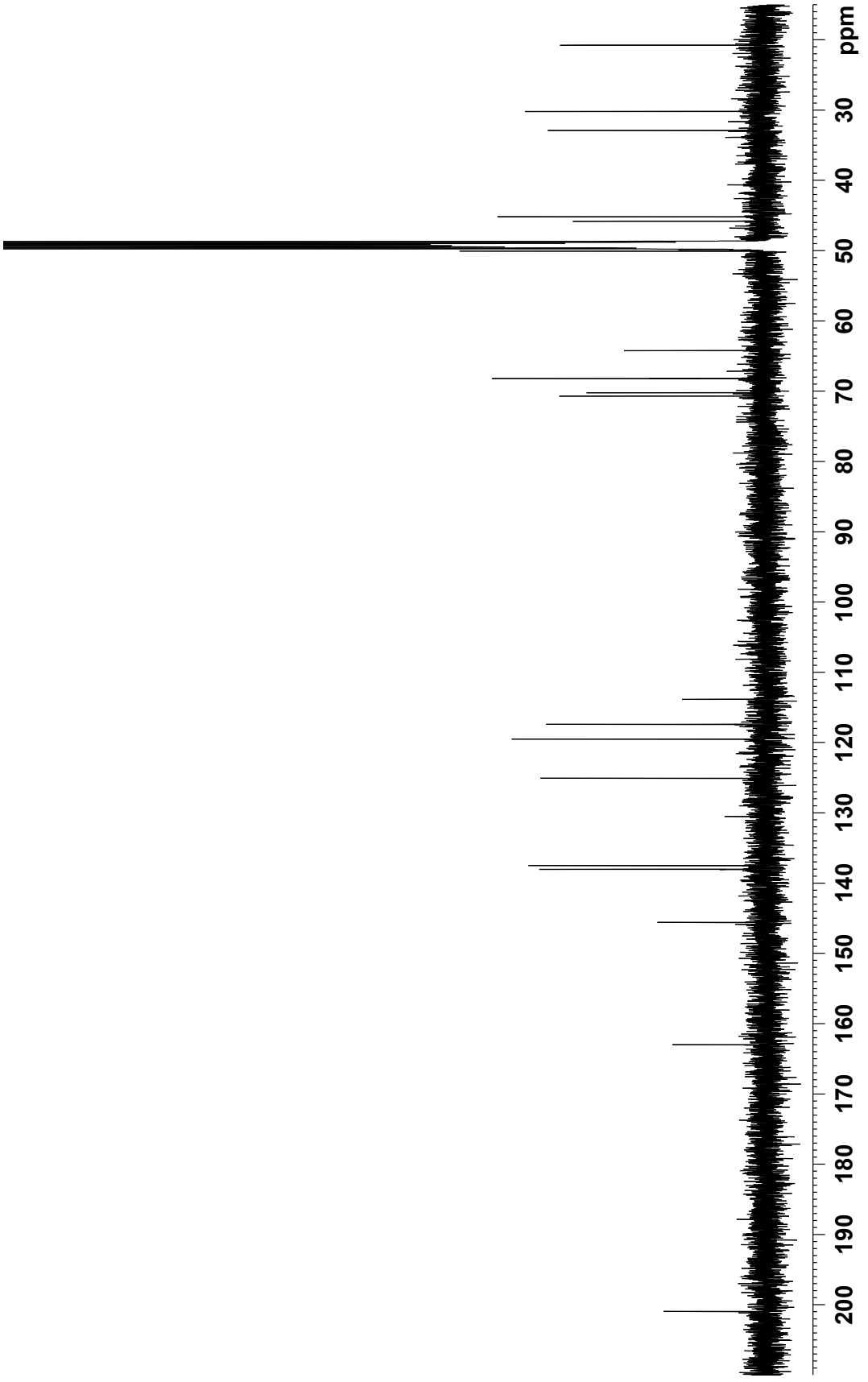

Figure S13. COSY spectrum of **15** (500 MHz, CD_3OD).

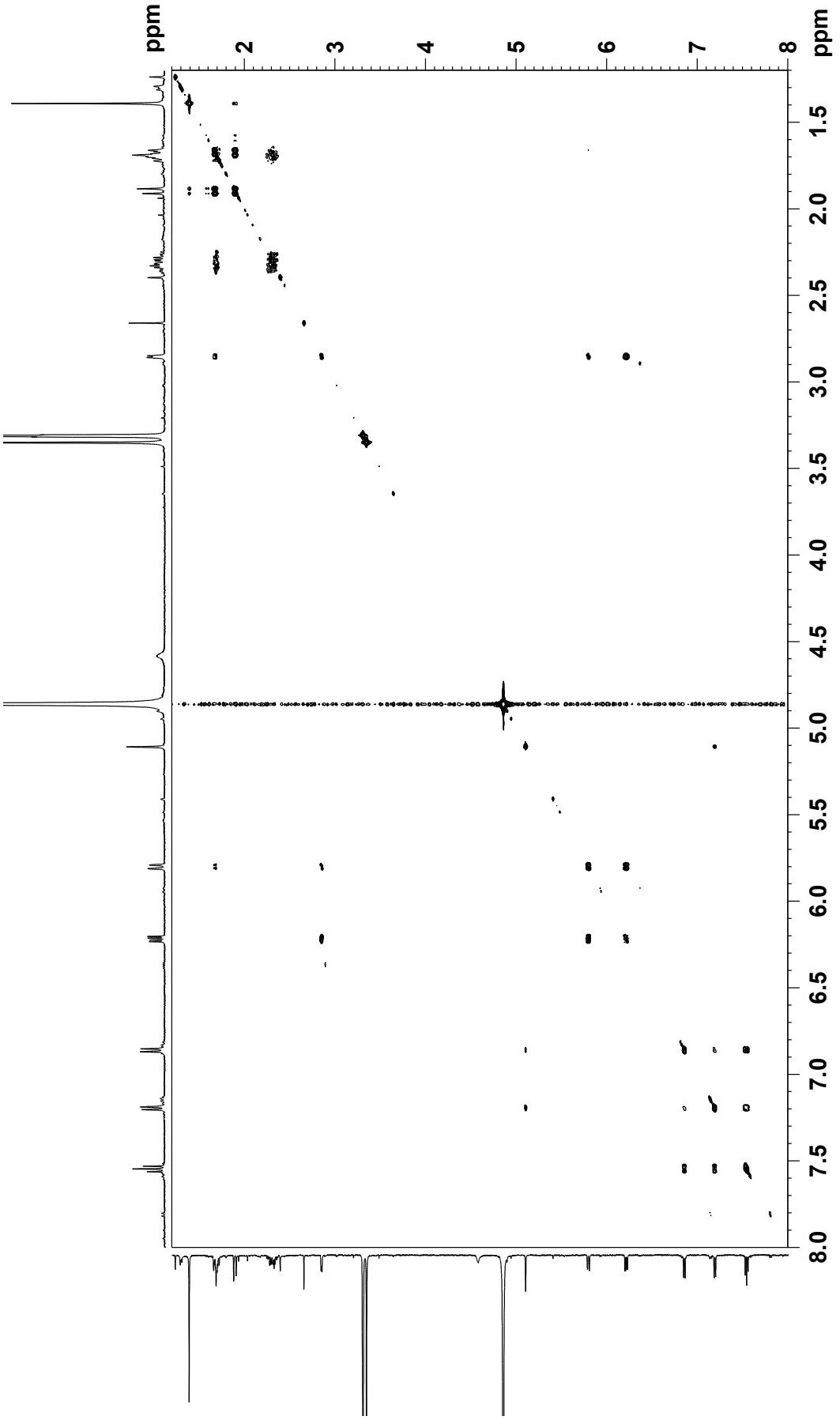

Figure S14. HSQC spectrum of **15** (500 MHz, CD_3OD).

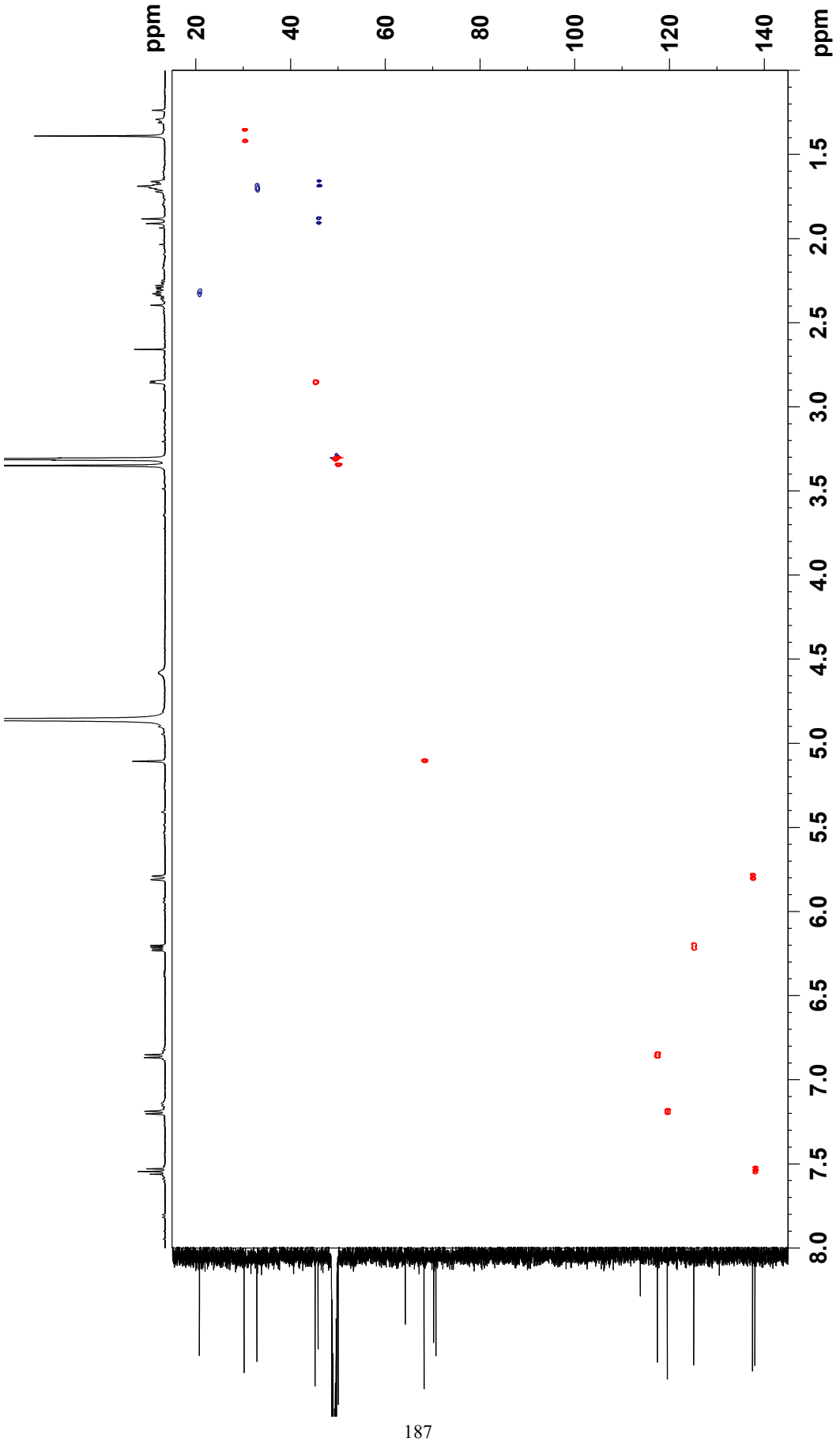

Figure S15. HMBC spectrum of **15** (500 MHz, CD_3OD).

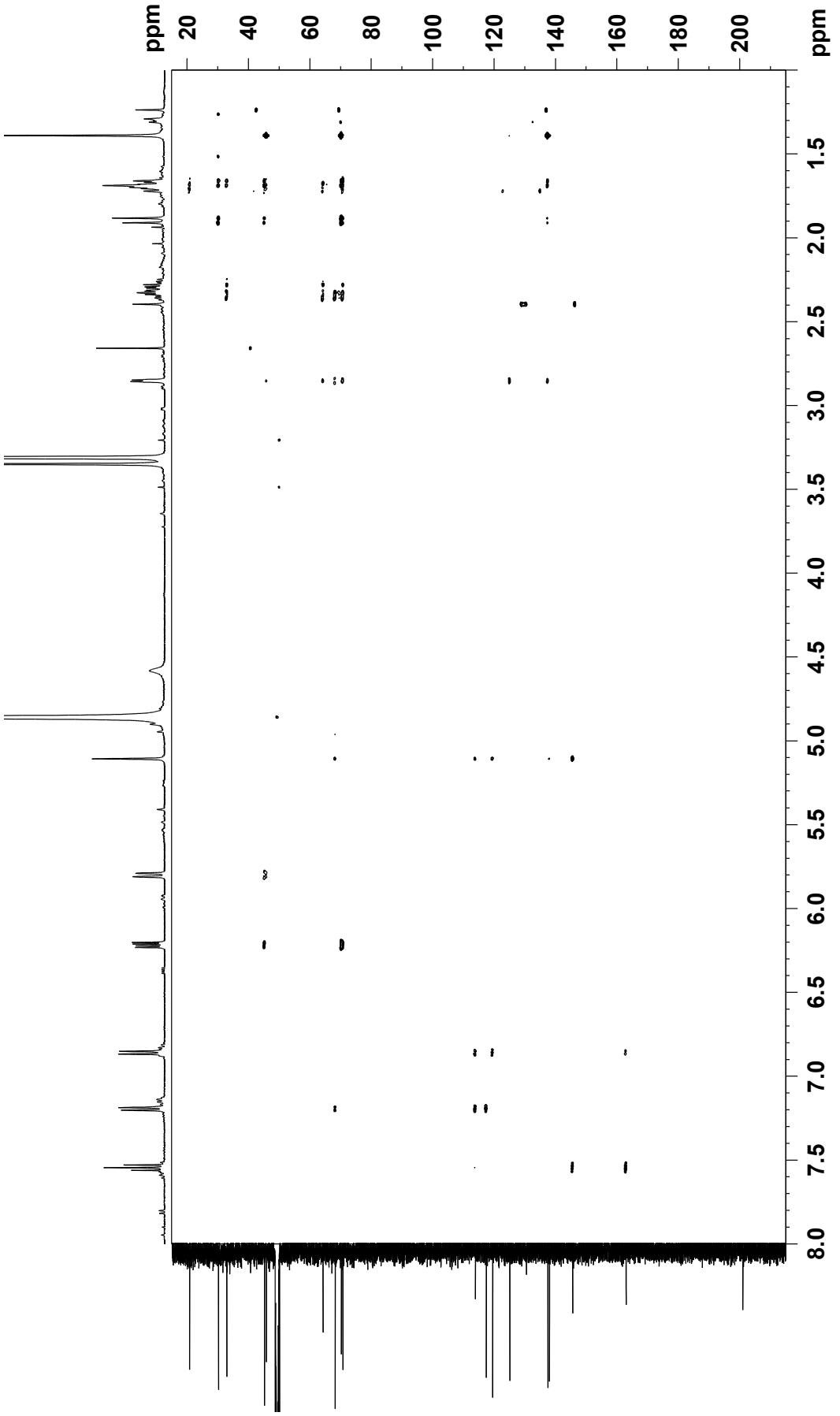

Figure S16. NOESY spectrum of **15** (500 MHz, CD_3OD).

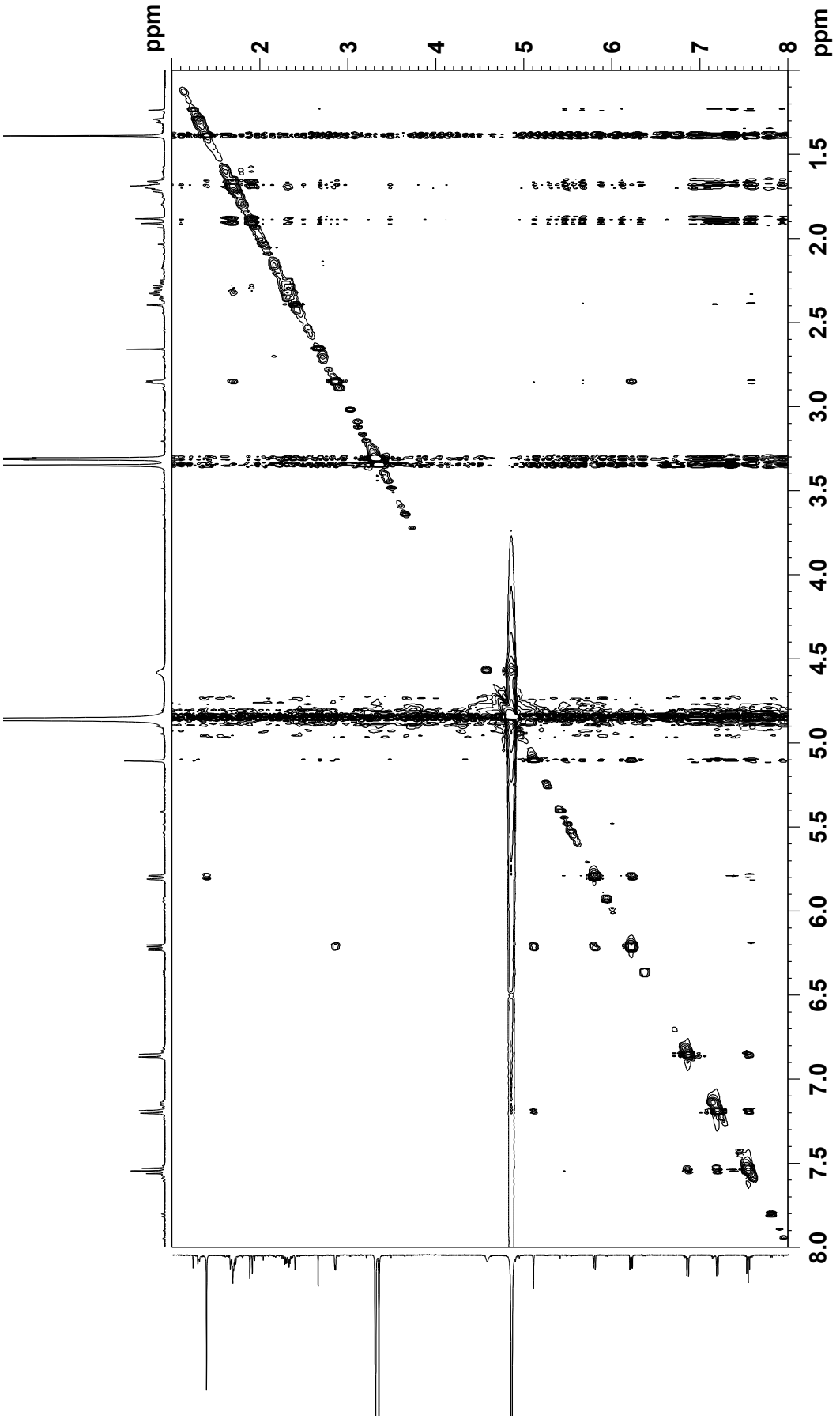

Figure S17. UV spectrum of kumemicinone C (**16**).

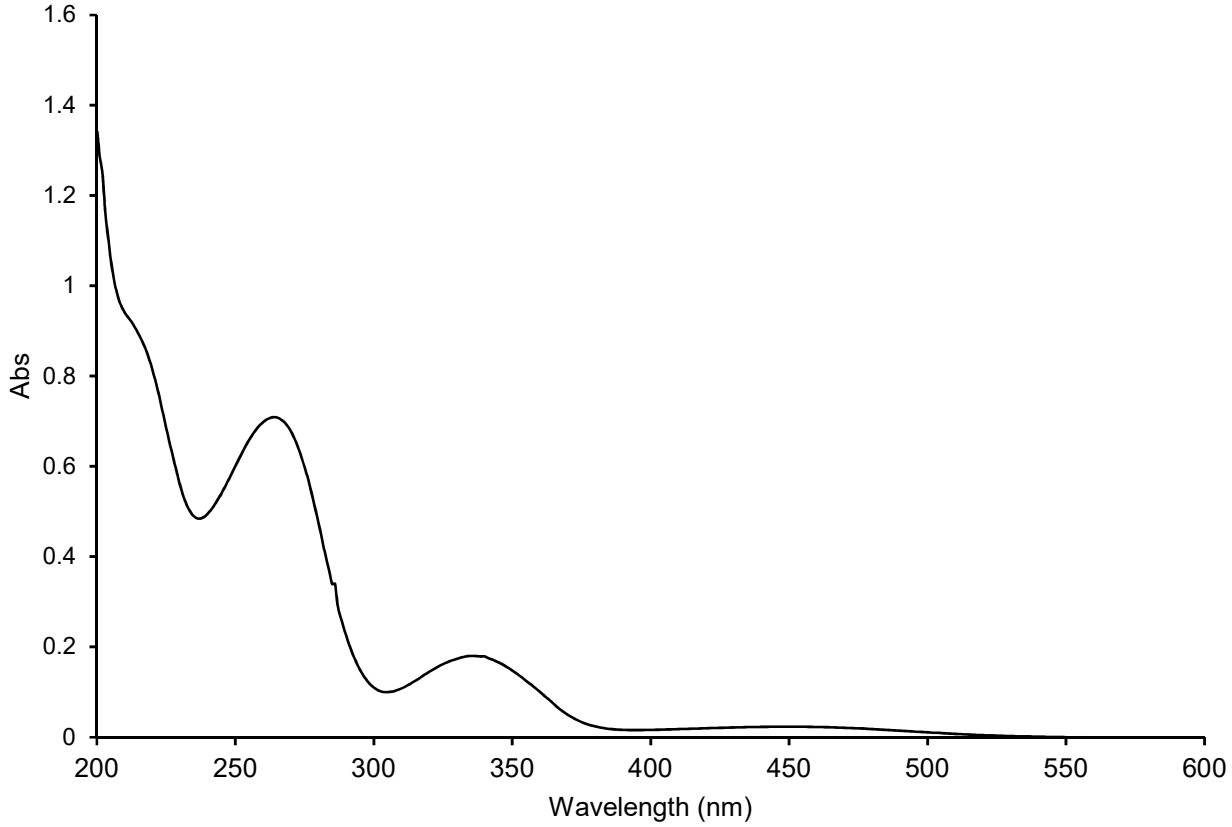

Figure S18. IR spectrum of **16**.

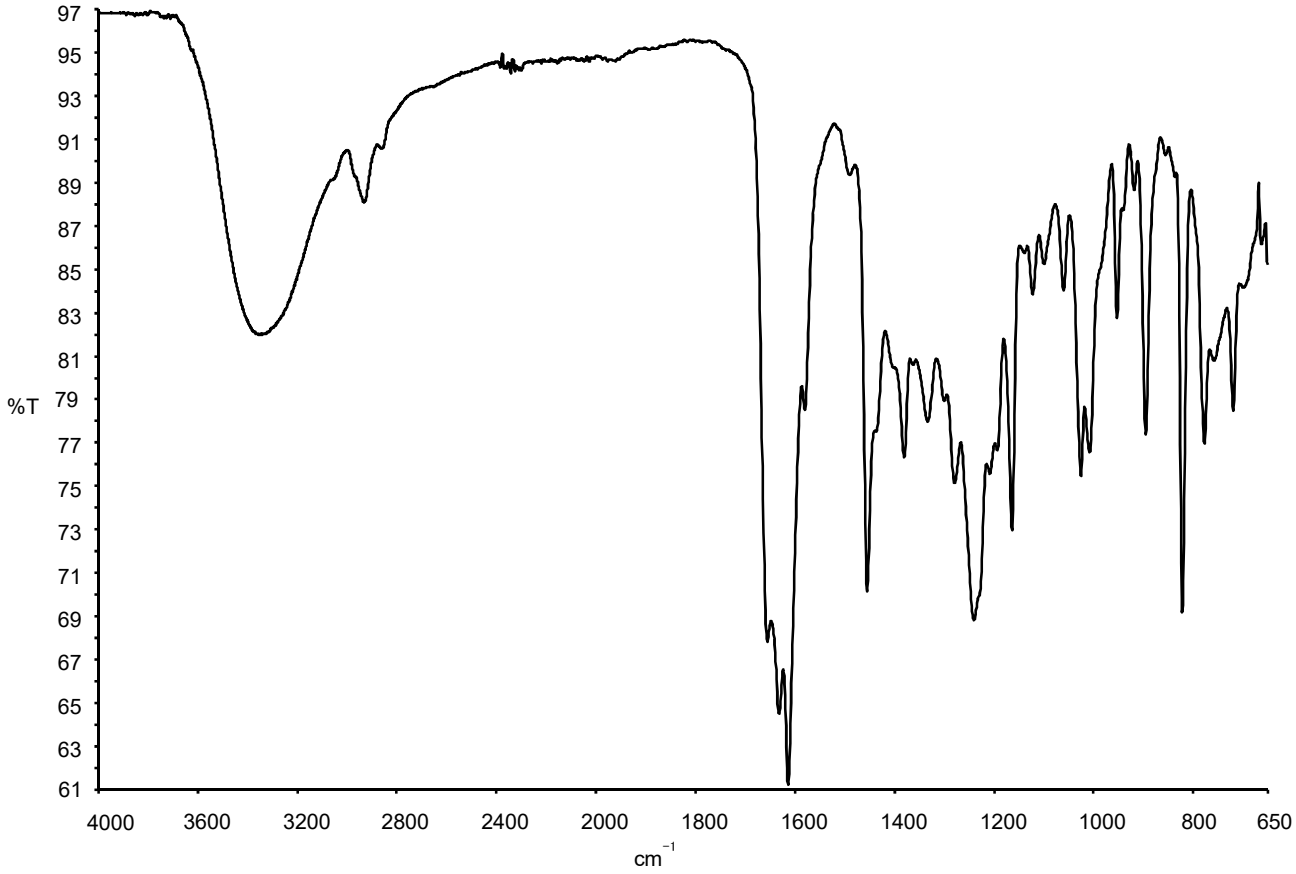

Figure S19. ^{1}H NMR spectrum of **16** (500 MHz, CD_3OD).

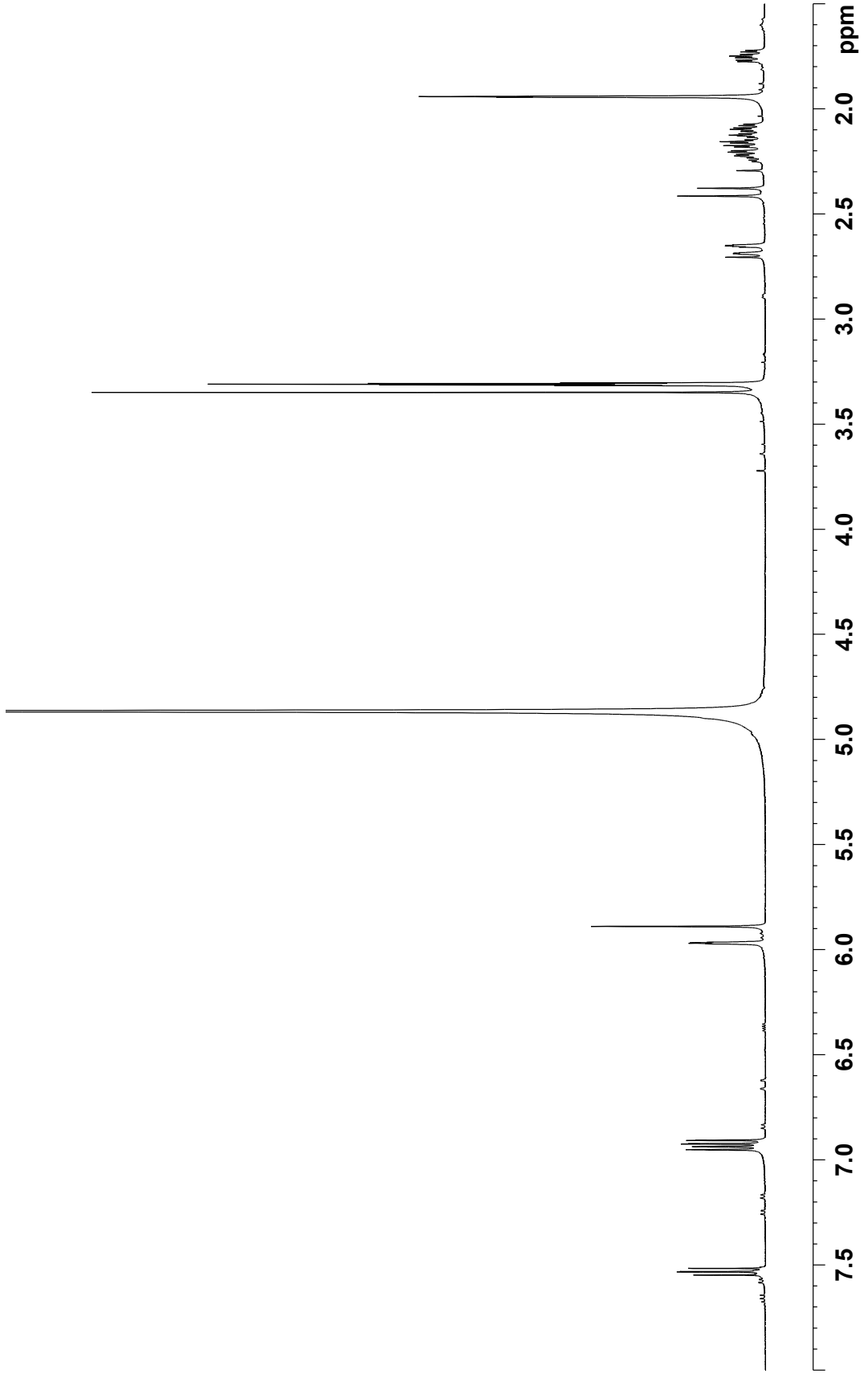

Figure S20. ^{13}C NMR spectrum of **16** (125 MHz, CD_3OD).

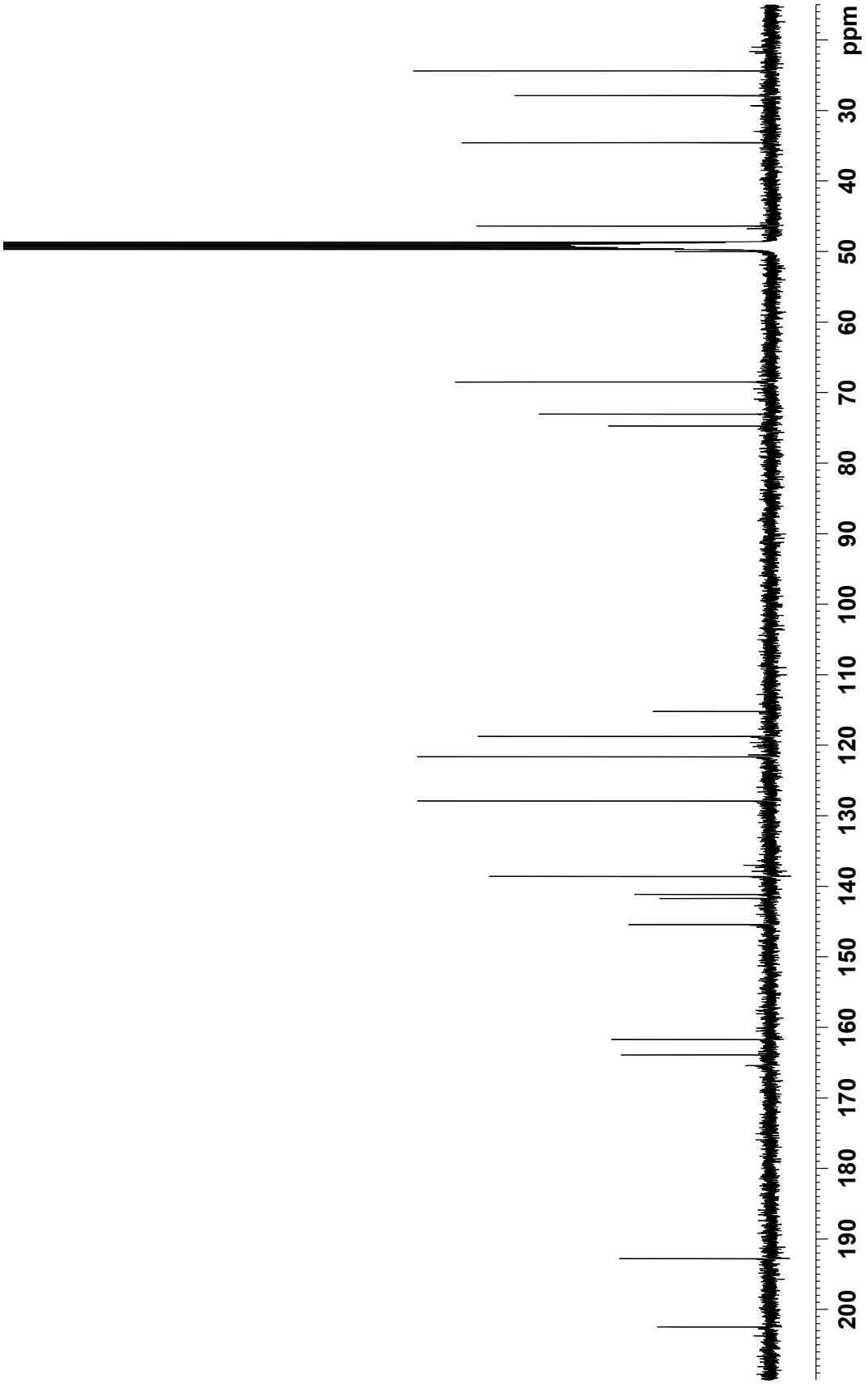

Figure S21. COSY spectrum of **16** (500 MHz, CD_3OD).

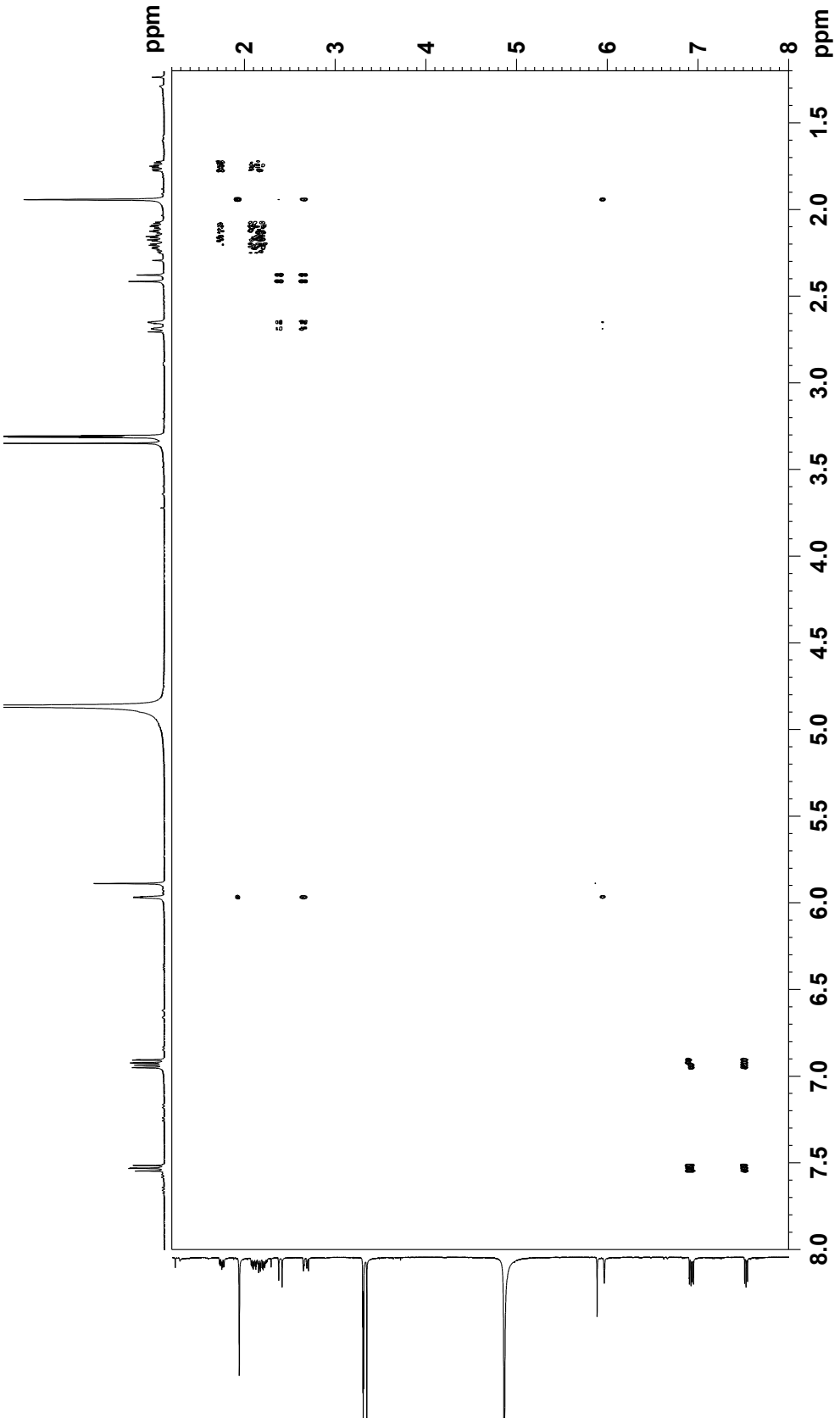

Figure S22. HSQC spectrum of **16** (500 MHz, CD_3OD).

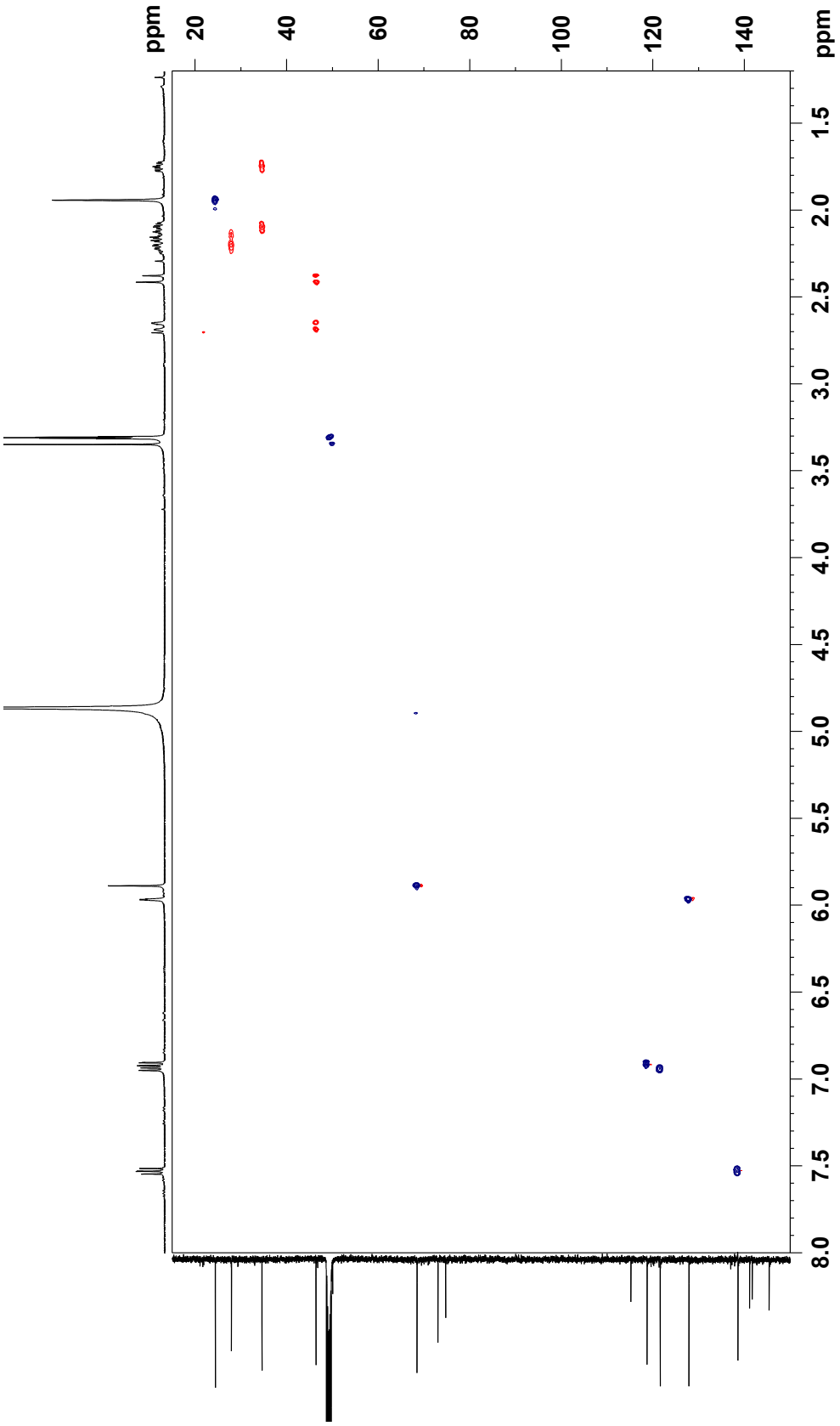

Figure S23. HMBC spectrum of **16** (500 MHz, CD_3OD).

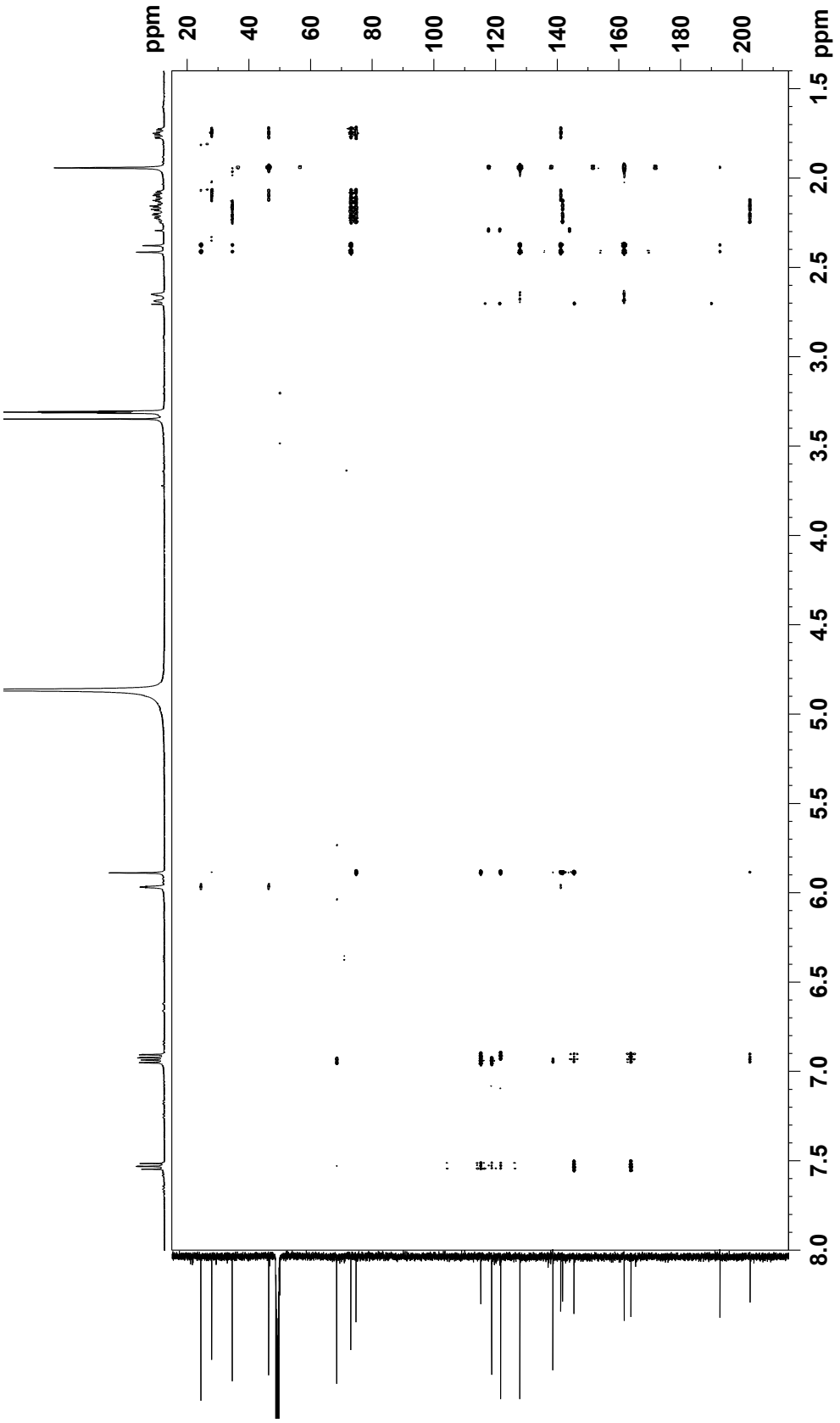

Figure S24. NOESY spectrum of **16** (500 MHz, CD_3OD).

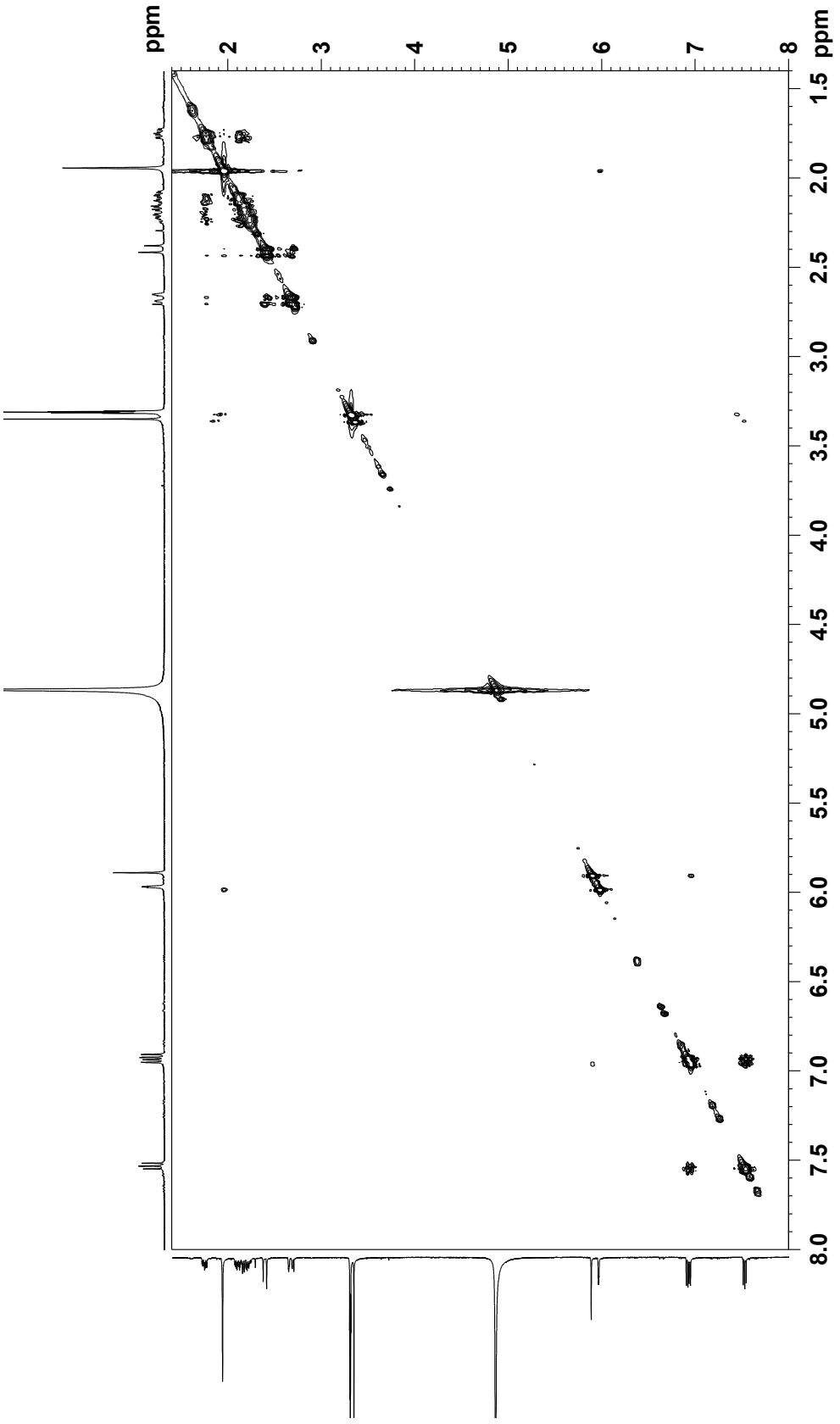

Figure S25. UV spectrum of kumemicinone D (**17**).

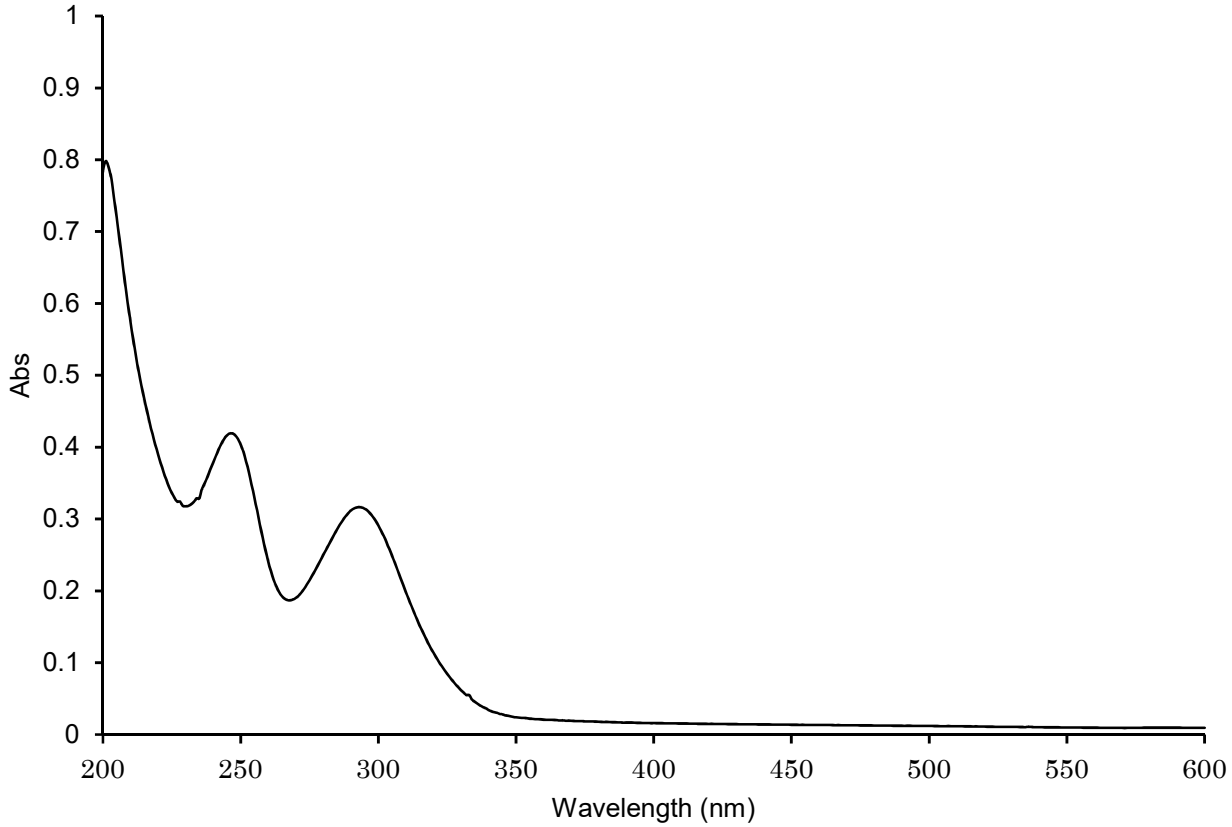

Figure S26. IR spectrum of **17**.

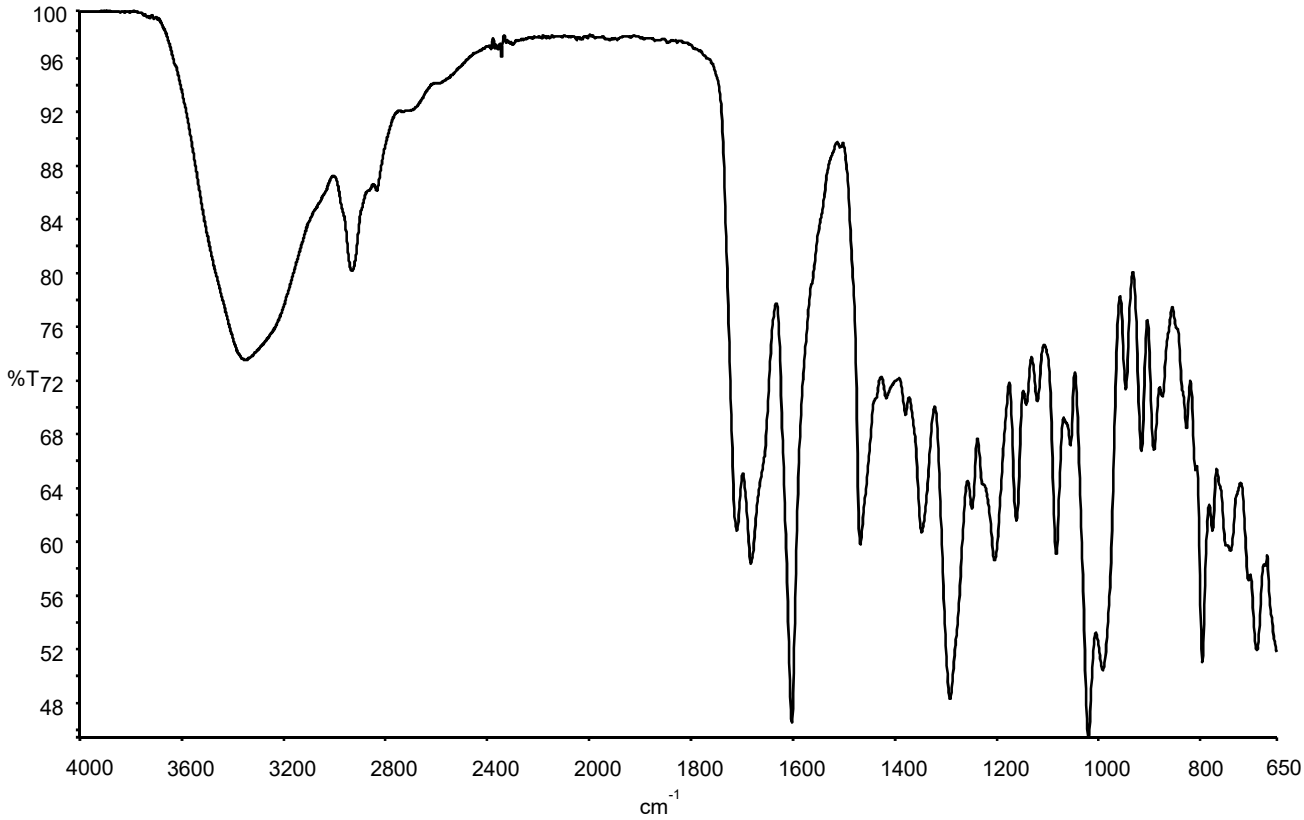

Figure S27. ^{1}H NMR spectrum of **17** (500 MHz, CD_3OD).

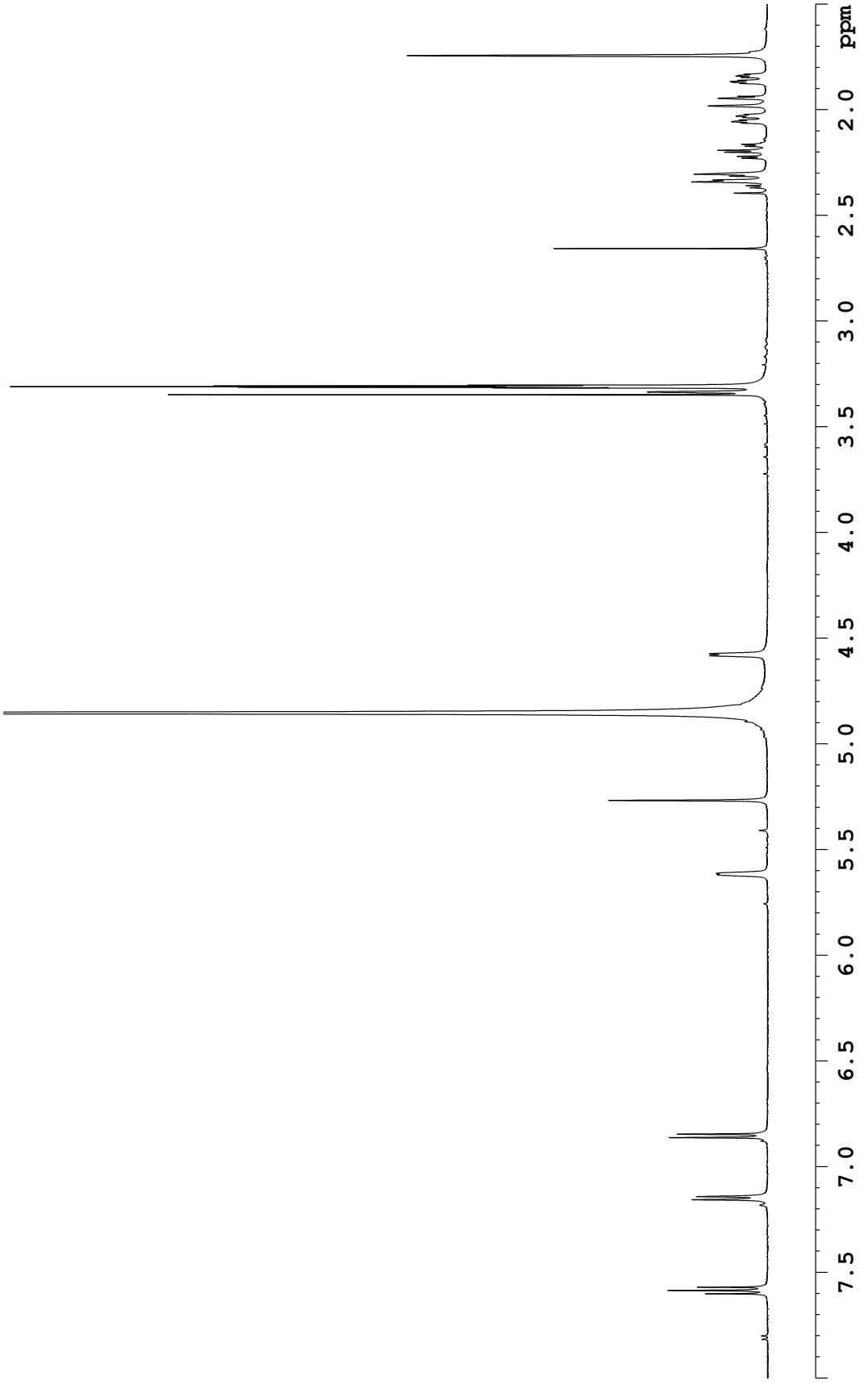

Figure S28. ^{13}C NMR spectrum of **17** (125 MHz, CD_3OD).

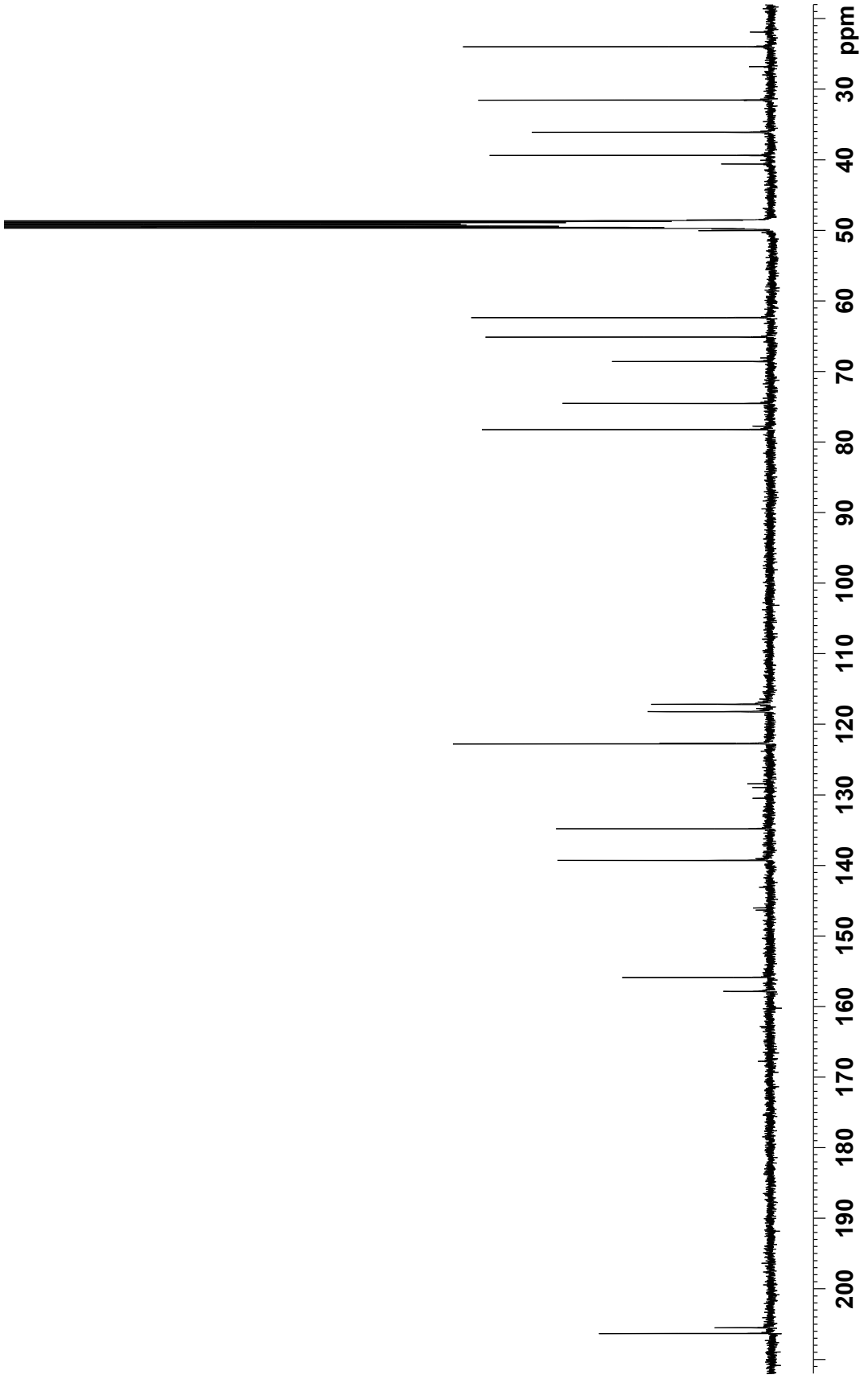

Figure S29. COSY spectrum of **17** (500 MHz, CD_3OD).

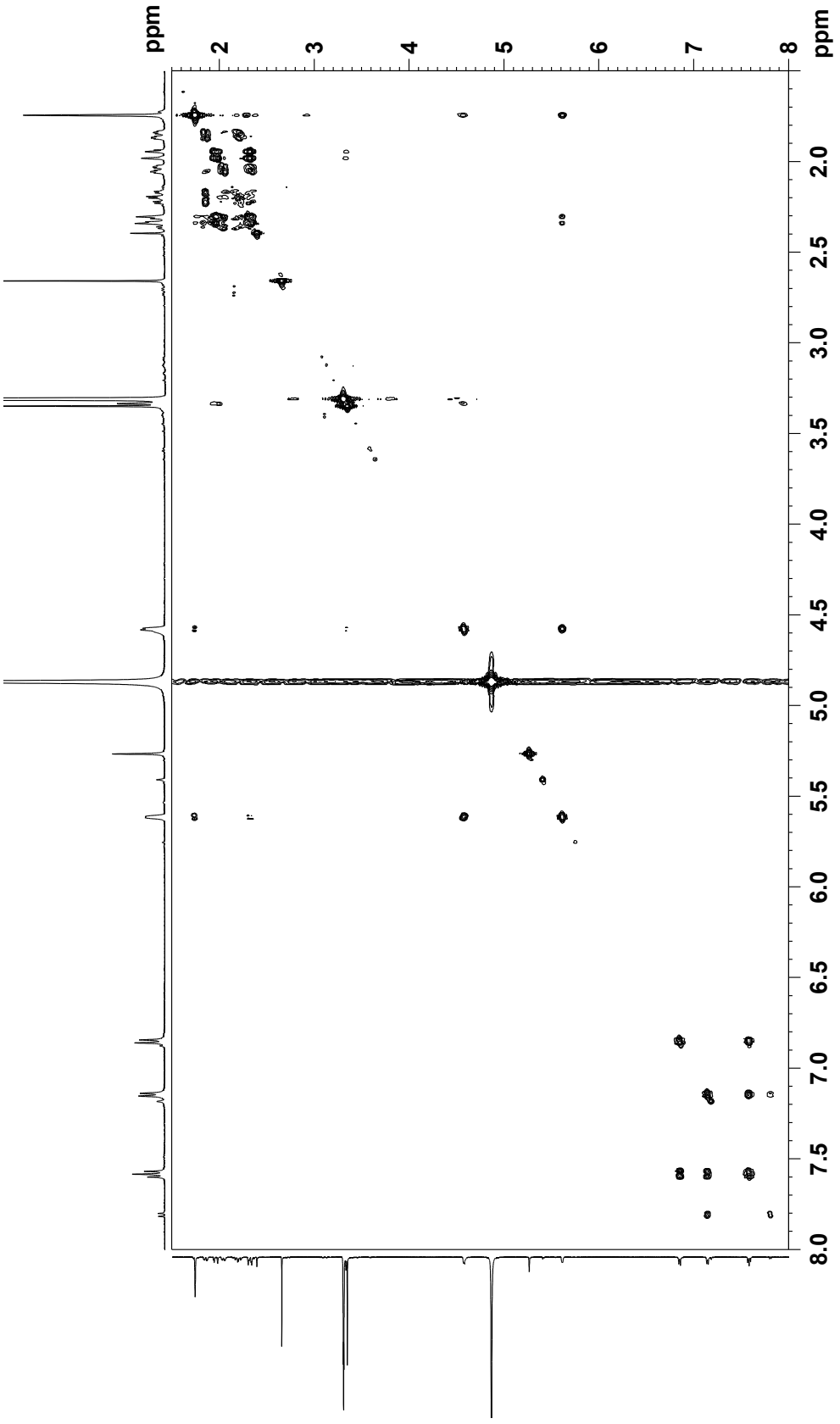

Figure S30. HSQC spectrum of **17** (500 MHz, CD_3OD).

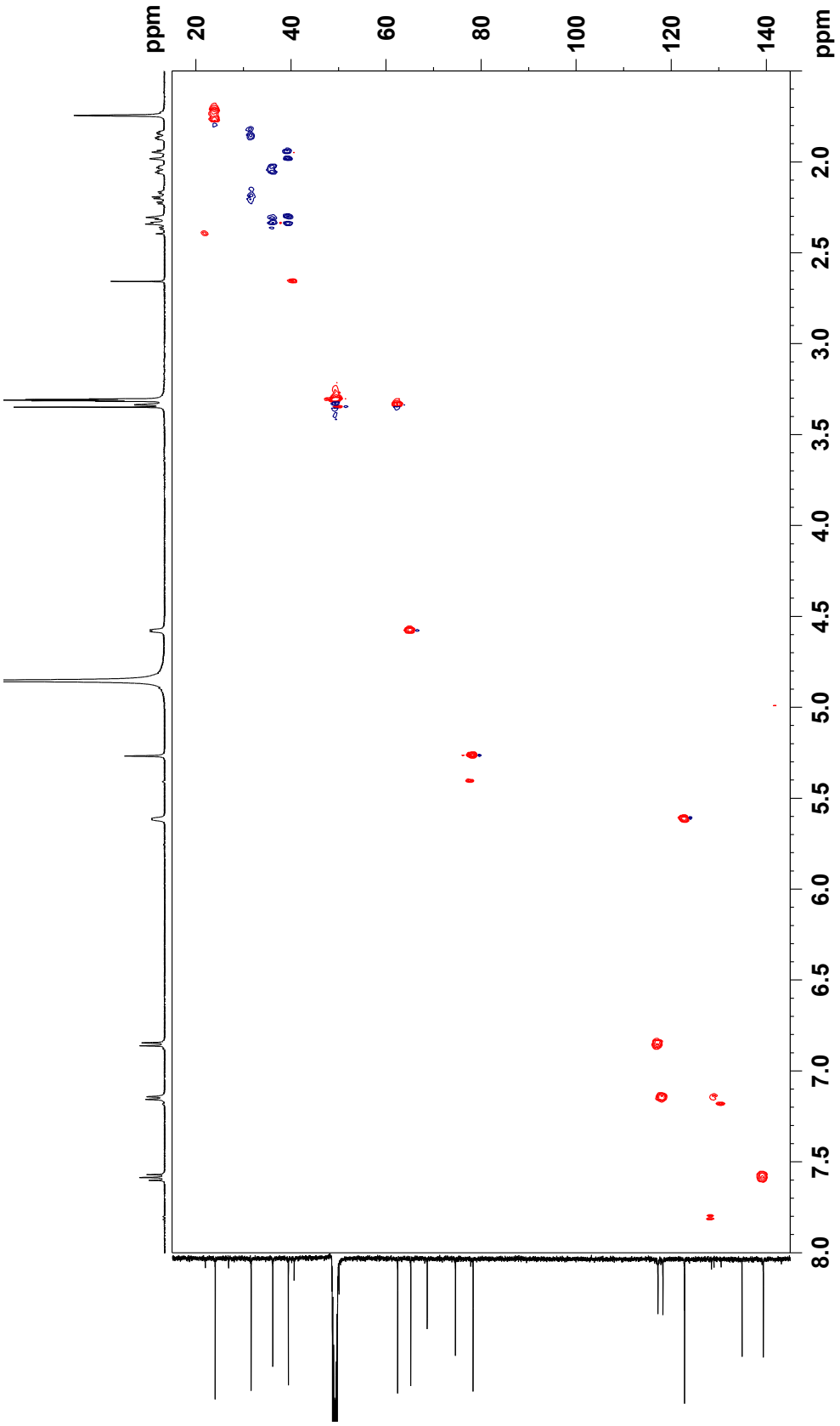

Figure S31. HMBC spectrum of **17** (500 MHz, CD_3OD).

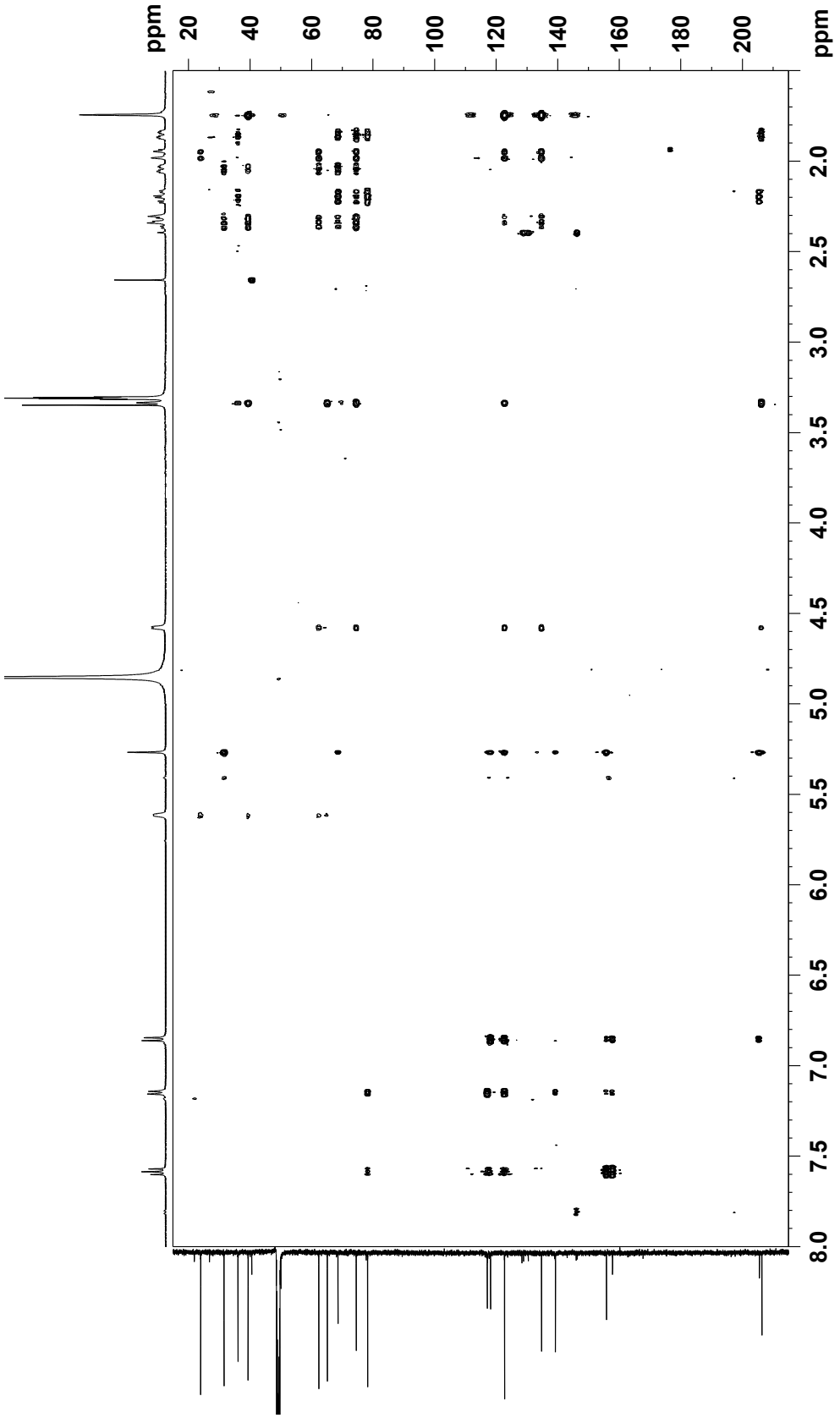

Figure S32. NOESY spectrum of **17** (500 MHz, CD_3OD).

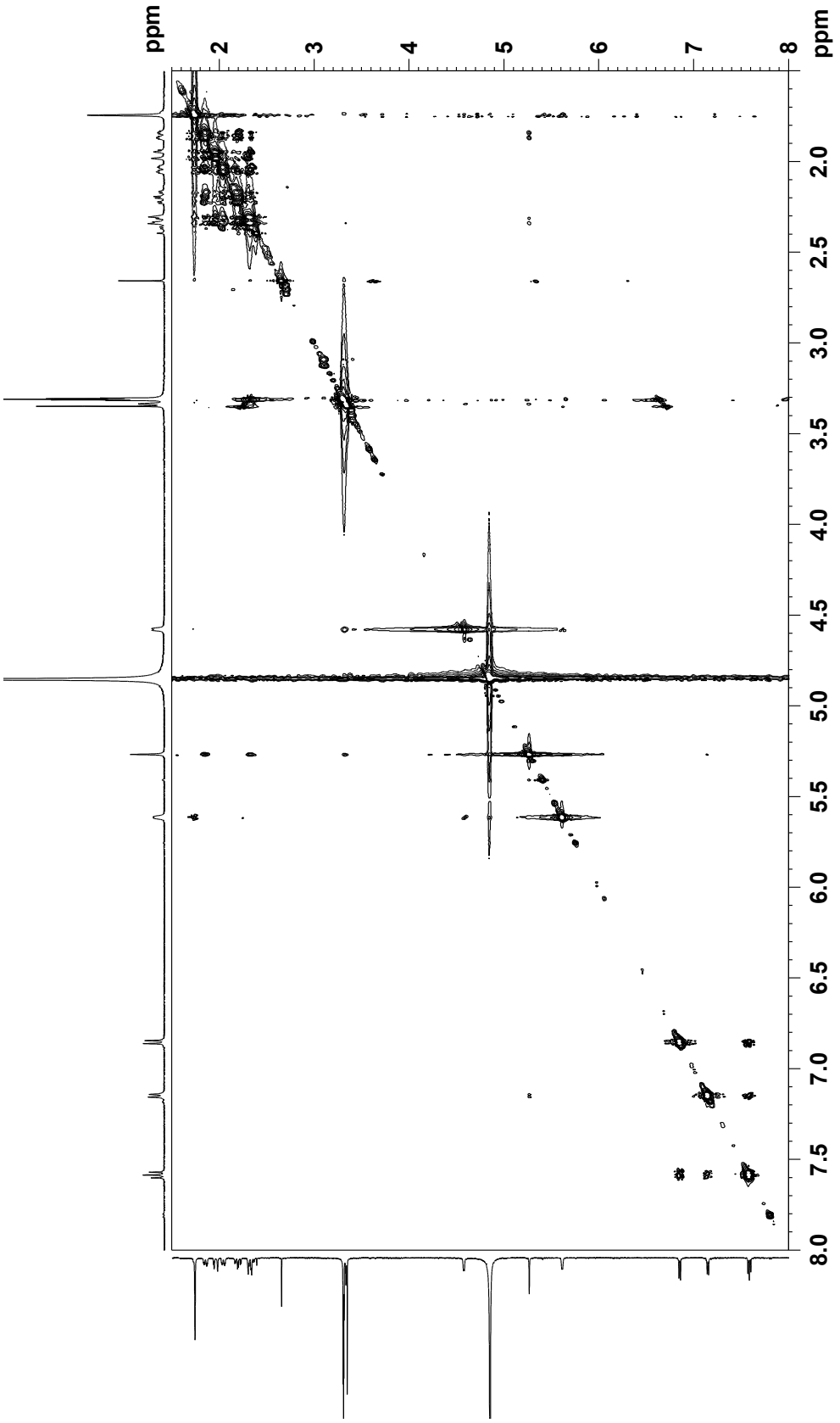

Figure S33. UV spectrum of kumemicinone E (**18**).

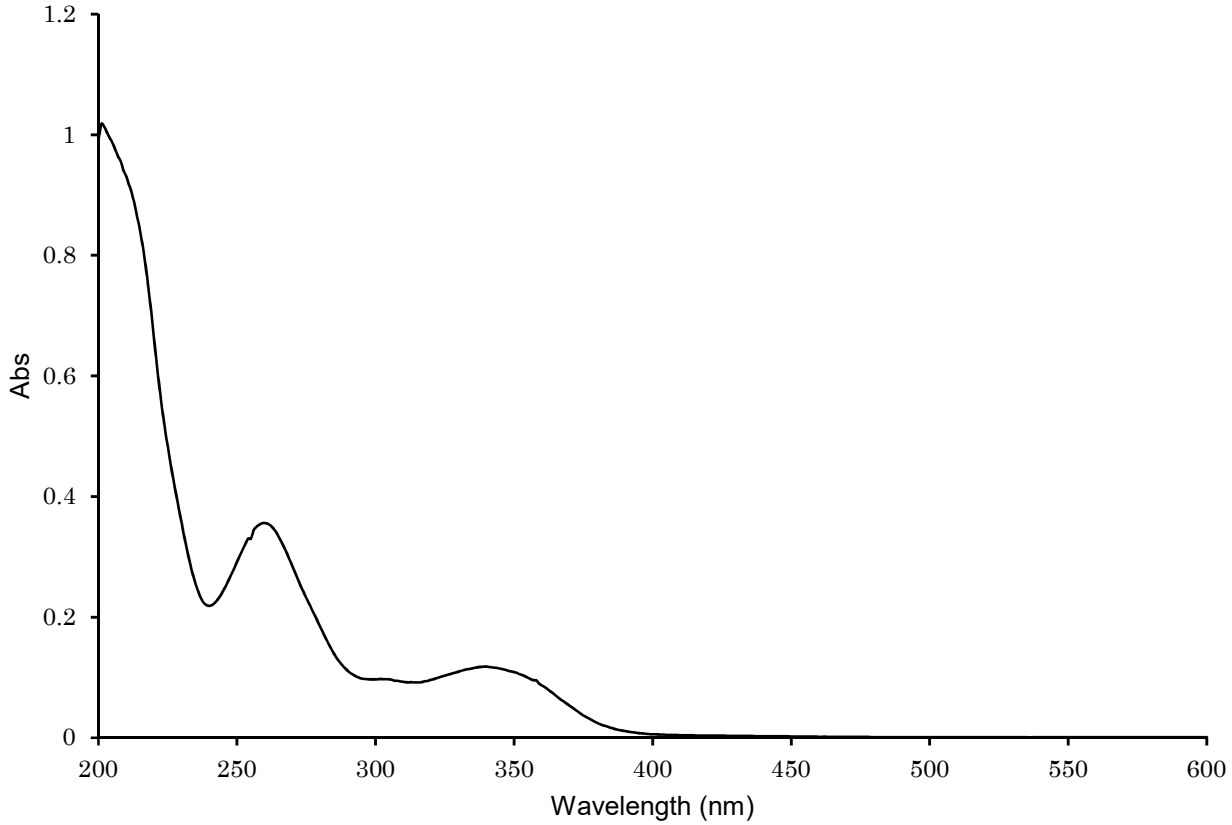

Figure S34. IR spectrum of **18**.

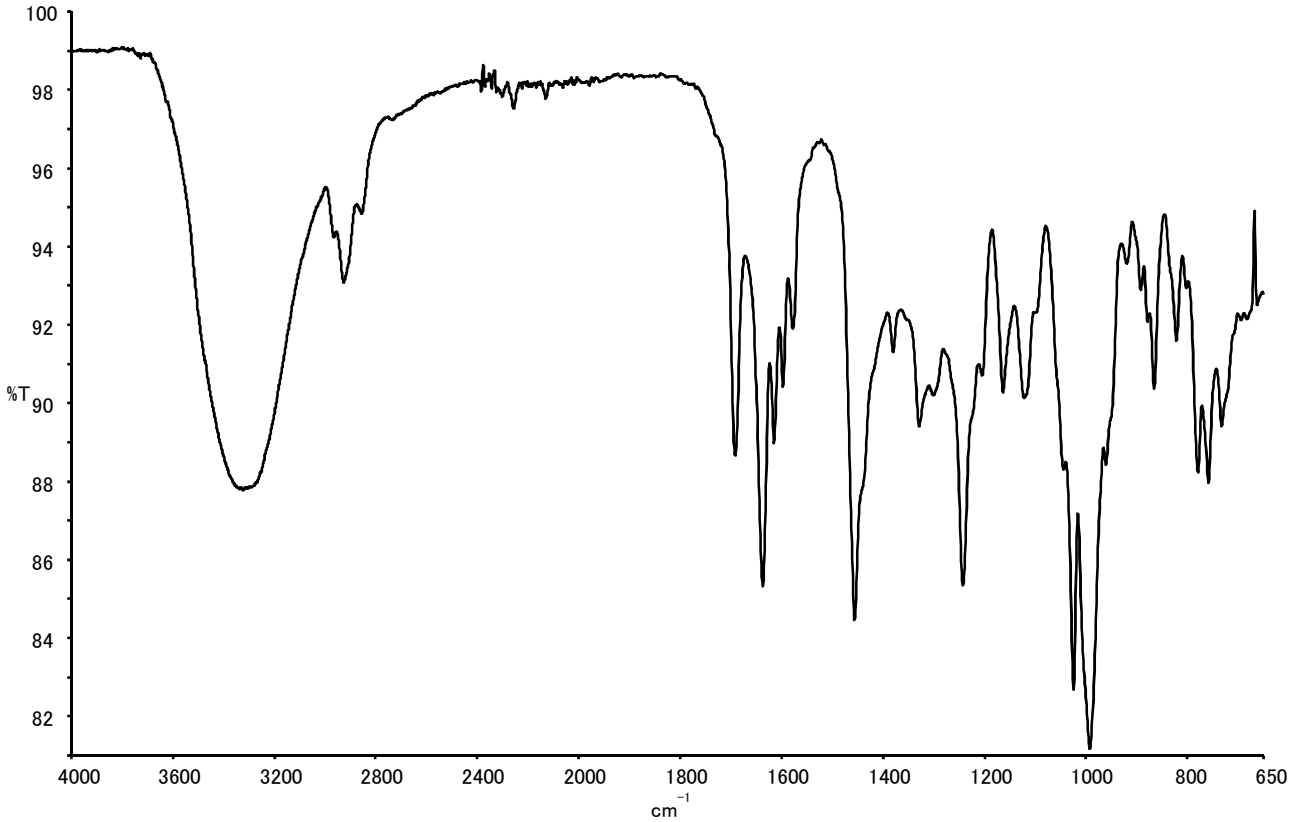

Figure S35. ^{1}H NMR spectrum of **18** (500 MHz, DMSO-d_6).

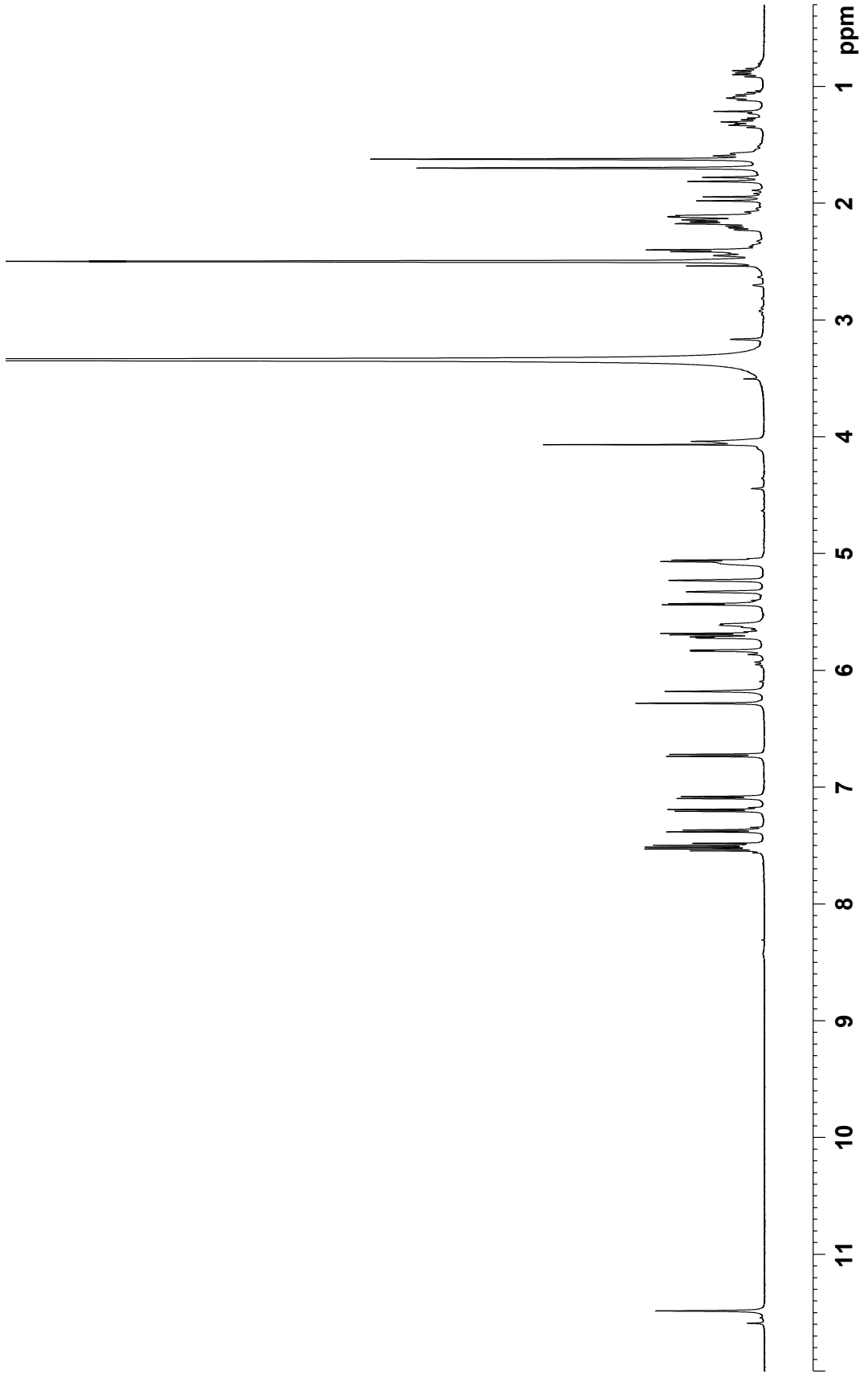

Figure S36. ^{13}C NMR spectrum of **18** (125 MHz, DMSO-d_6).

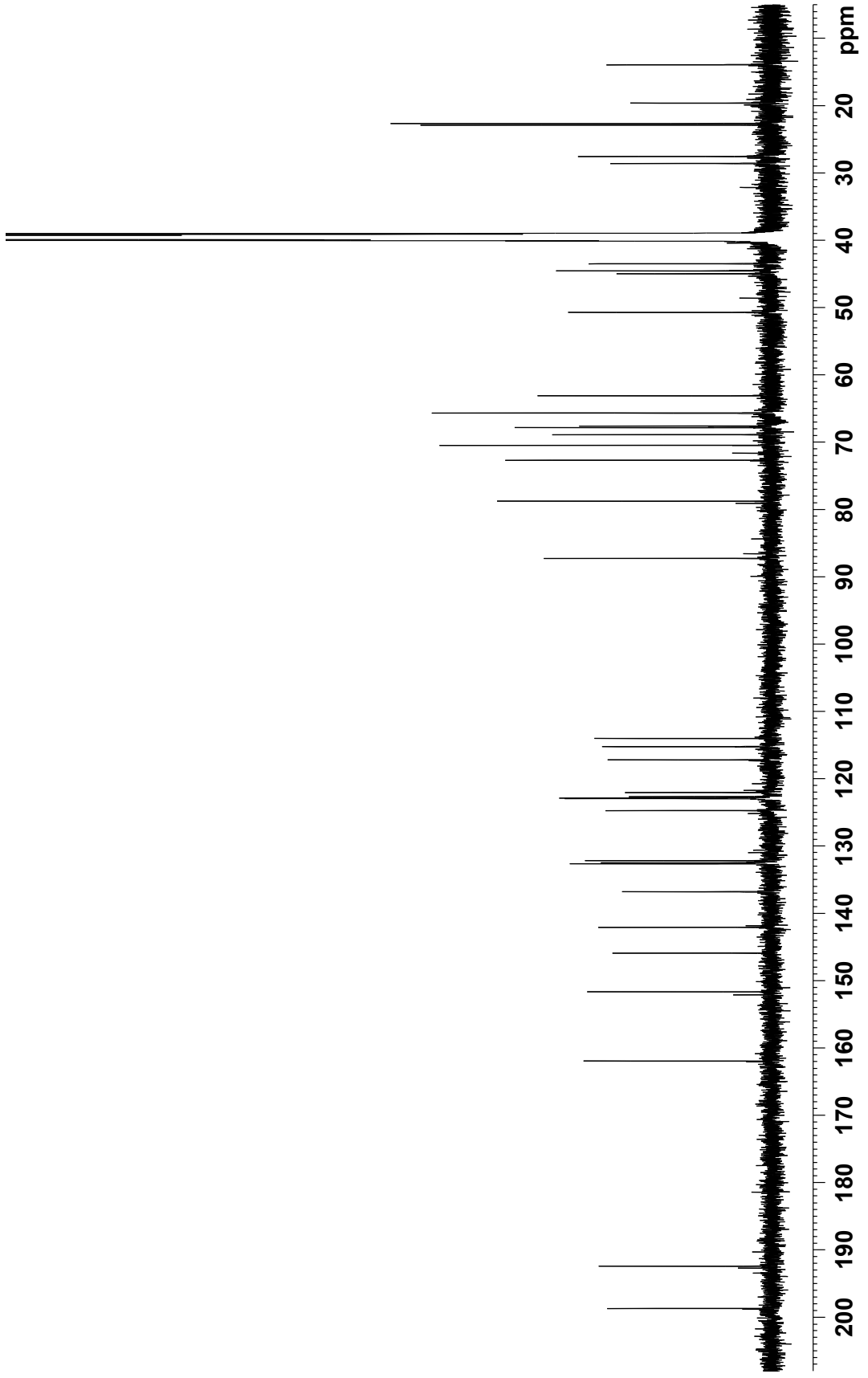

Figure S37. COSY spectrum of **18** (500 MHz, DMSO-d_6).

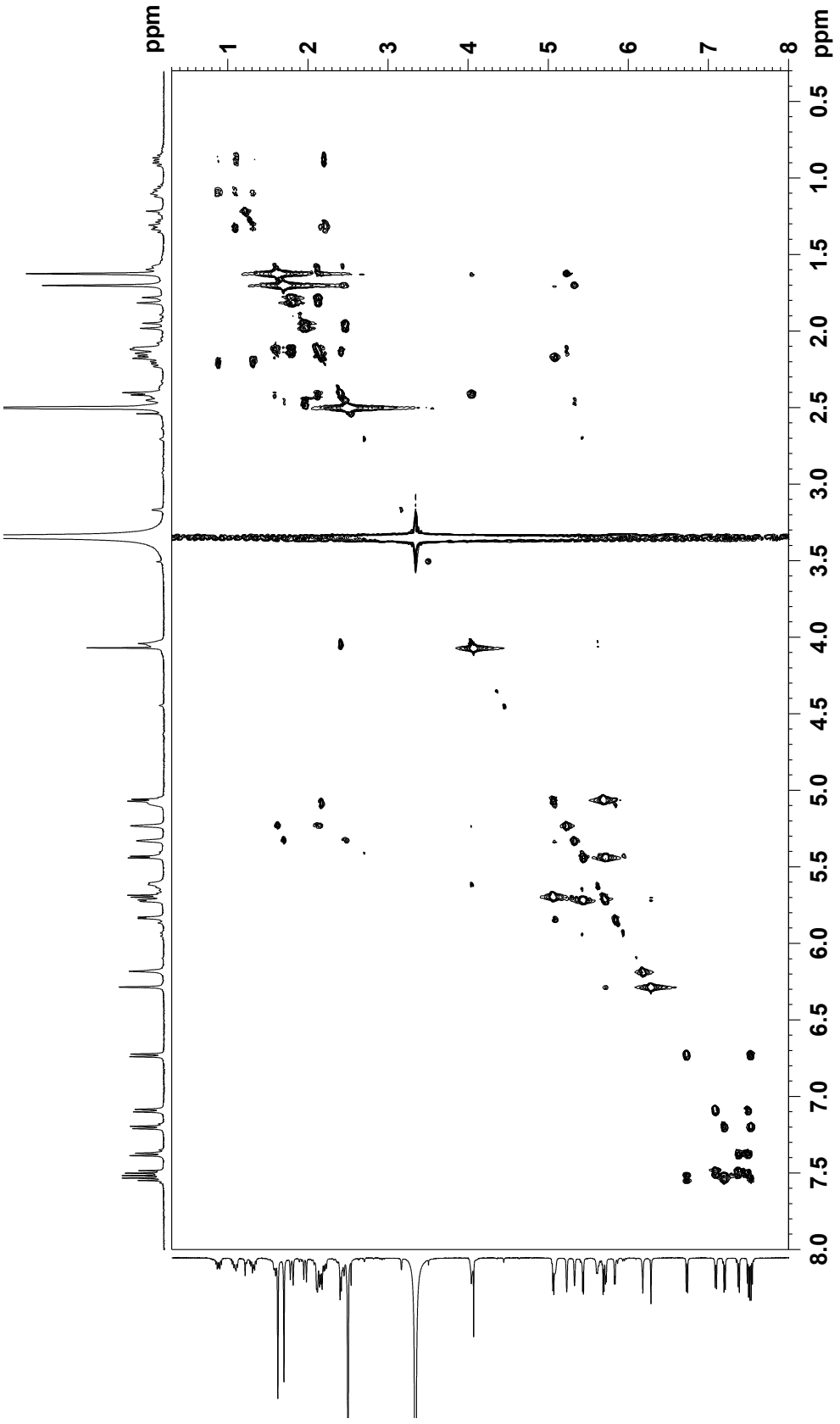

Figure S38. HSQC spectrum of **18** (500 MHz, DMSO-d_6).

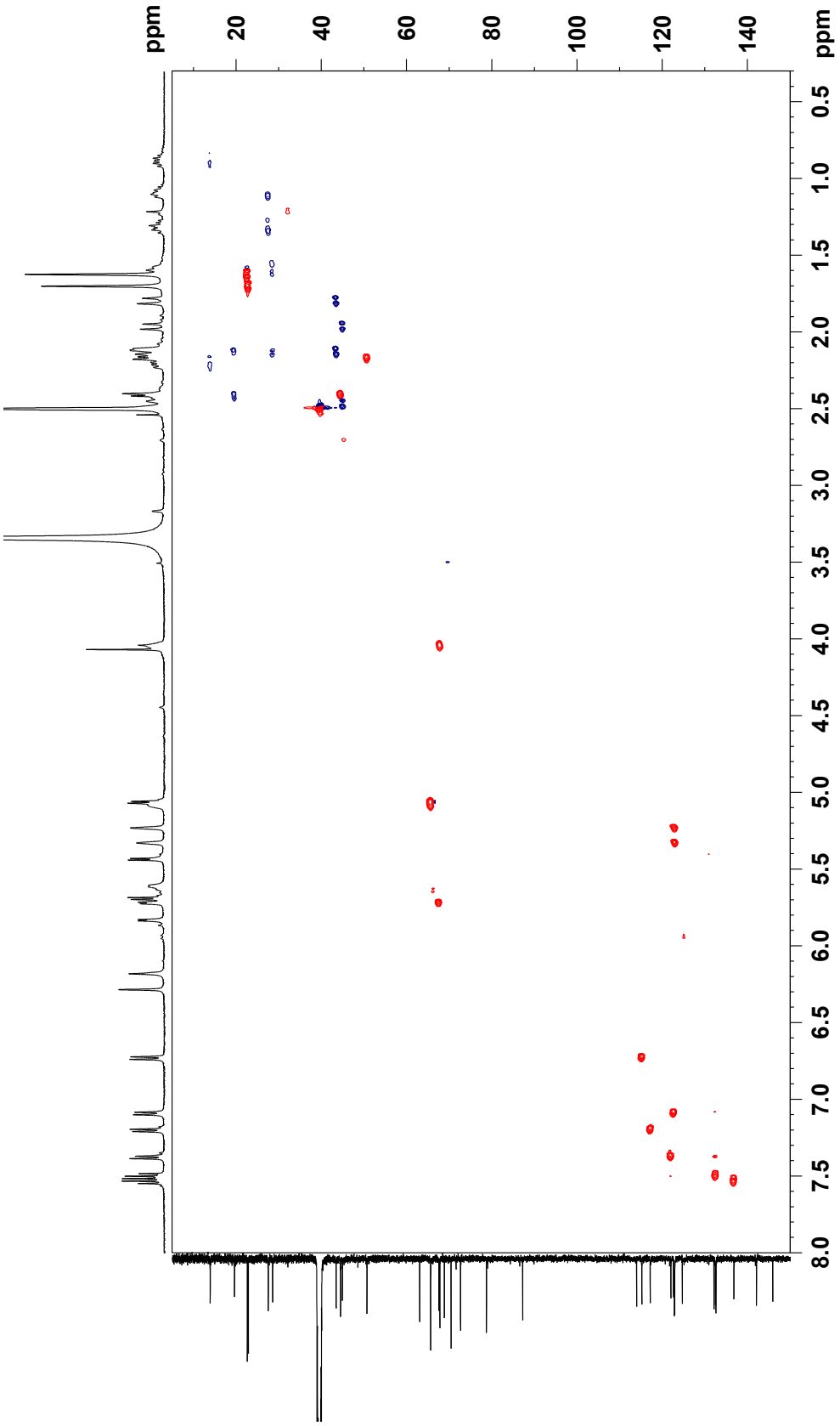

Figure S39. HMBC spectrum of **18** (500 MHz, DMSO-d_6).

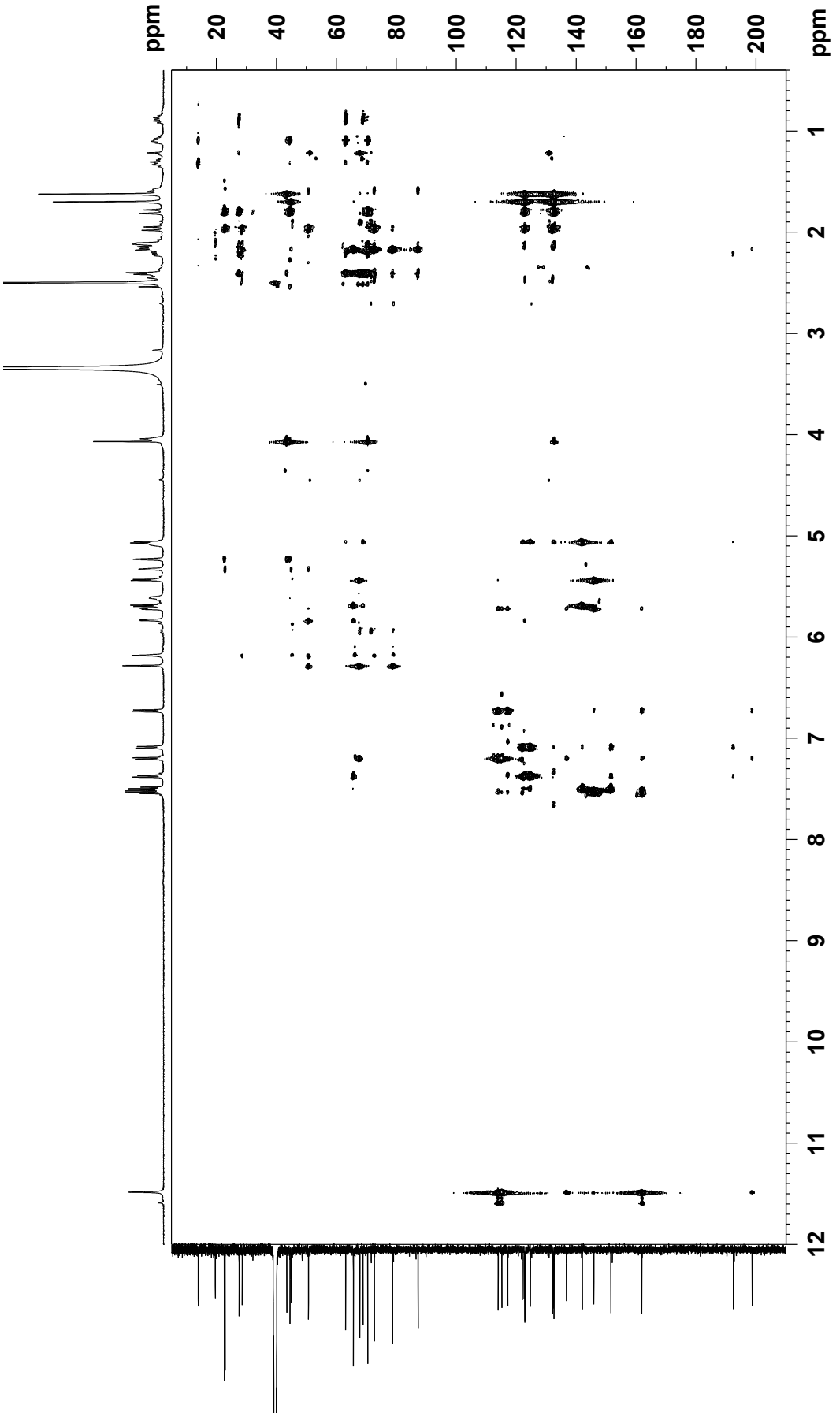

Figure S40. NOESY spectrum of **18** (500 MHz, DMSO-d_6).

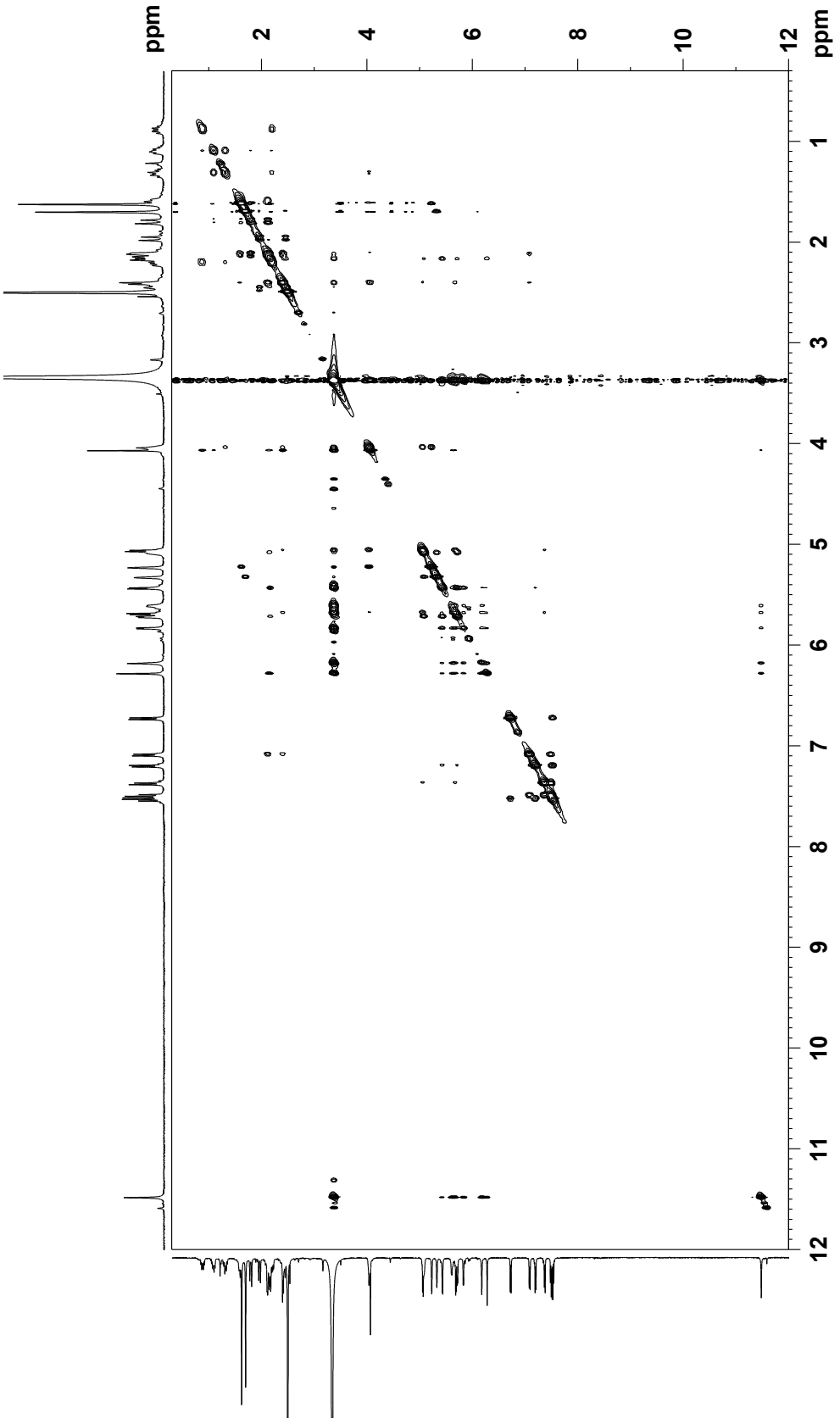

Figure S41. UV spectrum of kumemicinone F (**19**).

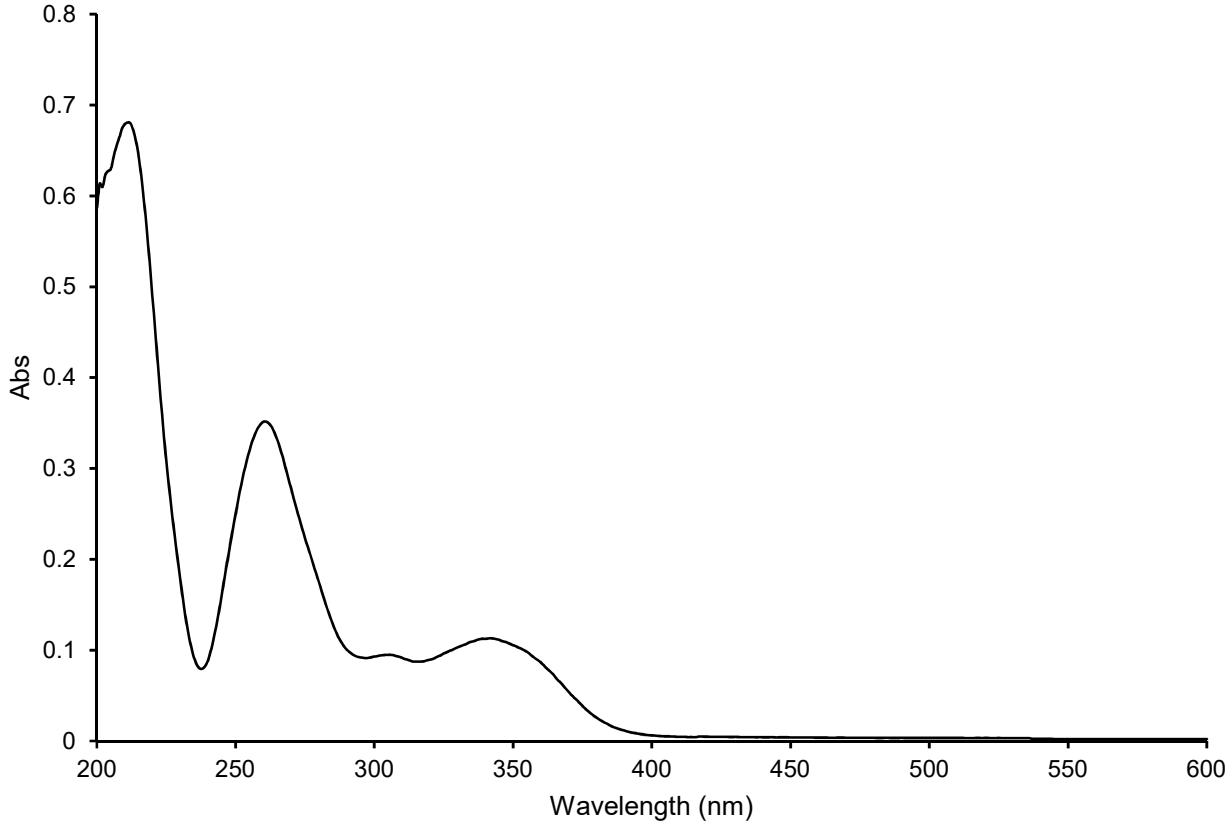

Figure S42. IR spectrum of **19**.

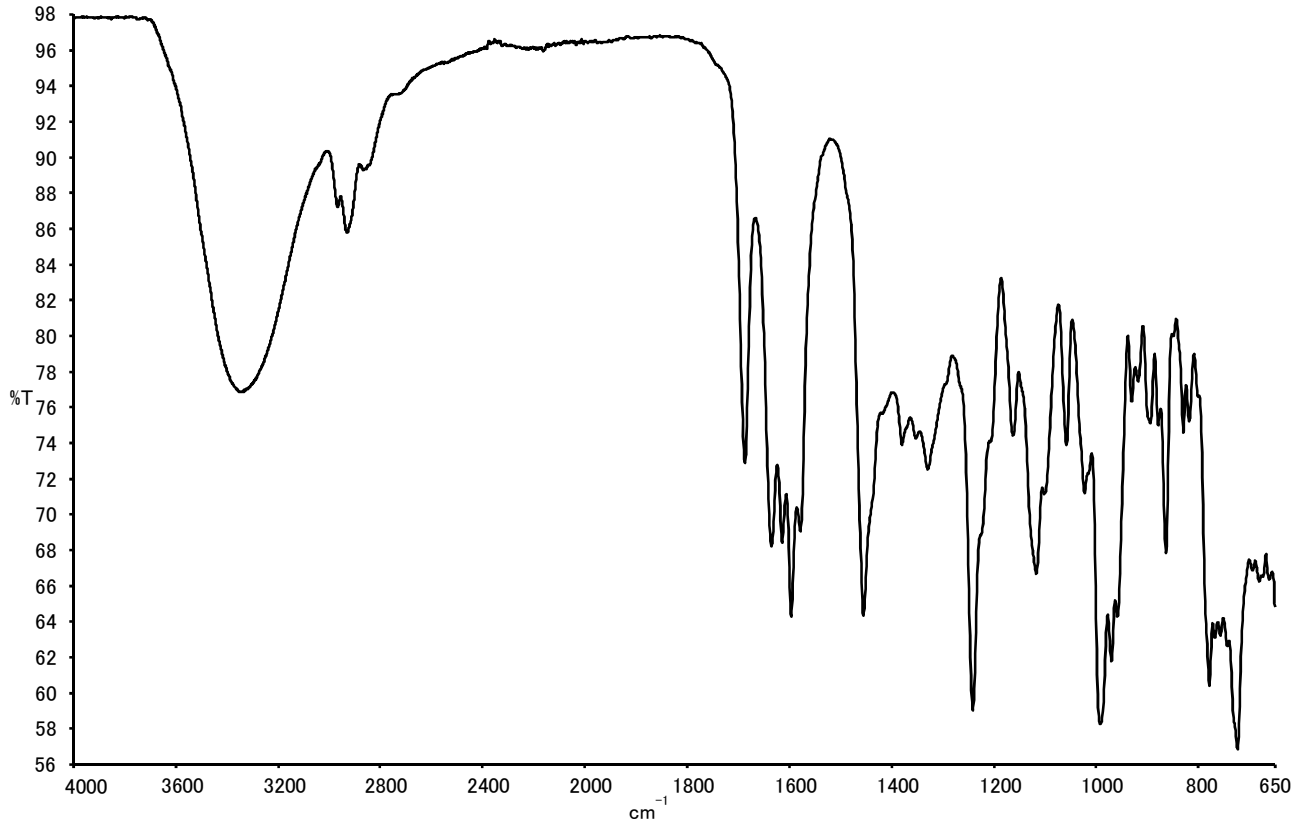

Figure S43. ^{1}H NMR spectrum of **19** (500 MHz, CD_3OD).

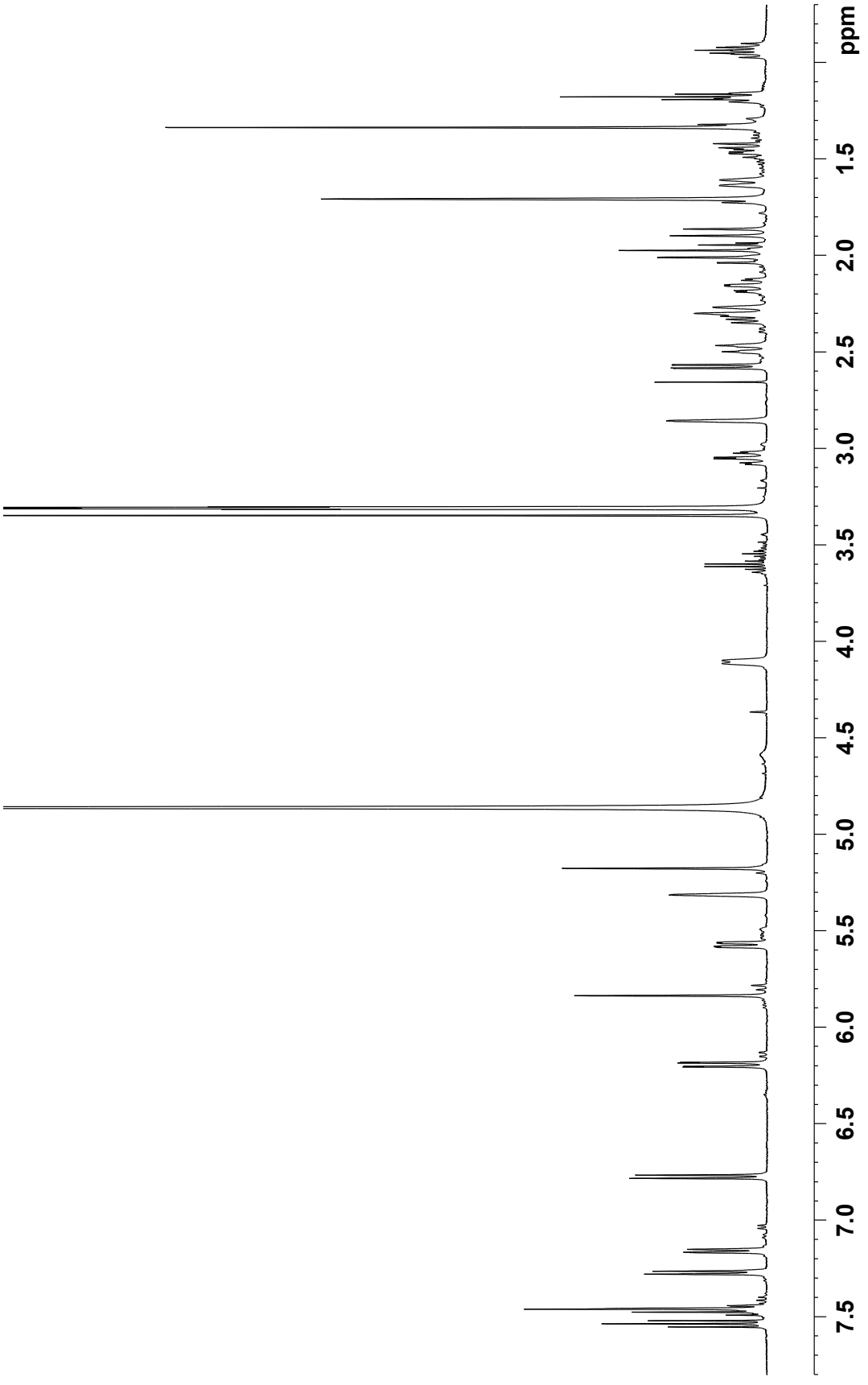

Figure S44. ^{13}C NMR spectrum of **19** (125 MHz, CD_3OD).

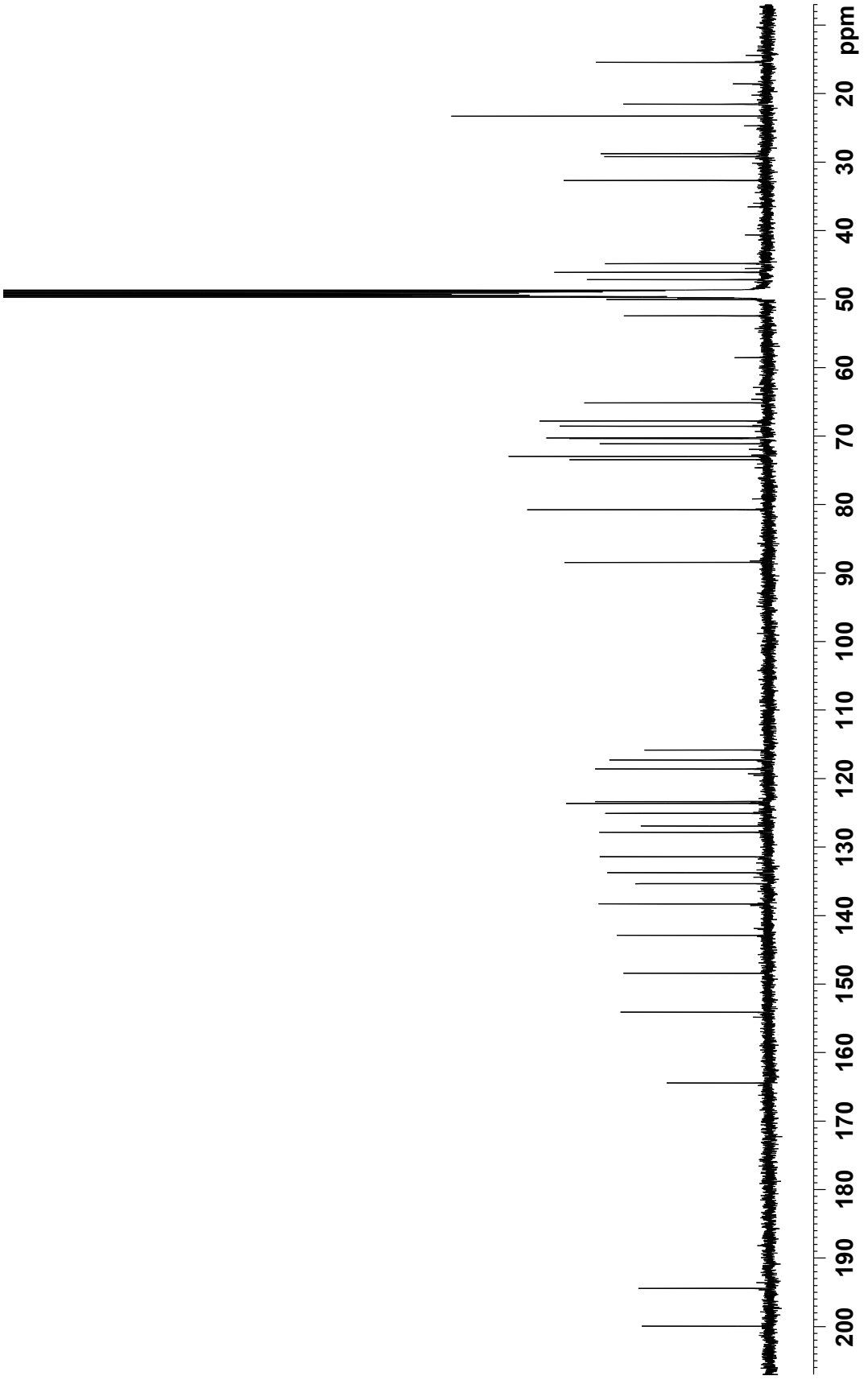

Figure S45. COSY spectrum of **19** (500 MHz, CD_3OD).

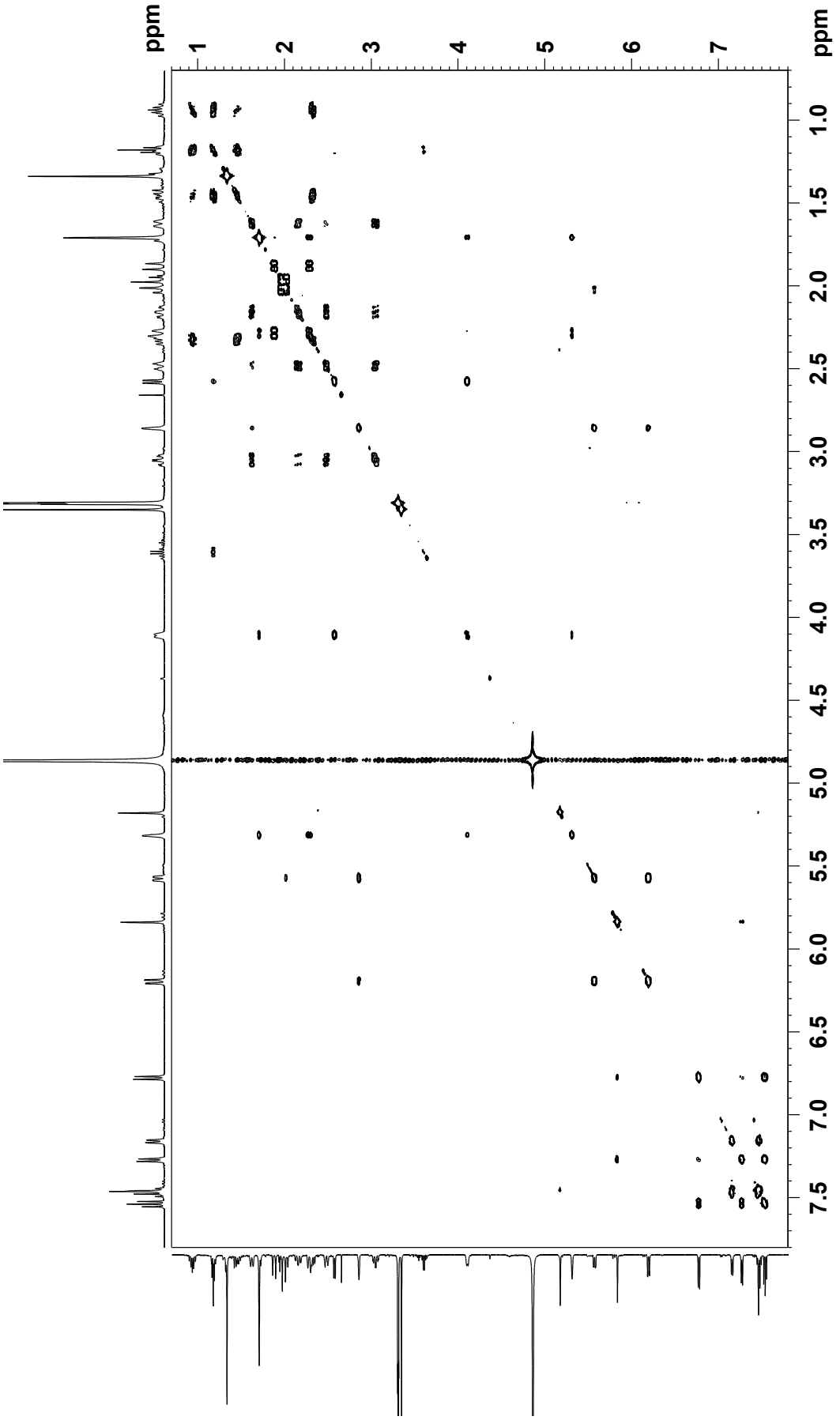

Figure S46. HSQC spectrum of **19** (500 MHz, CD_3OD).

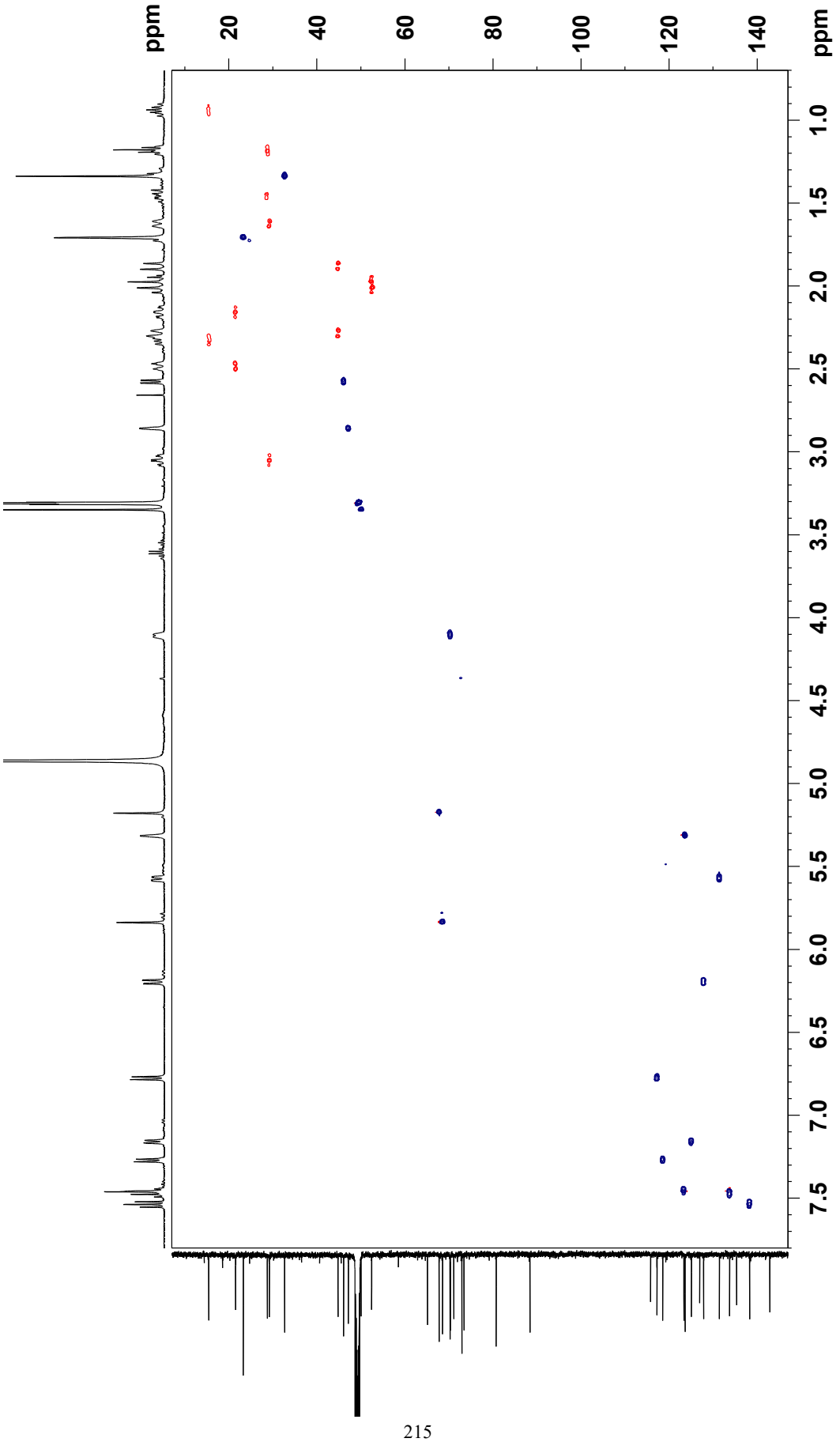

Figure S47. HMBC spectrum of **19** (500 MHz, CD_3OD).

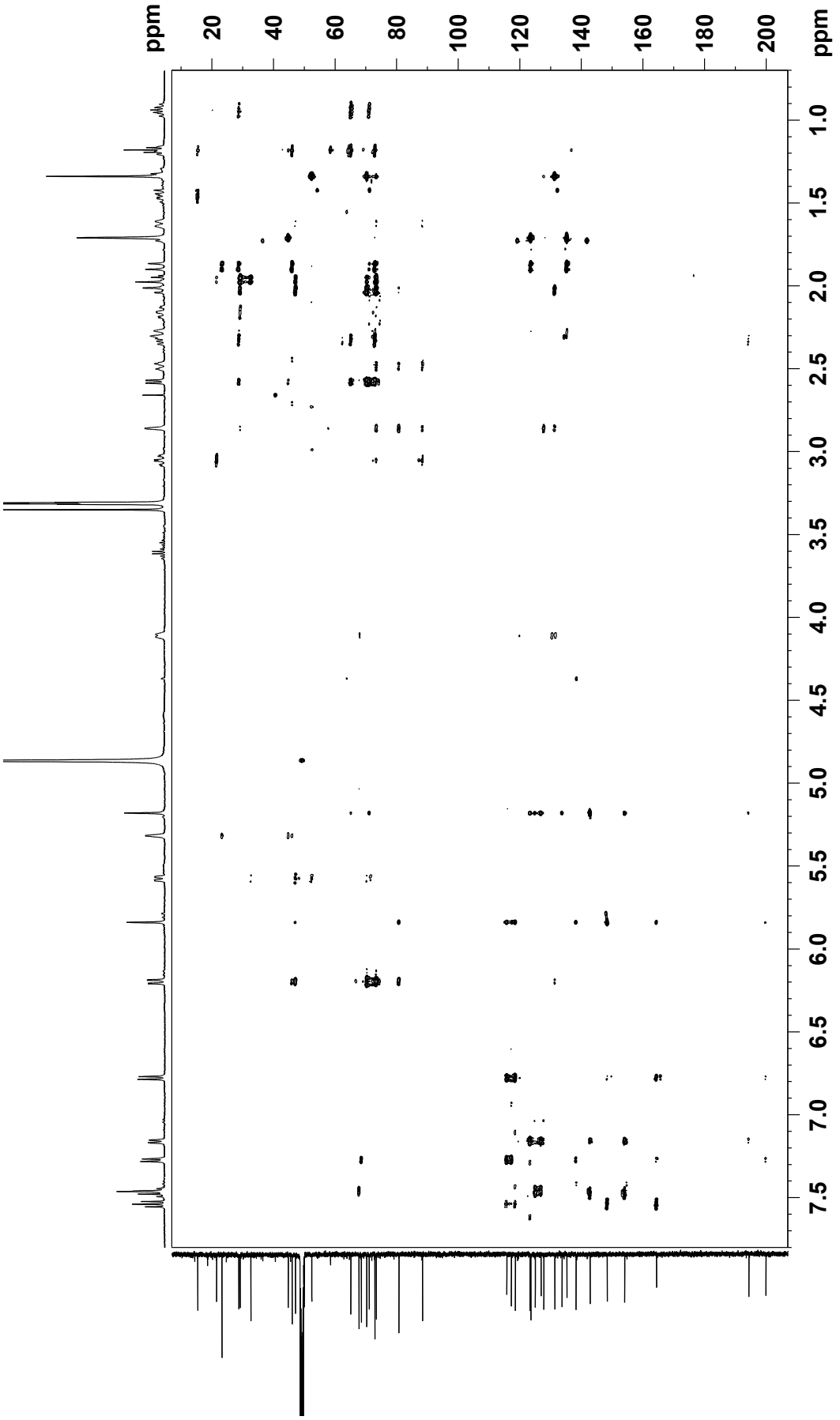

Figure S48. NOESY spectrum of **19** (500 MHz, CD_3OD).

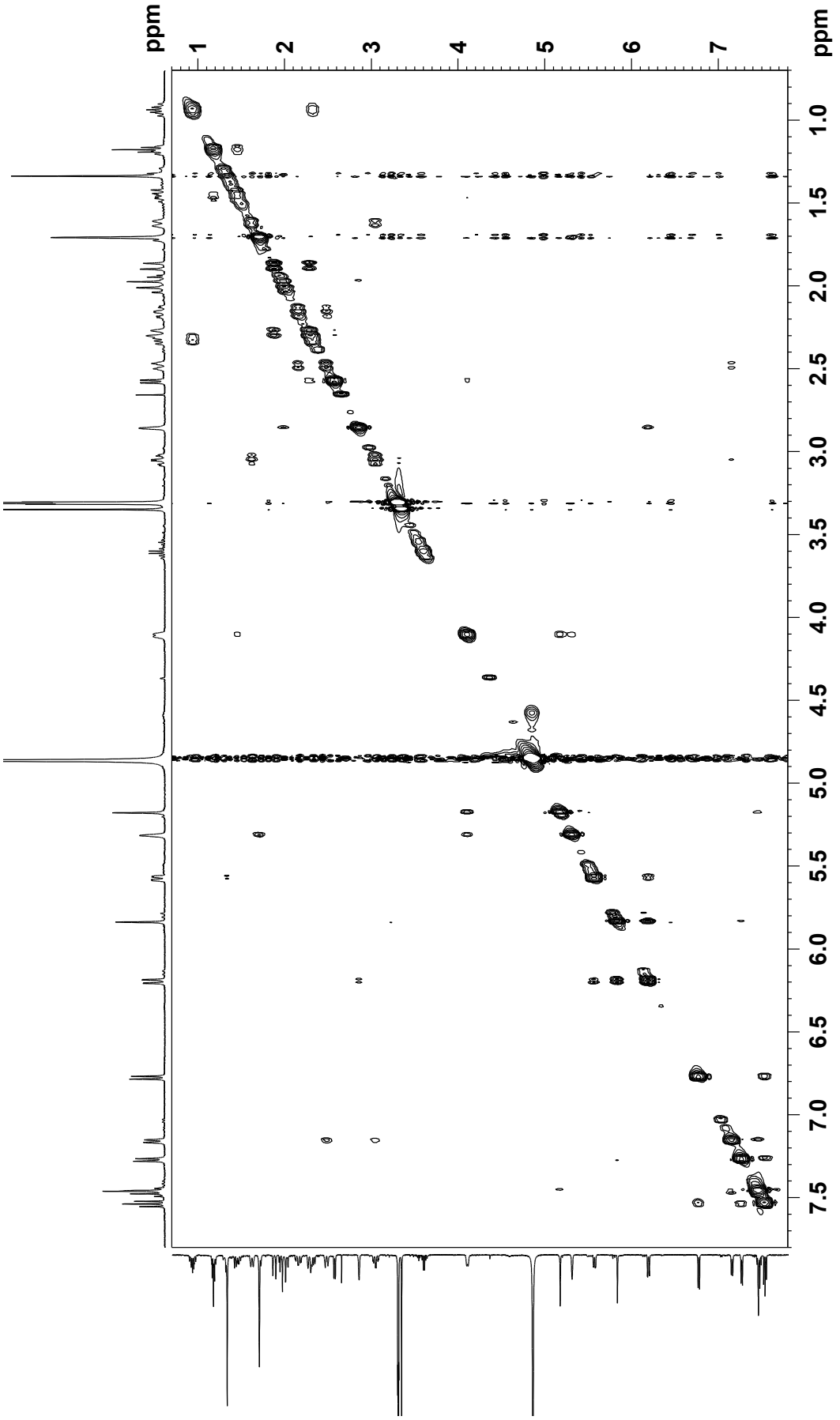

Figure S49. UV spectrum of kumemicinone G (**20**).

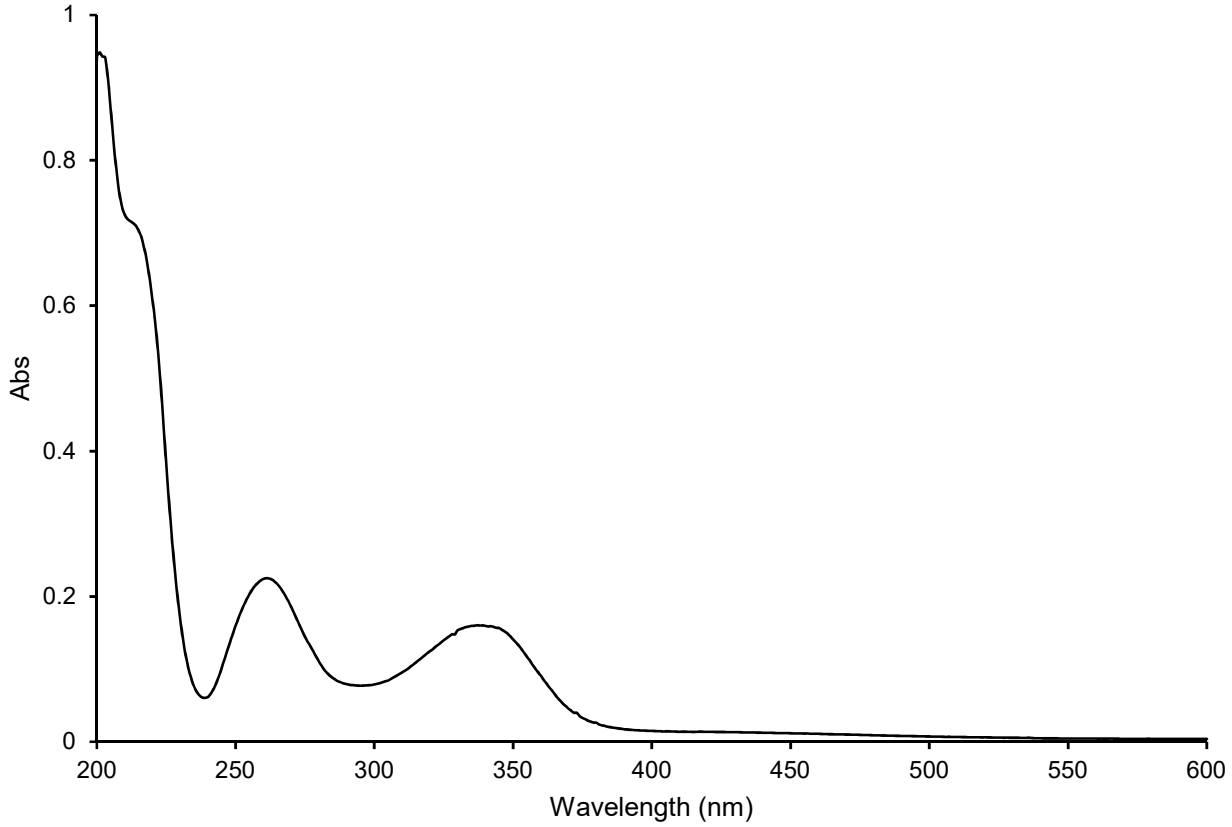

Figure S50. IR spectrum of **20**.

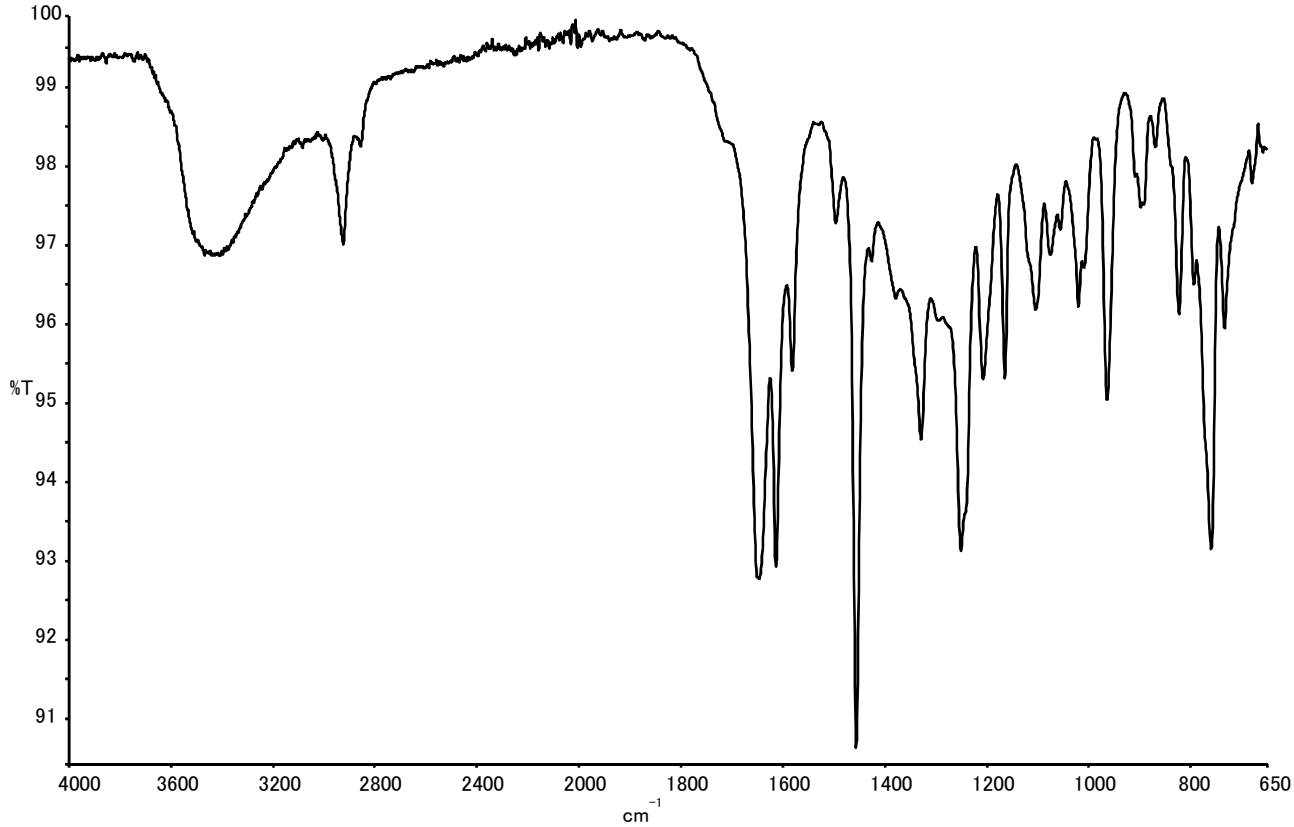

Figure S51. ^{1}H NMR spectrum of **20** (500 MHz, CD_3OD).

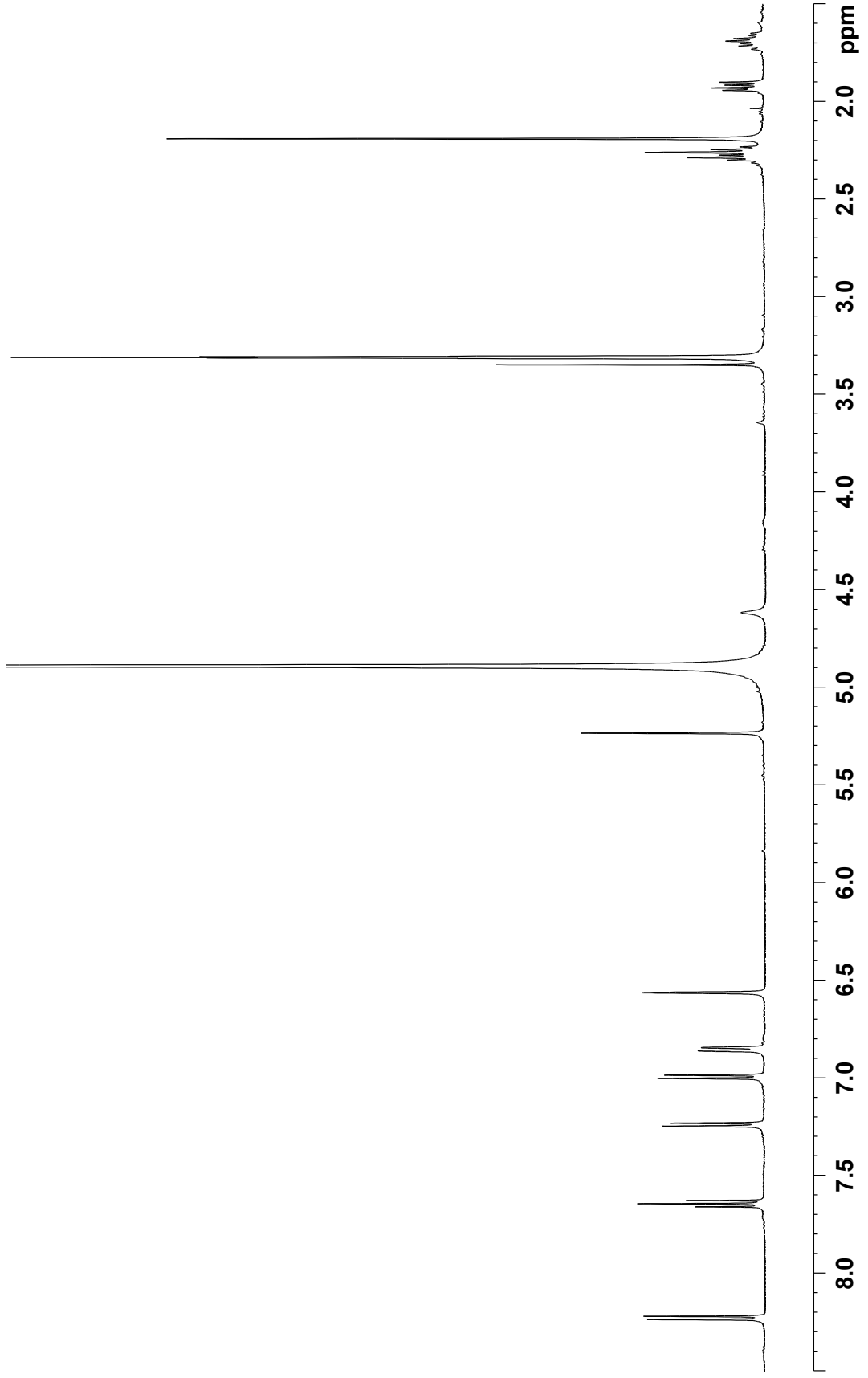

Figure S52. ^{13}C NMR spectrum of **20** (125 MHz, CD_3OD).

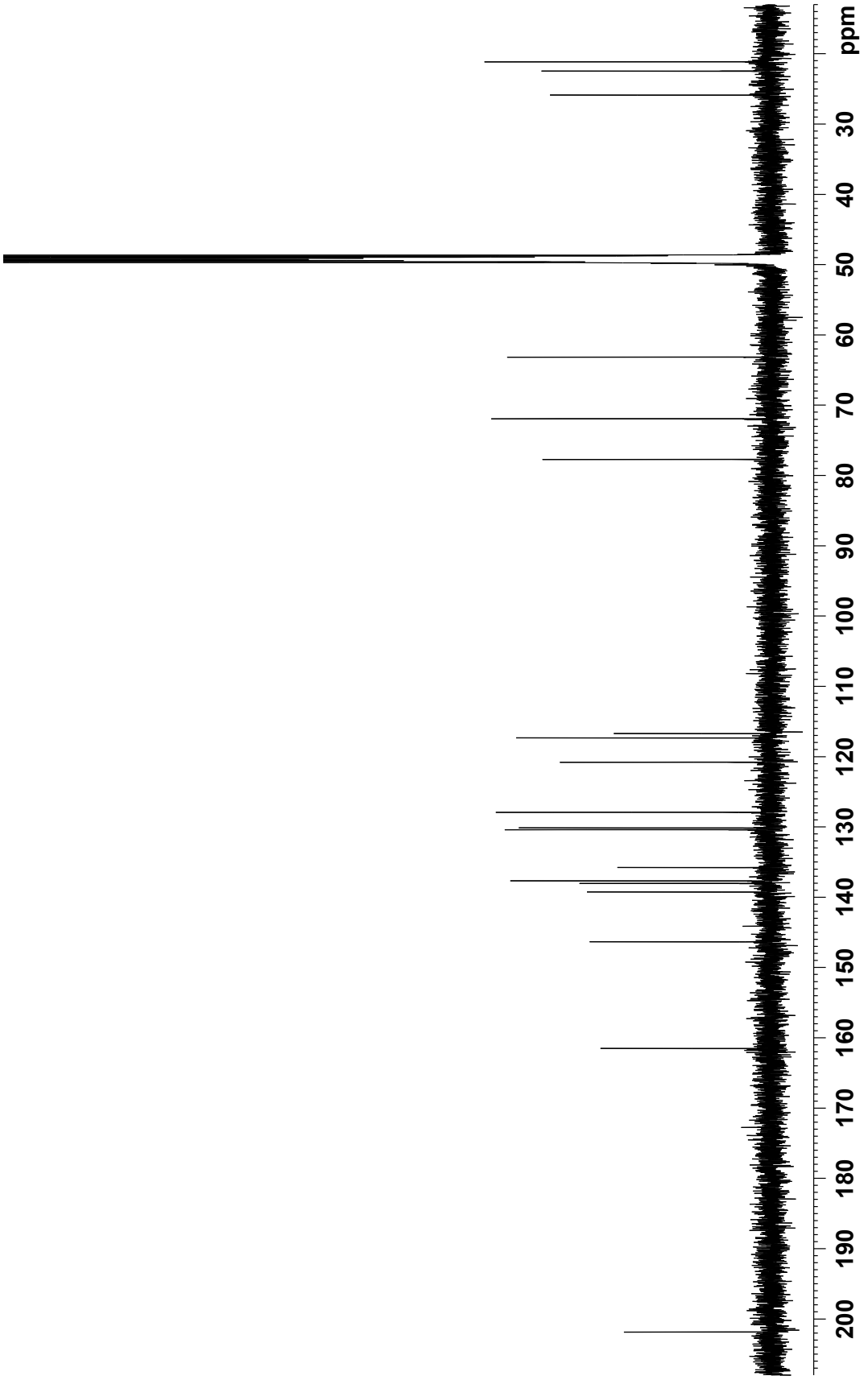

Figure S53. COSY spectrum of **20** (500 MHz, CD_3OD).

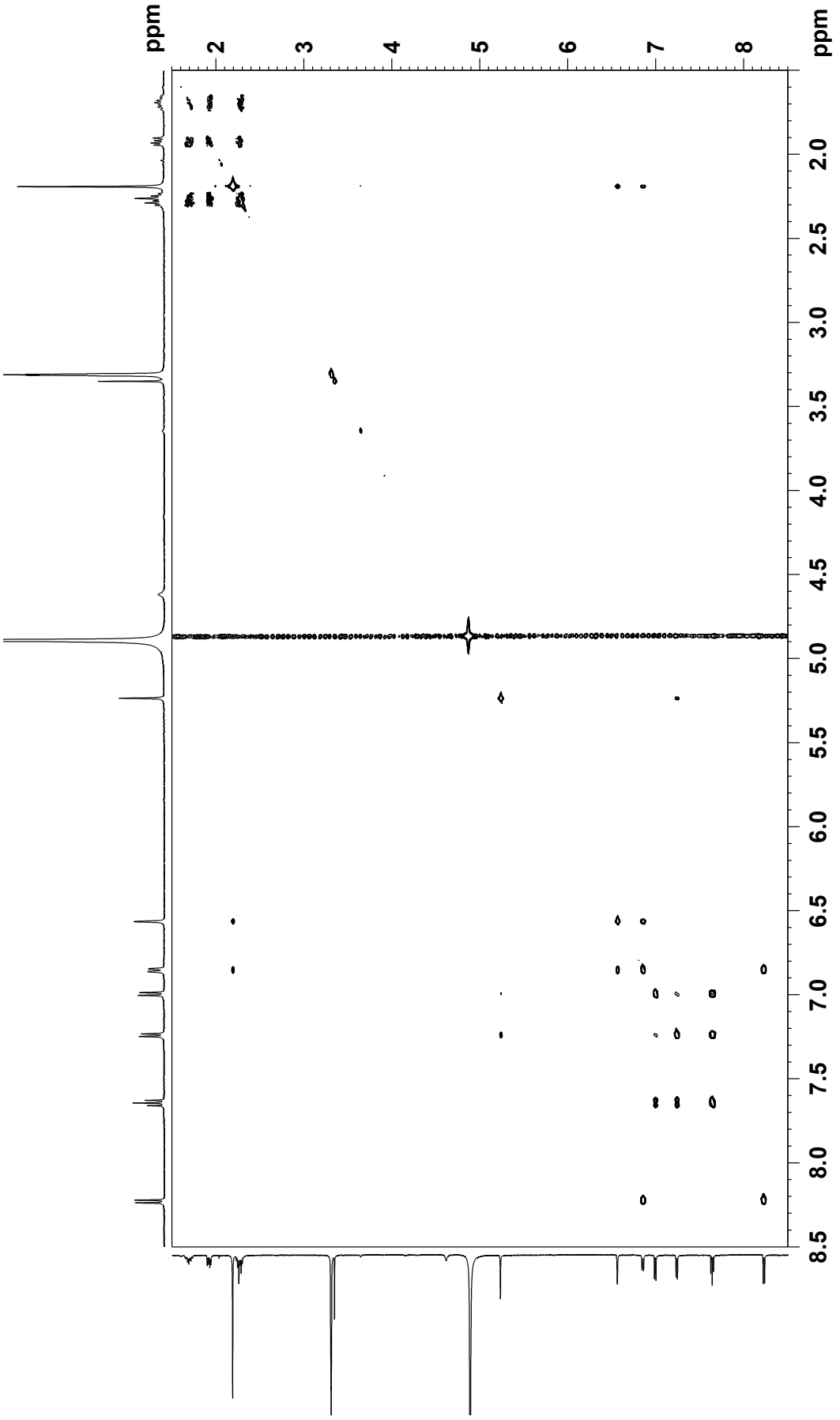

Figure S54. HSQC spectrum of **20** (500 MHz, CD_3OD).

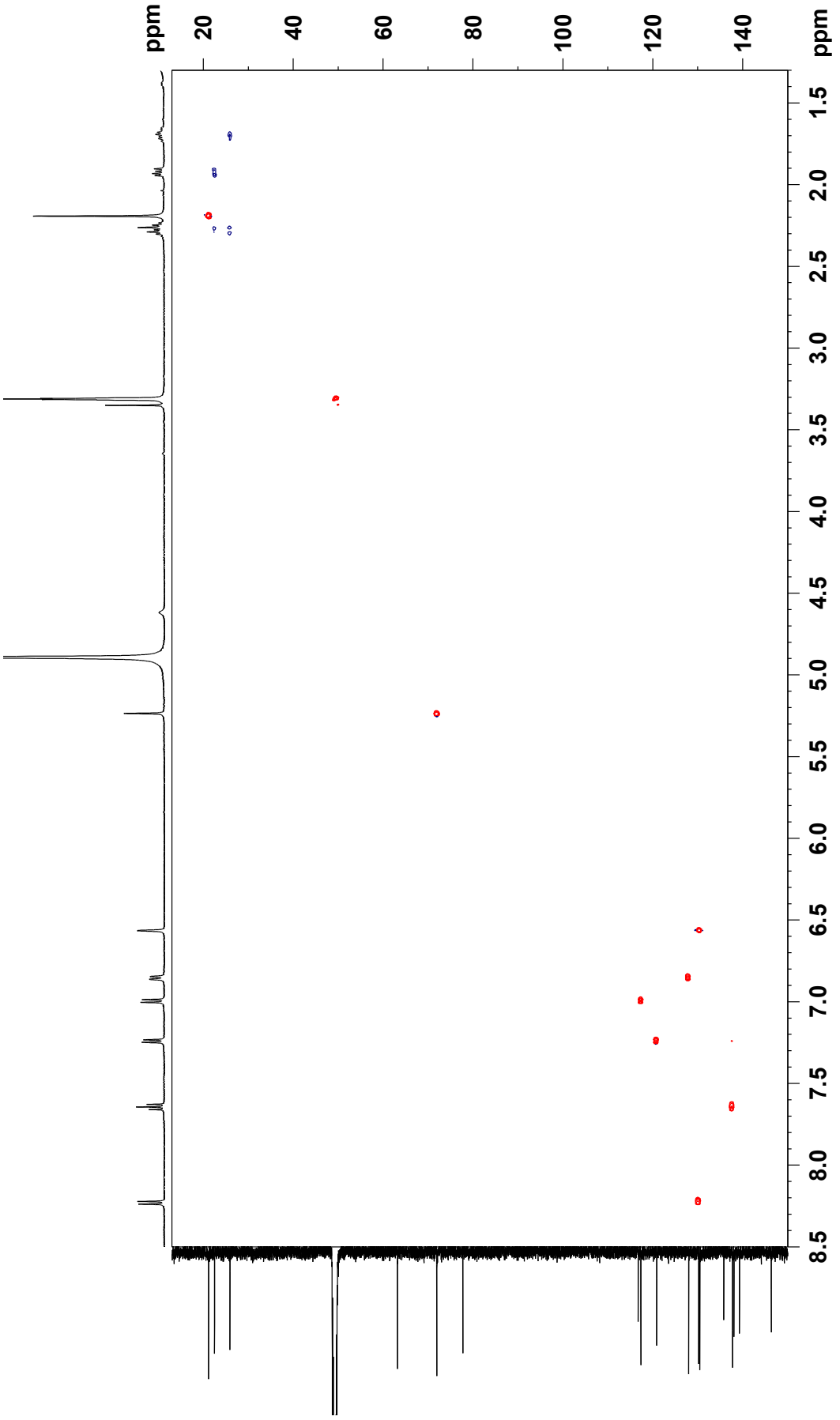

Figure S55. HMBC spectrum of **20** (500 MHz, CD_3OD).

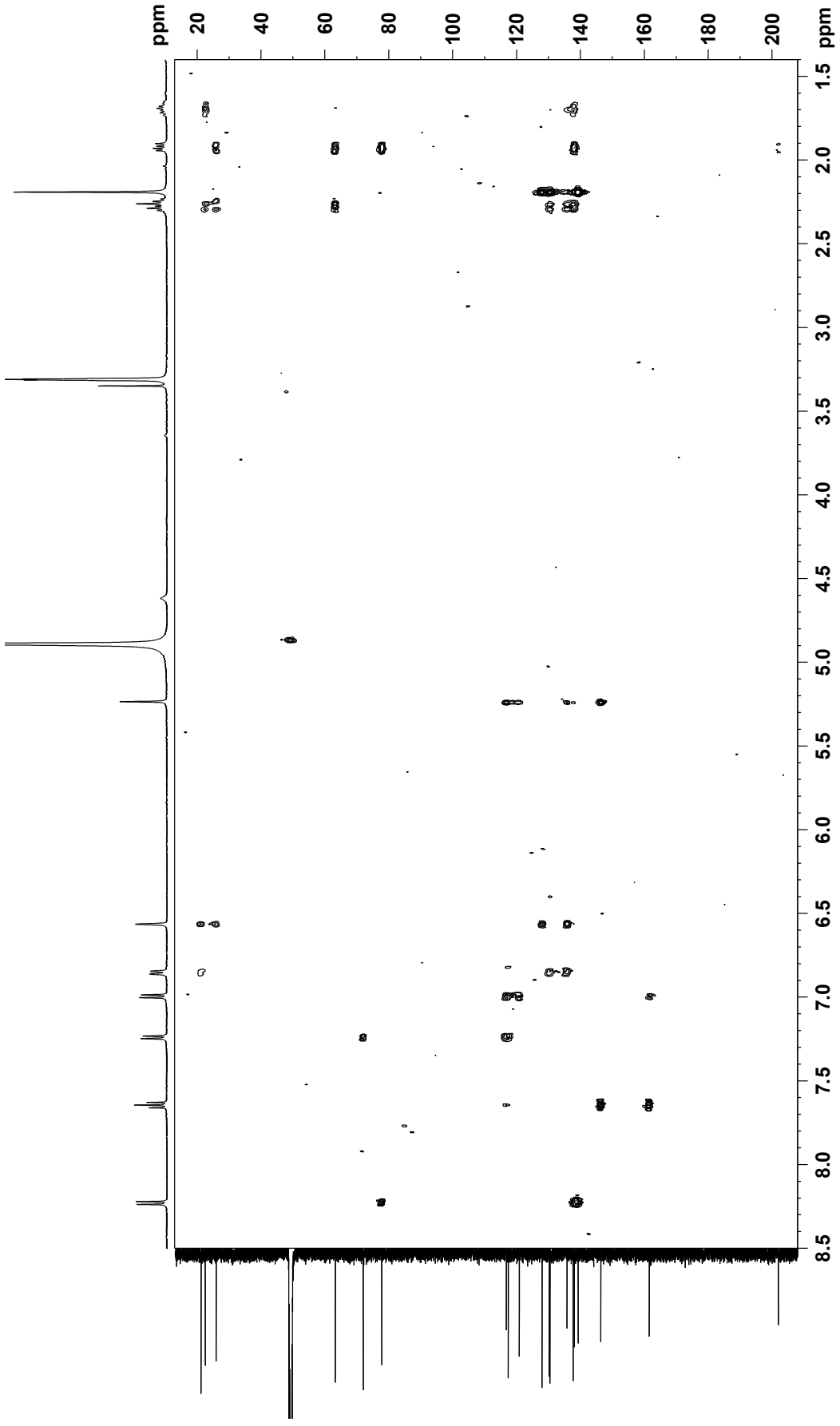

Figure S56. NOESY spectrum of **20** (500 MHz, CD_3OD).

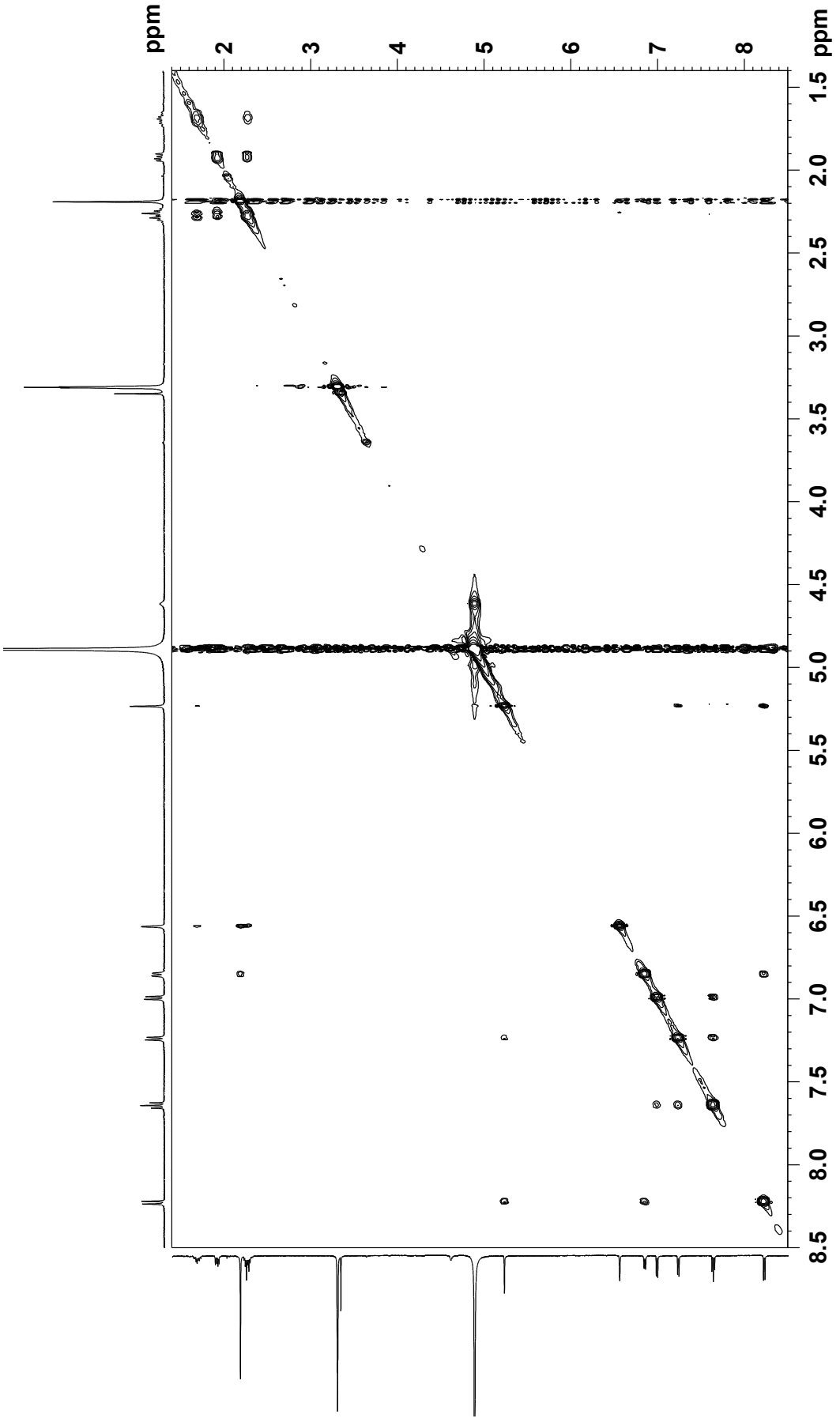

Figure S57. ^{1}H NMR spectrum of miaosporone E (**21**) (500 MHz, CD_3OD).

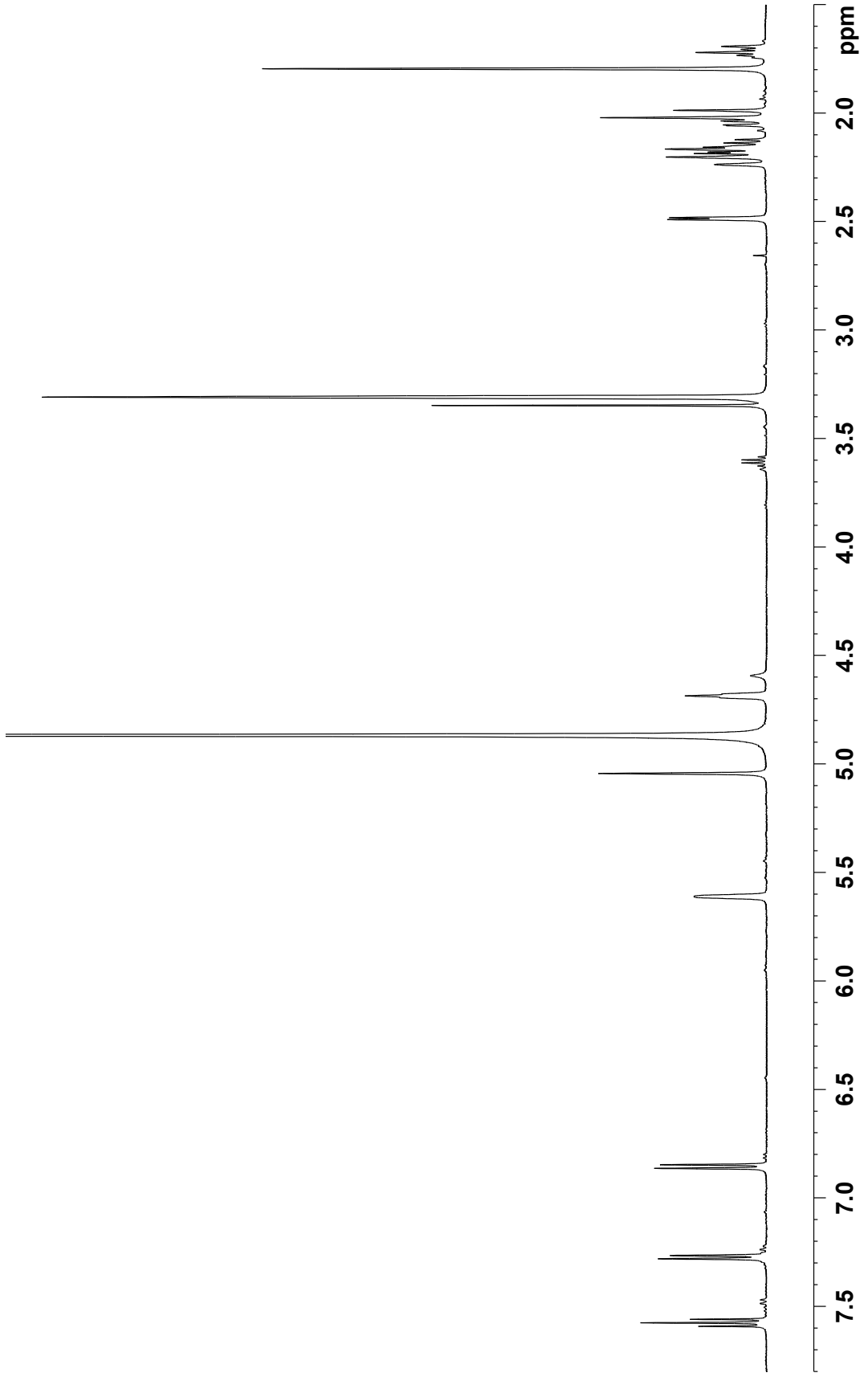

Figure S58. ^{13}C NMR spectrum of **21** (125 MHz, CD_3OD).

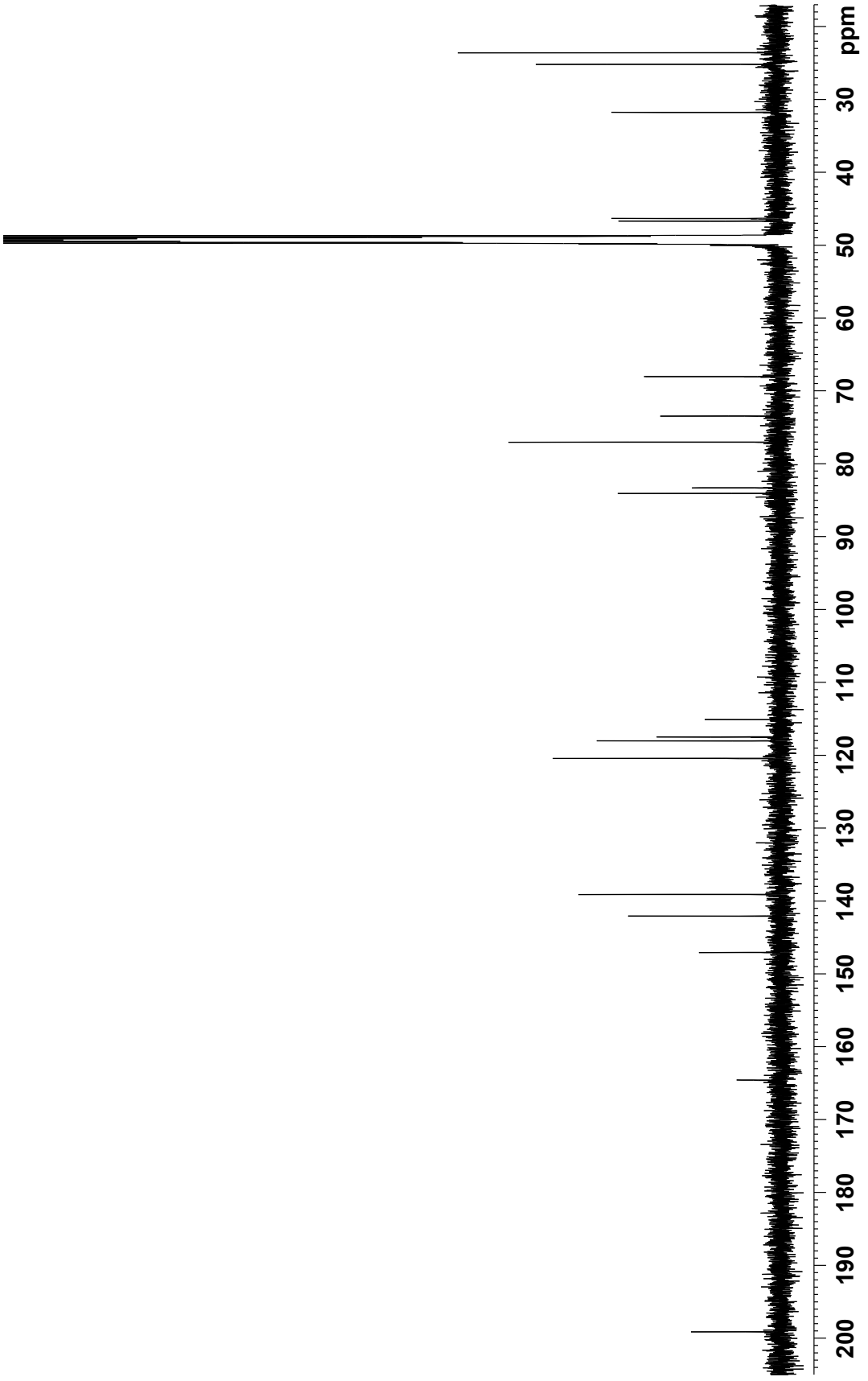

Figure S59. ^{1}H NMR spectrum of SF2315 B (**22)** (500 MHz, CD_3OD).

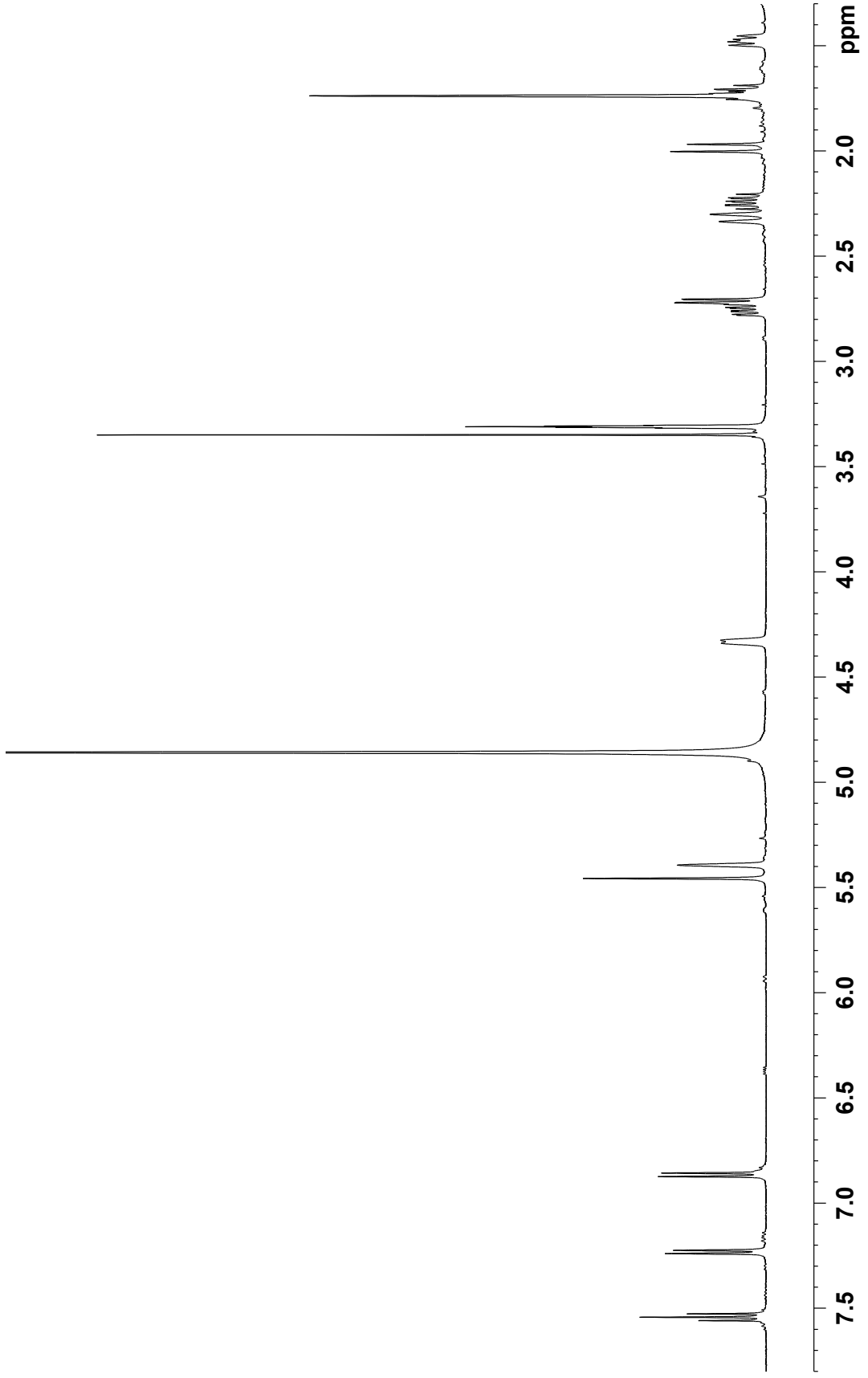

Figure S60. ^{13}C NMR spectrum of **22** (125 MHz, CD_3OD).

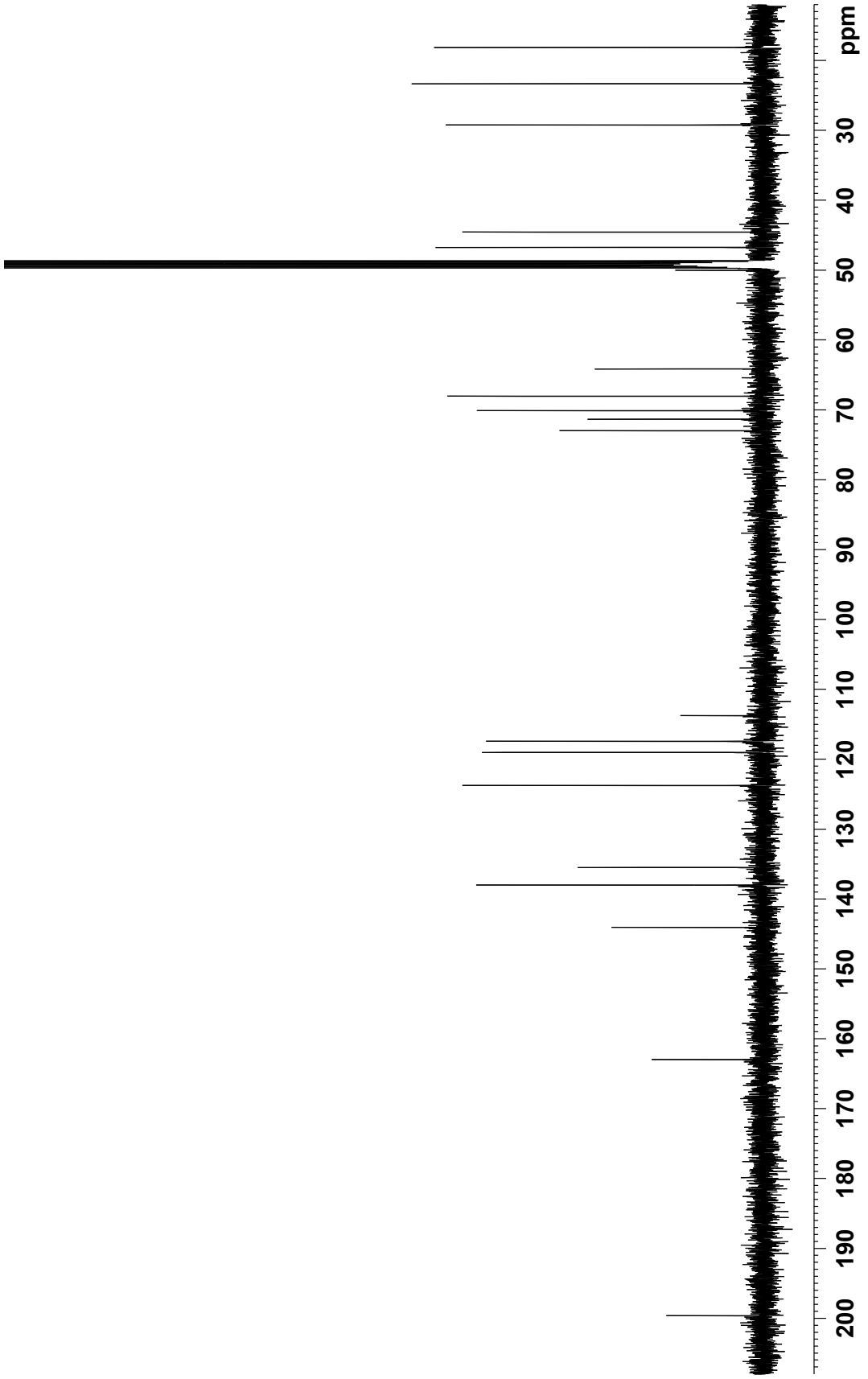

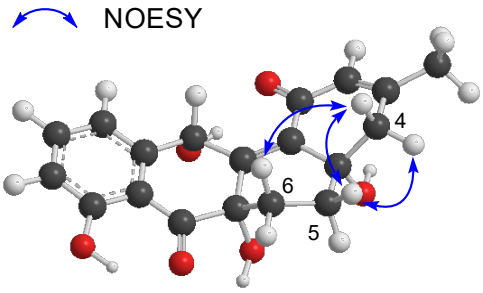

Figure S61. Key NOESY correlations supporting the relative configuration of **16**.

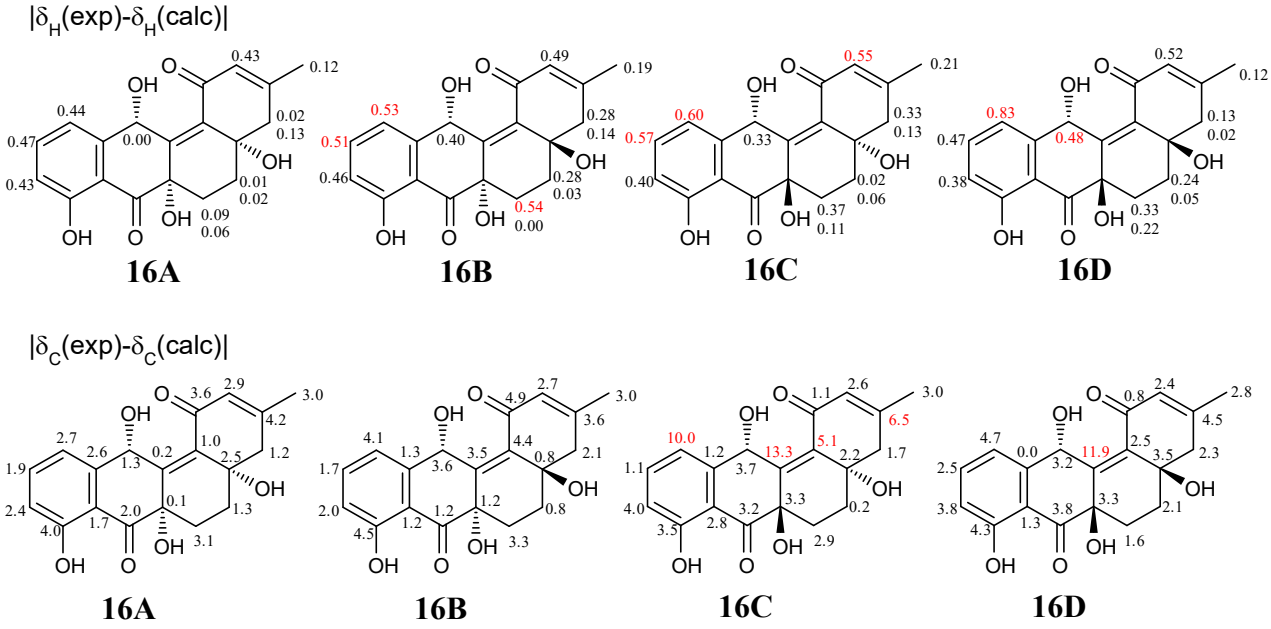

Figure S62. Four possible stereoisomers **16A**–**16D** for **16**. Absolute values of differences between the calculated and experimental ^{1}H and ^{13}C NMR chemical shifts are indicated

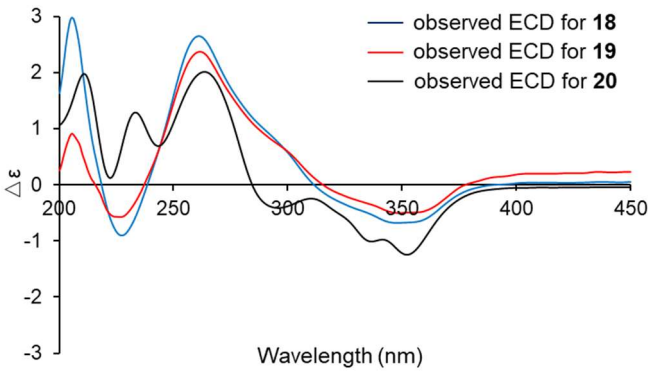

Figure S63. Experimental ECD spectra of **18**–**20**.

Table S1. DFT-calculated C^{13} and H^{1} NMR chemical shifts of four possible stereoisomers **16A**–**16D** for **16**.

position	δ_C(exp)	**16A**	**16B**	**16C**	**16D**	|exp-**16A**|	|exp-**16B**|	|exp-**16C**|	|exp-**16D**|
C1	192.8	189.2	187.9	191.7	193.6	3.6	4.9	1.1	0.8
C2	127.9	125.0	125.2	125.3	125.5	2.9	2.7	2.6	2.4
C3	161.7	165.9	165.3	168.2	166.2	4.2	3.6	6.5	4.5
C4	46.4	47.6	48.5	48.1	48.7	1.2	2.1	1.7	2.3
C4a	73.0	75.5	73.8	75.2	76.5	2.5	0.8	2.2	3.5
C5	34.6	35.9	35.4	34.8	36.7	1.3	0.8	0.2	2.1
C6	27.9	31.0	31.2	30.8	29.5	3.1	3.3	2.9	1.6
C6a	74.7	74.8	75.9	78.0	78.0	0.1	1.2	3.3	3.3
C7	202.5	200.5	203.7	199.3	198.7	2.0	1.2	3.2	3.8
C7a	115.2	113.5	114.0	112.4	113.9	1.7	1.2	2.8	1.3
C8	163.9	159.9	159.4	160.4	159.6	4.0	4.5	3.5	4.3
C9	118.7	116.3	116.7	114.7	114.9	2.4	2.0	4.0	3.8
C10	138.6	136.7	136.9	137.5	136.1	1.9	1.7	1.1	2.5
C11	121.6	118.9	117.5	111.6	116.9	2.7	4.1	10.0	4.7
C11a	145.4	142.8	144.1	146.6	145.4	2.6	1.3	1.2	0.0
C12	68.5	69.8	72.1	72.2	71.7	1.3	3.6	3.7	3.2
C12a	141.7	141.9	145.2	155.0	153.6	0.2	3.5	13.3	11.9
C12b	141.1	142.1	136.7	136.0	138.6	1.0	4.4	5.1	2.5
C13	24.4	27.4	27.4	27.4	27.2	3.0	3.0	3.0	2.8
					MAE[c]	2.2	2.6	3.8	3.2

position	δ_H(exp)	**3A**	**3B**	**3C**	**3D**	|exp-**3A**|	|exp-**3B**|	|exp-**3C**|	|exp-**3D**|
H2	5.96	6.39	6.45	6.51	6.48	0.43	0.49	0.55	0.52
H4a	2.39	2.41	2.67	2.72	2.52	0.02	0.28	0.33	0.13
H4b	2.67	2.80	2.81	2.80	2.69	0.13	0.14	0.13	0.02
H5a	2.09	2.10	2.37	2.11	1.85	0.01	0.28	0.02	0.24
H5b	1.75	1.77	1.78	1.81	1.80	0.02	0.03	0.06	0.05
H6a	2.14	2.05	1.60	1.77	1.81	0.09	0.54	0.37	0.33
H6b	2.20	2.14	2.20	2.31	2.42	0.06	0.00	0.11	0.22
H9	6.91	7.34	7.37	7.31	7.29	0.43	0.46	0.40	0.38
H10	7.53	8.00	8.04	8.10	8.00	0.47	0.51	0.57	0.47
H11	6.94	7.38	7.47	7.54	7.77	0.44	0.53	0.60	0.83
H12	5.89	5.89	6.29	6.22	6.37	0.00	0.40	0.33	0.48
H13	1.94	2.06	2.13	2.15	2.06	0.12	0.19	0.21	0.12
					MAE[c]	0.18	0.32	0.31	0.32

[c] MAE = mean absolute error (ppm)

Table S2. DFT-calculated NMR chemical shifts of four possible stereoisomers **17A**–**17D** for **18**.

position	δ C(exp)	**17A**	**17B**	**17C**	**17D**	|exp-**17A**|	|exp-**17B**|	|exp-**17C**|	|exp-**17D**|
C1	78.3	79.7	79.3	78.7	79.1	1.4	1.0	0.4	0.8
C2	68.6	72.5	71.9	70.6	71.2	3.9	3.3	2.0	2.6
C3	205.5	204.2	203.9	204.1	203.7	1.3	1.6	1.4	1.8
C3a	122.7	119.6	119.3	119.0	119.0	3.1	3.4	3.7	3.7
C4	157.8	154.3	154.4	154.7	154.7	3.5	3.4	3.1	3.1
C5	117.2	114.7	115.0	115.2	114.9	2.5	2.2	2.0	2.3
C6	139.2	137.5	137.8	137.9	138.0	1.7	1.4	1.3	1.2
C7	118.2	115.2	115.5	116.5	115.8	3.0	2.7	1.7	2.4
C7a	155.8	153.1	152.9	152.5	153.0	2.7	2.9	3.3	2.8
C1'	206.3	214.6	214.3	210.8	208.1	8.3	8.0	4.5	1.8
C3'	31.6	33.2	33.3	34.7	34.3	1.6	1.7	3.1	2.7
C4'	36.1	36.4	36.6	38.1	37.8	0.3	0.5	2.0	1.7
C4a'	74.6	76.6	77.5	77.3	75.8	2.0	2.9	2.7	1.2
C5'	39.4	48.3	46.7	39.9	41.7	8.9	7.3	0.5	2.3
C6'	134.8	140.4	135.2	133.8	136.9	5.6	0.4	1.0	2.1
C7'	122.8	120.3	123.2	124.5	121.3	2.5	0.4	1.7	1.5
C8'	65.2	66.3	67.9	69.5	67.8	1.1	2.7	4.3	2.6
C8a'	62.4	58.9	63.5	62.6	63.2	3.5	1.1	0.2	0.8
C9'	24.0	26.4	26.0	25.3	26.0	2.4	2.0	1.3	2.0
					MAE[c]	3.1	2.6	2.11	2.07

position	δ H(exp)	**17A**	**17B**	**17C**	**17D**	|exp-**17A**|	|exp-**17B**|	|exp-**17C**|	|exp-**17D**|
H1	5.27	5.39	5.38	5.44	5.41	0.12	0.11	0.17	0.14
H5	6.85	7.28	7.26	7.25	7.25	0.43	0.41	0.40	0.40
H6	7.59	8.10	8.09	8.13	8.11	0.51	0.50	0.54	0.52
H7	7.15	7.58	7.61	7.59	7.58	0.43	0.46	0.44	0.43
H3'a	2.20	3.01	2.76	2.18	2.14	0.81	0.56	0.02	0.06
H3'b	1.85	1.66	1.69	1.74	1.87	0.19	0.16	0.11	0.02
H4'a	2.04	1.96	1.97	1.96	2.03	0.08	0.07	0.08	0.01
H4'b	2.31	2.20	2.26	2.21	2.24	0.11	0.05	0.10	0.07
H5'a	2.32	2.50	2.57	2.45	2.38	0.18	0.25	0.13	0.06
H5'b	1.96	2.26	2.09	1.87	1.94	0.30	0.13	0.09	0.02
H7'	5.61	6.10	5.89	5.99	6.08	0.49	0.28	0.38	0.47
H8'	4.58	4.74	4.78	4.62	4.64	0.16	0.20	0.04	0.06
H8a'	3.34	3.12	3.00	3.37	3.33	0.22	0.34	0.03	0.01
H9'	1.74	1.83	1.80	1.80	1.82	0.09	0.06	0.06	0.08
					MAE[c]	0.29	0.26	0.18	0.17

[c] MAE = mean absolute error (ppm)

Figure S64. Partial ^{13}C NMR spectra of **20** for the oxymethine region measured in CD_3OD (blue) and CD_3OH (red).

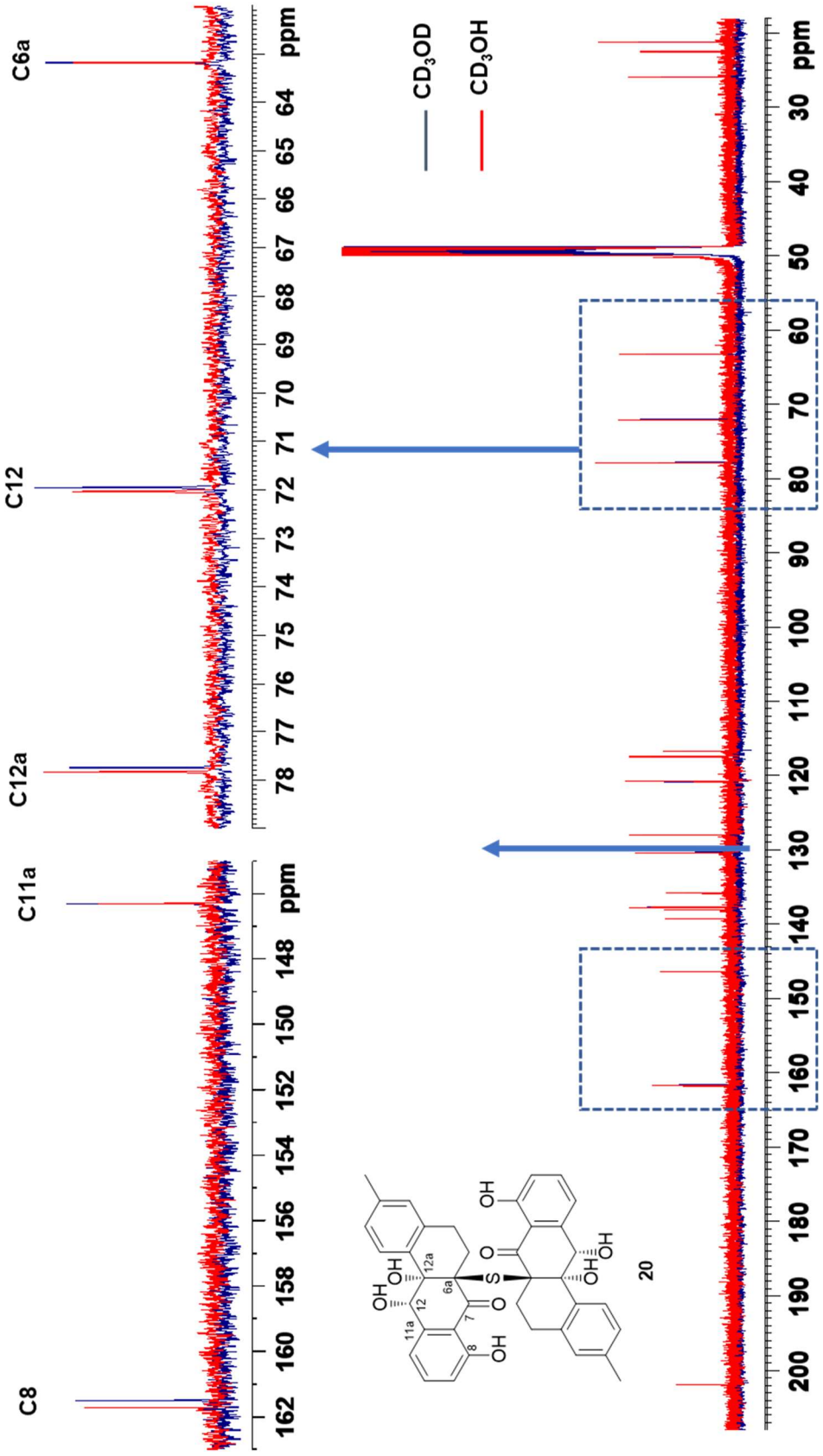

Figure S65. Process and results of HPLC detection after mixing SF2315B (**22**) with silica.

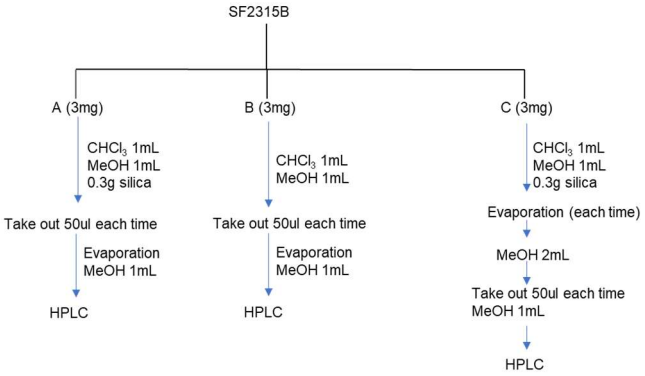

A (HPLC injection 10ul) 1 days

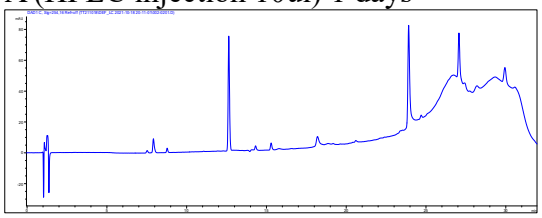

A (HPLC injection 20ul) 2 days

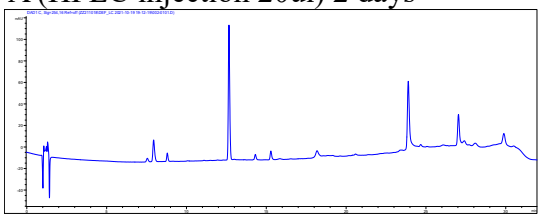

B (HPLC injection 10ul) 1 days

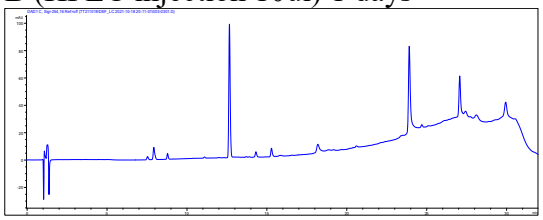

B (HPLC injection 20ul) 2 days

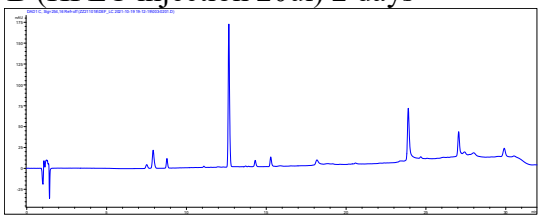

C (HPLC injection 10ul) 1 days

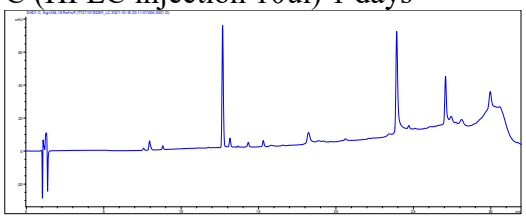

C (HPLC injection 20ul) 2 days

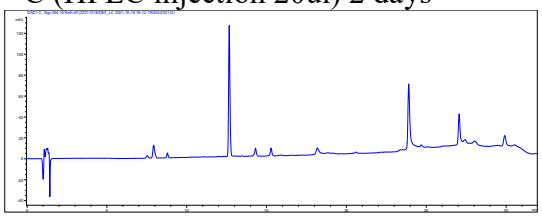

A (HPLC injection 20ul) 5 days

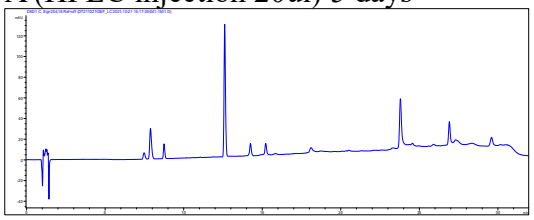

A (HPLC injection 20ul) 7 days

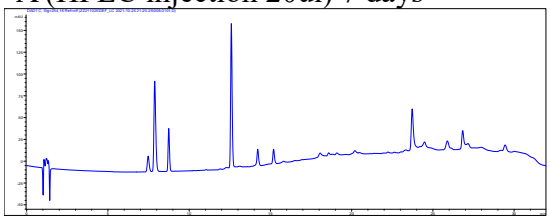

B (HPLC injection 20ul) 5 days

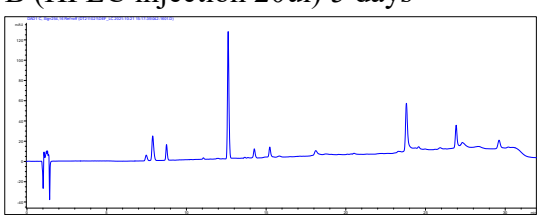

B (HPLC injection 20ul) 7 days

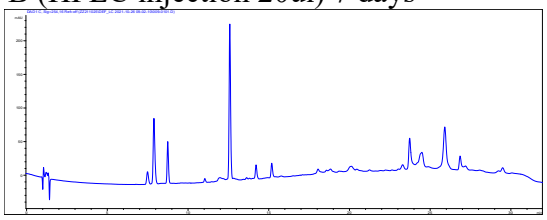

C (HPLC injection 20ul) 5 days

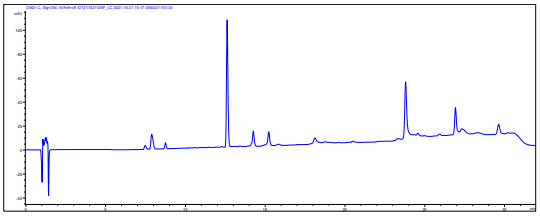

C (HPLC injection 20ul) 7 days

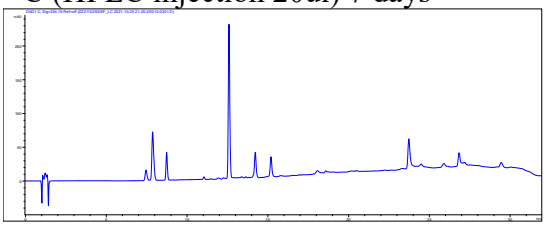

Table S3. ^{1}H and ^{13}C NMR Data for miaosporone E (**21**) and SF3215B (**22**) in CD_3OD.

	21			**22**		
no.	δ_C[b]	δ_H, mult (*J* in Hz)[a]	HMBC[a,c]	δ_C[b]	δ_H, mult (*J* in Hz)[a]	HMBC[a,c]
1	77.0	4.69, t (4.5)	2, 3, 4a, 12b	70.1	4.33, d (7.4)	3, 4a, 12b
2	120.4	5.61, s	1, 4, 13	123.7	5.39, s	4, 12b, 13
3	142.1			135.5		
4α	46.3	2.22[d]	2, 3, 4a, 5, 12b, 13	44.5	2.31, d (17.4)	2, 3, 4a, 5, 12b, 13
4β		2.01, (16.8)	2, 3, 4a, 5		1.98, d (17.4)	2, 3, 4a, 5
4a	73.4			73.0		
5α	31.8	2.15[d]	4a, 6, 6a	29.2	1.71, m	4a, 6, 6a, 12b
5β		1.71, m	6, 6a		1.47, m	4a, 6, 6a, 7
6α	25.2	2.16[d]	5		2.75, m	5, 6a, 12a
6β		2.03, m	5, 7, 6a, 12a	18.2	2.24, m;	4a, 5, 6a
6a	84.1			64.1		
7	199.1			199.6		
7a	115.1			113.7		
8	164.6			162.9		
9	117.5	6.86, d (8.5)	7a, 11	117.4	6.86, brd (8.4)	7, 7a, 8, 11
10	139.1	7.58, t (7.9)	8, 11a	138.0	7.54, t (8.0)	8, 11a
11	118.0	7.27, d (7.6)	7a, 9, 12	119.0	7.23, d (7.6)	7a, 8, 9, 12
11a	147.1			144.2		
12	68.0	5.04, s	7a, 11, 11a, 12b	68.0	5.5, s	7a, 11, 11a, 12a
12a	83.3			71.3		
12b	46.7	2.49, d (4.4)	1, 4, 4a, 5, 6a, 12a	46.8	2.71, d (7.7)	1, 4a, 5, 6a, 12a
13	23.6	1.80, s	2, 3, 4	23.4	1.73, s	2, 3, 4

[a] Recorded at 500 MHz
[b] Recorded at 125 MHz
[c] Proton showing HMBC correlations to indicated carbons
[d] Coupling constant not assignable due to signal overlapping

Table S4. Cartesian coordinates and energies of the most stable conformer of **14**.

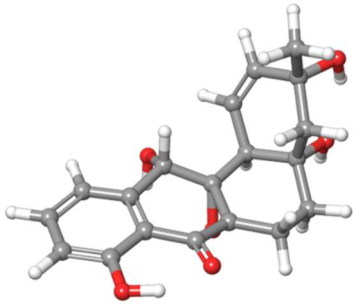

14

M06-2X/def2-TZVP-SMD(MeOH)//M06-2X/6-31G(d,p)-SMD(MeOH):		
Gibbs Free Energy (a.u.)	=	−1187.099135
M06-2X/def2-TZVP-SMD(MeOH):		
Electronic energy (a.u.)	=	−1187.420872
M06-2X/6-31G(d,p)-SMD(MeOH):		
Zero-point correction (a.u.)	=	0.368717
Thermal correction to Energy (a.u.)	=	0.389186
Thermal correction to Enthalpy (a.u.)	=	0.390130
Thermal correction to Gibbs Free Energy (a.u.)	=	0.321736

C	−0.05424	3.97298	−1.83142	C	0.04659	2.62282	−1.42218
C	1.31617	2.01372	−1.33958	C	2.44780	2.72825	−1.70215
C	2.32853	4.05207	−2.13686	C	1.09518	4.67809	−2.19860
C	−1.17089	1.86099	−1.14543	C	−1.07811	0.35882	−1.07064
C	0.25515	−0.25932	−0.85771	C	1.49502	0.61282	−0.78012
C	−2.35642	−0.35806	−0.72037	C	−2.12916	−1.86070	−0.60113
C	−0.95664	−2.20031	0.31693	C	0.37741	−1.66945	−0.25246
C	−1.17040	−1.65419	1.72934	C	−0.08450	−2.10055	2.71434
C	1.27962	−1.98476	2.07502	C	1.48389	−1.78005	0.77458
O	−1.23008	4.62111	−1.89799	O	−2.27514	2.39082	−1.01781
O	2.56758	−0.05916	−1.41751	O	−0.29607	−3.45642	3.12930
C	−0.14518	−1.27179	3.99080	O	−0.87270	−3.62208	0.45427
O	−0.33805	−0.21600	−2.15510	H	3.42189	2.25713	−1.63910
H	3.22003	4.60454	−2.41790	H	0.99189	5.70910	−2.51951
H	1.78346	0.70278	0.27350	H	−2.74498	0.05736	0.21403
H	−3.09680	−0.13792	−1.49586	H	−3.02757	−2.34411	−0.20566
H	−1.93102	−2.28932	−1.59117	H	−1.17166	−0.55945	1.68718
H	−2.14753	−1.97756	2.10752	H	2.13033	−2.10748	2.74433
H	−1.93126	4.02575	−1.55750	H	2.34580	−0.13578	−2.35831
H	−1.14056	−1.34918	4.43953	H	0.59089	−1.64311	4.71031
H	0.06823	−0.22008	3.78240	H	−0.69864	−4.01033	−0.41555
H	0.64966	−2.31281	−1.10166	H	2.49997	−1.71369	0.39510
H	−0.34750	−3.97552	2.31079				

Table S5. Cartesian coordinates and energies of the most stable conformer of **15**.

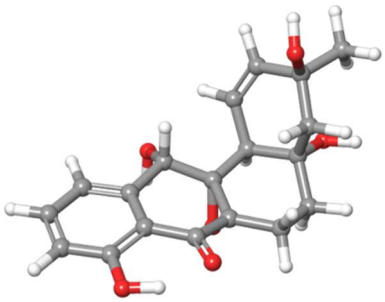

15

M06-2X/def2-TZVP-SMD(MeOH)//M06-2X/6-31G(d,p)-SMD(MeOH):		
Gibbs Free Energy (a.u.)	=	−1187.096421
M06-2X/def2-TZVP-SMD(MeOH):		
Electronic energy (a.u.)	=	−1187.416875
M06-2X/6-31G(d,p)-SMD(MeOH):		
Zero-point correction (a.u.)	=	0.368074
Thermal correction to Energy (a.u.)	=	0.388826
Thermal correction to Enthalpy (a.u.)	=	0.389770
Thermal correction to Gibbs Free Energy (a.u.)	=	0.320454

C	−2.18158	−1.78593	3.50148	C	−1.50509	−1.05326	2.49873
C	−0.31850	−0.36269	2.82199	C	0.14882	−0.37015	4.12741
C	−0.55037	−1.07074	5.11539	C	−1.70108	−1.77920	4.81385
C	−2.07756	−0.97153	1.15527	C	−1.56642	0.09413	0.22100
C	−0.25015	0.71793	0.50892	C	0.51947	0.32361	1.75701
C	−2.16285	0.09488	−1.16262	C	−1.52897	1.18149	−2.02259
C	−0.00056	1.12100	−2.02051	C	0.57122	1.37924	−0.61246
C	0.49106	−0.22910	−2.55486	C	2.01167	−0.35193	−2.66022
C	2.66720	0.26375	−1.44885	C	2.03903	1.01493	−0.54661
O	−3.29691	−2.49322	3.24998	O	−2.99140	−1.70315	0.77321
O	1.16830	1.47102	2.27713	O	2.26492	−1.76576	−2.66633
C	2.58998	0.24537	−3.94267	O	0.49595	2.19907	−2.81412
O	−1.46835	1.38566	0.83525	H	1.06015	0.16256	4.37319
H	−0.17722	−1.07159	6.13508	H	−2.24295	−2.33905	5.56855
H	1.32034	−0.36393	1.46215	H	−2.02673	−0.89610	−1.60504
H	−3.24185	0.25439	−1.07043	H	−1.87919	1.08656	−3.05640
H	−1.82995	2.17098	−1.66217	H	0.16242	−1.01735	−1.86801
H	0.02923	−0.43044	−3.52993	H	3.73448	0.06867	−1.34173
H	−3.47753	−2.45404	2.28681	H	0.48025	2.09294	2.55991
H	2.12357	−0.22662	−4.81336	H	2.42793	1.32313	−3.98839
H	3.66881	0.05576	−3.98338	H	0.20804	2.04777	−3.72642
H	0.48395	2.45854	−0.42854	H	2.59504	1.41490	0.29688
H	3.21338	−1.89253	−2.81356				

Table S6. Cartesian coordinates and energies of the most stable conformer of **16A**.

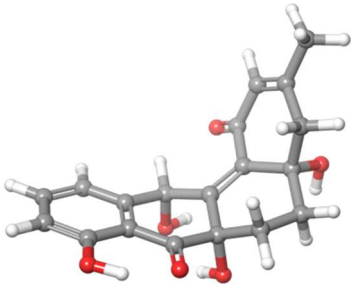

16A

M06-2X/def2-TZVP-SMD(MeOH)//M06-2X/6-31G(d,p)-SMD(MeOH):		
Gibbs Free Energy (a.u.)	=	−1185.934676
M06-2X/def2-TZVP-SMD(MeOH):		
Electronic energy (a.u.)	=	−1186.230270
M06-2X/6-31G(d,p)-SMD(MeOH):		
Zero-point correction (a.u.)	=	0.344507
Thermal correction to Energy (a.u.)	=	0.365556
Thermal correction to Enthalpy (a.u.)	=	0.366501
Thermal correction to Gibbs Free Energy (a.u.)	=	0.295594

C	−4.10618	0.01593	−0.79542	C	−2.84952	0.07089	−0.14580
C	−2.34649	−1.08621	0.48123	C	−3.08012	−2.26107	0.46979
C	−4.32214	−2.29956	−0.17251	C	−4.83500	−1.17771	−0.80171
C	−2.07924	1.31471	−0.14934	C	−0.72785	1.39266	0.58772
C	−0.09043	0.02559	0.76980	C	−1.03481	−1.06115	1.23051
C	0.18360	2.35956	−0.16242	C	1.58491	2.34005	0.42632
C	2.22550	0.95965	0.33203	C	1.23382	−0.14447	0.65283
C	2.84231	0.65722	−1.03430	C	3.31925	−0.76901	−1.15488
C	2.90054	−1.73483	−0.31515	C	1.90786	−1.48109	0.73596
O	−4.64088	1.07755	−1.41801	O	−2.50585	2.34005	−0.68244
O	−1.36251	−0.80911	2.60780	O	1.62928	−2.31773	1.58972
C	4.30025	−1.03985	−2.25049	O	3.31527	0.86787	1.25344
O	−1.02409	1.95910	1.86768	H	−2.68483	−3.14638	0.95790
H	−4.89299	−3.22301	−0.18284	H	−5.79505	−1.19566	−1.30643
H	−0.57178	−2.04420	1.13884	H	0.20114	2.07467	−1.22028
H	−0.25403	3.35848	−0.09971	H	2.23082	3.07436	−0.06520
H	1.52630	2.61001	1.48737	H	2.11463	0.85777	−1.83143
H	3.68842	1.33612	−1.19595	H	3.28100	−2.75060	−0.38409
H	−4.01585	1.83108	−1.31887	H	−0.55966	−0.98226	3.12410
H	3.89640	−0.69248	−3.20838	H	5.22242	−0.47450	−2.07400
H	4.54243	−2.10122	−2.32878	H	2.97082	1.03079	2.14385
H	−1.33768	1.23797	2.44151				

Table S7. Cartesian coordinates and energies of the most stable conformer of **16B**.

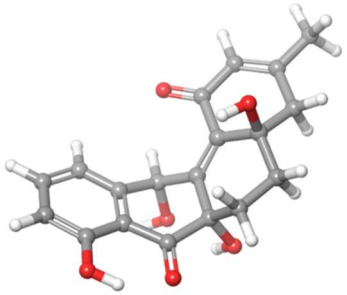

16B

M06-2X/def2-TZVP-SMD(MeOH)//M06-2X/6-31G(d,p)-SMD(MeOH):		
Gibbs Free Energy (a.u.)	=	−1185.935672
M06-2X/def2-TZVP-SMD(MeOH):		
Electronic energy (a.u.)	=	−1186.231606
M06-2X/6-31G(d,p)-SMD(MeOH):		
Zero-point correction (a.u.)	=	0.344259
Thermal correction to Energy (a.u.)	=	0.365385
Thermal correction to Enthalpy (a.u.)	=	0.366329
Thermal correction to Gibbs Free Energy (a.u.)	=	0.295934

C	−3.53064	0.06225	−2.27175	C	−2.32629	−0.42212	−1.72691
C	−1.10067	−0.07317	−2.33209	C	−1.06564	0.78252	−3.41590
C	−2.27054	1.29991	−3.91430	C	−3.48849	0.94432	−3.36035
C	−2.32902	−1.25490	−0.51750	C	−1.04723	−1.37703	0.34467
C	0.10299	−0.59591	−0.28649	C	0.13921	−0.74944	−1.78713
C	−1.38822	−0.83586	1.73380	C	−0.11308	−0.72614	2.55709
C	0.85019	0.29337	1.95115	C	0.91921	0.18641	0.43605
C	2.25204	0.12488	2.53861	C	3.30149	0.95721	1.85472
C	3.13512	1.39649	0.59449	C	1.93929	1.08754	−0.19163
O	−4.73564	−0.27107	−1.77804	O	−3.34395	−1.81582	−0.11188
O	0.07471	−2.15836	−2.03124	O	1.77748	1.55896	−1.31593
C	4.53275	1.25265	2.64868	O	0.46075	1.62941	2.28890
O	−0.73368	−2.75179	0.50457	H	−0.11678	1.04343	−3.87361
H	−2.25234	1.97891	−4.76132	H	−4.42458	1.32444	−3.75558
H	1.03579	−0.32488	−2.23665	H	−1.87721	0.14086	1.63529
H	−2.10658	−1.52058	2.19147	H	−0.32981	−0.41879	3.58438
H	0.37135	−1.70705	2.59284	H	2.21177	0.38326	3.60364
H	2.55238	−0.92890	2.47910	H	3.88751	2.00589	0.10101
H	−4.60871	−0.94879	−1.08326	H	−0.09189	−2.30204	−2.97394
H	4.96494	0.32068	3.03086	H	5.28406	1.77965	2.05774
H	4.27342	1.86076	3.52295	H	−0.36698	1.83641	1.83187
H	−0.41846	−3.06760	−0.35840				

Table S8. Cartesian coordinates and energies of the most stable conformer of **16C**.

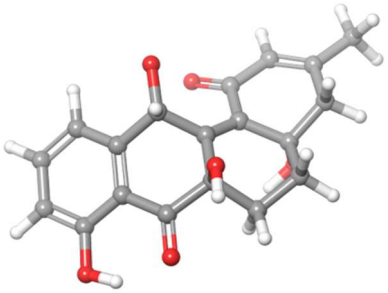

16C

M06-2X/def2-TZVP-SMD(MeOH)//M06-2X/6-31G(d,p)-SMD(MeOH):			
Gibbs Free Energy (a.u.)	=	−1185.934760	
M06-2X/def2-TZVP-SMD(MeOH):			
Electronic energy (a.u.)	=	−1186.229717	
M06-2X/6-31G(d,p)-SMD(MeOH):			
Zero-point correction (a.u.)	=	0.343855	
Thermal correction to Energy (a.u.)	=	0.364988	
Thermal correction to Enthalpy (a.u.)	=	0.365932	
Thermal correction to Gibbs Free Energy (a.u.)	=	0.294957	

C	2.72391	2.09087	−2.57990	C	2.09482	1.05101	−1.85927
C	1.04139	0.32725	−2.45906	C	0.60629	0.65194	−3.72978
C	1.21569	1.71284	−4.41450	C	2.26215	2.42670	−3.85777
C	2.51514	0.74384	−0.49506	C	1.69244	−0.23488	0.38302
C	0.31982	−0.47145	−0.23309	C	0.45596	−0.85168	−1.69735
C	1.61552	0.33494	1.79817	C	0.58826	−0.44598	2.59658
C	−0.80480	−0.23222	2.01208	C	−0.80726	−0.35890	0.49197
C	−1.78910	−1.24469	2.60118	C	−3.14347	−1.21936	1.95081
C	−3.30312	−0.74660	0.70133	C	−2.18012	−0.26756	−0.09841
O	3.75400	2.79149	−2.08057	O	3.52893	1.22897	0.00831
O	−0.65419	−1.43077	−2.32107	O	−2.37128	0.24250	−1.20698
C	−4.28368	−1.74471	2.75988	O	−1.32203	1.04893	2.38246
O	2.37996	−1.48341	0.36371	H	−0.19124	0.08317	−4.19289
H	0.86767	1.97370	−5.40952	H	2.74784	3.23756	−4.38976
H	1.22230	−1.63949	−1.70034	H	2.61060	0.27925	2.24666
H	1.34559	1.39657	1.74920	H	0.84024	−1.51134	2.56290
H	0.57129	−0.13308	3.64453	H	−1.37693	−2.25777	2.51076
H	−1.89138	−1.03779	3.67314	H	−4.27984	−0.70523	0.22729
H	3.99165	2.40878	−1.20850	H	−1.36940	−0.77132	−2.32231
H	−4.42846	−1.11644	3.64633	H	−5.21237	−1.77458	2.18729
H	−4.05167	−2.75244	3.12316	H	−0.80822	1.73518	1.93370
H	3.27710	−1.33381	0.70166				

Table S9. Cartesian coordinates and energies of the most stable conformer of **16D**.

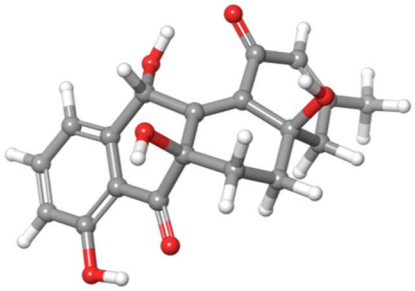

16D

M06-2X/def2-TZVP-SMD(MeOH)//M06-2X/6-31G(d,p)-SMD(MeOH):			
Gibbs Free Energy (a.u.)	=	−1185.931395	
M06-2X/def2-TZVP-SMD(MeOH):			
Electronic energy (a.u.)	=	−1186.227281	
M06-2X/6-31G(d,p)-SMD(MeOH):			
Zero-point correction (a.u.)	=	0.344136	
Thermal correction to Energy (a.u.)	=	0.365092	
Thermal correction to Enthalpy (a.u.)	=	0.366036	
Thermal correction to Gibbs Free Energy (a.u.)	=	0.295886	

C	−1.14524	2.26489	3.09503	C	−0.83047	1.88003	1.77094
C	−1.86851	1.66428	0.83918	C	−3.18638	1.85646	1.22830
C	−3.47944	2.26349	2.53301	C	−2.47644	2.46353	3.46683
C	0.57063	1.74345	1.36767	C	0.82526	1.63941	−0.14325
C	−0.18510	0.66496	−0.73226	C	−1.60649	1.19119	−0.59413
C	2.26302	1.27808	−0.46572	C	2.49451	−0.19882	−0.19370
C	1.62228	−1.05849	−1.10764	C	0.20377	−0.51211	−1.25300
C	1.54961	−2.48918	−0.56748	C	0.58044	−3.37045	−1.30363
C	−0.42453	−2.84367	−2.02515	C	−0.64424	−1.40191	−2.11660
O	−0.19923	2.46036	4.03104	O	1.50758	1.79758	2.16216
O	−2.61774	0.25457	−0.88032	O	−1.45091	−0.94086	−2.92671
C	0.79992	−4.84390	−1.19088	O	2.20816	−1.17458	−2.40722
O	0.48208	2.91688	−0.68182	H	−3.98624	1.67936	0.51948
H	−4.51437	2.41637	2.82380	H	−2.69364	2.76760	4.48516
H	−1.69944	2.06843	−1.25020	H	2.43047	1.51214	−1.52281
H	2.93319	1.90580	0.12763	H	3.53766	−0.47880	−0.36571
H	2.25991	−0.41955	0.85332	H	2.55499	−2.92483	−0.61822
H	1.26625	−2.46841	0.49259	H	−1.11101	−3.46892	−2.58938
H	0.67462	2.25466	3.63583	H	−2.57472	0.06520	−1.83101
H	0.85408	−5.13393	−0.13524	H	0.00681	−5.41348	−1.67863
H	1.76285	−5.11187	−1.64058	H	2.16721	−0.31184	−2.84391
H	1.13884	3.55686	−0.36677				

Table S10. Cartesian coordinates and energies of the most stable conformer of **17A**.

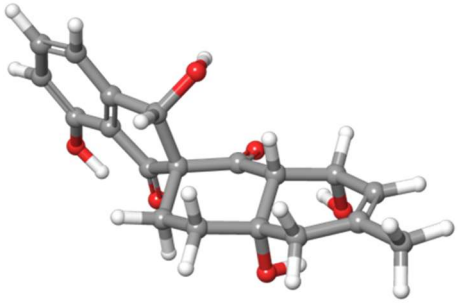

17A

M06-2X/def2-TZVP-SMD(MeOH)//M06-2X/6-31G(d,p)-SMD(MeOH):			
Gibbs Free Energy (a.u.)	=	−1187.129268	
M06-2X/def2-TZVP-SMD(MeOH):			
Electronic energy (a.u.)	=	−1187.448355	
M06-2X/6-31G(d,p)-SMD(MeOH):			
Zero-point correction (a.u.)	=	0.368134	
Thermal correction to Energy (a.u.)	=	0.389522	
Thermal correction to Enthalpy (a.u.)	=	0.390466	
Thermal correction to Gibbs Free Energy (a.u.)	=	0.319087	

C	3.28557	3.57455	0.03196	C	2.27715	2.62119	−0.15144
C	1.26028	2.79364	−1.08847	C	1.20832	3.93687	−1.86889
C	2.21865	4.89003	−1.68722	C	3.24570	4.72497	−0.75772
O	4.26817	3.40585	0.93722	C	0.26969	1.64459	−1.03878
C	0.92849	0.60847	−0.05924	C	2.12245	1.35315	0.54675
C	1.47088	−0.63741	−0.79677	C	0.35473	−1.57294	−1.24803
C	−0.51577	−2.02293	−0.07676	C	−1.12902	−0.80398	0.63881
C	−0.06990	0.20762	1.01952	C	−1.64292	−2.93837	−0.56277
C	−2.76042	−3.13518	0.43145	C	−2.91439	−2.34457	1.49768
C	−1.98158	−1.21977	1.84490	C	−3.70367	−4.26330	0.12886
O	−1.16309	−1.68719	2.92989	H	−1.77912	−0.29048	−0.08457
O	0.34427	−2.71707	0.82689	O	−0.03326	0.72100	2.12463
O	−1.01467	2.08888	−0.63741	O	2.85610	0.92057	1.42429
H	0.41650	4.09309	−2.59388	H	2.20767	5.79411	−2.28868
H	4.01665	5.47849	−0.63629	H	4.13218	2.55825	1.39948
H	0.12966	1.19416	−2.02529	H	2.06472	−0.30066	−1.65349
H	2.14254	−1.16831	−0.11544	H	−0.28271	−1.08514	−1.99391
H	0.78979	−2.46127	−1.71977	H	−2.07063	−2.53677	−1.49192
H	−1.20345	−3.91023	−0.82007	H	−3.72665	−2.52872	2.19794
H	−2.55545	−0.34970	2.18680	H	−4.13189	−4.14709	−0.87373
H	−3.16965	−5.22041	0.13465	H	−4.52027	−4.31432	0.85289
H	−0.66838	−0.91901	3.25613	H	−0.05609	−2.68570	1.71333
H	−0.91716	2.65104	0.14647				

Table S11. Cartesian coordinates and energies of the most stable conformer of **17B**.

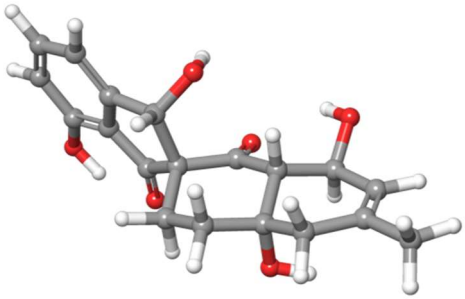

17B

M06-2X/def2-TZVP-SMD(MeOH)//M06-2X/6-31G(d,p)-SMD(MeOH):			
Gibbs Free Energy (a.u.)	=	−1187.129375	
M06-2X/def2-TZVP-SMD(MeOH):			
Electronic energy (a.u.)	=	−1187.447752	
M06-2X/6-31G(d,p)-SMD(MeOH):			
Zero-point correction (a.u.)	=	0.367788	
Thermal correction to Energy (a.u.)	=	0.389423	
Thermal correction to Enthalpy (a.u.)	=	0.390367	
Thermal correction to Gibbs Free Energy (a.u.)	=	0.318377	

C	−1.18434	−4.70321	0.26567	C	−1.02814	−3.31229	0.29473
C	−2.11740	−2.44879	0.38488	C	−3.40917	−2.94757	0.42839
C	−3.56620	−4.33910	0.39595	C	−2.48217	−5.21403	0.31820
O	−0.12782	−5.53445	0.18757	C	−1.67329	−0.99780	0.36533
C	−0.10145	−1.07076	0.36902	C	0.21870	−2.56418	0.24257
C	0.50845	−0.55095	1.68776	C	0.44605	0.96972	1.78413
C	1.16899	1.63790	0.61956	C	0.55005	1.19940	−0.72277
C	0.44367	−0.30615	−0.83178	C	1.11271	3.16045	0.73003
C	1.54655	3.87037	−0.53160	C	1.62973	3.23506	−1.70459
C	1.32130	1.77879	−1.91044	C	1.86540	5.32955	−0.38144
O	0.57360	1.66079	−3.11621	H	−0.48251	1.57678	−0.76169
O	2.52456	1.18470	0.67497	O	0.73265	−0.89483	−1.85960
O	−2.23099	−0.29400	−0.72884	O	1.34194	−3.04171	0.16535
H	−4.26944	−2.28908	0.48571	H	−4.56666	−4.75972	0.43335
H	−2.63101	−6.28847	0.29719	H	0.69004	−5.00380	0.16496
H	−2.01807	−0.46929	1.25891	H	−0.02801	−1.01360	2.52318
H	1.54973	−0.88393	1.73950	H	−0.59467	1.31341	1.79189
H	0.91068	1.30063	2.71922	H	0.09233	3.47606	0.98504
H	1.75191	3.46637	1.56820	H	1.94799	3.77352	−2.59607
H	2.26251	1.21740	−2.01995	H	1.01507	5.86332	0.05910
H	2.71331	5.47130	0.29856	H	2.10698	5.79144	−1.34164
H	0.52544	0.71292	−3.30949	H	3.06412	1.75770	0.11019
H	−2.10311	−0.81985	−1.53301				

Table S12. Cartesian coordinates and energies of the most stable conformer of **17C**.

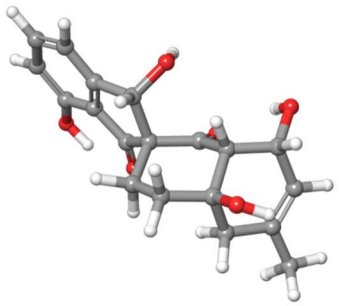

17C

M06-2X/def2-TZVP-SMD(MeOH)//M06-2X/6-31G(d,p)-SMD(MeOH):		
Gibbs Free Energy (a.u.)	=	−1187.126103
M06-2X/def2-TZVP-SMD(MeOH):		
Electronic energy (a.u.)	=	−1187.444871
M06-2X/6-31G(d,p)-SMD(MeOH):		
Zero-point correction (a.u.)	=	0.368083
Thermal correction to Energy (a.u.)	=	0.389620
Thermal correction to Enthalpy (a.u.)	=	0.390564
Thermal correction to Gibbs Free Energy (a.u.)	=	0.318768

C	−0.60999	−1.52091	−4.18014	C	−0.64434	−1.30834	−2.79736
C	−1.50611	−2.01845	−1.96211	C	−2.37556	−2.96078	−2.48535
C	−2.33961	−3.17557	−3.86947	C	−1.47766	−2.47580	−4.71373
O	0.22559	−0.83846	−4.98597	C	−1.39198	−1.53389	−0.52763
C	−0.12545	−0.60865	−0.53951	C	0.17918	−0.38973	−2.02350
C	1.11185	−1.30616	0.08184	C	1.11557	−1.29917	1.60956
C	0.86207	0.08533	2.19894	C	−0.50053	0.61303	1.68428
C	−0.44138	0.70053	0.17580	C	1.96277	1.09358	1.85267
C	1.58226	2.52483	2.16408	C	0.31178	2.88831	2.36957
C	−0.85876	1.93801	2.36417	C	2.71788	3.50618	2.19456
O	−2.02565	2.53197	1.81257	H	−1.26025	−0.14222	1.92398
O	0.78844	−0.09637	3.60818	O	−0.63680	1.73097	−0.44410
O	−2.57766	−0.87429	−0.11810	O	1.02524	0.37252	−2.46897
H	−3.06107	−3.51359	−1.85176	H	−3.00573	−3.91273	−4.30775
H	−1.46854	−2.66165	−5.78258	H	0.75408	−0.22043	−4.44839
H	−1.25386	−2.35937	0.17626	H	1.14345	−2.33659	−0.28796
H	2.00799	−0.80561	−0.29786	H	0.33808	−1.96757	1.99850
H	2.07995	−1.67030	1.97259	H	2.87032	0.81609	2.40373
H	2.22329	1.03492	0.78647	H	0.07079	3.92788	2.58779
H	−1.13158	1.70549	3.40149	H	3.27267	3.47916	1.24924
H	2.36454	4.52651	2.36139	H	3.43058	3.24863	2.98652
H	−1.81359	2.74296	0.89063	H	0.89658	0.76423	4.03931
H	−2.82888	−0.23447	−0.80187				

Table S13. Cartesian coordinates and energies of the most stable conformer of **17D**.

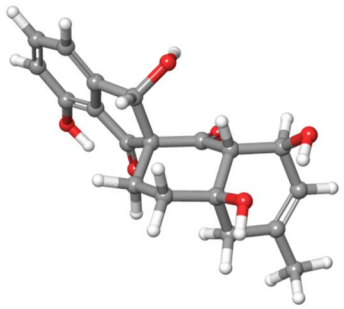

17D

M06-2X/def2-TZVP-SMD(MeOH)//M06-2X/6-31G(d,p)-SMD(MeOH):		
Gibbs Free Energy (a.u.)	=	−1187.127440
M06-2X/def2-TZVP-SMD(MeOH):		
Electronic energy (a.u.)	=	−1187.446371
M06-2X/6-31G(d,p)-SMD(MeOH):		
Zero-point correction (a.u.)	=	0.368108
Thermal correction to Energy (a.u.)	=	0.389669
Thermal correction to Enthalpy (a.u.)	=	0.390613
Thermal correction to Gibbs Free Energy (a.u.)	=	0.318931

C	−0.98475	−4.21026	1.46691	C	−0.98157	−2.84398	1.16388
C	−2.05001	−2.01186	1.49544	C	−3.16918	−2.52279	2.13151
C	−3.17187	−3.89025	2.43630	C	−2.10579	−4.73085	2.11619
O	0.05004	−5.01219	1.15176	C	−1.81735	−0.59990	0.98691
C	−0.32020	−0.60636	0.51790	C	0.07896	−2.08429	0.51666
C	0.60451	0.11991	1.52639	C	0.53966	1.64167	1.40733
C	0.74429	2.13724	−0.02420	C	−0.31863	1.51417	−0.94547
C	−0.21476	0.00496	−0.87662	C	2.13942	1.82314	−0.57007
C	2.27010	2.05860	−2.05648	C	1.20185	2.14166	−2.85481
C	−0.22374	2.04917	−2.37730	C	3.67553	2.16359	−2.57411
O	−0.88148	3.31135	−2.49309	H	−1.30591	1.77667	−0.54043
O	0.50259	3.54385	−0.08051	O	−0.08354	−0.68941	−1.86541
O	−2.74025	−0.26837	−0.03583	O	1.14129	−2.53120	0.10774
H	−4.01461	−1.89205	2.38530	H	−4.03334	−4.31826	2.94020
H	−2.13178	−5.78669	2.36434	H	0.73835	−4.48403	0.70724
H	−1.96554	0.14718	1.77173	H	0.31982	−0.19145	2.53723
H	1.62859	−0.22991	1.36282	H	−0.43746	2.00979	1.74189
H	1.30022	2.08975	2.05756	H	2.87439	2.43461	−0.02911
H	2.40944	0.77831	−0.35970	H	1.33788	2.31908	−3.92041
H	−0.78055	1.37312	−3.03419	H	4.25404	1.27360	−2.29926
H	3.69863	2.27049	−3.66126	H	4.18779	3.02335	−2.12675
H	−0.42763	3.89676	−1.86652	H	1.22681	3.99578	0.37684
H	−2.76424	−0.99372	−0.67854				

Table S14. Cartesian coordinates and energies of the most stable conformer of **20**.

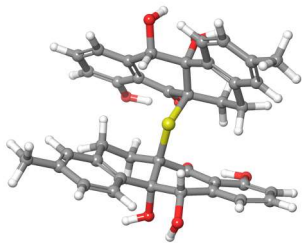

20

B3LYP-D3BJ/6-311+G(d,p)-IEFPCM(MeOH)//B3LYP-D3BJ/6-31G(d)-IEFPCM (MeOH):			
Gibbs Free Energy (a.u.)	=	−2468.792443	
B3LYP-D3BJ/6-311+G(d,p)-IEFPCM(MeOH):			
Electronic energy (a.u.)	=	−2469.370159	
B3LYP-D3BJ/6-31G(d)-IEFPCM(MeOH):			
Zero-point correction (a.u.)	=	0.648863	
Thermal correction to Energy (a.u.)	=	0.688750	
Thermal correction to Enthalpy (a.u.)	=	0.689694	
Thermal correction to Gibbs Free Energy (a.u.)	=	0.577716	

C	2.47765	−0.43978	3.74318	C	2.01910	−1.00443	2.52270
C	1.03065	−2.00985	2.54334	C	0.48510	−2.41064	3.75746
C	0.91015	−1.81295	4.94994	C	1.90039	−0.83800	4.95322
C	2.52748	−0.49074	1.25739	C	1.75212	−0.82201	−0.01029
C	1.38471	−2.34128	0.00717	C	0.56661	−2.71894	1.27698
C	2.57785	−0.51612	−1.26065	C	1.79599	−0.78569	−2.53990
C	0.96230	−2.04540	−2.49306	C	0.71442	−2.75360	−1.30222
C	0.37019	−2.48501	−3.68512	C	−0.46074	−3.60187	−3.74155
C	−0.69859	−4.29904	−2.54755	C	−0.11966	−3.88597	−1.35571
C	−1.08531	−4.05258	−5.03818	O	0.62851	−4.12595	1.48711
O	2.63580	−3.05451	0.17976	O	3.52441	0.24227	1.19332
O	3.43333	0.51037	3.77065	C	2.22201	2.81591	−2.73433
C	1.13485	2.59899	−1.84569	C	−0.16955	2.44468	−2.35858
C	−0.37301	2.46624	−3.73353	C	0.71263	2.63240	−4.60169
C	2.00219	2.81066	−4.11551	C	1.38920	2.47132	−0.41657
C	0.29793	1.85843	0.45031	C	−1.07362	2.49843	0.05952
C	−1.38703	2.30382	−1.45318	C	0.56601	2.10552	1.93555
C	−0.48465	1.44813	2.82120	C	−1.89502	1.57368	2.29280
C	−2.18536	2.00991	0.98646	C	−2.94734	1.18209	3.13191
C	−4.27932	1.20575	2.72416	C	−4.55468	1.64351	1.42003
C	−3.53011	2.04101	0.57234	C	−5.39220	0.77874	3.64809
O	−2.37742	3.24138	−1.86279	O	−0.89961	3.93219	0.19264
O	2.47206	2.79052	0.09409	O	3.48176	2.98635	−2.28616
S	0.08568	0.04327	0.01827	H	−0.25769	−3.20009	3.77466
H	0.46706	−2.12360	5.89157	H	2.24468	−0.37862	5.87352

H	−0.48595	−2.48349	1.10510
H	3.46578	−1.15600	−1.21147
H	2.48809	−0.83212	−3.38826
H	−1.34178	−5.17553	−2.55438
H	−0.81822	−3.38619	−5.86348
H	−2.17888	−4.07789	−4.96189
H	2.88281	−3.43262	−0.67913
H	−1.37900	2.37113	−4.12622
H	2.84728	2.95268	−4.78048
H	1.56780	1.77536	2.20528
H	−0.25827	0.38200	2.92892
H	−2.70550	0.84053	4.13640
H	−3.76434	2.39175	−0.42469
H	−5.97913	−0.03666	3.20888
H	−2.10529	4.07718	−1.43614
H	3.42764	3.02325	−1.29607
H	2.94746	0.50765	−1.23595
H	1.12509	0.05564	−2.74370
H	0.56602	−1.92233	−4.59571
H	−0.30169	−4.44717	−0.44803
H	−0.75986	−5.06612	−5.30210
H	1.56448	−4.35093	1.31981
H	3.75936	0.61125	2.83893
H	0.54427	2.63351	−5.67461
H	−1.82552	1.31455	−1.60125
H	0.56116	3.19203	2.07616
H	−0.42907	1.87193	3.83024
H	−5.58285	1.67511	1.06811
H	−6.08678	1.60591	3.83850
H	−5.00290	0.43606	4.61119
H	−1.34418	4.21060	1.00904

CHAPTER 6

Conclusion

Marine microorganisms are still largely underexploited in comparison with terrestrial microorganisms, for natural product screening. This study was conducted to evaluate the productivity of structurally new natural products by marine actinomycetes. As detailed discussed in Chapters 2 to 5, marine actinomycetes were isolated from three different unexploited sources, stony coral, sea slug and deep-sea water (DSW). HPLC-UV chemical screening was employed to find structurally novel bioactive compounds from these marine actinomycete strains. Specifically, two strains *Streptomyces*, isolated from stony coral and sea slug samples, and other two strains *Actinomadura.* isolated from DSW, were chosen and subjected to metabolite analysis.

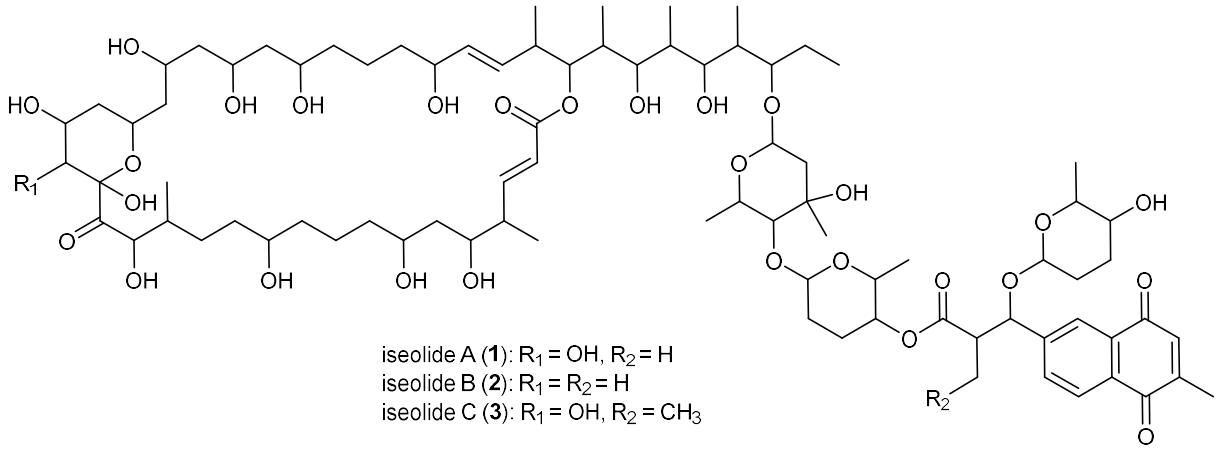

In Chapter 2, the first strain, *Streptomyces* sp. DC4-5 isolated from a stony coral *Dendrophyllia* sp., was collected at -20~25 m in depth near the coast of Minami-Ise, Mie prefecture, Japan. The isolated strain DC4-5 was identified as a member of genus *Streptomyces* on the basis of 99.2% similarity in the 16S rRNA gene sequence to *Streptomyces kronopolitis* NEAU-ML8^{T}. From the fermentation extract of this strain were isolated three new macrolides, iseolides A–C (**1**–**3**). Extensive analysis of one- and two-dimensional NMR data, coupled with MS/MS analytical data, revealed that iseolides are the new congeners of 36-membered macrolides, PM100117 and PM100118, previously reported from a marine-derived *Streptomyces*. Iseolides showed potent antifungal activity against a plant pathogen *Glomerella cingulate* NBRC5907 and human pathogens *Candida albicans* NBRC0197 and *Trichophyton rubrum* NBRC5467 with MIC in the range of 0.19 to 6.25 μg/mL.

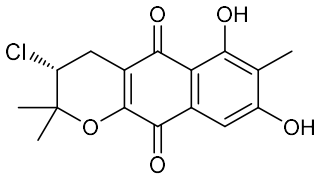

TMKS8A (**4**)

In Chapter 3, *Strepromyces* sp. TMKS8 was isolated from an air-breathing slug, *Paromoionchis tumidus*, collected at Mangkang mangrove forest, Semarang, Central Java, Indonesia. The 16S rRNA gene sequence analysis showed that strain TMKS8 belongs to the genus *Streptomyces* sp. Chemical investigation for structurally novel secondary metabolites from this marine actinomycete led to the discovery of one new chlorinated α-lapachone derivative, TMKS8A (**4**). The structure of **4** was determined by the analysis of NMR and MS spectral data, assisted by NMR chemical shift prediction using DFT-based calculation. Compound **4** displayed antimicrobial activity against Gram-positive bacteria with MIC values ranging from 6.25 to 12.5 μg/mL and cytotoxicity against murine leukemia P388 cells with IC_{50} 9.8 μM.

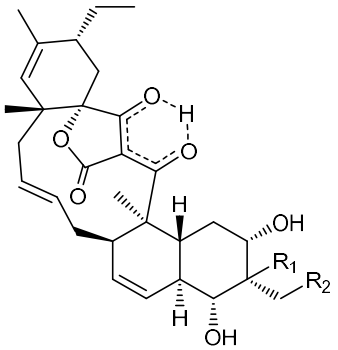

nomimicin B (**10**): $R_1 = R_2 = OH$
nomimicin C (**11**): $R_1 = OH$, $R_2 = H$
nomimicin A (**13**): $R_1 = R_2 = H$

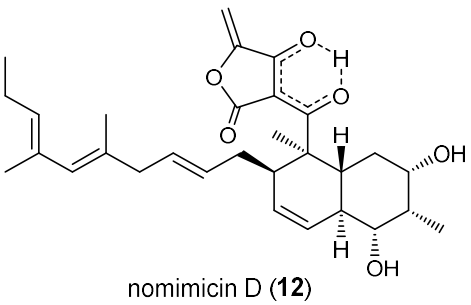

nomimicin D (**12**)

In Chapter 4, *Actinomadura* sp. AKA43 was isolated from the sea water sample collected at the Izu-Akazawa DSW pumping station in Shizuoka prefecture, Japan. A 16S rRNA gene sequence analysis revealed that strain AKA43 belongs to the genus *Actinomadura* sp. Fermentation and subsequent extraction, fractionation, and chromatographic separation led to the isolation of three new tetronate-class polyketides, nomimicins B–D (**11**–**12**). The structures of **10**–**12** were elucidated through the interpretation of NMR and MS analytical data and the absolute configurations were determined by combination of NOESY/ROESY and ECD analyses. Compounds **10**–**12**

showed antimicrobial activity against Gram-positive bacteria, *Kocuria rhizophila* ATCC9341 and *Bacillus subtilis* PCI219, with MICs in the range of 6.5 to 12.5 μg/mL. Compounds **10** and **11** also displayed cytotoxicity against P388 murine leukemia cells with IC_{50} at 33 and 89 μM, respectively.

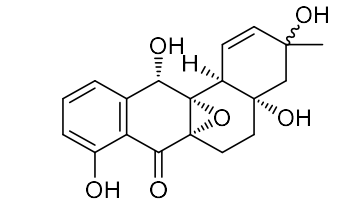

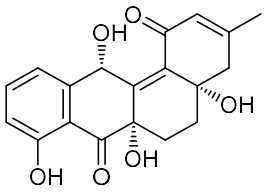
kumemicinone C (**16**)

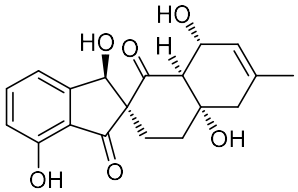
kumemicinone D (**17**)

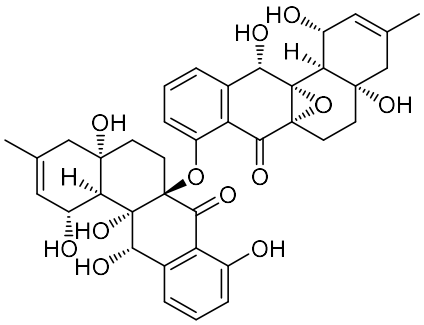
kumemicinone E (**18**)

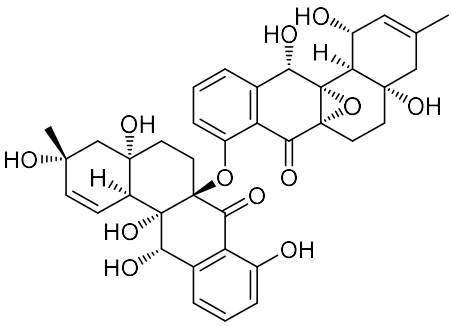
kumemicinone F (**19**)

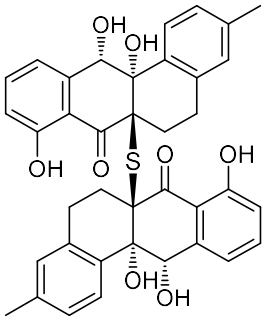
kumemicinone G (**20**)

In Chapter 5, *Actinomadura* sp. KD439 was isolated from suspended matter in sea water collected at -612 m near the coast of Kumejima Island, Okinawa, Japan. The producing strain KD 439 was identified as a member of the genus *Actinomadura* sp. by phylogenetic analysis based on 16S rRNA gene sequence similarity. Similarly, chemical investigation of secondary metabolites from this marine-derived actinomycete strain led to discovery of three new angucyclines, one skeletally rearranged product, and three dimeric angucyclines designated Kumemicinones A–G (**14**–**20**). Structures of **14**–**20** were determined through the interpretation of NMR and MS spectroscopic data and the absolute configurations were elucidated using quantum chemical calculations of NMR chemical shifts and ECD and X-ray diffraction. Compounds **14**–**20** exhibited cytotoxicity against P388 murine leukemia cells with IC_{50} values ranging from 1.8 to 53 μM.

In summary, four marine actinomycetes, two *Streptomyces* strains and two *Actinomadura* strains were subjected to analyze the secondary metabolites. Chromatographic separation of fermented products and NMR-based structure analysis resulted in the discovery of fourteen new bioactive compounds, including three

macrolides, iseolides A–C (**1**–**3**) with antifungal and cytotoxicity activity from *Streptomyces* sp. isolated from a stony coral, and one new chlorinated α-lapachone derivative, TMKS8A (**4**) with antimicrobial and cytotoxicity activities from *Streptomyces* sp. obtained from a sea slug, three new tetronate-class polyketides, nomimicins B–D (**11**–**12**) from *Actinomadura* isolated from suspended matter in deep sea water, and seven new angucyclines-class compounds kumemicinones A–G (**14**–**20**) with cytotoxicity activity from *Actinomadura* isolated from deep sea water. These results verify the usefulness of marine actinomycetes as a source of new bioactive natural products and actinomycetes collected from invertebrates and DSW are promising sources of novel bioactive natural products. In this study, the results substantiate that marine actinomycetes are promising resource for screening for new drug lead discovery.

Acknowledgements

I would like to express my deepest appreciation for my advisor Professor Yasuhiro Igarashi, Toyama Prefectural University, for his guidance, supervision, continuous encouragement, and valuable advice in completing this work.

I also would like to express my deepest gratitude to Associate Professor Naoya Oku, Assistant Professor Enjuro Harunari and Dr. Tao Zhou, Toyama Prefectural University, for their valuable guidance, supervision and encouragement throughout the course of this work.

And I also greatly appreciate all members of the Laboratory of Microbial Engineering, Biotechnology Center, Toyama Prefectural University.

Acknowledgements are also made to co-authors: Prof. Daisuke Urabe and Assistant Professor Keisuke Fukaya, Toyama Prefectural University, and Assoc. Prof. Yasuko In, Osaka University of Pharmaceutical Sciences, and Prof. Chiaki Imada, and Dr. Taehui Yang, Tokyo University of Marine Science and Technology, and Dr. Mada Triandala Sibero, Diponegoro University, Indonesia.

Finally, I am gratitude to my parents and my family members for their inspiration, support, and patience.

Publication List

1. Iseolides A–C, antifungal macrolides from a coral-derived actinomycete of the genus *Streptomyces*

Zhiwei Zhang, Tao Zhou, Enjuro Harunari, Naoya Oku, Yasuhiro Igarashi

The Journal of Antibiotics. 2020, 73: 534–541.

2. TMKS8A, an antibacterial and cytotoxic chlorinated α-lapachone, from a sea slug-derived actinomycete of the genus *Streptomyces*

Zhiwei Zhang, Mada Triandala Sibero, Akiho Kai, Keisuke Fukaya, Daisuke Urabe, Yasuhiro Igarashi

*The Journal of Antibiotics.*2021, 74: 464-469.

3. NomimicinsB–D, new tetronate-class polyketides from a marine-derived actinomycete of the genus *Actinomadura*

Zhiwei Zhang, Tao Zhou, Taehui Yang, Keisuke Fukaya, Enjuro Harunari, Shun Saito, Katsuhisa Yamada, Chiaki Imada, Daisuke Urabe, Yasuhiro Igarashi

Beilstein Journal of Organic Chemistry. 2021, 17: 2194-2202.

4. Kumemicinones A–G, cytotoxic angucyclinones from a deep sea-derived actinomycete of the genus *Actinomadura*

Zhiwei Zhang, Yasuko In, Keisuke Fukaya, Taehui Yang, Enjuro Harunari, Daisuke Urabe, Chiaki Imada, Naoya Oku, Yasuhiro Igarashi

Journal of Natural Products. 2022, 85:1098–1108.